UC Berkeley
UC Berkeley Electronic Theses and Dissertations

Title
Human Exposure to Urban Vehicle Emissions

Permalink
https://escholarship.org/uc/item/0nf849mt

Author
Apte, Joshua Schulz

Publication Date
2013

Peer reviewed|Thesis/dissertation

eScholarship.org Powered by the California Digital Library
University of California

Human Exposure to Urban Vehicle Emissions

By

Joshua Schulz Apte

A dissertation submitted in partial satisfaction of the

requirements for the degree of

Doctor of Philosophy

in

Energy and Resources

in the

Graduate Division

of the

University of California, Berkeley

Committee in charge:

Professor William W. Nazaroff, Chair
Professor Kirk R. Smith
Professor Robert A. Harley
Professor Julian D. Marshall

Fall 2013

Human Exposure to Urban Vehicle Emissions

Copyright © 2013

by Joshua Schulz Apte

Abstract

Human Exposure to Urban Vehicle Emissions

by

Joshua Schulz Apte

Doctor of Philosophy in Energy and Resources

University of California, Berkeley

Professor William W Nazaroff, Chair

This dissertation investigates human exposure to vehicular air pollutant emissions in urban areas. Since resources for protecting human health from the adverse consequences of inadvertent environmental releases are constrained, it is often desirable to identify sources and settings in which emissions controls could lead to especially high human health benefits per unit effort. The three measurement and modeling studies that comprise this dissertation aim to contribute towards this goal by advancing a mechanistic understanding of the relationship between urban vehicle emissions and subsequent human exposures. Two key themes that permeate these investigations include the exposure consequences of vehicle emissions in low-income settings such as developing world cities, and the role of dynamic processes in influencing the emissions-to-exposure relationship for urban air pollutant sources. Chapter 1 introduces each of the dissertation chapters and provides context and background related to the broader themes motivating the investigation.

In Chapter 2, I report on exposures to particulate matter (PM) in the megacity of New Delhi, India. Previous work has identified New Delhi as a hotspot for ambient PM pollution. To investigate the degree to which in-vehicle exposures can be represented by ambient fixed-site measurements in New Delhi, I undertook a multi-month field campaign in 2010. In-vehicle measurements focused on concentrations of fine particulate matter ($PM_{2.5}$), black carbon (BC) and ultrafine particles (UFP, measured by particle number count, PN) inside the cabins of auto-rickshaws, a common type of unenclosed vehicle in South Asia. Supplemental measurements considered PM levels inside conventional (enclosed) automobiles. Contemporaneously with the in-vehicle measurements, I conducted routine ambient monitoring of $PM_{2.5}$, BC and PN at a rooftop fixed site.

In-vehicle particle concentrations measured during this field campaign were substantially elevated relative to the levels recorded at the ambient monitoring site. Geometric mean concentrations inside the auto-rickshaw, averaged over ~160 h of 1 Hz data, were 190 $\mu g\ m^{-3}$ $PM_{2.5,}$ 42 $\mu g\ m^{-3}$ BC, and 280×10^3 particles cm^{-3}. These concentrations rank among the highest levels ever reported for routine transportation microenvironments. Short-duration peak concentrations (averaging time: 10 s), attributable to exhaust plumes of nearby vehicles, were greater than 300 $\mu g\ m^{-3}$ for $PM_{2.5}$, 85 $\mu g\ m^{-3}$ for BC, and 650×10^3 particles cm^{-3} for PN. In-vehicle $PM_{2.5}$ levels were 1.5× higher than the high ambient $PM_{2.5}$ concentrations (geometric

mean: 120 μg m^{-3}) in Delhi. In-vehicle BC and PN levels were more substantially elevated above background levels (respectively 3.6× and 8.4×). The especially high degree of elevation for PN suggests that in-vehicle exposures might account for a large fraction of daily PN exposure for auto-rickshaw users. The in-vehicle amplification for PN is likely attributable to proximity to a major PN source (traffic emissions) as well as dynamic loss processes such as coagulation that may remove UFP from ambient air.

A small subset of measurements collected inside conventional cars with open windows resulted in similar mean concentrations to contemporaneous measurements inside auto-rickshaws. In contrast, concentrations were somewhat lower inside automobiles with air conditioning, likely owing to dynamic in-vehicle particle removal mechanisms. Overall, this investigation concludes that in-vehicle exposures in New Delhi substantially exceed the high ambient background concentrations recorded at fixed sites.

Chapter 3 presents a global analysis of the population exposure implications of urban vehicle emissions using the intake fraction (*iF*) metric. Intake fraction is a dimensionless parameter that represents the fraction of a source's emissions that are ultimately inhaled by all exposed individuals. In this chapter, I develop and apply a model to estimate *iF* for spatially distributed, ground-level emissions (e.g., from vehicles) in 3646 worldwide urban areas, each with year-2000 population > 100,000. This large dataset of cities accounts for ~ 2.0 billion people, roughly ~70% of the year-2000 urban population. The investigation develops the first-ever *iF* estimates for urban emissions in many regions outside of North America and Europe, including for numerous megacities for which *iF* data did not previously exist.

In particular, Chapter 3 considers the intraurban *iF* for each of the cities in this dataset, which accounts for the inhalation exposure to an urban area's emissions that occurs within that same city. Base-case model runs consider an archetypal primary, conserved, non-reactive pollutant. Sensitivity scenarios consider primary pollutants with first-order decay. These broad classifications are representative of many health-relevant pollutants emitted by vehicles and other urban sources. Moreover, they provide a point of comparison for understanding the exposure implications of non-conserved and secondary pollutants, which are explored in more detail in Chapter 4.

For conserved primary pollutants, population-weighted median, mean, and interquartile range *iF* values are 26, 39, and 14 - 52 ppm, respectively, where 1 ppm signifies 1 g inhaled per tonne emitted. The global mean urban *iF* determined here is roughly twice as large as previous estimates for cities in the United States and Europe, owing primarily to the inclusion of cities with higher *iF* located outside of these two regions. Intake fractions vary among cities owing to differences in population size, population density, and meteorology. Sorting by size, population-weighted mean *iF* values are 65, 35, and 15 ppm, respectively, for cities with populations larger than 3 million, 0.6 – 3 million, and 0.1 – 0.6 million. For the 20 worldwide megacities in the dataset, the population-weighted mean intraurban *iF* is 83 ppm. Overall, mean *iF* values are greatest in Asia and lowest in land-rich high-income regions, owing primarily to differing patterns in urban form between these two regions. Among the 10 countries with the largest urban populations, population-weighted mean intraurban *iF* varies by a factor of 3. Intake fraction results for individual cities are predicted well by a parsimonious regression model that incorporates metrics of urban land area, population density, and meteorology.

Chapter 4 extends the concept of intake fraction to incorporate semivolatile organic emissions. The analysis emphasizes the consequences of these emissions for population exposure to organic particulate matter, which is a major constituent in both vehicle exhaust and ambient urban air. Organic aerosols (OA) blur traditional notions of primary and secondary pollutants owing to dynamic exchange of material between the vapor and particle phases. Dilution of fresh organic PM emissions (primary organic aerosol, POA) with ambient air typically causes a profound shift of material from particle to vapor phase. Relatively more volatile vapor-phase material is then "aged" into lower-volatility products over its residence time in a regional airshed via oxidation reactions initiated by photochemically produced radicals (e.g., the hydroxyl radical OH). In turn, these lower volatility products oxidized from evaporated emissions then condense to form quasi-secondary particles that make up the so-called oxidized primary organic aerosol (OPOA).

In this analysis, I update the definition of intake fraction to accommodate the cumulative contributions of population exposure to primary and quasi-secondary organic particles (i.e., POA and OPOA) as well as vapor-phase material to the overall intake fraction for semivolatile organic emissions. As in Chapter 3, the primary emphasis of the analysis is on vehicles and other urban, ground level emissions sources. Because photochemical aging at the regional scale is the major mechanism for converting evaporated POA material into OPOA, I develop and employ a nested multi-compartment mechanistic model to consider exposures at the urban, periurban and regional scales with a 400-km domain. Base-case model simulations consider an archetypal medium-sized US city (population 1.5 M); alternative cases include a model of *iF* for a global megacity (population 12 M). Key transformation processes for semivolatile emissions (e.g., dilution, partitioning, aging) are represented using the Volatility Basis Set (VBS) framework. A major goal of the modeling exercise is to contrast the magnitude and spatial distribution of *iF* for semivolatile organic emissions with patterns in *iF* for nonreactive pollutants.

For urban emissions of non-reactive particles, ~75% of domain-wide population intake occurs in the same urban compartment as emissions. In contrast, for semivolatile emissions, spatial patterns and gas-particle partitioning of intake depend substantially on emissions volatility. Low volatility organic emissions in urban areas produce predominantly intraurban, particle-phase exposures (similar to inert pollutants). As volatility of material emitted in urban areas increases, three key trends emerge that reduce particle-phase *iF*: (1) the overall proportion of population exposure that takes place in the particle phase decreases and the proportion of exposure in the gas phase increases, (2) photochemically aged material (OPOA) accounts for a larger fraction of particle-phase population intake, and (3) regional-scale exposures account for the predominant fraction of organic aerosol exposure attributable to urban precursor emissions.

Since higher volatility compounds account for a large fraction of motor vehicle emissions, the overall *iF* for organic particles attributable to urban semivolatile organic emissions is lower than for inert pollutants. For example, for the default emissions volatility distribution and considering the base-case model, the particle- and vapor-phase intake fractions for semivolatile emissions are respectively 3.1 ppm and 12.5 ppm. Thus, exposure to organic particle-phase material accounts for only ~ 20% of the population intake of all semivolatile organic emissions. For comparison, the *iF* for primary, non-reactive, conserved pollutants is substantially higher (*iF* ~ 16.9 ppm) and is only modestly attenuated for inert particles that are subject to loss via dry deposition (*iF* ~ 12.9 ppm).

The dissertation concludes with a summary and synthesis chapter (Chapter 5), which explores policy implications and provides recommendations for future research.

Acknowledgements

The process of researching and writing a dissertation is often likened to standing on the shoulders of giants. Nearly seven years ago, as a fresh-faced masters student at UC Berkeley, these anonymous giants conjured images in my minds eye of some craggy monolith of wisdom that I might scramble up to add a few pebbles of my own. Looking back, I realize I had it all wrong. My deepest debt is not to some faceless canon of knowledge, but to the family, friends, colleagues, and mentors who have encouraged and guided me so ably over these many years. It is the time that I have spent with these inspiring people that will be my most fond and enduring memory of graduate school.

First and foremost, I owe heartfelt thanks to each of my dissertation committee members: Rob Harley, Julian Marshall, Kirk Smith, and especially Bill Nazaroff, my chair. Rob deserves special credit for launching me on my dissertation research trajectory by piquing my interest in Indian auto-rickshaws in a CE218A class project. Rob, thank you for your constant support and wisdom. Julian's multifaceted contributions frequently transcended the normal roles of a dissertation advisor. Not merely a colleague, Julian has also enthusiastically played the role of co-conspirator, cheerleader, and friend. Julian, thank you for blazing the path at ERG before me, and for showing me time and again that success requires fun and hard work in equal measure. Kirk deserves special credit for pushing me to stretch my interests to incorporate the health effects of air pollution. I've benefited greatly from his distilled wisdom about environmental health policy, and his relentless encouragement for me to push the boundaries about how I think about problems and solutions. Thank you, Kirk. Finally, my greatest academic debt is to Bill Nazaroff, to his outstanding mentorship, and to his uncanny ability to lead by example. I've benefited tremendously from Bill's conscientious advice, and from his dedication, support, patience, generosity, and good humor. Bill, thank you for teaching me to set the bar high. It's been an honor to work with you.

A great many others have helped me along the way. From my time in India, I owe a great debt to the many who made my research in Delhi possible. Special thanks go to Alex Reich, Shyam Deshpande, Arvind Chel, and Geetanjali Kaushik for their dedicated contributions to data collection. Ambuj Sagar, Geetam Tiwari, and Anumita Roychowdhury were instrumental in inspiring and supporting my fieldwork. My friends Sarath Guttikunda and Puja Jawahar embodied a wide set of roles during my frequent visits to Delhi, including as advisors, collaborators, badminton partners, and ever-gracious hosts. In helping me prepare for my fieldwork in India I'm indebted to the support and generosity of Tom Kirchstetter, Hugo Destaillats, Melissa Lunden, Lara Gundel, and my father Mike Apte at LBNL; to Jeff Blair of AethLabs; and to my colleagues at UBC: Mike Brauer, Conor Reynolds, and Andy Grieshop. I'm especially grateful to Tom Kirchstetter for giving me free reign over his lab, and for helping me quickly move up the learning curve for particle instrumentation. I also owe fond thanks to the many others at LBNL who nurtured my early interests in energy research, including Dariush Arasteh, Steve Selkowitz, Christian Kohler, Howdy Goudey, Ashok Gadgil, Alan Meier, and Rick Diamond. At ERG, I am especially grateful for the encouragement, critiques, and contributions of the core faculty, and the tireless efforts of the ERG staff. Departed but not forgotten, Alex Farrell and Lee Schipper still loom larger-than-life in my memories. Heartfelt thanks are due to my ERGie classmates and friends for inspiration their and support, especially

to Sam Borgeson, Merrian Fuller, Anand Gopal, Fritz Kahrl, Derek Lemoine, Lindsey Fransen, Sintana Vergara, Zoe Chafe, Jalel Sager, and Amol Phadke. Likewise, I'll fondly remember the companionship and support of the AirHeads cohort in Davis Hall, especially Tim Dallmann, Brian MacDonald, Matt Vannucci, Seema Bhangar, Sharon Shearer, Nasim Mullen, Dev Millstein, Arman Shehabi, Bev Coleman, and George Ban-Weiss.

Funding for this work was provided by a number of sources, including the US EPA STAR Graduate Fellowship, a Fulbright-Nehru grant to India, and the Chang-Lin Tien and Philomathia Graduate Fellowships in the Environmental Sciences. I also benefited from the financial support of the International Council on Clean Transportation, and from the collaboration and encouragement of my ICCT colleagues Ray Minjares, Kate Blumberg, Sarah Chambliss, Gaurav Bansal, and Mazyar Zeinali.

Finally, my deep thanks and appreciation go to my family for a lifetime of support. To my parents and grandparents: thank you for your constant inspiration and encouragement, and for making me who I am today. To my brothers, thanks for keeping me sane, and for putting up with me after all these years of being a student. To my girlfriend, Meghana, thanks for your love, dedication, patience, and companionship in all of our many adventures over the years.

Joshua Apte
16 August 2013

Table of Contents

Abstract **1**

Acknowledgements ..... **i**

Table of Contents ..... **iii**

List of Tables ..... **viii**

List of Figures ..... **x**

Chapter 1: Introduction **1**

1.1 Context: Cities, urbanization, and motorization 1

1.2 Health effects of air pollution exposure 2

1.3 Air pollutant dynamics 4

1.4 Conceptual framework and dissertation outline 5

1.5 References 8

Chapter 2: Concentrations of fine, ultrafine, and black carbon particles in auto-rickshaws in New Delhi, India **14**

2.1. Introduction 14

2.2 Materials and methods 14

2.2.1 Site description and experimental design 14

In-vehicle measurements 15

Ambient air quality monitoring: Chittaranjan Park (CRP) and Lodhi Garden (LG) 16

Self-pollution 16

2.2.2 Instrumentation 17

Meteorological parameters 17

Continuous and integrated $PM_{2.5}$ measurements 17

Black carbon measurements 19

Ultrafine particle number concentration measurements 19

Other measurements and protocols 20

2.2.3 Quality control, data processing and analysis 20

2.3 Results and Discussion 21

2.3.1 In-vehicle concentrations: Auto-rickshaws 21

2.3.2 Contribution of proximate sources to in-vehicle exposure concentrations 22

Ratio of in-vehicle to ambient concentrations 22

Estimated coagulation time scale for ambient ultrafine particles 22

Nearby contributions to in-vehicle exposures 23

2.3.3 Seasonal and temporal variability in ambient and in-vehicle pollutant concentrations 24

2.3.4 Comparisons among vehicle types 25

2.3.5 Comparison to other megacities, and implications for time-integrated exposure 26

2.4 Conclusions 27

2.5 References 28

Chapter 3: Global intraurban intake fractions for primary air pollutants from vehicles and other distributed sources 46

3.1 Introduction 46

3.2 Methods 47

3.2.1 Intake fraction 47

3.2.2 Emissions – exposure concentration relationship 47

Model selection 47

One-compartment emissions-concentration model 48

3.2.3 Model input data 49

Meteorological data 49
Breathing rate 51
Data for each urban area 51
Emissions profile 51
3.2.4 Steady-state intake fraction 52
3.3 Results and discussion 53
3.3.1 Global and regional summary of intake fraction 53
Reduced-form model for intake fraction 53
Patterns of intake fraction by city size, world region, and country 54
Megacities 55
Time-of-day and seasonal patterns in iF 55
City ventilation per-capita dilution rate 56
3.3.2 Validation and comparison with prior research 56
3.3.3 Sensitivity analysis and limitations 57
3.4 Implications for policy 60
3.4 Conclusions 60
3.5 References 62
Chapter 4: Inhalation intake fraction for urban emissions of semi-volatile organic compounds from vehicles and other distributed sources 85
4.1 Introduction 85
4.2 Methods and conceptual framework 87
4.2.1 Fundamental considerations: Dynamics of semi-volatile compounds 87
Absorptive partitioning theory 87
Evolving partitioning 88
4.2.2 Nested multi-compartment model 92

4.2.3 Intake fraction for semi-volatile compounds in a multi-compartment system....94
4.2.4 Differential material balance....97
4.2.5 Other model input variables....100
Wind speed and mixing height....100
OH radical profiles and ambient temperatures....101
4.2.6 Emissions....102
4.3 Results and discussion....103
4.3.1 Concentration results....103
4.3.2 Intake fraction for primary nonreactive pollutants....105
4.3.3 Intake fraction for semi-volatile organic compounds....106
Base-case model....106
Megacity scenario....108
Contribution of beyond-urban emissions to urban exposures....109
4.3.4 Comparing metrics: source-oriented exposure vs. atmospheric burden....110
4.3.5 Sensitivity analyses....111
Emissions: magnitude and volatility....111
Meteorology and dispersion....112
Dry deposition....113
Compartment parameterization: population and land area....113
Photochemistry....114
4.3.6 Limitations and future research....115
4.4 Conclusions....116
4.5 References....118
5. Conclusions....138

5.1 Summary of results....138
5.2 Implications for policy and future research....140
5.2.1 Near-source exposures....141
5.2.2 Health effects of vehicle emissions....142
5.2.3 Sustainable transportation for an urbanizing world....143
5.3 References....146
6. Appendix A: Post-processing of aethalometer black carbon meaurements....150
References....154
7. Appendix B: Development of diurnal profiles for population breathing rates....157
References....158

List of Tables

Table 2-1. Monthly mean and range of meteorological parameters at the Chittaranjan Park (CRP) ambient site during morning (AM) and evening (PM) auto-rickshaw trips. 32

Table 2-2. Distribution of average particulate matter concentrations for 62 auto-rickshaw trips in New Delhi. 32

Table 2-3. Summary statistics for within-trip concentration distributions inside auto-rickshaws....33

Table 2-4. Sum-of-lognormals fit used to approximate New Delhi ambient particle size distribution....33

Table 2-5. Comparison of present study results with prior measurements in megacities and elsewhere....34

Table 3-1. Global summary of intraurban intake fraction, demographic parameters, and meteorology....68

Table 3-2. Population-weighted mean intake fraction (*iF*) by region and city size 68

Table 3-3. Regional summary of intraurban intake fraction, population density, & meteorology 68

Table 3-4. Population-weighted mean intraurban intake fraction for the 10 countries with largest population in cities 69

Table 3-5. Population-weighted mean intraurban intake fraction for all cities modeled, grouped by country 70

Table 3-6. Intake fraction results and summary data for 20 worldwide megacities 73

Table 3-7. Population-weighted mean per-capita dilution parameter (DR / LPD), grouped by region and city size 73

Table 3-8. Sensitivity of model results to meteorological inputs. 74

Table 3-9. Sensitivity of model results to other inputs. 74

Table 3-10. Parameter values for microenvironment sensitivity analysis 75

Table 4-1. Volatility basis set and assumed parameters for emitted material. 122

Table 4-2. Demographic parameters and sizing for base-case and megacity scenarios 122

Table 4-3. Concentrations of semivolatile material by compartment 122

Table 4-4. Intake fractions for urban emissions in base-case scenario 123

Table 4-5. Intake fractions for urban emissions in megacity scenario 124

Table 4-6. Key results from sensitivity scenarios 125

Table 4-7. Emissions volatility distribution for diesel generators 127

Table 5-1. Potential routes for reducing health and climate impacts from transportation 149

Table B-1. Activity-specific breathing rates for the US population 159

Table B-2. Apportionment of average person time by microenvironment and breathing rate for US population in NHAPS 159

List of Figures

Figure 2-1. Map of New Delhi indicating the main sampling route used in the study 36

Figure 2-2. Scatter plot of colocated gravimetric and time-averaged DustTrak PM2.5 concentration measurements. 37

Figure 2-3. Example data for one trip (29 March 2010) 38

Figure 2-4. Lognormal probability plots and box plots for trip-averaged auto- rickshaw concentrations 39

Figure 2-5. Example screen capture from auto-rickshaw video camera during on-road sampling 40

Figure 2-6. Traces of vehicle status and pollutant concentrations during experiment to investigate potential self-pollution contribution to in-vehicle exposures 41

Figure 2-7. Box plots of trip-averaged in-vehicle concentration attributable to near-roadway microenvironment 42

Figure 2-8. Decomposition of variability in concentrations into month-of-year and time-of-day components for ambient concentrations and in-vehicle measurements 43

Figure 2-9. Boxplots of $PM_{2.5}$, BC, and PN in-vehicle exposure concentrations sampled in May 2010, by vehicle type, showing concentrations and a measure of skew 44

Figure 2-10. Comparison of in-vehicle and ambient concentrations from this study and from other megacities 45

Figure 3-1. Comparison of base case diurnal breathing rate profile with three alternate profiles used for sensitivity analysis 76

Figure 3-2. Comparison of base case diurnal emissions profile with alternate profiles used for sensitivity analysis. 76

Figure 3-3. Log-probability plot for population-weighted global distribution of intraurban *iF* for emissions of primary, nonreactive pollutants from distributed groundlevel sources 77

Figure 3-4. Population-weighted distribution of intraurban intake fraction by city size and region 78

Figure 3-5. Map of nine world regions used for analysis. 79

Figure 3-6. Maps of intraurban intake fractions by continent 79

Figure 3-7. Variation in *iF* for emissions occurring at a specified time of day, expressed as a ratio of the time-dependent *iF* to time-averaged *iF* for a given city 83

Figure 3-8. Seasonal variation in *iF* for emissions occurring at a specified time of day, expressed as a ratio of the time-dependent *iF* to time-averaged *iF* for a given city 84

Figure 4-1. Model schematic and aging mechanism. 128

Figure 4-2. Geometry of 3 compartment nested model. 129

Figure 4-3. Diurnal cycle of urban mixing height and wind speed 130

Figure 4-4. Mean-normalized diurnal cycle of OH radical concentration 130

Figure 4-5. Assumed volatility distribution of emissions for default model runs 131

Figure 4-6. Diurnal variation in particle-phase partitioning coefficient and primary fraction of total OA mass 131

Figure 4-7. Source contributions to organic aerosol concentrations within the innermost urban compartment 132

Figure 4-8. Plots of OA intake fraction and population intake rate for urban emissions of organic semivolatile precursor material (vapors and particles). 133

Figure 4-9. Plots of vapor-phase intake fraction and population intake rate for urban emissions of organic semivolatile precursor material (vapors and particles). 133

Figure A-1. Effect of post-processing algorithm on aethalometer black carbon data 155

Figure A-2. Effect of filter loading correction on colocated BC measurements collected in the field study described in Chapter 2. 156

Figure B-1. Fraction of total person-time in NHAPS for each of four microenvironment groupings 160

Figure B-2. Fraction of US population time in each of five breathing rate modes by hour of day 160

Figure B-3. Diurnal breathing rate profile for the US population estimated using US EPA and NHAPS data 161

Chapter 1: Introduction

1.1 Context: Cities, urbanization, and motorization

This dissertation investigates practical and theoretical aspects of human exposure to vehicle air pollution in urban areas. In this chapter, I introduce the motivation and background for my research and summarize key themes and ideas that are explored in detail in subsequent chapters.

When I began my research for this dissertation in 2008, the size of the world's urban population had grown larger than that of the rural population for the first time in recorded history. In 1950, less than 30% of the world's population lived in cities. Under current forecasts, the world's cities will account for more than two-thirds of the human population by the year 2050 (United Nations, 2012). Urbanization will exceed total population growth. According to United Nations (UN) forecasts, roughly 2.7 billion more people will live in the cities of 2050 compared to the cities of 2010, while the world's total population will grow by only 2.4 billion people. The vast majority of this increase in the world's urban population will take place in the so-called economically developing world, especially in Africa (+860 million people) and in Asia (+1.5 billion people) (United Nations, 2012). The opportunities and challenges created by this urbanization will shape the lives of current generations, and perhaps the lives of many generations to come.

The activity that takes place in cities has outsized importance for the world's economy and environment. A disproportionate fraction of worldwide energy use is dedicated to satisfying the consumption and production demands of urban areas (Satterthwaite, 2008). In this dissertation, I focus one major urban energy end use, transportation, which accounts for a large (~25%) and growing fraction of primary energy consumption. As incomes rise, personal car ownership is increasing rapidly in many regions of the world ("motorization"). This expansion of private mobility brings newfound freedoms and economic opportunities, yet also imposes important societal externalities, such as injuries, congestion, and pollution (Gakenheimer, 1999; Pucher et al., 2005; Woodcock et al., 2009). The adverse environmental consequences of vehicle emissions span a broad range of spatial scales. For example, the exhaust emissions of an urban vehicle may influence population air pollutant exposures over spatial scales as short as 1 m and as long as 1000 km. The CO_2 contained in vehicle exhaust will mix thoroughly throughout the global atmosphere over its long atmospheric lifetime, thereby affecting the energy balance of the entire planet. While my interest in transportation systems is motivated in part by their global environmental impacts, I emphasize here the local and regional aspects of population air pollution exposure from urban vehicles.

It is instructive to remember that cities are mere specks on our landscape when viewed from above. As sensed by satellites from space, cities account for < 0.5% of the earth's land area (Schneider et al., 2009). The world's current urban population of ~3.6 billion people inhabits a land area of approximately 700,000 km^2, roughly equivalent to the area of France. The ratio of these two statistics implies a worldwide mean urban population density of ~ 5000 km^{-2}. Globally, urban population density varies substantially among world regions. Cities in high-income, land-rich countries (e.g., the USA) tend to be less dense than the global mean, while cities in many lower-income countries are substantially denser than the global mean.

Human air pollution exposure to mobile-source emissions has a complex relationship with urban population density (Marshall et al., 2005). On one hand, the urban form of dense cities offers the potential for lower per-capita emissions from transportation by reducing the demand for private mobility. On the other hand, populations in dense cities are exposed to pollution in close proximity and at lower levels of dilution. Issues of dilution and proximity are of central importance to this dissertation. I devote special attention to the conditions in developing world megacities, where the confluence of high-emitting vehicles with high urban population density results in very high air pollutant concentrations and exposures. The air quality challenges of megacities – the ~20-30 worldwide cities with more than 10 million inhabitants (Forstall et al., 2009) – are a well-acknowledged extreme case of the confluence of population, activity, emissions and exposure (Gurjar et al., 2010; Gurjar and Lelieveld, 2005; Mage et al., 1996; Molina and Molina, 2004). In many developing world cities, the effects of increasing private mobility can quickly outpace improvements in vehicle fleet emission factors (e.g., as has been the case in New Delhi) (Kumar et al., 2013). Moreover, if current population growth trends hold, the number of worldwide megacity inhabitants (currently over 300 million) seems likely increase, especially as other large fast-growing cities graduate into the "megacity" category. In short, the air quality challenges of the world's large cities will require substantial attention from engineers and policymakers for the foreseeable future.

1.2 Health effects of air pollution exposure

Air pollution is a major risk factor for ill health and premature mortality. For example, a systematic comparative risk assessment for the Global Burden of Disease project estimated that outdoor air pollution, as represented by ambient fine particulate matter ($PM_{2.5}$) exposure, was associated with ~3.2 million worldwide premature deaths in 2010 (Lim et al., 2012; Lozano et al., 2012). For comparison, HIV-AIDS and malaria were estimated to result in respectively ~ 1.5 million and ~ 1.2 million premature deaths in 2010 (Lim et al., 2012; Lozano et al., 2012). In short, air pollution represents a health hazard that is of comparable magnitude to other widely acknowledged global health risks.

Epidemiological studies form the basis for quantifying the population-level health risks of urban air pollution. While air pollution epidemiology has made great strides in the past decades, elucidating the health effects of urban air pollution is inherently fraught with challenge. The air that we breathe contains a multitude of compounds with plausible or identified adverse health effects. Concentrations often result from the emissions of multiple sources, as well as from the contributions of secondary formation processes. Owing to meteorology and common sources, the levels of multiple pollutants frequently vary collinearly in space and time, making it difficult to disentangle the adverse effect of one contaminant from another. Spatiotemporal variation in pollutant concentrations poses additional challenges. Concentrations measured at ambient fixed-site monitors are a widely available and commonly employed exposure metric. However, unlike fixed-site monitors, people move around their cities. As a metric of personal exposure, ambient concentrations are neither precise nor accurate. The exposure misclassification introduced by ambient monitors remains a major limitation to more precise elucidation of air pollution's health effects.

It is a testament to the skill and persistence of the epidemiological community that the evidence for air pollution's health effects is remarkably robust and consistent in spite of these myriad technical challenges. Among the major outdoor air pollutants with well-identified health

effects, fine particulate matter ($PM_{2.5}$) stands out as a pollutant with especially large population-level impacts. Epidemiological evidence links $PM_{2.5}$ exposure to elevated risks for several acute and chronic health outcomes, including respiratory disease, cardiovascular disease and premature mortality (Pope and Dockery, 2006; Brook et al., 2010). $PM_{2.5}$ is a ubiquitous urban pollutant, with major primary contributions from traffic, industry and power generation, as well as regional photochemical production from gaseous precursors. Long-term average $PM_{2.5}$ concentrations in US cities have improved over the past decades, such that the annual average $PM_{2.5}$ concentration among all ambient monitors in the US (predominantly urban sites; mean of all stations ~ 11-12 $\mu g\ m^{-3}$) nearly meets the World Health Organization annual air quality guideline of 10 $\mu g\ m^{-3}$ (Blanchard et al., 2011; US EPA, 2008; Schichtel et al., 2001). However, a large fraction of the world's population resides in areas with substantially higher $PM_{2.5}$ concentrations, including more than 500 million people who live in cities with annual-average concentrations exceeding 70 $\mu g\ m^{-3}$ (Brauer et al., 2012). Chapter 2 of this dissertation reports in detail on particle concentrations in New Delhi, one of the most polluted major cities in the world. While not the object of investigation here, extremes at the other (cleanest) end of the concentration spectrum also provide valuable information about the presence or absence of thresholds in the dose-response relationship for ambient air pollution. Emerging epidemiological evidence suggests sizeable long-term health effects of $PM_{2.5}$ even in some of the cleanest regions of the world (Crouse et al., 2012).

The acute health effects of $PM_{2.5}$ are widely documented by so-called "time-series" studies, in which transient increases in mortality are associated with individual air pollution episodes (Health Effects Institute, 2010a; Künzli et al., 2001; Pope and Dockery, 2006). While elegant, this type of study design is typically unable to detect the long-term development and progression of chronic disease that is thought to represent a major portion of air pollution's health effects (Künzli et al., 2001; Pope and Dockery, 2006). Indeed, long-term (i.e., multi-year to multi-decade) cohort studies typically report order-of-magnitude greater risks for chronic $PM_{2.5}$ exposures compared to short-term exposures (Dockery et al., 1993; Krewski et al., 2009; Künzli et al., 2001; Pope and Dockery, 2006). While such studies represent the gold standard for outdoor air pollution epidemiology in many regards, they are especially challenging to execute. The most ambitious such studies follow the survival of hundreds of thousands of individuals in dozens of cities for over a decade. Given the large cost associated with studies of this magnitude, these investigations have primarily been conducted in higher-income regions of the world.

The lack of epidemiological data from high-pollution, low-income portions of the world remains a major gap in the current state of knowledge about urban air pollution's health effects. A further limitation relates to the spatial scale of exposure assessment. Many cohort studies rely on a small number of urban-ambient concentration monitors to represent the exposures of thousands or tens of thousands of subjects. For pollution sources with pronounced spatial variability in exposure– such as traffic air pollution – coarse-scale exposure assessment techniques typically result in an underestimate of the true risk. Because of this exposure misclassification, risk estimates frequently increase when cohort studies are able to take advantage of more fine-scale exposure data (Jerrett et al., 2005). This dissertation aims to contribute towards a broad effort to better understand air pollution exposure at multiple spatial scales.

Several lines of evidence suggest that local-scale exposures to traffic air pollution pose health hazards in excess of what may be inferred from ambient air quality monitoring. Research from

around the world indicates that particle and gas-phase pollutant concentrations in transportation microenvironments – on and near roadways and inside vehicles – often exceed nearby ambient levels. Therefore, exposures of people while in transit and for those who live or work near roadways may not be well characterized by conventional air quality monitoring stations (Kaur et al., 2007). Several studies have found that residential proximity to roadways is associated with increased risk of premature mortality and other chronic health effects (Health Effects Institute, 2010b; Hoek et al., 2002). Short-term exposure to elevated in-vehicle particle concentrations has been associated with subclinical cardiovascular effects in healthy populations (Jacobs et al., 2010; Riediker et al., 2004), and may serve as a trigger of acute health effects such as myocardial infarction for susceptible individuals (Peters et al., 2004). Many other constituents of vehicle exhaust have well-identified adverse health effects. Black carbon – a product of incomplete combustion and a component of $PM_{2.5}$ – is associated with human carcinogens such as diesel exhaust (IARC, 1989; Benbrahim-Tallaa et al., 2012) and polycyclic aromatic hydrocarbons (IARC, 1983). Ultrafine particles (UFP; diameter < 0.1 μm) are abundant in vehicle exhaust (Kittelson, 1998) and represent an emerging public health concern (Sioutas et al., 2005; Oberdörster, 2001; Delfino et al., 2005). While this dissertation emphasizes human exposure to *particle* pollution from traffic, exposure to gas-phase pollutants also pose health risks. Examples of primary gas-phase pollutants that are especially elevated near roadways include CO, NO, NO_2 and benzene (Karner et al., 2010).

1.3 Air pollutant dynamics

It might seem self-evident that concentrations of vehicle-emitted pollutants are elevated to proximity to roadways. However, it is worthwhile to reflect on the processes and phenomena that govern human exposure to urban vehicle emissions. In this dissertation, I distinguish between two broad classes of pollutants based on the degree of physical and chemical processing that they experience over the transport timescales that govern human exposure to vehicle emissions. On one hand, more stable species (e.g., CO, CO_2) behave in an effectively conserved fashion. For conserved pollutants, advection is the dominant removal and dilution mechanism at the local, urban, and regional scales. On the other hand are so-called "dynamic" pollutants, which are removed or transformed rapidly relative to the timescales relevant for transport and human exposure. The physicochemical processes that transform or remove dynamic pollutants include phase change (i.e., evaporation and condensation), chemical reactions (e.g., oxidation or acid-base chemistry), and flux to surfaces (e.g., inertial impaction, gravitational settling, and diffusive mass transport). Because dynamic processes speed the rate of removal or transformation, dynamic pollutants tend to be depleted in more aged masses (Bhangar, 2010). Conversely, relative to ambient concentrations, concentrations of untransformed dynamic pollutants tend to be more sharply elevated in near-source region, such as on roadways. Accordingly, ambient air quality monitors are likely to be particularly inadequate for characterizing population exposures to urban emissions of dynamic pollutants. Mechanistic models that account for the behavior of dynamic pollutants can provide information about human exposures that occur under non-ambient conditions.

In this dissertation, I explicitly consider two pollutants that have important exposure-relevant dynamic behavior: ultrafine particles and semivolatile organic compounds. In the immediate near-source region, ultrafine particle size distributions evolve rapidly owing to a complex exchange of material between the gas and particle phase. Fresh ultrafine particles are nucleated

from semivolatile gas-phase material, while existing particles may grow in size owing to condensation of gas material onto existing particle surfaces, or conversely shrink via evaporation if below a critical diameter (Ketzel and Berkowicz, 2004; Zhang and Wexler, 2004; Zhang et al., 2004). Particle size distributions in on-road microenvironments are typically enriched in nucleation mode particles (count median diameter ~ 10-20 nm). Mixing, evaporation, condensation, coagulation, and deposition cause sharp shifts in the particle size distribution over the 100-500m required to reach conditions more typical of urban background levels (Ketzel and Berkowicz, 2004; Kumar et al., 2011; Zhang et al., 2004; Zhu et al., 2002). Compared to on-road conditions, particle size distributions in the urban background are depleted in ultrafine particles in general; the nucleation mode typical of fresh emissions is much less prominent in ambient air. Over longer timescales, vehicle emissions of organic particulate matter also experience substantial dynamic evolution. Since the organic particle constituents of vehicle exhaust are semivolatile, a substantial fraction of material that is present in the particle phase in concentrated exhaust plumes will evaporate into the gas phase under ambient conditions. Over the hours and days that follow emissions, photochemically initiated oxidation processes substantially reduce the volatility of evaporated primary material, leading to regional formation of secondary organic aerosol. Thus, dynamic processes cause aged air masses to be relatively depleted in primary emissions, but relatively enriched in secondary material.

1.4 Conceptual framework and dissertation outline

Because active remediation of outdoor air pollution is typically infeasible, efforts to improve air quality typically focus on reducing emissions. Air quality management includes deciding which sources to control and by how much. In classic environmental economics, a socially optimal control strategy is one that maximizes societal benefit at minimal cost. In real-world decision-making, policies are rarely optimal and not always rational. Nevertheless, given constrained resources for environmental protection, it is generally desirable to minimize the cost of reaching a given environmental health target (Cass and McRae, 1981) subject to consideration of other social values such as equity and justice. Therefore, it can be useful to prioritize control options on the basis of environmental health benefit achieved per unit cost of control.

It is generally infeasible to directly and prospectively infer the health benefits of a given air pollution control strategy. Useful proxy metrics are therefore required for policy making. Because different emissions sources differ greatly in their ability to cause human exposure, the mass emissions rate is generally a poor proxy for health effects (Roumasset and Smith, 1990; Smith, 1993; Marshall, 2005). Similarly, ambient concentrations are an inadequate proxy for emissions sources that cause appreciable population exposures at spatial scales that are much smaller than the urban-ambient length scale. The magnitude of this error is especially large for exposures that take place in the immediate proximity of an emissions source. It is likely that ambient concentrations underrepresent the contribution of urban vehicle emissions to near-source exposures. In Chapter 2, I investigate this hypothesis in detail using field measurements of in-vehicle exposures and ambient concentrations in New Delhi, India.

The inhalation intake rate – the product of breathing rate and exposure concentration – may be a more precise exposure metric than emissions or ambient concentrations (Evans et al., 2002; Marshall, 2005). The potential of emissions from a given source to result in population inhalation intakes is summarized by the intake fraction (*iF*) metric (Bennett et al., 2002). The intake fraction is a dimensionless ratio that quantifies the total fraction of emissions from a given

source or source category that is ultimately inhaled by an exposed population. Intake fraction information facilitates comparisons among source categories and exposure settings. For example, consider two major regulated source categories from the US: mobile sources (vehicles) and point sources (central power stations). Prior research indicates that ground-level urban vehicle emissions in the US have an *iF* that is roughly 10-20× greater than that of tall-stack central-station power plants, which tend to be located primarily outside of urban areas (Marshall, 2005; Heath et al., 2006). Accordingly, the control of a fixed unit of emissions from urban vehicle tailpipes may yield much greater intake reduction than the same quantity of emissions abatement from power plant stacks (Smith, 2002). If costs of control were similar for these two source categories, and if aggregate health damages scale proportionally to population intakes, then a given level of environmental health benefit could be achieved at much lower cost by controlling vehicle emissions. Further applications of the *iF* metric include cost-benefit and cost-effectiveness analyses, investigations of environmental equity, health risk assessment, and other studies that estimate the exposure consequences of emissions (Humbert et al., 2011; Lai et al., 2000; Rosenbaum et al., 2007).

This dissertation substantially addresses key data gaps related to the intake fraction of urban vehicle emissions in Chapters 3 and 4. In Chapter 3, I report new model estimates of the intraurban intake fraction of vehicle emissions of conserved, non-reactive pollutants in 3,646 worldwide urban areas with ~ 2 billion residents located on 6 continents. This analysis provides insight into the effects that global variation in meteorology and urban form has on the intake fraction of urban vehicle emissions. In Chapter 4, I develop and apply a model to investigate the *iF* of semivolatile organic emissions, which are an important reactive and non-conserved constituent of vehicle exhaust that make major contributions to near-source, urban-, and regional-scale $PM_{2.5}$ exposures.

It is worthwhile to briefly compare and contrast key aspects of the three investigations that comprise the core of this dissertation. A desire to better understand the exposure implications of urban vehicle emissions serves as the launching point for the dissertation, with the spatial scale of analysis radiating outward in each subsequent analysis. In Chapter 2, I focus on exposure conditions in a very near source region, namely the in-vehicle and on-road microenvironment in New Delhi. In Chapter 3, I consider urban-scale exposures on a global basis. In Chapter 4, I investigate exposures contributions at the intraurban, periurban, and regional scales. In consideration of the important role that particles have for health effects, Chapters 2 and 4 devote major emphasis to particle exposures attributable to urban vehicle emissions. Whereas Chapter 3 chiefly considers primary, non-reactive pollutants, Chapters 2 and 4 also aim to elucidate the role that dynamic processes play in influencing exposures. Finally, an interest in the environmental health consequences of urban motor vehicle emissions in low-income countries permeates all three investigations.

The modeling, data analysis, and measurement techniques that I employ here are drawn chiefly from the discipline of air quality engineering. The character of this dissertation is primarily analytical and deductive: the investigations contained herein aim to advance a mechanistic understanding of human exposure to urban vehicle emissions. However, my engagement with this topic owes a sizeable debt to many other domains of inquiry, especially environmental health, urban planning, and energy analysis. In keeping with the more prescriptive or even activist nature of these other intellectual traditions, I also seek to identify possible routes

for policy interventions to advance a more environmental sustainable and health-protective future.

1.5 References

Benbrahim-Tallaa, L., Baan, R.A., Grosse, Y., Lauby-Secretan, B., El Ghissassi, F., Bouvard, V., Guha, N., Loomis, D., Straif, K., 2012. Carcinogenicity of diesel-engine and gasoline-engine exhausts and some nitroarenes. *The Lancet Oncology* 13, 663-664.

Bennett, D.H., McKone, T.E., Evans, J.S., Nazaroff, W.W., Margni, M.D., Jolliet, O., Smith, K.R., 2002. Defining intake fraction. *Environmental Science & Technology* 36, 206A-211A.

Bhangar, S.V., 2010. *Human Exposure to Dynamic Air Pollutants: Ozone in Airplanes and Ultrafine Particles in Homes*. Ph.D. Dissertation, University of California, Berkeley.

Blanchard, C.L., Tanenbaum, S., Motallebi, N., 2011. Spatial and temporal characterization of $PM_{2.5}$ mass concentrations in California, 1980–2007. *Journal of the Air & Waste Management Association* 61, 339-351.

Brauer, M., Amann, M., Burnett, R.T., Cohen, A., Dentener, F., Ezzati, M., Henderson, S.B., Krzyzanowski, M., Martin, R.V., Van Dingenen, R., van Donkelaar, A., Thurston, G.D., 2012. Exposure assessment for estimation of the global burden of disease attributable to outdoor air pollution. *Environmental Science & Technology* 46, 652-660.

Brook, R.D., Rajagopalan, S., Pope, C.A., III, Brook, J.R., Bhatnagar, A., Diez-Roux, A.V., Holguin, F., Hong, Y., Luepker, R.V., Mittleman, M.A., Peters, A., Siscovick, D., Smith, S.C., Jr, Whitsel, L., Kaufman, J.D., 2010. Particulate matter air pollution and cardiovascular disease: An update to the scientific statement from the American Heart Association. *Circulation* 121, 2331-2378.

Cass, G.R., McRae, G.J., 1981. Minimizing the cost of air pollution control. *Environmental Science & Technology* 15, 748-757.

Crouse, D.L., Peters, P.A., van Donkelaar, A., Goldberg, M.S., Villeneuve, P.J., Brion, O., Khan, S., Atari, D.O., Jerrett, M., Pope, C.A., Brauer, M., Brook, J.R., Martin, R.V., Stieb, D., Burnett, R.T., 2012. Risk of nonaccidental and cardiovascular mortality in relation to long-term exposure to low concentrations of fine particulate matter: A Canadian national-level cohort study. *Environmental Health Perspectives* 120, 708-714.

Delfino, R.J., Sioutas, C., Malik, S., 2005. Potential role of ultrafine particles in associations between airborne particle mass and cardiovascular health. *Environmental Health Perspectives* 113, 934-946.

Dockery, D.W., Pope, C.A., Xu, X., Spengler, J.D., Ware, J.H., Fay, M.E., Ferris, B.G., Speizer, F.E., 1993. An association between air pollution and mortality in six U.S. cities. *New England Journal of Medicine* 329, 1753-1759.

Evans, J.S., Wolff, S.K., Phonboon, K., Levy, J.I., Smith, K.R., 2002. Exposure efficiency: An idea whose time has come? *Chemosphere* 49, 1075-1091.

Forstall, R.L., Greene, R.P., Pick, J.B., 2009. Which are the largest? Why lists of major urban areas vary so greatly. *Tijdschrift voor Economische en Sociale Geografie* 100, 277-297.

Gakenheimer, R., 1999. Urban mobility in the developing world. *Transportation Research Part A - Policy and Practice* 33, 671-689.

Gurjar, B.R., Lelieveld, J., 2005. New directions: Megacities and global change. *Atmospheric Environment* 39, 391-393.

Gurjar, B.R., Jain, A., Sharma, A., Agarwal, A., Gupta, P., Nagpure, A.S., Lelieveld, J., 2010. Human health risks in megacities due to air pollution. *Atmospheric Environment* 44, 4606-4613.

Health Effects Institute, 2010a. *Outdoor Air Pollution and Health in the Developing Countries of Asia: A Comprehensive Review*, Boston, MA. Special Report 18. Available from: http://pubs.healtheffects.org/view.php?id=349.

Health Effects Institute, 2010b. *Traffic-Related Air Pollution: A Critical Review of the Literature on Emissions, Exposure, and Health Effects*, Boston. Special Report 17. Available from: http://pubs.healtheffects.org/view.php?id=334.

Heath, G.A., Granvold, P.W., Hoats, A.S., Nazaroff, W.W., 2006. Intake fraction assessment of the air pollutant exposure implications of a shift toward distributed electricity generation. *Atmospheric Environment* 40, 7164-7177.

Hoek, G., Brunekreef, B., Goldbohm, S., Fischer, P., van den Brandt, P.A., 2002. Association between mortality and indicators of traffic-related air pollution in the Netherlands: a cohort study. *The Lancet* 360, 1203-1209.

Humbert, S., Marshall, J.D., Shaked, S., Spadaro, J.V., Nishioka, Y., Preiss, P., McKone, T.E., Horvath, A., Jolliet, O., 2011. Intake fraction for particulate matter: Recommendations for life cycle impact assessment. *Environmental Science & Technology* 45, 4808-4816.

IARC, 1983. Polynuclear Aromatic Compounds, Part 1, Chemical, Environmental and Experimental Data. *International Agency for Research on Cancer (IARC) Monographs on the Evaluation of Carcinogenic Risks to Humans* 32.

IARC, 1989. Diesel and Gasoline Engine Exhausts and Some Nitroarenes. *International Agency for Research on Cancer (IARC) Monographs on the Evaluation of Carcinogenic Risks to Humans* 46.

Jacobs, L., Nawrot, T., de Geus, B., Meeusen, R., Degraeuwe, B., Bernard, A., Sughis, M., Nemery, B., Panis, L., 2010. Subclinical responses in healthy cyclists briefly exposed to traffic-related air pollution: An intervention study. *Environmental Health* 9, Art. 64.

Jerrett, M., Burnett, R.T., Ma, R., Pope, C.A., III, Krewski, D., Newbold, K.B., Thurston, G., Shi, Y., Finkelstein, N., Calle, E.E., Thun, M.J., 2005. Spatial analysis of air pollution and mortality in Los Angeles. *Epidemiology* 16, 727-736.

Karner, A.A., Eisinger, D.S., Niemeier, D.A., 2010. Near-roadway air quality: Synthesizing the findings from real-world data. *Environmental Science & Technology* 44, 5334-5344.

Kaur, S., Nieuwenhuijsen, M.J., Colvile, R.N., 2007. Fine particulate matter and carbon monoxide exposure concentrations in urban street transport microenvironments. *Atmospheric Environment* 41, 4781-4810.

Ketzel, M., Berkowicz, R., 2004. Modelling the fate of ultrafine particles from exhaust pipe to rural background: An analysis of time scales for dilution, coagulation and deposition. *Atmospheric Environment* 38, 2639-2652.

Kittelson, D.B., 1998. Engines and nanoparticles: a review. *Journal of Aerosol Science* 29, 575-588.

Krewski, D., Jerrett, M., Burnett, R.T., Ma, R., Hughes, E., Shi, Y., Turner, M.C., Pope, C.A., Thurston, G., Calle, E.E., Thun, M.J., Beckerman, B., DeLuca, P., Finkelstein, N., Ito, K., Moore, D.K., Newbold, K.B., Ramsay, T., Ross, Z., Shin, H., Tempalski, B., 2009. *Extended follow-up and spatial analysis of the American Cancer Society study linking particulate air pollution and mortality,* Health Effects Institute, Boston, MA. Research Report 140. Available from: http://pubs.healtheffects.org/view.php?id=315.

Kumar, P., Ketzel, M., Vardoulakis, S., Pirjola, L., Britter, R., 2011. Dynamics and dispersion modelling of nanoparticles from road traffic in the urban atmospheric environment—A review. *Journal of Aerosol Science* 42, 580-603.

Kumar, P., Jain, S., Gurjar, B.R., Sharma, P., Khare, M., Morawska, L., Britter, R., 2013. New Directions: Can a "blue sky" return to Indian megacities? *Atmospheric Environment* 71, 198-201.

Künzli, N., Medina, S., Kaiser, R., Quenel, P., Horak, F., Jr., Studnicka, M., 2001. Assessment of deaths attributable to air pollution: Should we use risk estimates based on time series or on cohort studies? *American Journal of Epidemiology* 153, 1050-1055.

Lai, A.C.K., Thatcher, T.L., Nazaroff, W.W., 2000. Inhalation transfer factors for air pollution health risk assessment. *Journal of the Air & Waste Management Association* 50, 1688-1699.

Lim, S.S., Vos, T., Flaxman, A.D., Danaei, G., Shibuya, K., Adair-Rohani, H., Amann, M., Anderson, H.R., Andrews, K.G., Aryee, M., Atkinson, C., Bacchus, L.J., Bahalim, A.N., Balakrishnan, K., Balmes, J., Barker-Collo, S., Baxter, A., Bell, M.L., Blore, J.D., Blyth, F., Bonner, C., Borges, G., Bourne, R., Boussinesq, M., Brauer, M., Brooks, P., Bruce, N.G., Brunekreef, B., Bryan-Hancock, C., Bucello, C., Buchbinder, R., Bull, F., Burnett, R.T., Byers, T.E., Calabria, B., Carapetis, J., Carnahan, E., Chafe, Z., Charlson, F., Chen, H., Chen, J.S., Cheng, A.T.-A., Child, J.C., Cohen, A., Colson, K.E., Cowie, B.C., Darby, S., Darling, S., Davis, A., Degenhardt, L., Dentener, F., Des Jarlais, D.C., Devries, K., Dherani, M., Ding, E.L., Dorsey, E.R., Driscoll, T., Edmond, K., Ali, S.E., Engell, R.E., Erwin, P.J., Fahimi, S., Falder, G., Farzadfar, F., Ferrari, A., Finucane, M.M., Flaxman, S., Fowkes, F.G.R., Freedman, G., Freeman, M.K., Gakidou, E., Ghosh, S., Giovannucci, E., Gmel, G., Graham, K., Grainger, R., Grant, B., Gunnell, D., Gutierrez, H.R., Hall, W., Hoek, H.W., Hogan, A., Hosgood III, H.D., Hoy, D., Hu, H., Hubbell, B.J., Hutchings, S.J., Ibeanusi, S.E., Jacklyn, G.L., Jasrasaria, R., Jonas, J.B., Kan, H., Kanis, J.A., Kassebaum, N., Kawakami, N., Khang, Y.-H., Khatibzadeh, S., Khoo, J.-P., Kok, C., Laden, F., Lalloo, R., Lan, Q., Lathlean, T., Leasher, J.L., Leigh, J., Li, Y., Lin, J.K., Lipshultz, S.E., London, S., Lozano, R., Lu, Y., Mak, J., Malekzadeh, R., Mallinger, L., Marcenes, W., March, L., Marks, R., Martin, R., McGale, P., McGrath, J., Mehta, S., Mensah, G.A., Merriman, T.R., Micha, R., Michaud, C., Mishra, V., Hanafiah, K.M., Mokdad, A.A., Morawska, L., Mozaffarian, D., Murphy, T., Naghavi, M., Neal, B., Nelson, P.K., Nolla, J.M., Norman, R., Olives, C., Omer, S.B., Orchard, J., Osborne, R., Ostro, B., Page, A., Pandey, K.D., Parry, C.D., Passmore, E., Patra, J., Pearce, N., Pelizzari, P.M., Petzold, M., Phillips, M.R., Pope, D., Pope Iii, C.A., Powles, J., Rao, M., Razavi, H., Rehfuess, E.A., Rehm, J.T., Ritz, B., Rivara, F.P., Roberts, T., Robinson, C., Rodriguez-Portales, J.A., Romieu, I., Room, R., Rosenfeld, L.C., Roy, A., Rushton, L., Salomon, J.A., Sampson, U., Sanchez-Riera, L.,

Sanman, E., Sapkota, A., Seedat, S., Shi, P., Shield, K., Shivakoti, R., Singh, G.M., Sleet, D.A., Smith, E., Smith, K.R., Stapelberg, N.J., Steenland, K., Stöckl, H., Stovner, L.J., Straif, K., Straney, L., Thurston, G.D., Tran, J.H., Van Dingenen, R., van Donkelaar, A., Veerman, J.L., Vijayakumar, L., Weintraub, R., Weissman, M.M., White, R.A., Whiteford, H., Wiersma, S.T., Wilkinson, J.D., Williams, H.C., Williams, W., Wilson, N., Woolf, A.D., Yip, P., Zielinski, J.M., Lopez, A.D., Murray, C.J., Ezzati, M., 2012. A comparative risk assessment of burden of disease and injury attributable to 67 risk factors and risk factor clusters in 21 regions, 1990–2010: A systematic analysis for the Global Burden of Disease Study 2010. *The Lancet* 380, 2224-2260.

Lozano, R., Naghavi, M., Foreman, K., Lim, S., Shibuya, K., Aboyans, V., Abraham, J., Adair, T., Aggarwal, R., Ahn, S.Y., Alvarado, M., Anderson, H.R., Anderson, L.M., Andrews, K.G., Atkinson, C., Baddour, L.M., Barker-Collo, S., Bartels, D.H., Bell, M.L., Benjamin, E.J., Bennett, D., Bhalla, K., Bikbov, B., Abdulhak, A.B., Birbeck, G., Blyth, F., Bolliger, I., Boufous, S., Bucello, C., Burch, M., Burney, P., Carapetis, J., Chen, H., Chou, D., Chugh, S.S., Coffeng, L.E., Colan, S.D., Colquhoun, S., Colson, K.E., Condon, J., Connor, M.D., Cooper, L.T., Corriere, M., Cortinovis, M., de Vaccaro, K.C., Couser, W., Cowie, B.C., Criqui, M.H., Cross, M., Dabhadkar, K.C., Dahodwala, N., De Leo, D., Degenhardt, L., Delossantos, A., Des Jarlais, D.C., Dharmaratne, S.D., Dorsey, E.R., Driscoll, T., Duber, H., Ebel, B., Erwin, P.J., Espindola, P., Ezzati, M., Feigin, V., Flaxman, A.D., Forouzanfar, M.H., Fowkes, F.G.R., Franklin, R., Fransen, M., Freeman, M.K., Gabriel, S.E., Gakidou, E., Gaspari, F., Gillum, R.F., Gonzalez-Medina, D., Halasa, Y.A., Haring, D., Harrison, J.E., Havmoeller, R., Hay, R.J., Hotez, P.J., Hoy, D., Jacobsen, K.H., James, S.L., Jasrasaria, R., Jayaraman, S., Johns, N., Karthikeyan, G., Kassebaum, N., Keren, A., Khoo, J.-P., Knowlton, L.M., Kobusingye, O., Koranteng, A., Krishnamurthi, R., Lipnick, M., Lipshultz, S.E., Ohno, S.L., Mabweijano, J., MacIntyre, M.F., Mallinger, L., March, L., Marks, G.B., Marks, R., Matsumori, A., Matzopoulos, R., Mayosi, B.M., McAnulty, J.H., McDermott, M.M., McGrath, J., Mensah, G.A., Merriman, T.R., Michaud, C., Miller, M., Miller, T.R., Mock, C., Mocumbi, A.O., Mokdad, A.A., Moran, A., Mulholland, K., Nair, M.N., Naldi, L., Narayan, K.M.V., Nasseri, K., Norman, P., O'Donnell, M., Omer, S.B., Ortblad, K., Osborne, R., Ozgediz, D., Pahari, B., Pandian, J.D., Rivero, A.P., Padilla, R.P., Perez-Ruiz, F., Perico, N., Phillips, D., Pierce, K., Pope Iii, C.A., Porrini, E., Pourmalek, F., Raju, M., Ranganathan, D., Rehm, J.T., Rein, D.B., Remuzzi, G., Rivara, F.P., Roberts, T., De León, F.R., Rosenfeld, L.C., Rushton, L., Sacco, R.L., Salomon, J.A., Sampson, U., Sanman, E., Schwebel, D.C., Segui-Gomez, M., Shepard, D.S., Singh, D., Singleton, J., Sliwa, K., Smith, E., Steer, A., Taylor, J.A., Thomas, B., Tleyjeh, I.M., Towbin, J.A., Truelsen, T., Undurraga, E.A., Venketasubramanian, N., Vijayakumar, L., Vos, T., Wagner, G.R., Wang, M., Wang, W., Watt, K., Weinstock, M.A., Weintraub, R., Wilkinson, J.D., Woolf, A.D., Wulf, S., Yeh, P.-H., Yip, P., Zabetian, A., Zheng, Z.-J., Lopez, A.D., Murray, C.J., Denenberg, J., Hoen, B., 2012. Global and regional mortality from 235 causes of death for 20 age groups in 1990 and 2010: A systematic analysis for the Global Burden of Disease Study 2010. *The Lancet* 380, 2095-2128.

Mage, D., Ozolins, G., Peterson, P., Webster, A., Orthofer, R., Vandeweerd, V., Gwynne, M., 1996. Urban air pollution in megacities of the world. *Atmospheric Environment* 30, 681-686.

Marshall, J.D., 2005. *Inhalation of vehicle emissions in urban environments*. Ph.D. Dissertation, University of California, Berkeley.

Marshall, J.D., McKone, T.E., Deakin, E., Nazaroff, W.W., 2005. Inhalation of motor vehicle emissions: Effects of urban population and land area. *Atmospheric Environment* 39, 283-295.

Molina, M.J., Molina, L.T., 2004. Megacities and atmospheric pollution. *Journal of the Air & Waste Management Association* 54, 644-680.

Oberdörster, G., 2001. Pulmonary effects of inhaled ultrafine particles. *International Archives of Occupational and Environmental Health* 74, 1-8.

Peters, A., von Klot, S., Heier, M., Trentinaglia, I., Hörmann, A., Wichmann, H.E., Löwel, H., 2004. Exposure to traffic and the onset of myocardial infarction. *New England Journal of Medicine* 351, 1721-1730.

Pope, C.A., Dockery, D.W., 2006. Health effects of fine particulate air pollution: Lines that connect. *Journal of the Air & Waste Management Association* 56, 709-742.

Pucher, J., Korattyswaropam, N., Mittal, N., Ittyerah, N., 2005. Urban transport crisis in India. *Transport Policy* 12, 185-198.

Riediker, M., Cascio, W.E., Griggs, T.R., Herbst, M.C., Bromberg, P.A., Neas, L., Williams, R.W., Devlin, R.B., 2004. Particulate matter exposure in cars is associated with cardiovascular effects in healthy young men. *American Journal of Respiratory and Critical Care Medicine* 169, 934-940.

Rosenbaum, R.K., Margni, M., Jolliet, O., 2007. A flexible matrix algebra framework for the multimedia multipathway modeling of emission to impacts. *Environment International* 33, 624-634.

Roumasset, J.A., Smith, K.R., 1990. Exposure trading: An approach to more efficient air pollution control. *Journal of Environmental Economics and Management* 18, 276-291.

Satterthwaite, D., 2008. Cities' contribution to global warming: Notes on the allocation of greenhouse gas emissions. *Environment and Urbanization* 20, 539-549.

Schichtel, B.A., Husar, R.B., Falke, S.R., Wilson, W.E., 2001. Haze trends over the United States, 1980–1995. *Atmospheric Environment* 35, 5205-5210.

Schneider, A., Friedl, M.A., Potere, D., 2009. A new map of global urban extent from MODIS satellite data. *Environmental Research Letters* 4, 044003.

Sioutas, C., Delfino, R.J., Singh, M., 2005. Exposure assessment for atmospheric ultrafine particles (UFPs) and implications in epidemiologic research. *Environmental Health Perspectives* 113, 947-955.

Smith, K.R., 1993. Fuel combustion, air pollution exposure, and health: The situation in developing countries. *Annual Review of Energy and the Environment* 18, 529-566.

Smith, K.R., 2002. Place makes the poison: Wesolowski Award Lecture — 1999. *Journal of Exposure Analysis and Environmental Epidemiology* 12, 167 - 171.

United Nations, 2012. *World Urbanization Prospects, the 2011 Revision*, United Nations, Department of Economic and Social Affairs, Population Division, New York. ST/ESA/SER.A/322.

US EPA, 2008. *Chapter 2: Air, in U.S. EPA's 2008 Report on the Environment (Final Report)*, U.S. Environmental Protection Agency, Washington, DC. EPA/600/R-07/045F (NTIS PB2008-112484).

Woodcock, J., Edwards, P., Tonne, C., Armstrong, B.G., Ashiru, O., Banister, D., Beevers, S., Chalabi, Z., Chowdhury, Z., Cohen, A., Franco, O.H., Haines, A., Hickman, R., Lindsay, G., Mittal, I., Mohan, D., Tiwari, G., Woodward, A., Roberts, I., 2009. Public health benefits of strategies to reduce greenhouse-gas emissions: Urban land transport. *The Lancet* 374, 1930-1943.

Zhang, K.M., Wexler, A.S., 2004. Evolution of particle number distribution near roadways--Part I: analysis of aerosol dynamics and its implications for engine emission measurement. *Atmospheric Environment* 38, 6643-6653.

Zhang, K.M., Wexler, A.S., Zhu, Y.F., Hinds, W.C., Sioutas, C., 2004. Evolution of particle number distribution near roadways. Part II: the 'Road-to-Ambient' process. *Atmospheric Environment* 38, 6655-6665.

Zhu, Y.F., Hinds, W.C., Kim, S., Shen, S., Sioutas, C., 2002. Study of ultrafine particles near a major highway with heavy-duty diesel traffic. *Atmospheric Environment* 36, 4323-4335.

Chapter 2: Concentrations of fine, ultrafine, and black carbon particles in auto-rickshaws in New Delhi, India

2.1. Introduction

New Delhi, India, is among the ten largest metropolitan areas worldwide, with an estimated year-2003 population of 18.6 million people (Forstall et al., 2009). Particulate air pollution has been a longstanding problem in Delhi. Ambient concentrations of $PM_{2.5}$ and PM_{10} (mass concentrations of airborne particles with aerodynamic diameters, d_p, less than 2.5 and 10 μm, respectively) are regularly among the highest in the world and frequently an order of magnitude larger than in US cities (Mage et al., 1996; Gurjar et al., 2008; Tiwari et al., 2013). Air quality management efforts in Delhi devote special attention to vehicle emissions. Many private and public transit vehicles have been converted to operate using compressed natural gas (CNG) fuel, and two-stroke vehicles are being phased out of use (Reynolds and Kandlikar, 2008). However, owing to rapid increases in private motor vehicle use, the Delhi transportation sector remains a large and growing source of air pollution in that metropolis (Narain et al., 2010).

In-vehicle and near-roadway air pollution exposures pose a potentially important health hazard amplification that is not captured by traditional ambient pollution monitoring systems (Jacobs et al., 2010; Kaur et al., 2007; Peters et al., 2004; Riediker et al., 2004; Boogaard et al., 2010). Relatively few studies have investigated in-traffic exposures to particulate air pollution in developing-world megacities (Han and Naeher, 2006). Such exposures are of concern owing to high-emitting vehicle fleets, rapid increases in vehicle use, and long exposure durations in and near traffic. For example, a 1997 study in Delhi reported that concentrations of $PM_{5.0}$ and CO inside vehicles exceeded the high urban background concentrations by 1.5-10×, depending on vehicle type (Saksena et al., 2007).

In view of the limited data on this important air quality issue, I undertook an investigation of the ambient and in-vehicle concentrations in New Delhi of three constituents of vehicle exhaust: fine particles ($PM_{2.5}$), black carbon (BC), and ultrafine particle number (PN). To my knowledge, the research reported here constitutes the first published study that characterizes in-vehicle exposure concentrations to BC and PN on the Indian subcontinent. In addition, the measurements presented here apparently represent one of the largest datasets for real-time, in-vehicle particle concentrations sampled anywhere.

2.2. Materials and methods

2.2.1 Site description and experimental design

New Delhi is India's capital and one of the country's more affluent cities. The region experiences cool winters (Dec – Jan); a brief, transitional spring (Feb – Mar); hot and dry summers (Apr – Jun); a hot and humid monsoon season (Jul - Sep); and a warm and dry post-

monsoon season (Oct – Nov). This study, conducted from February 2010 through May 2010, spans the early spring through mid-summer period in Delhi. In this study, in-vehicle concentration measurements were collected primarily inside auto-rickshaws, a semi-enclosed, three-wheeled vehicle that offers little evident protection from exhaust plumes in outside air. Auto-rickshaws are ubiquitous in many South Asian cities, serving a function similar to a conventional taxi but at lower fares (Tiwari, 2003; Harding and Hussein, 2010). The ~55,000 auto-rickshaws in New Delhi, comprising ~1% of the vehicle fleet, handle ~4% of non-pedestrian person-trips. For comparison, there were ~5 million registered private vehicles in Delhi in 2008 (Harding and Hussein, 2010; Narain et al., 2010). During measurement sessions, nearby traffic consisted of motorcycles, auto-rickshaws, light-duty passenger vehicles (LDV), three-wheeled cargo vehicles, small trucks, and buses. The most common fuels in use were gasoline, diesel, and CNG. Heavy-duty trucks are prohibited from being driven in Delhi during daytime hours (6:00 – 21:00). Diesel-fueled cars comprise a substantial – although not dominant – fraction of the Delhi LDV fleet (Harding and Hussein, 2010).

In-vehicle measurements

I measured in-vehicle concentrations on 40 weekdays (total sampling time ~180 h) during February 22 to May 26, 2010. Auto-rickshaw measurements (31 days, 62 trips, 160 h) were primarily conducted inside a single Bajaj model RE-4S TSR vehicle, the most common model in Delhi (Harding and Hussein, 2010). This open-sided vehicle holds 1-4 occupants in an interior volume of ~1 m^3, has a maximum speed of 50-60 km h^{-1}, and is powered by a 300 cm^3 displacement, 5-6 kW four-stroke compressed natural gas (CNG) engine. Instruments were carried inside the vehicle in a padded backpack designed to limit instrument tilt and vibration. Sampling lines for all instruments were situated to measure at a typical breathing height for a passenger in the center of the rear passenger seat. Supplemental experiments suggest that self-pollution from the auto-rickshaw's own exhaust did not make a substantial contribution to in-vehicle concentrations either while stopped or when traveling (See section on self-pollution below). Drivers and research staff were nonsmokers.

I selected the sampling route (one-way length: 19.5 km, Figure 2-1) to reflect the range of traffic conditions typical of south and central Delhi. The route connects an upper-income neighborhood, Chittaranjan Park (CRP), with a central commercial district, Connaught Place (CP). The route passes through residential, commercial, and office districts and incorporates several road types, including narrow residential streets, 2-4 lane arterial roads with traffic signals, and 6-8 lane arterial roads with flyover intersections. The route was driven round-trip twice per sampling day: once during morning (08:30-11:30) and once during evening commute times (17:45-20:45; total travel: 78 km d^{-1}). Field staff stopped midway through the route to measure ambient pollutant concentrations for 30 min inside a large urban park (see next section). Drivers were instructed to drive as they normally would, which in Delhi involves frequently changing lanes to avoid stopped vehicles and to reach the front of the queue at signals. As is typical of many Indian cities, traffic speeds were low. The median trip-integrated arithmetic mean speed was 18 km h^{-1} (10% trimmed range: 15-20 km h^{-1}). In the final sampling month (May 2010, 9 trips), the route was shortened by 2 km (~5%) owing to terrorism concerns at CP; overall traffic speeds and trip duration remained similar for the shortened route.

In addition to the primary sampling program, I explored variability in exposure concentrations with vehicle type and ventilation setting, as follows. Concentrations were measured in the driver's side rear seat of a common car model (Tata Indica) on 15 trips on the same route and times-of-day, May 17 to 26. I configured the car either with open windows (5 trips) or with minimal air intake (10 trips). During open-window (OW) trips, windows were lowered halfway and the ventilation system was off. During trips with minimal air intake (RC), windows were closed, air conditioning was active, and the ventilation system was set to recirculate air at medium fan speed.

Ambient air quality monitoring: Chittaranjan Park (CRP) and Lodhi Garden (LG)

This study incorporated routine ambient air measurements in the Chittaranjan Park (CRP) neighborhood and inside Lodhi Garden (LG) park. The start of the sampling route was located at CRP, in south Delhi. Air-quality monitoring was performed continuously at this location. Like other affluent neighborhoods in Delhi, CRP (area, A = 1.1 km^2, population density = 16,000 people km^{-2}) contains 3-5 story residential buildings and dense shade tree cover; vehicle traffic is largely restricted to a few main roads. Monitoring was conducted on a building rooftop (height 13 m) situated 200-250 m from the nearest roadway with continuous vehicle flow, and 1000 m from the nearest major arterial roadway. Instruments were housed in a 1-m^3 sampling enclosure with 24-h power supply via electricity with battery backup. Local sources of air pollution were only observed occasionally and included vehicle traffic, wood and leaf combustion for heating and cooking outdoors (e.g., by security guards), trash burning, and construction activity.

Measurements at LG (A = 0.3 km^2) occurred during a 15-20 min period midway through each morning and evening mobile monitoring session. There were no evident major emissions sources in the park and the sampling location (~1 m above ground) was more than 230 m from the nearest roadway.

Self-pollution

Concentrations inside the auto-rickshaw have the potential to be meaningfully influenced by entrainment of the auto-rickshaw's own exhaust into the passenger compartment (self-pollution). In order to determine whether self-pollution made a substantial contribution to in-vehicle concentrations, I conducted the following experiment. The test consisted of repeatedly driving around a 600 m single-lane loop that formed the perimeter of a forested park near the CRP site. In-vehicle sampling was conducted on a weekend morning to minimize encounters with other vehicles. The test auto-rickshaw was fitted with a vibration transducer (Onset Corporation, Bourne, MA) to record engine on/off status. At the start of each circuit around the park, the auto-rickshaw paused with engine running for 1-2 min. After completing the loop (average speed: 14 km h^{-1}, maximum speed 18 km h^{-1}), the vehicle's engine was shut off immediately, and remained off for 1-2 min. This protocol (engine start, 1-2 min idle, drive loop, engine off 1-2 min) was repeated a total of 5 times. During the test, I continuously measured $PM_{2.5}$, BC, and PN; BC measurements were discarded due to instrument malfunction. Mean wind speed at CRP was 1.6 m s^{-1} during the test. The results of this experiment, described in detail in in §2.3.1, indicated that self-pollution was not a major contributor to in-vehicle concentrations.

2.2.2 Instrumentation

Meteorological parameters

I employed a weather station (Model PWS-1000TD, Zephyr Instruments, East Granby, CT) to record meteorological parameters at CRP. The instrument was situated 2 m above roof height (15 m above ground level). Temperature (*T*), relative humidity (*RH*), wind speed (*WS*) and direction, and precipitation were logged at 5-min intervals over the entire study duration (14 weeks). The study was conducted between early spring (February, mean daily temperature range 16-27 ºC) and peak summer (April – May, 30-44 ºC). The interquartile range (IQR) wind speed was 0.7-1.3 m s^{-1}, primarily from the NE. Little rainfall occurred during the study (< 2 cm $month^{-1}$). Trip-averaged meteorological data are reported in Table 2-1.

Continuous and integrated $PM_{2.5}$ measurements

$PM_{2.5}$ concentrations were measured using two DustTrak aerosol monitors (model 8520, TSI, Inc., Shoreview, MN). This instrument uses a laser photometer to determine real-time PM mass concentration based on 90º light scattering (Arku et al., 2008). Instruments were fitted with manufacturer-supplied $PM_{2.5}$ inlet nozzles and impactors. Each day, internal pumps were adjusted to the specified 1.7 L min^{-1} flow rate. The instrument zero point was calibrated daily using an external HEPA filter. One DustTrak was continuously operated (except during maintenance) at the ambient sampling location (CRP) from February 16 to April 23. A second DustTrak was used for mobile sampling between February 16 and May 26 and for ambient measurements after April 23. A short length (< 30 cm) of conductive tubing (6 mm in diameter) was used to minimize particle loss. The DustTrak's recording interval was 1 s at LG and in-vehicle, and 30 s at CRP.

The DustTrak's light-scattering measurement technique is subject to error because the amount of light scattered by particles depends on relative humidity and particle properties such as shape, size, and refractive index (Arku et al., 2008; Chakrabarti et al., 2004; Ramachandran et al., 2003). I applied two corrections to minimize error. First, I accounted for real-time effects of *RH* on instrument response using the approach of Ramachandran et al. (2003):

$$PM2.5_{RH\text{-}corrected} = \frac{PM2.5_{raw}}{CF},\ CF = 1 + 0.25\frac{RH^2}{(1-RH)} \qquad [2.1]$$

Here, *RH* is the most recent 5-min average *RH* at CRP, expressed as a fraction of 100%. Although equation [2.1] is unstable for very high relative humidity ($RH \rightarrow 1$), the instantaneous relative humidity never exceeded 65% during measurements. The trip-averaged *RH* correction factor (*CF*) was moderate during late February (mean: 1.17, maximum: 1.22) and small during other months (mean: 1.05, maximum: 1.15).

To calibrate the DustTrak optical-to-mass response for New Delhi's aerosol, I developed a calibration relationship based on filter samples. A total of 36 gravimetric filter measurements were collected side-by-side with the DustTrak inside auto-rickshaws (16 samples) and at the Chittaranjan Park (CRP) ambient site (20 samples) between late March and early June 2010. I employed an SKC PEM $PM_{2.5}$ impactor (MSP Corporation, Shoreview, MN) and an SKC Leland

Legacy sampling pump operating at 10 L min^{-1} (SKC, Inc, Eighty Four, PA) to achieve a 2.5 µm aerodynamic diameter size cut on the sample aerosol, which was collected on a preweighed 37-mm Teflon filters held by a rigid, porous backing plate. The median air volume sampled was 1.6 m^3 (10% trimmed range: 0.86 – 4.3 m^3).

Filter samples were conditioned for 24-72 hours before each weighing using a controlled chamber equilibrated to 35-45% RH and 22-25 ºC. Each filter was discharged of static electricity using a ^{210}Po source and weighed pre- and post-sampling on a 0.1 µg precision Sartorius SE-2 Microbalance (Sartorius AG, Göttingen, Germany) at Lawrence Berkeley National Laboratory (LBNL) in Berkeley, CA, USA. A total of 18 blank filters were retained for quality control, of which 3 were stored at LBNL, 11 were taken to India and returned unhandled, and 4 handling blanks were loaded and unloaded into the filter apparatus at the CRP ambient site but without turning on the pump. Of the 36 non-blank filters sampled, four were rejected during the post-sampling weighing session owing to visible damage, such as separation of the filter medium from its support ring, thereby yielding the 32 samples employed in analysis. All blank filters recorded a loss in weight between the first and second weighing sessions (January 2010 and June 2010, respectively). To correct for this change in weight, I added the mean weight change for the handling blanks (8.5 µg) to each sample weight before calculating final gravimetric $PM_{2.5}$ concentrations.

I developed a calibration curve to represent the relationship between the gravimetric $PM_{2.5}$ concentration and the time-averaged, RH-corrected $PM_{2.5}$ concentrations reported by the colocated DustTrak. Figure 2-2 presents scatter plots of DustTrak and gravimetric $PM_{2.5}$ concentration measurements for the 32 valid sampling sessions. Exploratory data analysis revealed that simple linear regressions performed poorly in describing the relationship between DustTrak and gravimetric $PM_{2.5}$ measurements, especially at relatively low ambient concentrations for Delhi (< 75 µg m^{-3}). A power law regression relationship satisfactorily fit the observed data while also accommodating the zero calibration point:

$$G^* = a(D)^b \qquad [2.2]$$

Here, G^* is the modeled gravimetric $PM_{2.5}$ concentration (units: µg m^{-3}), D is the RH-corrected real-time DustTrak $PM_{2.5}$ concentration, and a and b are empirically determined fitting parameters via linear regression of the log-transformed data points. To account for the nonlinear behavior of the power law relationship, I used an iterative fitting algorithm and obtained the following calibration relationship:

$$PM2.5_{gravimetric} = 3.91\ (PM2.5_{RH\text{-}corrected})^{0.706} \qquad [2.3]$$

Here, $PM2.5_{gravimetric}$ represents the estimated gravimetric-equivalent concentration, based on *RH*-corrected DustTrak measurements, and both mass concentration determinations have units of µg m^{-3}. Over all 60 sampling trips, the mean ratio of gravimetric-calibrated to RH-corrected $PM_{2.5}$ concentration was 0.74 for in-vehicle measurements, and 0.91 for ambient measurements. For the 32 individual filter samples, the root-mean-square error (RMSE) of the individual modeled gravimetric concentrations was 32 µg m^{-3} (coefficient of variation: 23%). I estimate the mean ± 95% CI bias of the calibration relationship to be 0 ± 9.1%. This uncertainty in the calibration relationship modestly reduces the precision of estimated mean $PM_{2.5}$ concentrations.

Ratio comparisons between ambient and in-vehicle concentrations (γ, φ, see §2.3.2) are not affected by this uncertainty.

Black carbon measurements

I measured black carbon (BC) concentrations in-vehicle and at CRP using two portable aethalometers (model AE-51 "microAeth," Magee Scientific, Berkeley, CA). These instruments report BC concentration at 1-s intervals by measuring changes in light attenuation ($\lambda = 880$ nm) on a disposable filter through which sample air is drawn at 100 – 150 cm^3 min^{-1}.

Aethalometer measurements required substantial post-processing. The aethalometer frequently recorded spurious concentration "spikes" of ± 200 – 2000 μg m^{-3} BC when exposed to mild mechanical shock or vibration. As controlled testing of the instrument revealed a distinctive pattern for this spurious signal, I was able to remove nearly all occurrences of these spikes by developing and applying a custom post-processing algorithm to the 1 Hz raw signal from the instrument (see Appendix A).

Previous laboratory and field experiments have revealed that the default aethalometer algorithm underestimates BC concentration as filter BC mass increases, especially when sampling highly light-absorbing particles (Jimenez et al., 2007; Kirchstetter, 2007; Kirchstetter and Novakov, 2007). I corrected for this effect using the empirical relationship of Kirchstetter and Novakov (2007), which was subsequently found in a study of heavy-duty diesel exhaust plumes (Ban-Weiss et al., 2009) to yield good agreement between thermal-optical analysis and aethalometer measurements of BC:

$$BC = BC_o \left(0.88\,Tr + 0.12\right)^{-1} \qquad [2.4]$$

Here, BC is the corrected black carbon concentration, BC_o is the instrument-reported concentration, and $Tr = \exp(-ATN / 100)$ is the aethalometer filter transmission that is calculated from the instrument-reported attenuation coefficient (ATN). I applied equation [2.4] to all BC measurements. Trip-averaged correction factors (BC/BC_o) for in-vehicle BC measurements were greater than those for ambient measurements (medians: 1.58 in-vehicle, 1.23 ambient) owing to the more rapid filter loading experienced in on-road sampling conditions.

Ultrafine particle number concentration measurements

Ultrafine particle number concentrations (PN) were measured using a portable condensation particle counter (CPC, model CPC 3007, TSI Inc., Shoreview, MN; frequency: 1 Hz). Although this instrument detects particles in the size range 10 nm < d_p < 1 μm, PN is a reasonable proxy for UFP (d_p < 0.1 μm) under the conditions encountered in this study. Above the manufacturer-established concentration limit of 100,000 particles cm^{-3}, measurements are subject to undercounting because of particle coincidence errors (Knibbs et al., 2007; Westerdahl et al., 2005). To extend the effective maximum concentration limit of the instrument, I constructed an apparatus described by Ban-Weiss et al. (2009), which diluted the influent sample by ~5.5×. The device split the sample into two unequal paths: ~15% of flow passed through a 0.6 mm orifice (O'Keefe Controls, Trumbull, CT) and ~85% of flow passed through a HEPA filter. The flows were rejoined before entering the instrument. To ensure stable performance of the dilution

system, I replaced the HEPA filter every 2-4 weeks and measured the dilution ratio daily. Over the life of each filter, measured dilution ratios were within 10-20% of the median value for that filter. For each filter used, I applied the median measured dilution ratio to all PN measurements made during the period of use of that filter (range: 5.39-5.95).

With the dilution system in place, concentrations still exceeded the 100,000 particles cm^{-3} threshold for 5% of measurements. I used the following equation to account for undercounting (Westerdahl et al., 2005) and dilution:

$$PN = PN_{diluted} \times DF,\ PN_{diluted} = \begin{cases} 38456 \exp\left(PN_{raw} \times 10^{-5}\right), & PN_{raw} > 10^5 \\ PN_{raw}, & PN_{raw} < 10^5 \end{cases} \quad [2.5]$$

Here, all PN parameters are in units of particles cm^{-3}; PN_{raw} represents instrument-measured PN; and DF is the dilution factor (whose average over all trips was ~5.5). Including this correction for readings above 100,000 particles cm^{-3} only slightly increased the overall trip average PN concentrations (median increase: 3%; 10% trimmed range: 2 – 8% increase). As only one CPC was available, ambient PN levels reported here reflect the average of three mean concentrations: at LG mid-trip and at CRP for the 30-min periods immediately preceding and following each in-vehicle sampling period.

Other measurements and protocols

I used a handheld GPS receiver (model GPSMap 60Csx, Garmin, Inc., Olathe, KS) to record position (accuracy: ± 3-5 m) and speed of the sampling vehicle at 1 Hz frequency. This GPS device was used to synchronize instrument clocks daily. During each trip, video recordings of road conditions were collected through the front window. Field staff also manually recorded visual observations of local traffic conditions, high-emitting vehicles, and prominent non-vehicular emissions (e.g., roadside trash burning). Staff checked all instruments every 15 min to ensure proper operation, and malfunctioning instruments were restarted when possible.

2.3 Quality control, data processing and analysis

Real-time measurements were downloaded, inspected, and archived immediately following each sampling session. Potential data quality issues (missing data, negative or otherwise spurious readings) were flagged for subsequent evaluation and resolution. I developed custom software written in MATLAB (Mathworks, Inc., Natick, MA) to import, synchronize, and combine datasets and to apply corrections and calibrations. I censored a small number of records owing to instrument malfunction or substantial missing data. Figure 2-3 presents illustrative data.

To ensure consistency between the paired instruments used to measure ambient and in-vehicle concentrations, I colocated both aethalometers and both DustTraks at CRP for the 30 min immediately before and after each sampling session. The DustTrak used for ambient measurements indicated a consistent bias of -7.3 ± 3.0 μg m^{-3} $PM_{2.5}$ relative to the instrument used for in-vehicle measurements and gravimetric calibrations. To remove the mean bias, I adjusted the ambient instrument's measurements by +7.3 μg m^{-3}. Colocated measurements of BC agreed closely after applying the loading correction and spike-removing algorithm to the aethalometer data and so were not further adjusted.

For each session, microenvironment, and pollutant, I computed time-integrated arithmetic mean concentrations and concentration rank-percentiles for the 1-Hz series. When simultaneous in-vehicle and ambient measurement was not possible (PN; some days of $PM_{2.5}$ measurement), I imputed ambient levels as the arithmetic mean of the time-averaged values for the three short-duration ambient measurements: LG (mid-trip) and CRP (30 min before and after in-vehicle sampling). I validated this approach for the ~40 sessions in which simultaneous real-time ambient $PM_{2.5}$ and BC data were collected. The imputed and actual mean concentrations agree well (median bias <5%, Pearson's r^2 of 0.89 for $PM_{2.5}$ and 0.85 for BC). As only a single CPC was available, it was not possible to directly validate this approach for PN. Quality control and data processing reduced the concentration datasets from ~3×10^6 observations per pollutant to, respectively, 60, 47 and 50 matched pairs of arithmetic mean in-vehicle and ambient $PM_{2.5}$, BC, and PN collected on a total of 62 trips.

2.3. Results and discussion

2.3.1 In-vehicle concentrations: Auto-rickshaws

Particle concentrations measured in auto-rickshaws were high. Trip-averaged concentrations were approximately lognormally distributed (Figure 2-4), with geometric means of 190 μg m^{-3} for $PM_{2.5}$, 42 μg m^{-3} for BC, and 280 × 10^3 particles cm^{-3} for PN (Table 2-2). Concentrations were elevated in-vehicle relative to ambient measurements at CRP, which had geometric means of 130 μg m^{-3} for $PM_{2.5}$, 12 μg m^{-3} for BC, and 35 × 10^3 particles cm^{-3} for PN. Over all trips, the arithmetic mean incremental in-vehicle (auto-rickshaw minus ambient) concentration was 58 ± 8.0 μg m^{-3} for $PM_{2.5}$, 29 ± 2.6 μg m^{-3} for BC, and (250 ± 20) × 10^3 particles cm^{-3} for PN (mean ± 95% CI). For context, note that annual average $PM_{2.5}$ among all ambient monitors in the US (sites predominantly urban) was 11.5 μg m^{-3} during 2006-2008 (US EPA, 2008).

There were frequent short-duration (~10 – 100 s) concentration peaks for all monitored pollutants. The 95th percentile of 10-s averaged concentrations exceeded the trip arithmetic mean concentration by ~1.6 – 2.3× (Table 2-3). Video data (e.g., Figure 2-5) suggest that many transient high concentrations ($PM_{2.5}$ > 500 μg m^{-3}, BC > 400 μg m^{-3}, PN > 10^6 particles cm^{-3}) may be attributable to visibly high-emitting vehicles, a finding that is consistent with recent laboratory emissions tests of New Delhi auto-rickshaws linking visible plumes with high $PM_{2.5}$ emissions (Reynolds et al., 2011).

Over all trips, 1-min average concentrations of the individual pollutants were only weakly correlated with each other within individual time series: mean Pearson's r^2 were 0.33, 0.10, and 0.12, respectively, for correlations of $PM_{2.5}$-BC, $PM_{2.5}$-PN, and BC-PN. Trip average in-vehicle concentrations were moderately correlated with ambient concentrations: over all trips, Pearson's r^2 for contemporaneous ambient and in-vehicle arithmetic mean concentrations were 0.65, 0.42, and 0.31 for $PM_{2.5}$, BC, and PN, respectively.

Supplemental measurements described in §2.2.1 provided no evidence of substantial self-pollution. During this self-pollution experiment, mean in-vehicle concentrations of $PM_{2.5}$ and PN were moderately lower than levels measured at CRP immediately following the self-pollution test (Figure 2-6). In-vehicle $PM_{2.5}$ and PN concentrations during the test did not indicate the large and frequent variability that was typical of the main exposure measurements (compare with

Figure 2-3). Moreover, there was no pattern in pollutant concentrations that correlated with engine on/off status. I observed one PN spike of ~80 × 10^3 cm^{-3} midway through the second test iteration. The origin of this concentration spike is unclear; I noted passing a two-stroke motorcycle at approximately the same time. The ratio of mean (median) concentration during periods with engine on to mean (median) concentration during periods with engine off was 1.02 (1.02) for $PM_{2.5}$ and 1.08 (0.99) for PN. An unpaired two-sample *t*-test indicated that the difference in mean pollutant concentration between periods with engine on and periods with engine off was statistically indistinguishable from zero (p = 0.12 for $PM_{2.5}$, p = 0.34 for PN). Overall, the results of this experiment are consistent with the hypothesis that the dominant contribution to in-vehicle concentrations along the main measurement route is from sources other than the sampling auto-rickshaw.

2.3.2 Contribution of proximate sources to in-vehicle exposure concentrations

Ratio of in-vehicle to ambient concentrations

To the extent that in-vehicle concentrations differ systematically from ambient concentrations, ambient air quality measurements may not adequately represent in-traffic exposures. The in-vehicle to ambient concentration ratio (γ) is a metric that can usefully characterize this difference. In theory, this ratio will be greater for pollutants that are predominantly emitted on roadways. Furthermore, among those pollutants emitted primarily on roadways, the ratio will be higher for nonconserved pollutants that decay on time scales that are as fast or faster than the air transit time from emission site to ambient receptor. A review of 25 studies reported that a typical value of γ for primary, vehicle-derived conserved pollutants is ~4:1 (Marshall et al., 2003). For each of the pollutants measured in this study, I computed the distribution of γ over all trips (Table 2-3). For BC – a primary, conserved pollutant and a marker for vehicle emissions – the arithmetic mean value of γ was 3.6 (95% CI: 3.1 – 4.1), which is comparable to the value reported by Marshall et al. For $PM_{2.5}$, the mean value of γ was 1.5 (95% CI: 1.4 – 1.6). This value is substantially lower than for BC. That this result is less than for BC is not surprising because $PM_{2.5}$ is a conserved, regional pollutant; thus, in-vehicle concentrations are only moderately elevated above the high background levels. Receptor modeling for Delhi conducted in 2001 suggests that road dust and vehicle emissions each account for only ~20-25% of ambient $PM_{2.5}$ during the spring (Chowdhury et al., 2007). Interestingly, in-vehicle levels of PN were highly elevated above the ambient background; for PN, γ was 8.4 (95% CI: 7.3 – 9.6). This finding, too, is qualitatively consistent with expectations. PN, a strong marker for vehicle exhaust plumes, is a nonconserved pollutant. Coagulation, evaporation, and deposition onto surfaces can remove ultrafine particles at time scales that compete with the residence time of air in urban areas. (For advection across New Delhi, at a scale of 40-50 km with wind speeds of 1-2 m s^{-1}, the advective transport time scale is ~5 – 10 h.) Mönkkönen et al. (2004) observed evidence of a strong coagulation sink for UFP in New Delhi. In the following section, I estimate a timescale of ~0.3 – 3 h for coagulation of 10 – 100 nm particles for ambient conditions in New Delhi.

Estimated coagulation time scale for ambient ultrafine particles

As previous work in New Delhi has identified coagulation as a possible sink for ambient ultrafine mode particles (Mönkkönen et al., 2004; Mönkkönen et al., 2005; Laakso et al., 2006), I

present here calculations to demonstrate the plausibility of relatively rapid coagulation of ambient UFP. To estimate the coagulation timescale $\tau_{coag,i}$ for the coagulation of a single particle of diameter i onto a polydisperse aerosol, I used a modified version of the coagulation coefficient presented by Seinfeld and Pandis (2006) :

$$\tau_{coag,i} \sim \frac{1}{\int_{1\,\mathrm{nm}}^{10\,\mu m} \left[\frac{\mathrm{d}N}{\mathrm{d}\log\left(d_p\right)} \beta\left(d_p, i\right) \right] \mathrm{d}\log\left(d_p\right)} \qquad [2.6]$$

Here, $\beta(d_{p.}, i)$ represents the coagulation coefficient ($cm^3\ s^{-1}$) for a single particle of size i coagulating onto particles of size D_p, and $dN/d\log(d_p)$ (cm^{-3}) represents the particle size distribution of the aerosol acting as the coagulation "sink." This version of the coagulation timescale equation allows for the possibility that the single particle will coagulate with either a larger or a smaller particle. Note that this form of the coagulation coefficient differs from another coagulation timescale (e.g., Westerdahl et al., 2009), which evaluates the characteristic time for a particle of size i to coagulate with a particle of diameter larger than itself.

I computed β using the Fuchs form of the Brownian coagulation coefficient (Seinfeld and Pandis, 2006) for T = 20 ºC. For these estimates, I employ the particle size distribution (PSD) for ambient air in New Delhi, as reported by Laakso et al. (2006) for October – November 2002. The distribution is idealized as the sum of three lognormal components with geometric mean diameters of 11, 44, and 147 nm (Table 2-4). To evaluate the timescale for coagulation of a single particle with diameter i onto the New Delhi ambient aerosol, I used the PSD reported by Laasko et al. as the basis for determining $dN/d\log(d_p)$ and numerically integrated equation [2.6] using 100 logarithmically spaced steps per decade of particle size d_p. I repeated this procedure for particles in the size range 10 nm – 1 μm, which roughly corresponds to the particle size range detected by the CPC used here. I estimate that $\tau_{coag,i}$ is in the range of 0.2 – 1.5 h for particles of diameter range 10 – 100 nm. Averaging over the entire PSD > 10 nm, the mean coagulation timescale is ~1 h. However, the PN reported by Laakso et al. (2006) was ~68×10^3 particles cm^{-3}, which is roughly twice the level observed at the CRP ambient monitoring site during this study. To evaluate the effect of lower ambient concentrations, I scaled the number concentration of the PSD so that the total PN was equivalent to the mean ambient PN concentration measured here, 35×10^3 particles cm^{-3}. Doing so resulted in longer coagulation time scales, with a range of ~0.3 – 3 h for particles in the size range of 10 – 100 nm. Averaged over all particle sizes > 10 nm in the rescaled PSD, I estimate that the mean coagulation timescale is ~2 h at this lower concentration. I therefore conclude that coagulation may be a significant sink for ambient PN in New Delhi, since the corresponding time scales have are much shorter than the urban-air residence time of ~5-15 h, based on the ratio of the urban length scale, 40-50 km, to the typical 1-2 m s^{-1} near-surface wind speed.

Nearby contributions to in-vehicle exposures

I infer the contribution of roadway emissions to in-vehicle exposures by computing the difference between mean in-vehicle and ambient (CRP) concentrations for each of the 62 trips. I

estimate the fraction of the in-vehicle concentration attributable to the roadway microenvironment (φ) as

$$\varphi = \left(C_{veh} - C_{amb}\right) / C_{veh} = 1 - \gamma^{-1} \quad [2.7]$$

Here, for a given sampling session, C_{veh} is the mean in-vehicle concentration and C_{amb} is the mean ambient concentration at CRP. As illustrated in Figure 2-7, φ was smallest for $PM_{2.5}$ (mean ± 95% CI: 30 ± 4%), intermediate for BC (68 ± 3%) and greatest for PN (86 ± 1%). The values of this metric indicate that in-vehicle concentrations of BC and PN are dominated by local (near and on-roadway) emissions.

As noted above, BC and UFP (and thus PN) are more specific markers of vehicle emissions than is $PM_{2.5}$. The ratio of concentrations for these two pollutants to $PM_{2.5}$ is an indicator of the extent to which microenvironmental concentrations are influenced by vehicle emissions. Over all trips, the mean ratio of BC:$PM_{2.5}$ was twice as high in the auto-rickshaw cabin as it was at the ambient site (in-vehicle BC:$PM_{2.5}$ = 0.23; ambient BC:$PM_{2.5}$ = 0.10). The ratio of PN:$PM_{2.5}$ was ~5× higher inside the auto-rickshaw cabin than for ambient measurements (in-vehicle PN:$PM_{2.5}$: 1.4×10^9 particles μg^{-1} ; ambient PN:$PM_{2.5}$: 0.3×10^9 particles μg^{-1}).

2.3.3 Seasonal and temporal variability in ambient and in-vehicle pollutant concentrations

I used unbalanced two-way analysis of variance (ANOVA) to decompose the variability in ambient (Figure 2-8a) and in-vehicle (Figure 2-8b) concentrations into time-of-day (AM vs. PM), day-of-week, and seasonal (month) components. Holding time of day constant, there was a statistically significant declining trend in ambient levels for all three pollutants during the February – May study period (Figure 2-8a). This decline was most pronounced for $PM_{2.5}$ and BC. It is possible that this decrease in ambient concentrations is partially attributable to Delhi's seasonally dependent patterns of 1) atmospheric mixing and 2) emissions from solid fuel combustion for heat. Similar trends were noted in another recent analysis of ambient $PM_{2.5}$ and BC in New Delhi (Tiwari et al., 2013). In addition to the seasonal trends, there was a statistically significant time-of-day trend for ambient $PM_{2.5}$ levels throughout the study period. Evening commute-time (6-9 PM) ambient concentrations were typically lower than morning (9 AM – noon) commute-time ambient concentrations (median difference: ~25%). There was not a statistically significant difference in ambient BC and PN concentrations between AM and PM commute hours.

Considering in-vehicle concentrations (Figure 2-8b), there were statistically significant ($p < 0.05$) time-of-day trends for $PM_{2.5}$ and BC, but not for PN. Interestingly, morning-versus-evening differences were of opposite sign for $PM_{2.5}$ and BC. On average, $PM_{2.5}$ and BC concentrations were, respectively, 10% lower and 46% higher in the evening as compared with the morning commutes. The reasons for the different behavior among the three species are not known. It is plausible that the time-of-day pattern of in-vehicle concentrations reflects a superposition of temporal trends for ambient levels and in the on-roadway increment in exposure. Compared to BC, ambient $PM_{2.5}$ concentrations represent a larger overall fraction of in-vehicle $PM_{2.5}$ exposure. The strong decline in ambient $PM_{2.5}$ concentrations between morning and evening (Figure 2.8a) is clearly evident in the in-vehicle $PM_{2.5}$ signal as well (Figure 2.8b).

In contrast, as noted above, there were no statistically significant differences in ambient BC between the morning and evening measurement sessions. Overall, the increment for in-vehicle concentrations above the ambient levels was typically greater in the evening than in morning for both $PM_{2.5}$ and BC, which may reflect influences from temporal patterns of emissions and/or atmospheric transport and dispersion. Wind speeds were ~60% lower in the evening than in the morning (Table 2-1), a characteristic that would be consistent with relatively higher contributions of vehicle emissions to on-roadway concentrations during the evening commutes. Finally, based on tests using ANOVA by day of week and multi-factorial ANOVA by day of week, time of day, and month, I did not detect any consistent day-of-week differences in concentration. Sampling was limited to Monday through Friday, so any weekend effects would not have been detected.

There was a statistically significant downward trend for in-vehicle $PM_{2.5}$ and PN concentrations between February and May. For $PM_{2.5}$, the seasonal concentration decrease was similar for in-vehicle and ambient conditions, suggesting that urban-scale trends (e.g., fuel use for heating, average mixing height) are responsible for observed seasonal changes for in-vehicle concentrations (e.g., Tiwari et al., 2013). In contrast, seasonal decreases for PN were noticeably larger for in-vehicle than for ambient conditions. Changes in temperatures might explain this in-vehicle/ambient PN difference, owing to shifts in gas-particle partitioning of semivolatile UFP constituents and the CPC's 10-nm particle size cut-point. Specifically, particles that would have been larger than 10 nm at lower temperatures might shrink via evaporation to diameters smaller than 10 nm at higher temperatures. The proportion of particles that are small (~10 nm) is expected to be higher near-source (on-roadway air, with fresh emissions) than in ambient air (more aged aerosols).

2.3.4 Comparisons among vehicle types

I examined differences by vehicle type for the trip-average concentration inside auto-rickshaws, cars with open windows (OW; no fan ventilation), and cars with ventilation set to recirculate air (RC; windows closed and air conditioning on) in May (Figure 2-9a). There was no statistically significant difference between concentrations in auto-rickshaws and OW cars. However, concentrations were substantially lower inside RC cars than in the auto-rickshaw, with mean ± 95% CI concentration difference of 61 ± 33 μg m^{-3} for $PM_{2.5}$, 12 ± 11 μg m^{-3} for BC, and (130 ± 41) × 10^3 particles cm^{-3} for PN. Concentration ratios (RC car: auto-rickshaw) were ~0.6 for $PM_{2.5}$, 0.7 for BC and 0.4 for PN. Relative to auto-rickshaw concentrations, the range of instantaneous in-vehicle concentrations (Figure 2-9b) was reduced for OW cars, and more substantially reduced for RC cars, as would be expected given the reduced air-exchange rates for such vehicles (Fruin et al., 2011; Ott et al., 2008; Hudda et al., 2012). If the auto-rickshaw PN exposure concentration measurements are similar to outdoor on-road levels, then the in-vehicle to outdoor PN ratio for the RC cars tested here (~0.4) is within the range (~0.2 – 0.6) reported in previous US studies (Zhu et al., 2007; Hudda et al., 2012). To the extent that concentrations in auto-rickshaws reflect on-road levels, then travelers using other unenclosed transport modes (such as motorcycles, which account for ~20% of total trips in Delhi) may also experience trip-averaged exposures of similarly high magnitude. Further research is warranted to investigate exposures for unenclosed transport modes with driving patterns distinct from those of auto-rickshaws.

2.3.5 Comparison to other megacities, and implications for time-integrated exposure

In-vehicle concentrations reported here are ~2-10× greater than in-vehicle and on-road concentrations previously reported for other megacities (London, Los Angeles, Beijing, Hong Kong; see Figure 2-10). Mean BC exposure concentrations in Delhi auto-rickshaws were roughly twice those measured on Beijing roads during the daytime and ~3–30× greater than those measured on Los Angeles arterial roadways and freeways with varying levels of diesel heavy duty vehicle (HDV) traffic (Fruin et al., 2008; Westerdahl et al., 2005; Westerdahl et al., 2009). Although few HDV were in use during measurements, the BC levels in Delhi are higher than reported elsewhere. This finding might indicate that LDV in Delhi are high-emitters of BC, perhaps because of the substantial (~30%) and growing market share of diesel LDV in India (Narain et al., 2010).

Table 2-5 reports concentration values from a selection of other worldwide studies of in-vehicle and on-road air quality (Boogaard et al., 2009; Bukowiecki et al., 2003; Chan et al., 2002; Fruin et al., 2008; Kaur et al., 2005; Kittelson et al., 2004; Knibbs and de Dear, 2010; Westerdahl et al., 2009). A global review of 47 studies of commuter exposure to UFP reported geometric mean PN ~5-8× lower than measured in Delhi auto-rickshaws, depending on transport mode (Knibbs et al., 2011). However, there have been few prior investigations of in-vehicle exposure to PN in developing world megacities. Compared to the measurements reported here, a study of particle exposures in Jakarta vehicles (Both et al., 2013) found similar PN concentrations inside cars (mean: 294,000 cm^{-3}) and substantially higher levels inside buses (mean: 401,000 cm^{-3}). Auto-rickshaw PN exposure concentrations were 3× higher in Delhi than measured on Beijing roads during the daytime and comparable to levels measured there during diesel HDV-dominated nighttime traffic (Westerdahl et al., 2009). Moreover, the Delhi measurements were largely conducted during time periods of strong vertical mixing (daytime, high mixing height), likely in contrast with the nighttime measurements in Beijing. As has been observed by others, ambient PN levels are remarkably similar for New Delhi, Beijing, and Los Angeles, despite substantial diversity in demographics, source types, and emissions among these cities (Laakso et al., 2006). This observation may be influenced by the high mass concentration providing an effective coagulation sink for UFP under more highly polluted conditions. Finally, note that the instruments used in this study may underreport total PN relative to the instruments used in other studies because of differences in the minimum size cutpoint (10 nm here, versus 3-7 nm in some other studies (Table 2-5).

High in-vehicle concentrations in Delhi would lead to high time-integrated exposures. For example, a typical time-integrated exposure during an average daily commute (1.9 h d^{-1} for auto-rickshaw users (Saksena et al., 2007)) is ~530 × 10^3 particles cm^{-3} h d^{-1}, which is larger than any of (a) estimates for entire-day PN exposures for urban California residents (~330 × 10^3 particles cm^{-3} h d^{-1} (Fruin et al., 2008)), (b) the average in-home exposure contributions for residents of seven San Francisco Bay Area single-family homes (~300 × 10^3 particles cm^{-3} h d^{-1} (Bhangar et al., 2011)) and (c) the average for occupants of Beijing high-rise apartments (~290 × 10^3 particles cm^{-3} h d^{-1} (Mullen et al., 2011)). During a typical daily work shift (10 – 16 h; Harding and Hussein, 2010), auto-rickshaw drivers may receive very high PN exposures, on the order of (2,000 – 3,000) × 10^3 particles cm^{-3} h d^{-1}. Of course, for most auto-rickshaw commuters, time spent in traffic accounts for a relatively small fraction of the total number of hours in a day. Accordingly, time spent in other microenvironments in the Delhi region – especially in

combustion-impacted indoor settings – is likely to contribute a substantial fraction of total time-integrated exposures, especially for BC and $PM_{2.5}$. In contrast, because of the very substantial level of in-vehicle elevation for PN (γ = 8.4), time spent commuting might account for a large proportion of the overall time-integrated daily PN exposure for auto-rickshaw users.

2.4. Conclusions

This study measured in-vehicle exposure concentrations to particulate air pollution for auto-rickshaw and car commuters during three months in New Delhi, India. The analysis reports one of the first sets of PN and BC exposure concentration measurements inside auto-rickshaws, a ubiquitous transport mode in South Asian urban areas. It also represents one of the longest-duration measurement campaigns of real-time, in-vehicle PN and BC concentrations anywhere. Auto-rickshaw exposure concentrations of $PM_{2.5}$, BC, and PN were very high in comparison with in-vehicle concentrations measured in other cities around the world. Short-duration trips by auto-rickshaw in New Delhi result in time-integrated exposures to particulate air pollution comparable to or greater than full-day exposures that would be experienced by residents of many urban areas in high-income countries.

Auto-rickshaw exposure concentrations were ~1.5× to 8× larger than, and only moderately correlated with, levels measured at an urban background site. Correspondence between ambient and in-vehicle measurements was greatest for $PM_{2.5}$, probably because of the high regional background from secondary $PM_{2.5}$. In contrast, in-vehicle BC and PN exposures were predominantly attributable to in- and near-roadway sources. These results reinforce previously published findings that ambient monitoring often provides a poor proxy for in-vehicle exposures to vehicle-emitted pollutants.

Over the past decade, Delhi has made strong steps towards reducing vehicle emissions of PM, especially with the conversion of much of the city's bus fleet from diesel to CNG fuel (Reynolds and Kandlikar, 2008). Despite these efforts, $PM_{2.5}$, BC, and PN concentrations in Delhi's auto-rickshaws are among the highest values reported in the literature for routine exposures in transportation microenvironments. These measurements in auto-rickshaws may be representative of other open-window or unenclosed vehicles in Delhi, India. Three current trends suggest that the public health risks that are likely to be associated with these high exposures may persist and even worsen in the future. First, vehicle ownership and use are growing rapidly in Delhi and other Indian cities. Second, diesel LDVs are increasingly popular in India. Without effective emission controls, a trend toward increasing diesel LDV use is likely to be accompanied by increasing on-road BC emissions and concentrations. Third, increased adoption of CNG may reduce $PM_{2.5}$ emissions from spark-ignition engines, but at the cost of higher PN emissions (Mönkkönen et al., 2005). Further study of exposure to particulate air pollution is warranted in other populous South Asian cities, which have different vehicle fleets (older vehicles, more heavy-duty vehicles and two wheelers) and different fuel mixes (less CNG, more diesel and gasoline) in comparison to New Delhi.

2.5 References

Arku, R.E., Vallarino, J., Dionisio, K.L., Willis, R., Choi, H., Wilson, J.G., Hemphill, C., Agyei-Mensah, S., Spengler, J.D., Ezzati, M., 2008. Characterizing air pollution in two low-income neighborhoods in Accra, Ghana. *Science of The Total Environment* 402, 217-231.

Ban-Weiss, G.A., Lunden, M.M., Kirchstetter, T.W., Harley, R.A., 2009. Measurement of black carbon and particle number emission factors from individual heavy-duty trucks. *Environmental Science & Technology* 43, 1419-1424.

Bhangar, S., Mullen, N.A., Hering, S.V., Kreisberg, N.M., Nazaroff, W.W., 2011. Ultrafine particle concentrations and exposures in seven residences in northern California. *Indoor Air* 21, 132-144.

Boogaard, H., Borgman, F., Kamminga, J., Hoek, G., 2009. Exposure to ultrafine and fine particles and noise during cycling and driving in 11 Dutch cities. *Atmospheric Environment* 43, 4234-4242.

Boogaard, H., Kos, G.P.A., Weijers, E.P., Janssen, N.A.H., Fischer, P.H., van der Zee, S.C., de Hartog, J.J., Hoek, G., 2010. Contrast in air pollution components between major streets and background locations: Particulate matter mass, black carbon, elemental composition, nitrogen oxide and ultrafine particle number. *Atmospheric Environment* 45, 650-658.

Both, A.F., Westerdahl, D., Fruin, S., Haryanto, B., Marshall, J.D., 2013. Exposure to carbon monoxide, fine particle mass, and ultrafine particle number in Jakarta, Indonesia: Effect of commute mode. *Science of The Total Environment* 443, 965-972.

Bukowiecki, N., Dommen, J., Prévôt, A.S.H., Weingartner, E., Baltensperger, U., 2003. Fine and ultrafine particles in the Zürich (Switzerland) area measured with a mobile laboratory: An assessment of the seasonal and regional variation throughout a year. *Atmopheric Chemistry and Physics* 3, 1477-1494.

Chakrabarti, B., Fine, P.M., Delfino, R., Sioutas, C., 2004. Performance evaluation of the active-flow personal DataRAM $PM_{2.5}$ mass monitor (Thermo Anderson pDR-1200) designed for continuous personal exposure measurements. *Atmospheric Environment* 38, 3329-3340.

Chan, L.Y., Lau, W.L., Lee, S.C., Chan, C.Y., 2002. Commuter exposure to particulate matter in public transportation modes in Hong Kong. *Atmospheric Environment* 36, 3363-3373.

Chowdhury, Z., Zheng, M., Schauer, J.J., Sheesley, R.J., Salmon, L.G., Cass, G.R., Russell, A.G., 2007. Speciation of ambient fine organic carbon particles and source apportionment of PM2.5 in Indian cities. *Journal of Geophysical Research* 112, D15303.

Forstall, R.L., Greene, R.P., Pick, J.B., 2009. Which are the largest? Why lists of major urban areas vary so greatly. *Tijdschrift voor Economische en Sociale Geografie* 100, 277-297.

Fruin, S., Westerdahl, D., Sax, T., Sioutas, C., Fine, P.M., 2008. Measurements and predictors of on-road ultrafine particle concentrations and associated pollutants in Los Angeles. *Atmospheric Environment* 42, 207-219.

Fruin, S.A., Hudda, N., Sioutas, C., Delfino, R.J., 2011. Predictive model for vehicle air exchange rates based on a large, representative sample. *Environmental Science & Technology* 45, 3569-3575.

Gurjar, B.R., Butler, T.M., Lawrence, M.G., Lelieveld, J., 2008. Evaluation of emissions and air quality in megacities. *Atmospheric Environment* 42, 1593-1606.

Han, X., Naeher, L.P., 2006. A review of traffic-related air pollution exposure assessment studies in the developing world. *Environment International* 32, 106-120.

Harding, S., Hussein, A., 2010. *On the Road to Nowhere? Auto Rickshaws in Delhi: The System, Problems and Recommendations*, New Delhi. Available from: http://www.amanpanchayat.org/documents/reports/simon-auto-final.doc.

Hudda, N., Kostenidou, E., Sioutas, C., Delfino, R.J., Fruin, S.A., 2012. Vehicle and driving characteristics that influence in-cabin particle number concentrations. *Environmental Science & Technology* 45, 8691-8697.

Jacobs, L., Nawrot, T., de Geus, B., Meeusen, R., Degraeuwe, B., Bernard, A., Sughis, M., Nemery, B., Panis, L., 2010. Subclinical responses in healthy cyclists briefly exposed to traffic-related air pollution: An intervention study. *Environmental Health* 9, Art. 64.

Jimenez, J., Claiborn, C., Larson, T., Gould, T., Kirchstetter, T.W., Gundel, L., 2007. Loading effect correction for real-time aethalometer measurements of fresh diesel soot. *Journal of the Air & Waste Management Association* 57, 868-873.

Kaur, S., Nieuwenhuijsen, M., Colvile, R., 2005. Personal exposure of street canyon intersection users to PM2.5, ultrafine particle counts and carbon monoxide in Central London, UK. *Atmospheric Environment* 39, 3629-3641.

Kaur, S., Nieuwenhuijsen, M.J., Colvile, R.N., 2007. Fine particulate matter and carbon monoxide exposure concentrations in urban street transport microenvironments. *Atmospheric Environment* 41, 4781-4810.

Kirchstetter, T.W., 2007. *Evaluating Past and Improving Present and Future Measurements of Black Carbon Particles in the Atmosphere*, California Energy Commission - Public Interest Energy Research Program Report CEC‐500‐2007‐042.

Kirchstetter, T.W., Novakov, T., 2007. Controlled generation of black carbon particles from a diffusion flame and applications in evaluating black carbon measurement methods. *Atmospheric Environment* 41, 1874-1888.

Kittelson, D.B., Watts, W.F., Johnson, J.P., 2004. Nanoparticle emissions on Minnesota highways. *Atmospheric Environment* 38, 9-19.

Knibbs, L.D., de Dear, R.J., Morawska, L., Coote, P.M., 2007. A simple and inexpensive dilution system for the TSI 3007 condensation particle counter. *Atmospheric Environment* 41, 4553-4557.

Knibbs, L.D., de Dear, R.J., 2010. Exposure to ultrafine particles and $PM_{2.5}$ in four Sydney transport modes. *Atmospheric Environment* 44, 3224-3227.

Knibbs, L.D., Cole-Hunter, T., Morawska, L., 2011. A review of commuter exposure to ultrafine particles and its health effects. *Atmospheric Environment* 45, 2611-2622.

Laakso, L., Koponen, I.K., Mönkkönen, P., Kulmala, M., Kerminen, V.-M., Wehner, B., Wiedensohler, A., Wu, Z., Hu, M., 2006. Aerosol particles in the developing world; A

comparison between New Delhi in India and Beijing in China. *Water, Air, and Soil Pollution* 173, 5-20.

Mage, D., Ozolins, G., Peterson, P., Webster, A., Orthofer, R., Vandeweerd, V., Gwynne, M., 1996. Urban air pollution in megacities of the world. *Atmospheric Environment* 30, 681-686.

Marshall, J.D., Riley, W.J., McKone, T.E., Nazaroff, W.W., 2003. Intake fraction of primary pollutants: Motor vehicle emissions in the South Coast Air Basin. *Atmospheric Environment* 37, 3455-3468.

Mönkkönen, P., Uma, R., Srinivasan, D., Koponen, I.K., Lehtinen, K.E.J., Hämeri, K., Suresh, R., Sharma, V.P., Kulmala, M., 2004. Relationship and variations of aerosol number and PM_{10} mass concentrations in a highly polluted urban environment —New Delhi, India. *Atmospheric Environment* 38, 425-433.

Mönkkönen, P., Koponen, I.K., Lehtinen, K.E.J., Hämeri, K., Uma, R., Kulmala, M., 2005. Measurements in a highly polluted Asian mega city: Observations of aerosol number size distribution, modal parameters and nucleation events. *Atmospheric Chemistry and Physics* 5, 57-66.

Mullen, N.A., Liu, C., Zhang, Y., Wang, S., Nazaroff, W.W., 2011. Ultrafine particle concentrations and exposures in four high-rise Beijing apartments. *Atmospheric Environment* 45, 7574-7582.

Narain, S., Roychowdhury, A., Mathur, H.B., Chattopadhyay, V., Chandola, P., Sen, J., 2010. *Mobility Crisis: Agenda for Action 2010*, Centre for Science and Environment, New Delhi, India. ISBN: 978-81-86906-51-4.

Ott, W., Klepeis, N., Switzer, P., 2008. Air change rates of motor vehicles and in- vehicle pollutant concentrations from secondhand smoke. *Journal of Exposure Science and Environmental Epidemiology* 18, 312-325.

Peters, A., von Klot, S., Heier, M., Trentinaglia, I., Hörmann, A., Wichmann, H.E., Löwel, H., 2004. Exposure to traffic and the onset of myocardial infarction. *New England Journal of Medicine* 351, 1721-1730.

Ramachandran, G., Adgate, J.L., Pratt, G.C., Sexton, K., 2003. Characterizing indoor and outdoor 15 minute average $PM_{2.5}$ concentrations in urban neighborhoods. *Aerosol Science and Technology* 37, 33-45.

Reynolds, C.C.O., Kandlikar, M., 2008. Climate impacts of air quality policy: Switching to a natural gas-fueled public transportation system in New Delhi. *Environmental Science & Technology* 42, 5860-5865.

Reynolds, C.C.O., Kandlikar, M., Badami, M.G., 2011. Determinants of PM and GHG emissions from natural gas-fueled auto-rickshaws in Delhi. *Transportation Research Part D: Transport and Environment* 16, 160-165.

Riediker, M., Cascio, W.E., Griggs, T.R., Herbst, M.C., Bromberg, P.A., Neas, L., Williams, R.W., Devlin, R.B., 2004. Particulate matter exposure in cars is associated with cardiovascular effects in healthy young men. *American Journal of Respiratory and Critical Care Medicine* 169, 934-940.

Saksena, S., Prasad, R.K., Shankar, V.R., 2007. Daily exposure to air pollutants in indoor, outdoor and in-vehicle microenvironments: A pilot study in Delhi. *Indoor and Built Environment* 16, 39-46.

Seinfeld, J.H., Pandis, S.N., 2006. *Atmospheric Chemistry and Physics: From Air Pollution to Climate Change*, 2nd edition, Wiley-Interscience, Hoboken, NJ.

Tiwari, G., 2003. Transport and land-use policies in Delhi. *Bulletin of the World Health Organization* 81, 444-450.

Tiwari, S., Srivastava, A.K., Bisht, D.S., Parmita, P., Srivastava, M.K., Attri, S.D., 2013. Diurnal and seasonal variations of black carbon and $PM_{2.5}$ over New Delhi, India: Influence of meteorology. *Atmospheric Research* 125–126, 50-62.

US EPA, 2008. *Chapter 2: Air, in U.S. EPA's 2008 Report on the Environment (Final Report)*, U.S. Environmental Protection Agency, Washington, DC. EPA/600/R-07/045F (NTIS PB2008-112484).

Westerdahl, D., Fruin, S., Sax, T., Fine, P.M., Sioutas, C., 2005. Mobile platform measurements of ultrafine particles and associated pollutant concentrations on freeways and residential streets in Los Angeles. *Atmospheric Environment* 39, 3597-3610.

Westerdahl, D., Wang, X., Pan, X., Zhang, K.M., 2009. Characterization of on-road vehicle emission factors and microenvironmental air quality in Beijing, China. *Atmospheric Environment* 43, 697-705.

Zhu, Y.F., Eiguren-Fernandez, A., Hinds, W.C., Miguel, A.H., 2007. In-cabin commuter exposure to ultrafine particles on Los Angeles freeways. *Environmental Science & Technology* 41, 2138-2145.

Table 2-1. Monthly mean and range of meteorological parameters at the Chittaranjan Park (CRP) ambient site during morning (AM) and evening (PM) auto-rickshaw trips.

Month	**Hours**	**Temperature (ºC)**		**Relative humidity (%)**		**Wind speed (m s^{-1})**	
(2010)	(trips)	AM	PM	AM	PM	AM	PM
Feb	23 (8)	26 (24-27)	23 (23-24)	52 (48-56)	56 (52-60)	0.9 (0.3-1.5)	0.2 (0.1-0.5)
Mar	62 (22)	33 (27-39)	30 (25-34)	35 (19-46)	37 (23-51)	0.6 (0.3-0.9)	0.3 (0.1-0.7)
Apr	48 (16)	41 (38-44)	37 (33-38)	16 (12-29)	21 (16-33)	0.5 (0.2-1.1)	< 0.15
May	41 (16)	39 (34-43)	37 (28-40)	26 (12-48)	23 (13-52)	0.6 (0.3-1.1)	0.4 (0-1.1)

Table 2-2. Distribution of average particulate matter concentrations for 62 auto-rickshaw trips in New Delhi. [a]

Pollutant	**Location**	**AM (SD)**	**GM (GSD)**	**Median**	**Min**	**P_{10}**	**P_{90}**	**Max**
$PM_{2.5}$	Auto-Rickshaw	200 (46)	190 (1.26)	200	110	130	260	340
(μg m^{-3})	Ambient	140 (52)	130 (1.45)	140	69	82	220	260
N = 60	Difference	58 (31)	47 (2.50)	56	0.19	22	91	160
BC	Auto-Rickshaw	43 (12)	42 (1.31)	43	22	29	57	77
(μg m^{-3})	Ambient	13 (6.3)	12 (1.61)	13	3.6	6.5	23	34
N = 47	Difference	29 (9.0)	29 (1.36)	27	10	21	40	63
PN	Auto-Rickshaw	290 (77)	280 (1.35)	280	69	200	380	500
(10^3 cm^{-3})	Ambient	38 (12)	35 (1.47)	37	9.8	24	51	67
N = 50	Difference	250 (71)	260 (1.41)	240	46	180	340	460

[a] "Difference" represents the trip-average concentration in the the auto-rickshaw microenvironment minus the concentration determined for the ambient site at Chittaranjan Park (CRP). Abbreviations: AM – arithmetic mean, SD - arithmetic standard deviation, GM – geometric mean, GSD – geometric standard deviation, P_{10} and P_{90} – 10^{th} and 90^{th} percentiles of distribution of trip-average concentrations.

Table 2-3. Summary statistics for within-trip concentration distributions inside auto-rickshaws. [a]

Pollutant		Auto-Rickshaw Concentrations P_5 GM (GSD)		P_{95} GM (GSD)		Max GM (GSD)		Ratio Mean Auto: Mean Ambient (γ) AM	Ratio P_{95} Auto: Mean Auto AM	Ratio P_{95} Auto: Mean Ambient AM
$PM_{2.5}$	($\mu g\ m^{-3}$)	110	(1.4)	300	(1.2)	690	(1.4)	1.5	1.5	2.4
BC	($\mu g\ m^{-3}$)	12	(1.5)	88	(1.3)	400	(2.1)	3.6	2.1	7.8
PN	($10^3\ cm^{-3}$)	53	(1.4)	650	(1.4)	1600	(1.6)	8.4	2.3	20

[a] "P_5" and "P_{95}" indicate, respectively, the 5th and 95th percentile 10-s averaged concentration measurement for a given commute trip; Max indicates the maximum 10-s averaged concentration measurement for that trip. Measures of central tendency (AM = arithmetic mean, GM = geometric mean) and of spread (GSD = geometric standard deviation) are for the distribution of values over all 47-60 trips with available data. Concentration ratios were computed for each individual trip; the value reported here is the AM of the distribution of ratios over all trips. See text for description of **γ**, the ratio of trip-averaged in-vehicle to ambient concentration.

Table 2-4. Sum-of-lognormals fit used to approximate New Delhi ambient particle size distribution (Laakso et al., 2006)

	N_{tot} [a] (particles cm^{-3})	GMD [b] (nm)	*GSD* [c] (-)
Nucleation mode	5150	11	1.4
Aitken mode	37930	44	1.8
Accumulation mode	22680	147	1.6

[a] N_{tot} – total number count for each mode
[b] *GMD* – Geometric count mean diameter
[c] *GSD* – Geometric standard deviation

Table 2-5. Comparison of present study results with prior measurements in megacities and elsewhere.[a]

(A) *Exposure Studies*									
Study	**City/Microenvironment**	**Year**	**Hours**	**$PM_{2.5}$** ($\mu g\ m^{-3}$)		**BC** ($\mu g\ m^{-3}$)		**PN** ($10^3\ cm^{-3}$)[c]	
				Ambient	**Vehicle**	**Ambient**	**Vehicle**	**Ambient**	**Vehicle**
Present study	**New Delhi, India**								
	Auto-Rickshaw	2010	~160	140	190	10	43	35[(10)]	280[(10)]
	Car (AC)		~20	120	110	9	29	30[(10)]	100[(10)]
	Car (Non AC)		~10	120	170		49		180[(10)]
Kaur et al., 2005	**London, UK**	2003							
	Car / Arterial			9.9	38	-	-	-	100[(20)]
	Bus / Arterial			-	35	-	-	-	100[(20)]
	Bicycle / Arterial			-	34	-	-	-	94[(20)]
Boogaard et al., 2009	**11 Dutch Cities**	2006	~30						
	Car / Arterial			-	49[b]	-	-	~10[(10)]	26[(10)]
	Bicycle / Cycle Path			-	44[b]	-	-	~10[(10)]	24[(10)]
Knibbs and de Dear, 2010	**Sydney, Australia**	2004							
	Bus			-	30[b]	-	-	-	84[(10)]
	Car			-	22[b]	-	-	-	75[(10)]
Both et al., 2013	**Jakarta, Indonesia**	2005							
	Bus				91				294[(10)]
	Car				117				401[(10)]
Chan et al., 2002	**Hong Kong, China**	2000							
	Bus (AC)			-	51	-	-	-	-
	Bus (Non AC)				93				
	Tram (on roadway)			-	110	-	-	-	-

Table 2-5, continued

(B) *On-Road Concentration Studies*

Study	City / Microenvironment	Year	Hours	$PM_{2.5}$ (μg m^{-3})		BC (μg m^{-3})		PN (10^3 cm^{-3}) [c]	
				Ambient	On-road	Ambient	On-road	Ambient	On-road
Westerdahl et al., 2009	**Beijing, China**								
	BJ - *Arterials / Day-LDV*	2007	~10	-	-	3.4	22	27(6)	82(6)
	BJ* - *Arterials / Night-HDV* [d]			-	-	11	60	19(6)	290(6)
Fruin et al., 2008	**Los Angeles, USA**								
	LA - *Residential/LDV*	2003	~15	7.9	23	0.74	1.5	13(7)	33(7)
	LA* - *Urban/HDV* [d]			17	54	1.5	12	26(7)	190(7)
Kittelson et al., 2004	**Minneapolis, USA**								
	Freeways	2003	~20	-	-	-	-	9.4(3)	400(3)
Bukowiecki et al., 2003	**Zürich, Switzerland**								
	Arterials	2000	~5	-	-	-	-	5-15(3)	30-50(3)

[a] Values are central tendency results from each study (geometric mean when available, otherwise arithmetic mean). Abbreviations: "$PM_{2.5}$" – fine particle mass, "BC" – black carbon, "PN" – particle number concentration, "LDV" – light-duty vehicle, "HDV" – heavy-duty vehicle.

[b] TSI DustTrak aerosol photometer used without adjustment for humidity or mass-based calibration against local aerosol, indicating possible overestimate.

[c] Superscripts on PN concentrations indicate minimum particle diameter (nm) detected by instrument for given study.

[d] BJ * and LA* refer to extreme conditions measured in those cities. See caption for Figure 2.10.

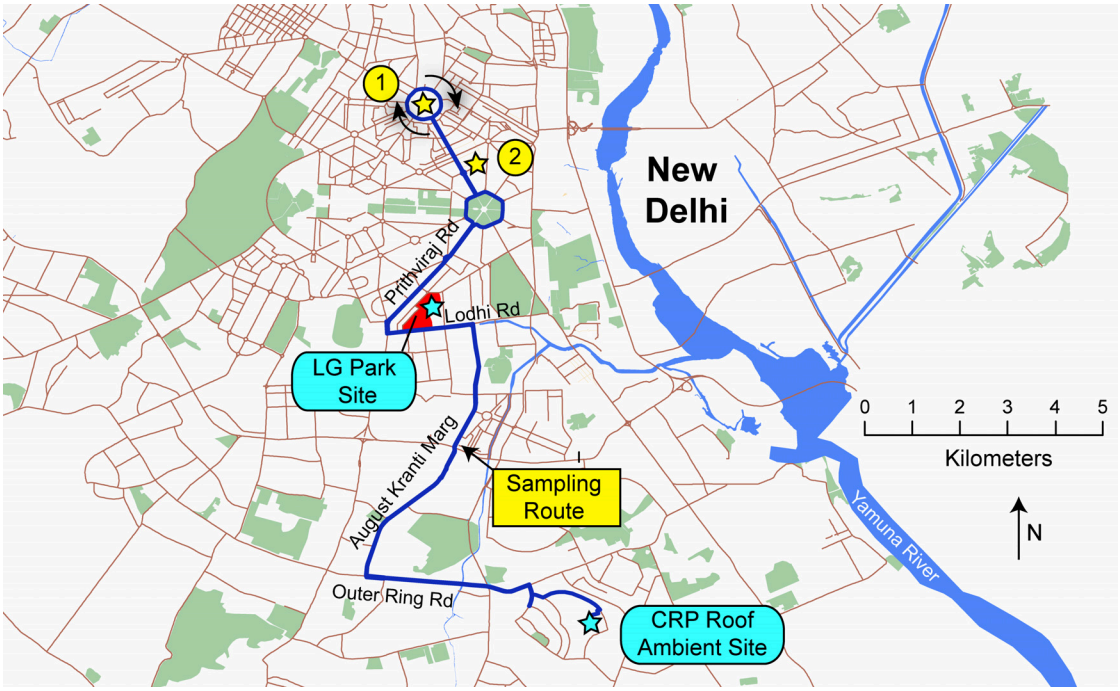

Figure 2-1. Map of New Delhi indicating the main sampling route used in the study. Each trip was driven out-and-back once each during AM and PM commute hours from the ambient monitoring site (Chittaranjan Park, CRP) to central New Delhi. Trips turned back at Connaught Place (CP; point 1 on map) during Feb – April (total distance: 39 km) and at Shrimant Madhav Rao Scindia Marg (point 2 on map) during May (total distance: 37 km). Each trip stopped at Lodhi Garden park (LG) for 30 minutes of ambient measurements.

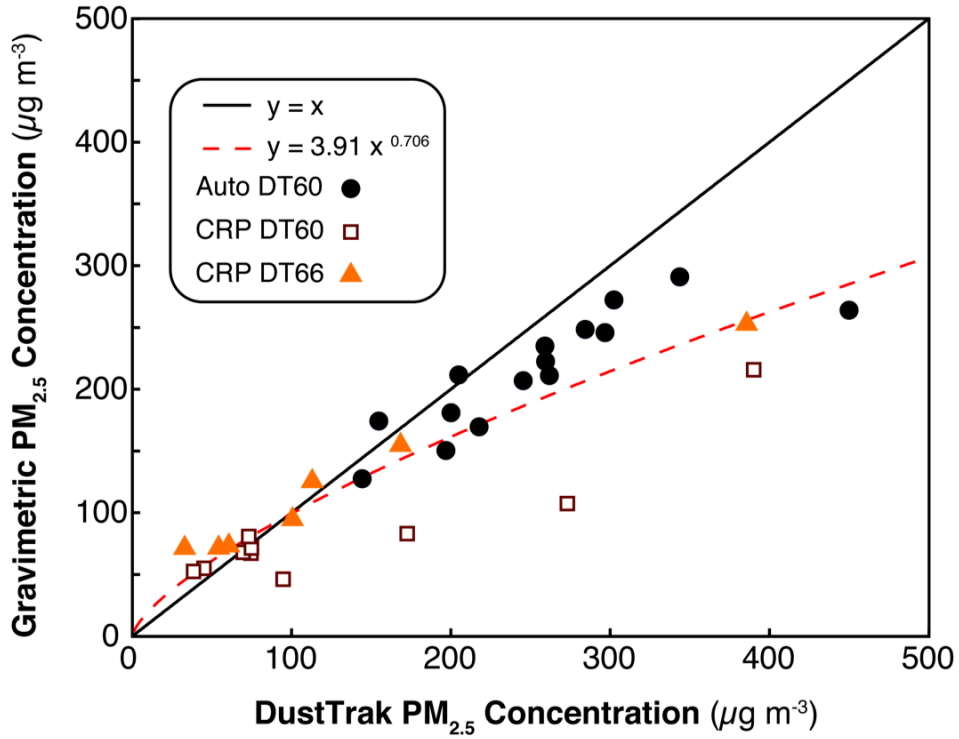

Figure 2.2. Scatter plot of colocated gravimetric and time-averaged DustTrak $PM_{2.5}$ concentration measurements. Points are plotted separately by measurement microenvironment ("auto" = auto-rickshaw, "CRP" = Chittaranjan Park ambient site) and by serial number of the TSI DustTrak used ("DT60", "DT66"). The dashed line indicates the best-fit calibration relationship.

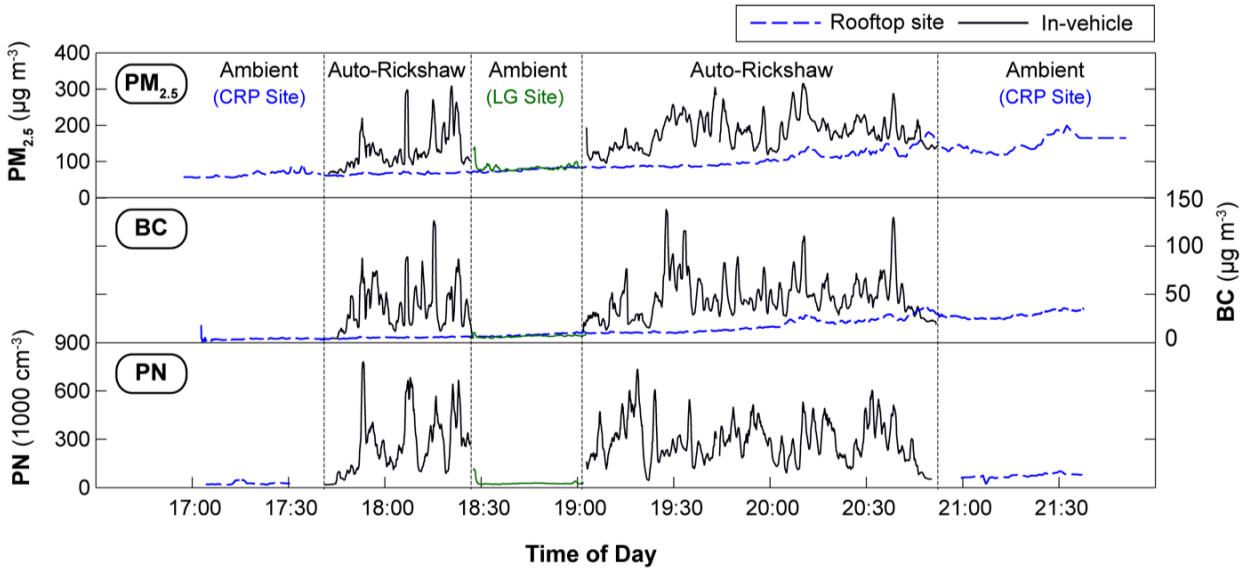

Figure 2-3. Example data for one trip (29 March 2010). For clarity, plotted concentrations were smoothed using a 60-s moving average filter.

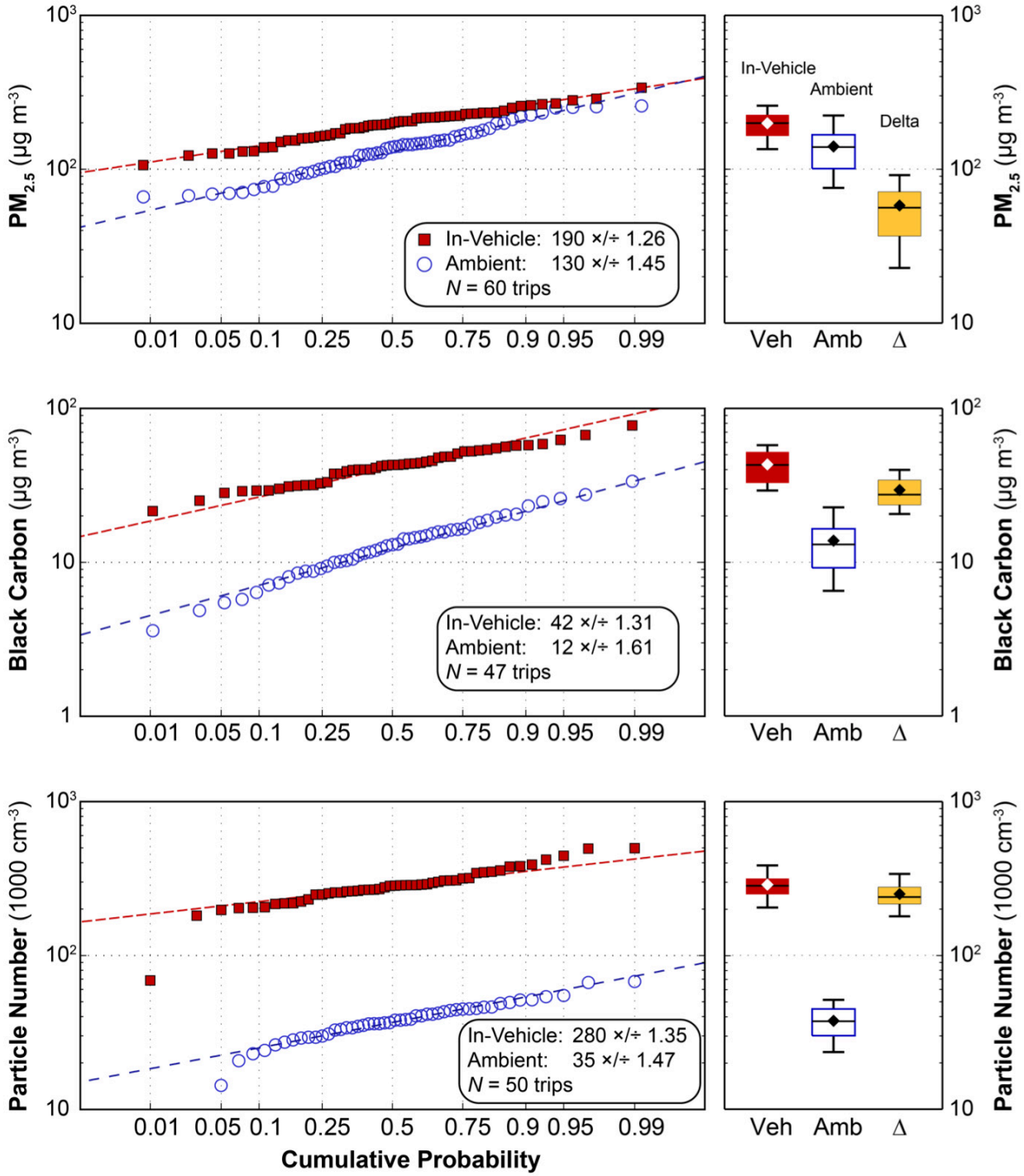

Figure 2-4. Lognormal probability plots (left) and box plots (right) for trip-averaged auto-rickshaw concentrations. For left frames, lines indicate the best-fit lognormal distribution for each microenvironment and pollutant. Text boxes report geometric mean ×/÷ geometric standard deviation for each pollutant; *N* represents the number of valid, complete trips sampled for each pollutant. Here and elsewhere, box plots display the following distributional parameters: median (central horizontal line), mean (diamond), 25th and 75th percentiles (box), and 10th and 90th percentile (whiskers). Incremental in-vehicle concentrations (Δ, "delta") are calculated as the difference between the mean in-vehicle and ambient concentration during each trip.

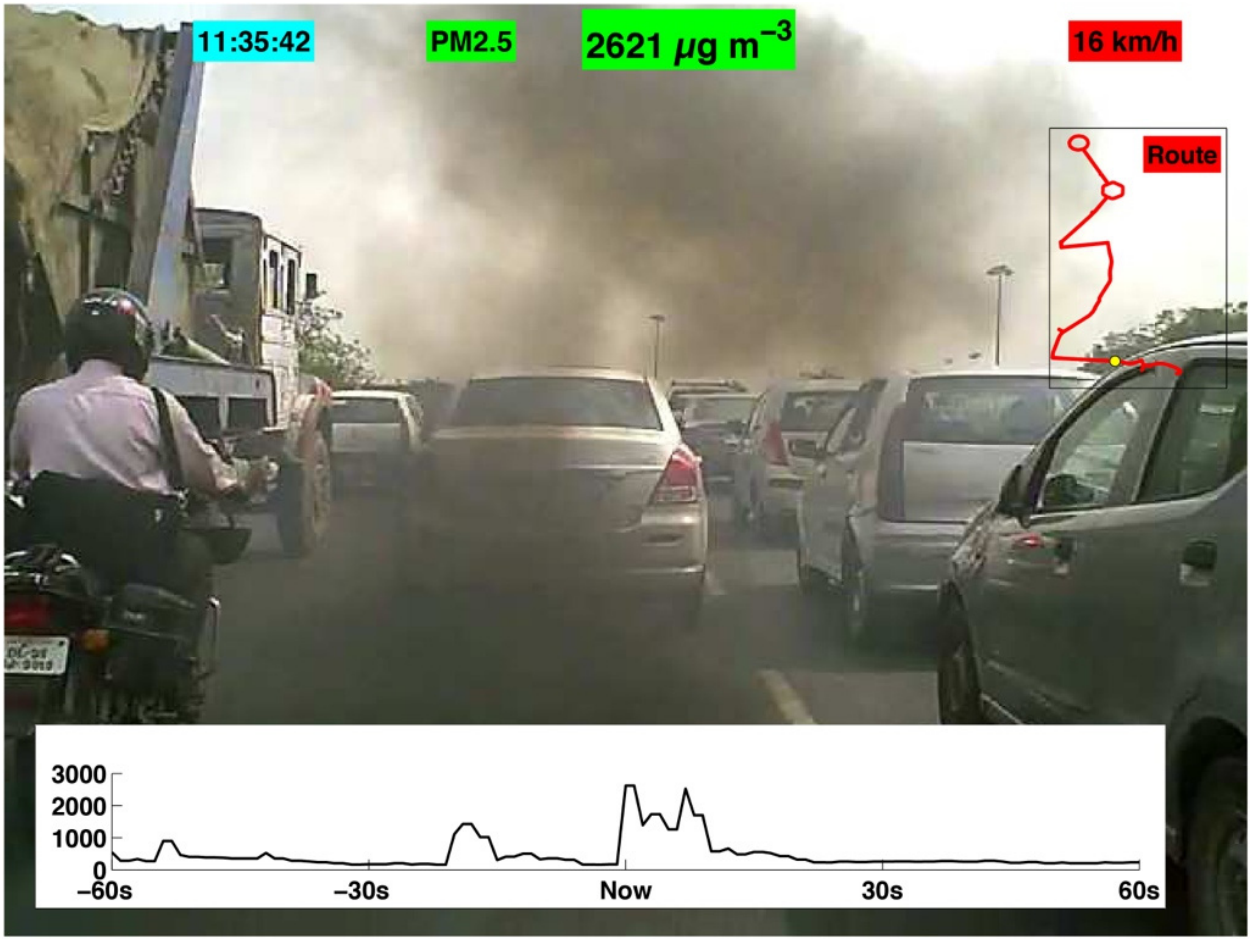

Figure 2-5. Example screen capture from auto-rickshaw video camera during on-road sampling. Concentration displayed (2621 μg m^{-3}) is calibrated DustTrak $PM_{2.5}$ concentration. Time series plotted at bottom displays ± 1 minute of 1 Hz $PM_{2.5}$ data about the displayed video frame for comparison. The high in-cabin concentration is predominantly attributable to the exhaust plume of the passing garbage truck at left. This scene occurred during stop-and-go traffic at the crest of an elevated flyover ramp on New Delhi's Outer Ring Road.

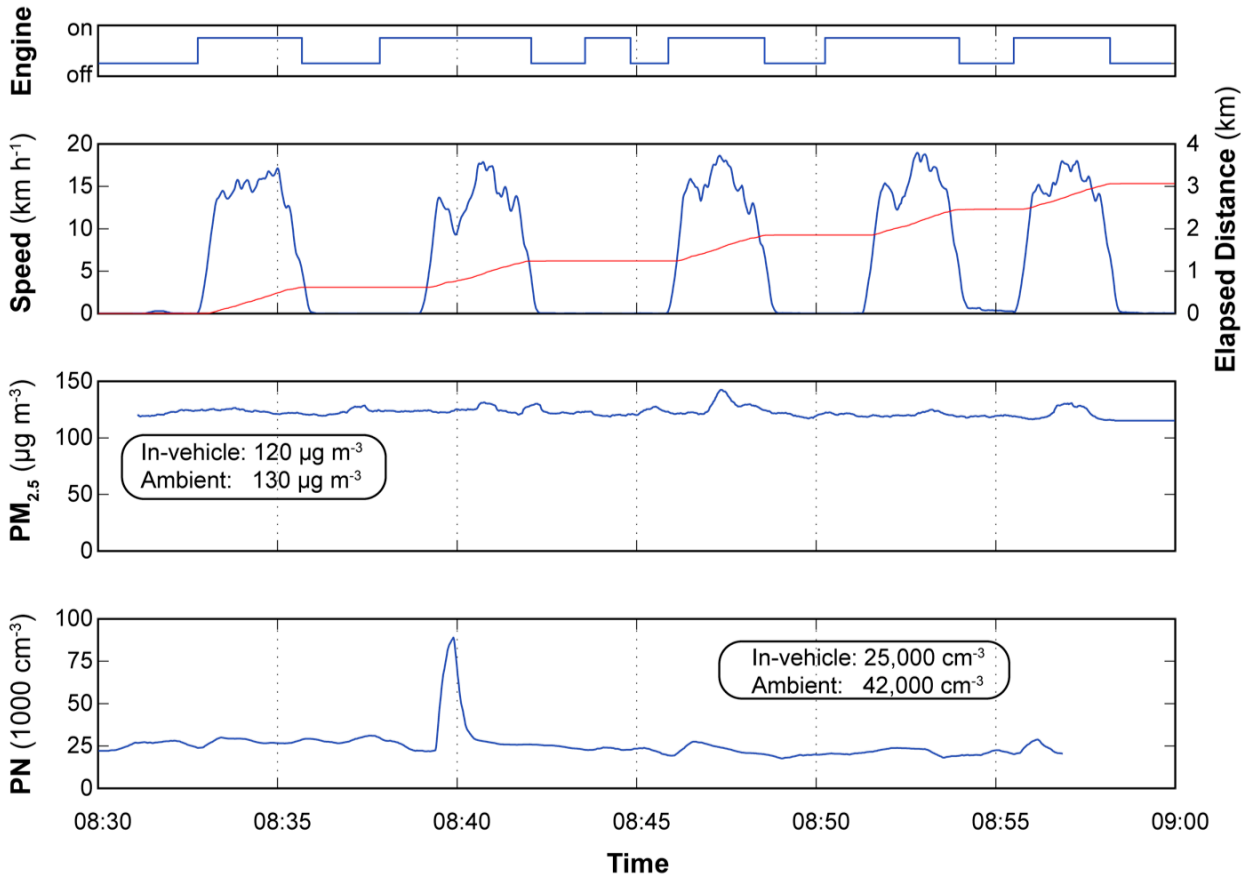

Figure 2-6. Traces of vehicle status and pollutant concentrations during an experiment to investigate potential self-pollution contribution to in-vehicle exposures. Elapsed distance (red line) indicates the cumulative distance traveled around the ~600 m sampling loop over all iterations of the test. Note the relatively low and stable pollutant concentrations inside the auto-rickshaw (compare with Figure 2-3).

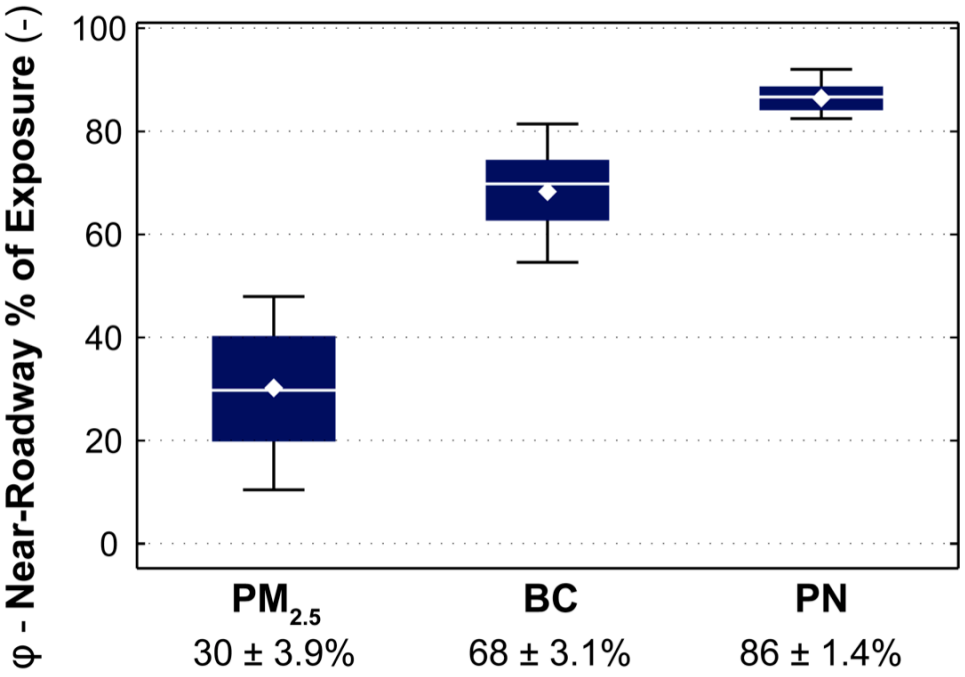

Figure 2-7. Box plots of trip-averaged in-vehicle concentration attributable to near-roadway microenvironment (φ, see text). Numbers indicate mean ± 95% confidence interval.

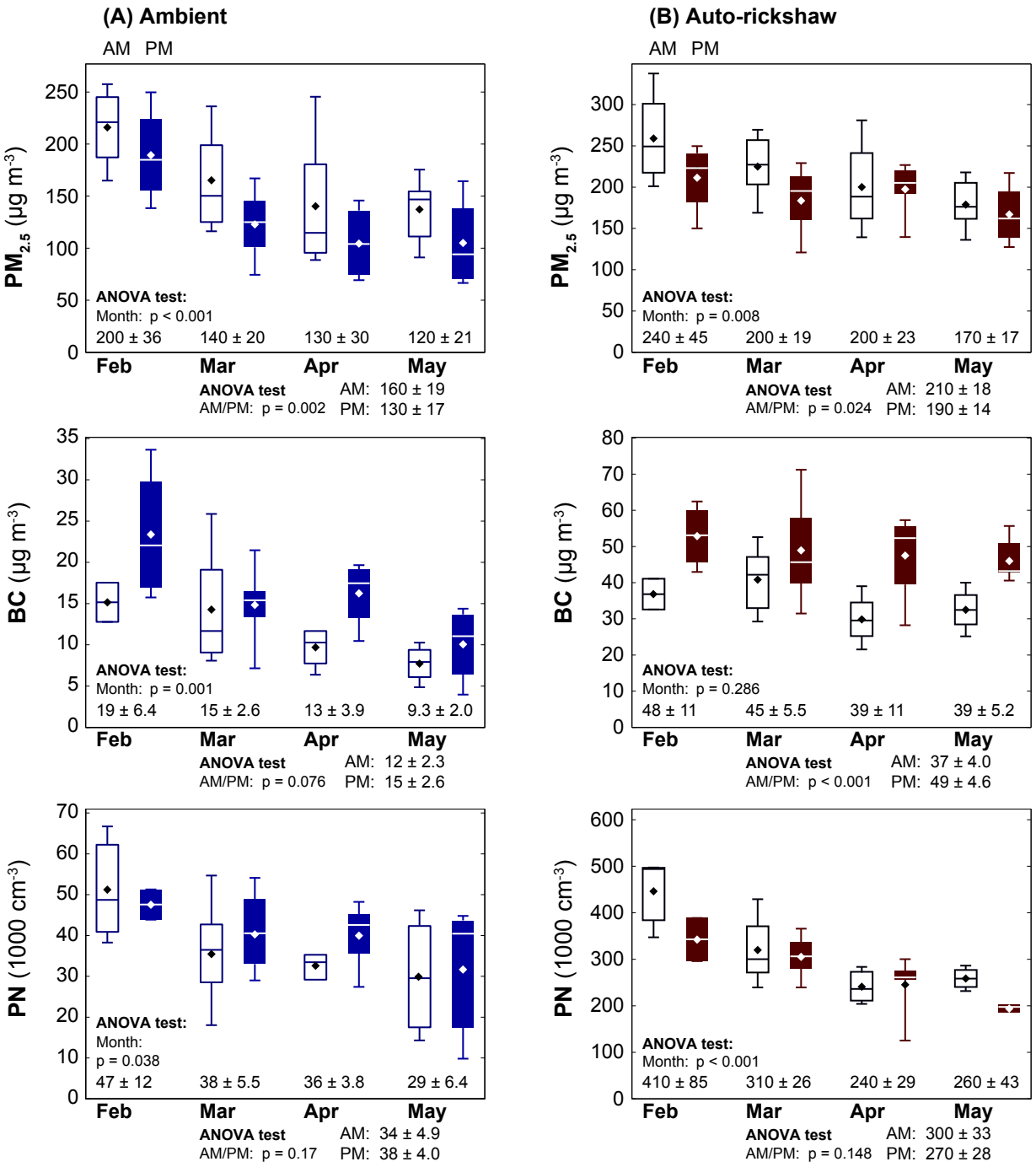

Figure 2-8. Decomposition of variability in concentrations into month-of-year and time-of-day components for ambient concentrations (A, left side) and in-vehicle measurements (B, right side). Box plots indicate the distribution of concentrations for morning and evening samples during each month of the field campaign. Arithmetic mean ± 95% CI concentrations are indicated for each month (inside frames) and separately by morning and evening sampling periods (below frames). *P*-values represent the result of unbalanced two-factor ANOVA test for effect of month and time-of-day on total concentration variability.

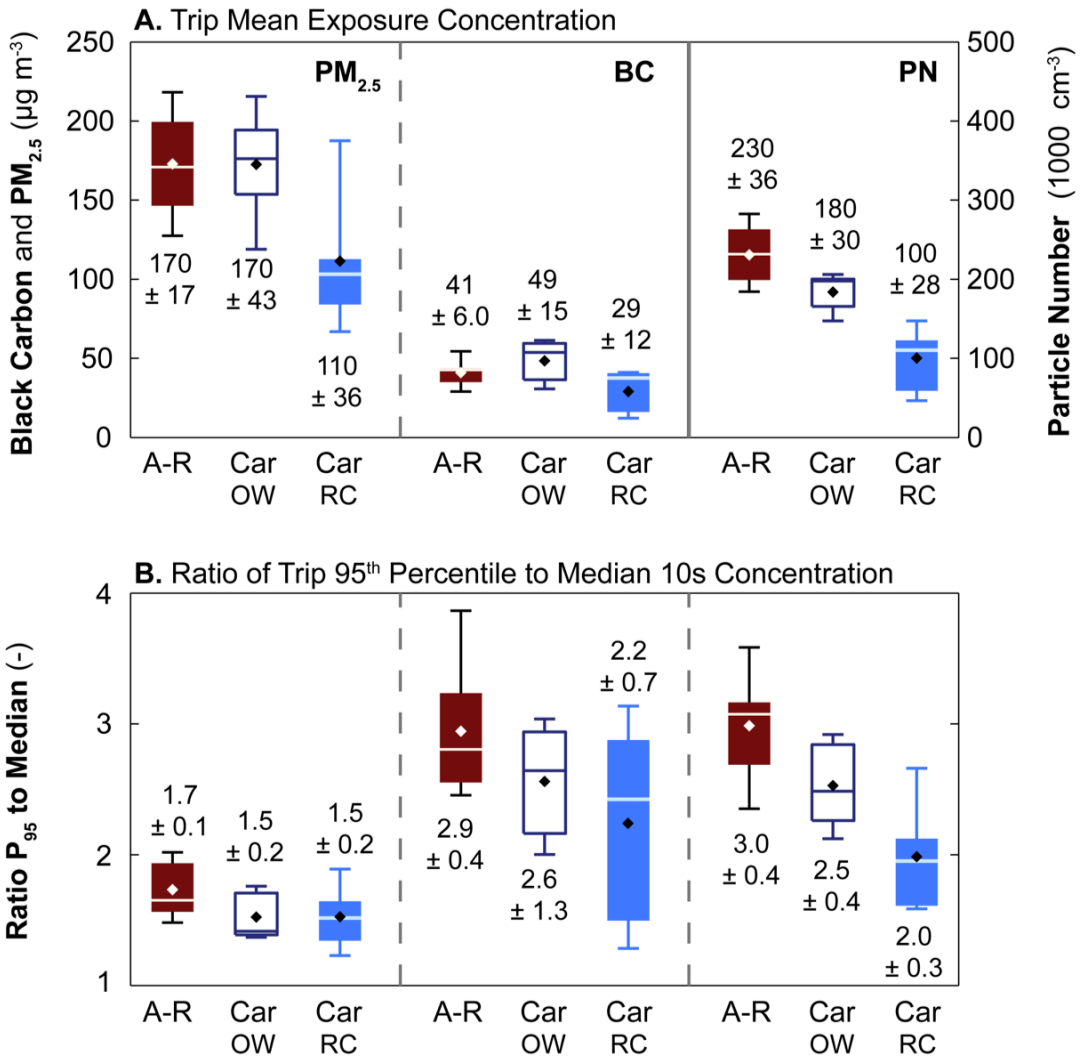

Figure 2-9. Boxplots of $PM_{2.5}$, BC, and PN in-vehicle exposure concentrations sampled in May 2010, by vehicle type, showing (A) concentrations and (B) a measure of skew (ratio of each trip's 95th percentile [P95] to median concentration based on 10-s averages of concentration). Vehicle types: A-R, auto rickshaw; Car OW, Tata Indica with windows open; Car RC, Tata Indica with windows closed, air conditioning on, and ventilation set to recirculate air. Left axis indicates PM2.5 and BC concentrations; right axis indicates PN concentration. Text displays arithmetic mean ± 95% CI. Total number of trips: auto-rickshaw (16), OW car (5), RC car (10).

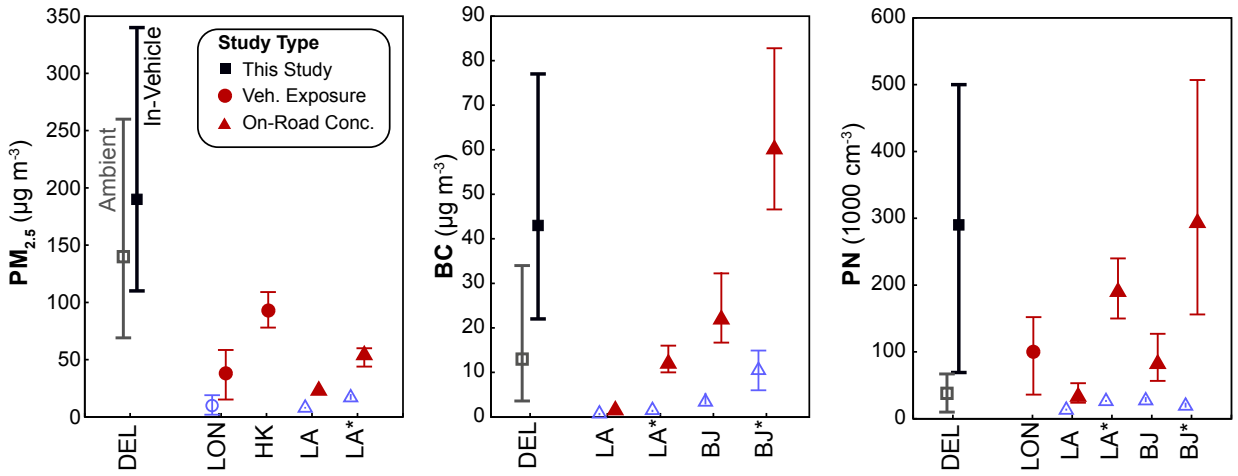

Figure 2-10. Comparison of in-vehicle (solid) and ambient (open) concentrations from this study (Delhi, DEL) and from other megacities. Whisker plots indicate means and range of observations. In-vehicle studies were for cars (London, LON; Kaur et al., 2005) and non-AC buses (Hong Kong, HK; Chan et al., 2002). Mobile on-road measurements were for Los Angeles (LA; Fruin et al., 2008) and Beijing (BJ; Westerdahl et al., 2009). Extreme conditions in these cities are plotted as LA* (freeway with extensive heavy-duty truck traffic) and BJ* (truck dominated night traffic).

Chapter 3: Global intraurban intake fractions for primary air pollutants from vehicles and other distributed sources

3.1. Introduction

Efforts to protect human populations from air pollution typically focus on reducing emissions. An essential element of air quality management therefore relates to the identification and prioritization of sources for control. The potential of an emissions source to adversely affect human health can be understood schematically to vary as function of three properties: (1) the quantity of material emitted by the source, (2) the relationship between emissions and subsequent population exposures to those materials and (3) the health effects that occur as a consequence of exposures (Marshall and Nazaroff, 2006). Since sources differ with respect to each of these properties, sources with similar emissions rates can impose markedly different public health risks (Roumasset and Smith, 1990; Smith, 1993; Tsai, 1999). Accordingly, air quality policy and risk assessment requires data and models that can link air pollutant emissions to exposures and health effects. In this chapter, I use the intake fraction metric to explore one aspect of this relationship, the linkage between emissions and subsequent inhalation intakes.

The intake fraction is a dimensionless parameter quantifies the ability of an emissions source or source category to result in population inhalation exposures. Specifically, *iF* summarizes the emissions-to-intake relationship as the fraction of emitted material that is ultimately inhaled by an exposed population (Bennett et al., 2002b). The intake fraction of emissions varies spatiotemporally and by the type of source. Key determinants of intake fraction include the size of the exposed population; proximity between people and emissions; and the environmental persistence of a pollutant (Marshall and Nazaroff, 2006).

This chapter investigates the intake fraction of emissions from urban vehicles and other ground-level, spatially distributed sources. Among the major sources of outdoor of air pollution, urban vehicle emissions have especially high intake fraction, since releases occur at ground level in close proximity to human populations (Lai et al., 2000; Evans et al., 2002; Marshall and Nazaroff, 2006). Reported *iF* values for nonreactive motor vehicle emissions include these results: 0.1 – 0.5 ppm for US rural areas (Greco et al., 2007b); 3 – 21 ppm for US cities of typical size (Evans et al., 2002; Marshall et al., 2005); and 29 – 280 ppm for three global megacities (Los Angeles, Mexico City, and Hong Kong) (Luo et al., 2010; Marshall et al., 2003; Stevens et al., 2007). An *iF* of 10 ppm (i.e., 10^{-5}) means that an exposed population inhales an aggregate increment of 10 grams per tonne emitted. For context, note that the *iF* for urban vehicle emissions typically exceeds the *iF* of central-station power plants and other tall-stack sources by roughly an order of magnitude (e.g.,Heath et al., 2006; Humbert et al., 2011).

Prior investigations of *iF* for urban vehicle emissions have emphasized conditions for North America and Europe. Determinants of *iF* such as meteorology and urban form may differ on other continents. Moreover, vehicle use is increasing rapidly in countries such as China and India for which few *iF* estimates exist (Baidya and Borken-Kleefeld, 2009; Chang et al., 2009; He et

al., 2005; Ji et al., 2012; Pucher et al., 2005). In this chapter, I model, analyze and compare *iF* data on a global basis. Specifically, I use a modeling approach to estimate intraurban *iF* values for distributed ground-level primary pollutant emissions for all worldwide cities with year-2000 population of 100,000 or more. In aggregate, this set of 3646 cities contains 2.0 billion people (for year 2000), including ~1 billion people in Asia. A goal of this study is to elucidate global patterns of intraurban *iF* among countries, regions, and cities of varying sizes. I extend a mechanistic model used in earlier studies (Stevens et al., 2007; Marshall et al., 2005) to incorporate global datasets of demographic and meteorological parameters as model inputs. This investigation is motivated by trying to better understand the exposure consequences of urban vehicle emissions. The results may be informative for any broadly distributed source of ground-level emissions to outdoor urban air.

3.2. Methods

3.2.1 Intake fraction

Intake fraction for atmospheric emissions can be evaluated as

$$\text{Intake fraction } (iF) = \frac{\text{Population intake}}{\text{Total emissions}} = \frac{\int_{T_1}^{\infty}\left(\sum_{i=1}^{P}\left(C_i(t)\times Q_i(t)\right)\right)\,\mathrm{d}t}{\int_{T_1}^{T_2} E(t)\;\mathrm{d}t}\;, \qquad [3.0]$$

where T_1 and T_2 are the starting and ending times of emissions; P is the number of people exposed; $Q_i(t)$ is the volumetric breathing rate ($m^3\ s^{-1}$) for individual i at time t; $C_i(t)$ is the incremental concentration ($g\ m^{-3}$) at time t in individual i's breathing zone that is attributable to the emissions; and, $E(t)$ is the emission rate ($g\ s^{-1}$) at time t (Marshall et al., 2003). The integrals in equation [3.0] are evaluated numerically, as detailed below. Intake fraction is a dimensionless parameter, since the numerator and denominator are both expressed in units of mass per time. Historically, a variety of similar, conceptually related formulations have been used to explore the relationship between emissions and exposures (Bennett et al., 2002b), including metrics such as the inhalation transfer factor (Lai et al., 2000), exposure efficiency (Evans et al., 2002), and exposure effectiveness (Smith, 1993).

3.2.2 Emissions – exposure concentration relationship

Model selection

Intake fractions depend on the relationship between emissions and exposure concentrations. Previous studies have employed various methods with differing levels of complexity and data requirements. Examples include one-compartment Eulerian models (Evans et al., 2002; Humbert et al., 2011; Marshall et al., 2005), Gaussian plume models (Heath and Nazaroff, 2007; Zhou et al., 2006), coarse-grid Eulerian models (Stevens et al., 2007; Tainio et al., 2009), empirical estimates using tracers of opportunity (Loh et al., 2009; Marshall et al., 2003; Ries et al., 2009; Stevens et al., 2007), and intentional tracer-gas experiments (Marshall and Behrentz, 2005).

In this paper, I designate all urban areas with population at least 100,000 as "cities." For the large number of cities considered here, an efficient approach is needed that can provide good estimates with a reasonable level of effort per city. I consider spatially distributed ground-level emissions sources (e.g., vehicles) and use a one-compartment Eulerian model. This model is employed to estimate the intraurban *iF* for emissions in each city, i.e., the *iF* associated with residents' inhalation of emissions from their city.

Compared to alternatives, there are several advantages of the one-compartment Eulerian model. (1) Input data are available globally using uniform methods. (2) Studies comparing *iF* estimated using this model have found similar results as compared with using empirical data or complex air-dispersion models (Marshall et al., 2003; Marshall et al., 2005). (3) Because this type of model is widely used (Bennett et al., 2002a; Cahill and Mackay, 2003; Stevens et al., 2005), the results reported here can be directly applied as model input parameters. (4) The one-compartment model is readily scaled in size for each location studied. Among the limitations of this approach are that (1) the model excludes within-urban variability (i.e., emissions are assumed mix uniformly throughout the urban airshed), (2) I have not evaluated *iF* for secondary pollutants or for non-conserved species with other than first-order decay, and (3) as applied here, I only consider intraurban exposures. Previous findings suggest that for estimating *iF* for individual cities, this approach is accurate within a factor of ~2 or better for primary pollutants (Marshall et al., 2003; Marshall et al., 2005; Stevens et al., 2007). I judge this accuracy to be acceptable given the efficiency of the approach; global intraurban *iF* values reported here vary by much more than a factor of 2. Chapter 4 of this dissertation addresses two of the limitations noted above through (1) consideration of regional exposures to urban emissions out to 400 km away from an urban source and (2) incorporating the dynamic partitioning behavior and atmospheric aging of semivolatile organic emissions.

One-compartment emissions-concentration model

The dynamic one-compartment Eulerian model is derived from mass-balance considerations. The model is embodied by the following equation, which I adapted from the presentation of Seinfeld and Pandis (2006) to the primary-pollutant concentration increment resulting from a given quantity of emissions:

$$\frac{\mathrm{d}C(t)}{\mathrm{d}t} = \frac{E(t)}{LWH(t)} - C(t)\left(k + \frac{u(t)}{L} + \phi\frac{1}{H(t)}\frac{\mathrm{d}H}{\mathrm{d}t}\right) \qquad [3.0]$$

Here, $C(t)$ is the incremental concentration attributable to the emissions source (g m^{-3}), which varies with time, t (seconds); $E(t)$ is the emission rate from the source under consideration (g s^{-1}); L and W are the windward and crosswind dimensions, respectively (m), of the model domain; $H(t)$ is the atmospheric mixing height (m); k is the first-order decay constant (s^{-1}); and $u(t)$ is the wind speed averaged over mixing height (m s^{-1}). The parameter ϕ accounts for dilution of contaminated urban air by clean air aloft, during periods of increasing mixing height, as follows: $\phi=0$ when $\mathrm{d}H/\mathrm{d}t$ is non-positive (H decreasing or constant), and $\phi=1$ when $\mathrm{d}H/\mathrm{d}t$ is positive (H increasing). Stevens et al. (2007) used a similar dynamic mass balance equation to estimate the *iF* of conserved pollutants. Equation [3.0] modifies that approach to incorporate pollutants that undergo first-order decay with rate constant, k. Base-case *iF* analyses are presented in this paper

for conserved, non-reactive emissions ($k = 0$). Many important vehicle-emitted species — such as carbon monoxide (CO), benzene, and primary (i.e., directly-emitted) constituents of fine particulate matter ($PM_{2.5}$), including black carbon particles — are reasonably modeled as conserved within urban areas, since $k << u/L$. Sensitivity cases are simulated for decaying pollutants with 10-h and 100-h half-lives ($k = 1.7\ d^{-1}$ and $0.17\ d^{-1}$, respectively). Example species in these classes are acetaldehyde and toluene (~10 h half life) and methyl tertiary butyl ether (MTBE, ~100 h half life) (Atkinson, 2000).

For the primary pollutants considered here, the *iF* is independent of the time-averaged emissions rate (Lai et al., 2000). Likewise, the intraurban primary-pollutant *iF* for any source is, by definition, independent of background concentrations imposed by other sources and by regional transport. Consequently, city-specific emissions and concentration data are not required as model inputs. Instead, an arbitrary emissions rate in equation [3.2] is used to simulate the urban-average concentration that results from a given unit of emissions. The results of equation [3.2] are then applied to the intake fraction relationship embodied in equation [3.1]. Two simplifying assumptions are then made to assess the attributable population inhalation intake rate $\sum_{i=1}^{P}\left(Q_i(t)\times C_i(t)\right)$ as defined in equation [3.1]. First, it is assumed that attributable personal exposure concentrations $C_i(t)$ in this summation are adequately represented on a population-average basis by the urban-average attributable concentration $C(t)$. It is further assumed that variability in instantaneous exposure concentrations among individuals is not substantially correlated with variability among individuals in instantaneous breathing rates. These two assumptions allow the above summation to be simplified to $C(t)\times\sum_{i=1}^{P}\left(Q_i(t)\right)$, thereby obviating the need to model inhalation intakes at the individual level. Sensitivity analyses (§3.3.3) consider the possible effect on *iF* of systematic variation among microenvironments in the relationship between personal-average incremental exposure concentrations $C_i(t)$ and the urban-average incremental exposure concentration $C(t)$.

In implementation, equation [3.0] is converted from differential to finite-difference form, and the model simulates a series of time steps. Short time steps are employed: 7.5 minutes, for a 3-year simulation of each urban area. I assumed a constant annual-average emission rate for all cities in the dataset and specified initial and upwind boundary conditions for each city as $C = 0$. I tested the numerical integration to ensure it behaves as expected for these conditions: (1) in simple scenarios with known outcome (e.g., step-change for one input parameter), and (2) by matching inputs and outputs from Stevens et al. (2007). Discretization errors resulting from numerical integration of equation [3.0] are estimated to be less than 1%.

3.2.3 Model input data

Meteorological data

I acquired location-specific and time-resolved mixing heights and wind speeds for years 2007-2009 from NASA's Modern-Era Retrospective Analysis for Research and Applications (MERRA) (Rienecker et al., 2011). MERRA uses the Goddard Earth Observing System (GEOS) atmospheric model to assimilate historical meteorological and climatological observations into a

global dataset with high spatiotemporal resolution (1/2º longitude × 2/3º latitude × 1 h; in mid latitudes, these values correspond to a spatial resolution of ~56 × 74 km). Each city in the dataset was matched to the nearest MERRA grid point. The median distance between the centroid of each city's urbanized land area and the corresponding MERRA grid point was 23 km (10% trimmed range: 10–34 km).

MERRA data provide wind speed at a standard 10-meter reference height. To obtain mixing-height-averaged wind speed, I employed a truncated power-law relationship (Seinfeld and Pandis, 2006; Stevens et al., 2007) for wind speed versus height. The following empirical power-law relationship represents the wind speed at a specific time ($u(z,t)$; units: m s^{-1}) as a function of height (z, units: m) (Hanna et al., 1982; Seinfeld and Pandis, 2006; Stevens et al., 2007):

$$u\left(z,t\right) = u_{\text{ref}}(t) \times \left(\frac{z}{H_{\text{ref}}}\right)^{p} \quad \text{for } z \le H_{\max} \qquad [3.1]$$

$$u\left(z,t\right) = \text{constant} = u_{\text{ref}}(t) \times \left(\frac{H_{\max}}{H_{\text{ref}}}\right)^{p} \quad \text{for } z > H_{\max} \qquad [3.2]$$

Here, $u_{\text{ref}}(t)$ is the wind speed (m s^{-1}) at the reference height at a specific time, H_{ref} is the reference height (10 m), $H_{\max}$ is the cutoff height (m) above which wind speed is assumed constant, and p is an empirical constant (dimensionless) that can vary with surface roughness and atmospheric stability. I use 200 m as the cutoff height (Hanna et al., 1982) and $p = 0.32$, which is an appropriate value for neutrally stable conditions in urban areas (Heath, 2006; Irwin, 1979; Seinfeld and Pandis, 2006). In sensitivity analyses, I consider alternate values for the cutoff height ($H_{\max}$ = 100 m, ∞) and the wind profile exponent (p = 0.25, 0.37, which covers a range of stability conditions). The following integral relation describes the time-dependent mixing-depth averaged wind speed $u(t)$:

$$u(t) = \frac{1}{H(t)} \int_{0}^{H(t)} u\left(z,t\right) dz \qquad [3.3]$$

Substituting equations [3.1] and [3.2] into equation [3.3], the following analytic solutions are obtained:

$$u(t) = \frac{u_{\text{ref}}(t)}{p+1}\left(\frac{H(t)}{H_{ref}}\right)^{p} \quad \text{for } z \le H_{\max} \qquad [3.4]$$

$$u(t) = \frac{H_{\max}\left[\frac{u_{\text{ref}}(t)}{p+1}\left(\frac{H_{\max}}{H_{ref}}\right)^{p}\right] + \left(H(t) - H_{\max}\right)\left[u_{\text{ref}}(t)\left(\frac{H_{\max}}{H_{ref}}\right)^{p}\right]}{H(t)} \quad \text{for } z > H_{\max} \qquad [3.5]$$

Breathing rate

Volumetric breathing rates for populations follow diurnal patterns, owing to variations in levels of physical activity and in physiological processes (e.g., circadian rhythm) (Stephenson et al., 2000; US EPA, 2009a; US EPA, 2009b). Few datasets are available to characterize the temporal pattern of breathing rate for large urban populations. Here, I develop a diurnal profile using time-activity data from a large probability-based sample of the US population (Klepeis et al., 2001) and activity-dependent inhalation rates (US EPA, 2009a; US EPA, 2009b) (see Appendix B). Note that this time-dependent treatment of breathing contrasts with some other intake fraction analyses (e.g., Stevens et al., 2007; Greco et al., 2007a), where the population inhalation rate is treated as a time-invariant multiplier in Equation [3.0].

Relative to the time-integrated mean, the diurnal profile varies from 47% lower (0300 h – 0400 h) to 33% higher (at 1500 h). For base-case and sensitivity analyses, the time-integrated mean breathing rate was taken to be 14.5 m^3 $person^{-1}$ d^{-1}, consistent with long-term average inhalation rates recommended by the US Environmental Protection Agency (USEPA) (US EPA, 2009b). This metabolically derived value is comparable to those used in other recent *iF* analyses (range: 13 – 14.5 m^3 $person^{-1}$ d^{-1}) (Humbert et al., 2011; Luo et al., 2010; Ries et al., 2009), and lower than the upper-bound breathing rate value of 20 m^3 $person^{-1}$ d^{-1} employed in some studies (Greco et al., 2007b; Stevens et al., 2007). To test the sensitivity of the results to the inferred time-pattern of population breathing, I considered four alternative patterns (Figure 3-1): constant; a sinusoidal daily cycle (amplitude: ±25% of the mean) (Stephenson et al., 2000); and two previously-published profiles for the USA (Marshall et al., 2003; Marshall et al., 2006).

Data for each urban area

I estimated intake fractions for the 3646 worldwide urban areas that each had at least 100,000 inhabitants in year 2000, utilizing a dataset compiled by Angel et al. (Angel et al., 2010; Angel et al., 2011). The total population in this dataset (2.0 billion) accounts for 71% of the total year-2000 global urban population, and 32% of global population (Angel et al., 2011). The following information is available for each city: population, land area (A, units: km^2, derived from satellite data (Schneider et al., 2009)) and location (latitude and longitude). In cases where a contiguous urbanized area spans several administrative units (e.g., for "conurbations" or "urban agglomerations"), this database generally provides a single population and land area estimate for the urban portion of the entire metropolitan region. To my knowledge, this database contains the most consistent and comprehensive global set of urban population and land area data available (Potere et al., 2009). Each city is idealized as occupying a square-plan urban footprint ($L = W = A^{0.5}$), so that urban ventilation is independent of variation in the wind direction. I consider variations in the aspect ratio, $\alpha = L/W$, as a sensitivity parameter.

Emissions profile

Since concentrations of primary nonreactive or first-order decaying pollutants scale linearly with emissions, intake fractions are independent of emission rates that are constant. However, because breathing rates and meteorology vary systematically, diurnal emission rate patterns can influence the intake fraction. For base-case analyses, I developed an "archetypal" diurnal

emissions profile based on mobile source emission inventories for Beijing, China (Huo et al., 2009), Mexico City, Mexico (Stevens et al., 2007), and New Delhi, India (Guttikunda, 2011).

Diurnal profiles of vehicle emissions depend on temporal patterns in the activity and composition of a vehicle fleet. Moreover, emissions profiles vary among cities and pollutants. Detailed data on the diurnal timing of vehicle emissions are not available for a large sample of global cities. However, some commonalities among the emissions profiles should be expected. First, vehicle activity (vehicle-km h^{-1}) is typically greatest during daytime hours. Second, especially in large cities, the relative abundance of heavy-duty vehicles (HDV) is often higher at night, owing to traffic conditions, logistics considerations or local regulations (Sathaye et al., 2010; Westerdahl et al., 2009; Guttikunda, 2011). For many pollutants (e.g., $PM_{2.5}$), HDV have higher emissions factors (g emission per vehicle-km) than do light-duty vehicles (LDV). Accordingly, the diurnal profile of emissions from all vehicle classes may be less variable than the diurnal profile of vehicle activity.

Each simulation utilized a single diurnal profile. I did not account for weekday – weekend differences in the timing of emissions or breathing rates. The base-case emissions profile is defined as the average of the diurnal profiles (dimensionless, relative emissions per hour) for Mexico City, Mexico ($PM_{2.5}$, all mobile sources), New Delhi, India (CO, all mobile sources), and Beijing, China (CO, LDV) (Guttikunda, 2011; Huo et al., 2009; Stevens et al., 2007). Sensitivity of results to the choice of diurnal profile was tested using the following alternative cases (Fig 3-2): (a) time-invariant emissions ("flat"), (b) individual diurnal profiles from the above cities, and (c) diurnal vehicle activity data (LDV+HDV vehicle km h^{-1}) from the US EPA National Emissions Inventory ("USA NEI") (US EPA, 2011). Among all profiles considered, the "flat" and New Delhi emissions profiles have the highest relative emissions during nighttime and lowest relative emissions during daytime, while the reverse is true for the USA NEI activity dataset.

3.2.4 Steady-state intake fraction

As a complement to the time-dependent numerical solution described above, I illustrate here an approximate analytical solution that aids in conceptual interpretation of the results. Substituting the steady-state solution for equation [3.0] into equation [3.0] yields the following relationship for the *iF* of a conserved species in a square-plan urban area (Evans et al., 2002; Lai et al., 2000; Marshall et al., 2005):

$$iF \sim \overline{Q_i} \times \left(P/\sqrt{A} \right) \times \left(\overline{1/uH} \right) = \overline{Q_i} \times LPD \times DR^{-1} \sim \frac{\text{Population breathing rate}}{\text{Urban ventilation rate}} \qquad [3.5]$$

This relationship can be decomposed into three parameter groups that provide insight into the key drivers of *iF* (Marshall et al., 2005). The first term, $\overline{Q_i}$, is the time-averaged per-capita mean breathing rate (units: $m^3\ s^{-1}\ person^{-1}$). The second group, linear population density (*LPD* = $P/\sqrt{A}$, units: persons m^{-1}), is a property of a city's urban form that represents the mean population per unit length (in the windward direction) of urbanized land (Marshall, 2007;

Marshall et al., 2005). The final parameter group, normalized dilution rate (DR) $= \left(\overline{1/uH}\right)^{-1}$, characterizes atmospheric dilution (wind speed times mixing height; units: $m^2\ s^{-1}$) (Marshall et al., 2005). For each city, *DR* is computed as the long-term harmonic mean of the product of linearly interpolated hourly values of *u* and *H*. The ratio *DR*/*LPD* can be intuitively understood as an effective per-capita atmospheric dilution rate available for an urban area. The intraurban intake fraction is proportional to the ratio of the population breathing rate to this per-capita atmospheric dilution rate ($iF \sim \overline{Q_i} \times [DR / LPD]^{-1}$).

3.3. Results and discussion

3.3.1 Global and regional summary of intake fraction

Table 3-1 presents summary metrics of population-weighted and unweighted distributions of *iF* values. Among all cities, the population-weighted mean intraurban *iF* for distributed ground-level emissions of conserved pollutants is 39 ppm (IQR: 14 - 52 ppm). Population-weighted results are computed by weighting each city's *iF* by its population (i.e., equal weight per person), whereas unweighted results treat each city as a distinct unit with equal weight (Marshall et al., 2005). Because *iF* is correlated with population, weighted metrics better reflect the distribution of *iF* over the global population of city inhabitants. For the remainder of this chapter, I employ population-weighted metrics of *iF* unless stated otherwise. All reported results reflect the full numerical solution to the *iF* model as outlined in 3.2.2.

Intake fraction varies over almost three orders of magnitude among all cities (full range: 0.6 - 260 ppm; 10%-trimmed range: 7.7 – 80 ppm). The population-weighted distribution of *iF* conforms well to a lognormal form (geometric mean, GM: 26 ppm, geometric standard deviation, GSD: 2.5, Figure 3-3). Respectively 530, 260 and 120 million people live in cities with *iF* values greater than 50 ppm, 75 ppm, and 100 ppm.

Reduced-form model for intake fraction

Variation in *iF* among cities is predicted well by a parsimonious regression model using this three-parameter fit:

$$iF = 74.0\ \text{ppm} \times (LPD)^{0.980} \times (DR)^{-0.876} \times (A)^{-0.0497} \qquad [3.5]$$

where *LPD* is specified in units of m^{-1}, *DR* is given in $m^2\ s^{-1}$, and *A* is specified in m^2. This regression can be used with reasonable accuracy to rapidly estimate *iF* for any city in the global dataset ($r^2 = 0.99$, root-mean-square prediction error 9%). In addition, the reduced-form model provides a framework for understanding how variation in *iF* is governed by urban form and meteorology. Globally, *LPD* is more variable than is *DR* (interquartile ranges are 57 – 220 persons m^{-1} for *LPD* and 370 – 550 $m^2\ s^{-1}$ for *DR*). Holding other variables constant, an IQR increase in linear population density results in a 3.8× increase in *iF*, while an IQR reduction in normalized dilution rate results in only a 42% increase in *iF*.

Patterns of intake fraction by city size, world region, and country

Larger cities tend to have higher *iF* values (Figure 3-4, Table 3-2). To illustrate, I divide the city dataset into three population-based groupings of nearly equal total population: small cities with between 100,000 and 600,000 inhabitants (32% of total city population), medium cities with 600,000 - 3 million inhabitants (34%), and large cities with > 3 million inhabitants (34%). Population-weighted mean intraurban *iF* for these three groupings are, respectively, 15, 35, and 65 ppm. Variation in *iF* by city size is principally attributable to the strong correlation between *LPD* and urban population. On average, each 1% increase in city population is associated with a 0.57% increase in *LPD* ($r^2 = 0.62$). Interestingly, *LPD* is much more variable among the three different city size groupings than is population density (mean *LPD*: 50, 130, 310 persons m^{-1}; mean density: 110, 150, 120 persons m^{-2}). The dilution rate (*DR*) is uncorrelated with population ($r^2 = 0.013$).

Intake fractions differ substantially among geographic regions (Table 3-3, Figures 3-4, 3-5, and 3-6). Following Angel et al. (Angel et al., 2010; Angel et al., 2011), I group the world into nine clusters that reflect varying land-use patterns (Figure 3-5). Among these regions, mean intraurban *iF* varies by 2.7× (Table 3-3). Regions with especially high mean intraurban *iF* values include South and Central Asia (SCA, mean: 55 ppm), Southeast Asia (SEA, 48 ppm), East Asia and the Pacific (EAP, 44 ppm), and sub-Saharan Africa (SSA, 43 ppm). By contrast, the intraurban *iF* is comparatively low for land-rich developed countries (LRD, 20 ppm). Comparing Asia with North and Central America highlights regional properties of urban settlement (Figure 3-4). The Asian cities mapped in Figure 3-6B have high mean intraurban *iF* (48 ppm) and large total population (914 million, ~45% of all global city inhabitants). Of all cities with intraurban *iF* ≥ 100 ppm ($n = 24$ cities), 75% ($n = 18$) are in Asia and 50% ($n = 12$) are in China. For the cities in North and Central America mapped in Figure 3-6A, the overall mean *iF* is 33 ppm. Mean *iF* is especially low for US and Canadian cities (respectively 21 ppm and 20 ppm) where cities have especially low population density, and higher in Mexico (65 ppm) and Colombia (75 ppm).

Regional patterns of *iF* are independent of city size, such that similar trends in *iF* emerge within each of the small, medium and large city groupings (Figure 3-4). As a result, *iF* for smaller cities in some regions may be greater than those for more populous cities elsewhere. For example, the mean *iF* for small cities in the East Asia and Pacific region (EAP, 22 ppm) is greater than that for medium cities in land-rich developed countries (LRD, 15 ppm).

Country-average intraurban *iF* varies by more than a factor of three among the ten countries with the largest urban populations (Table 3-4). Mean intraurban *iF* values in Mexico (65 ppm), Indonesia (53 ppm), India (51 ppm), Japan (50 ppm), South Korea (46 ppm) and China (44 ppm) are greater than in Indonesia (40 ppm), Russia (32 ppm), Germany (30 ppm) and the United States. Table 3-5 provides a database of population-weighted mean intraurban *iF* values for all countries considered here.

Regional variation in *iF* is attributable to urban form and meteorology (Table 3-3). For example, the high mean *iF* value in South and Central Asia (41% greater than global mean) is attributable to high *LPD* (37% greater than global mean) and weaker-than-average dilution (*DR* 9% below global mean). Similarly, relatively low *iF* in land-rich developed countries (47% lower than global mean) is explained by low *LPD* (36% lower than global mean) and more

favorable atmospheric dilution (*DR* 11% greater than global mean). The range in *LPD* among the nine regions is roughly twice as large as the range for *DR* (Table 3-3). However, local patterns in wind speed and mixing height give rise to apparent "hotspots" where meteorology has a more pronounced role influencing *iF*. For example, *DR* is ~30-60% lower than the global average in the Indo-Gangetic Plain (Pakistan; northern India; Bangladesh) and in heavily forested equatorial regions (Amazon and Congo River basins; parts of Indonesia). Globally, spatial variation in long-term *DR* depends more on variation in wind speed than on variation in mixing height.

Megacities

The air quality challenge of megacities (population > 10 million) has received considerable attention (Butler et al., 2008; Chan and Yao, 2008; Gurjar et al., 2008; Gurjar and Lelieveld, 2005; Guttikunda et al., 2005; Mage et al., 1996; Molina and Molina, 2004; Parrish and Zhu, 2009; Wang et al., 2010). The 20 megacities in this dataset account for ~15% of total city population (300 million people) and have population-weighted mean *iF* of 83 ppm (IQR: 48 – 94 ppm; range: 25 - 260 ppm). Four megacities have intake fractions that exceed 100 ppm: New Delhi, India; Kolkata, India; Dhaka, Bangladesh; and Mexico City, Mexico (Figure 3-6, Table 3-6). Although overall population density for megacities is nearly the same as the global mean for cities of all sizes (mean: 125 persons ha^{-1}), the *LPD* in megacities is 2.5× the global urban average (410 [megacities] versus 170 [global average]; units: persons m^{-1}), owing to megacities' large spatial extent (mean area: 2300 km^2).

The total intraurban population intake ($E \times iF$) of emissions in megacities may be especially high. Megacities have been identified elsewhere as emissions "hotspots" (Butler et al., 2008; Guttikunda et al., 2005; Parrish and Zhu, 2009). High *iF* in megacities magnifies the exposure relevance of these emissions. For example, consider a hypothetical pollutant emitted on an equal per-capita basis everywhere. For that pollutant, a city's total intraurban intake would scale with the product of population and *iF*. Under such conditions, the world's 20 megacities would themselves account for 32% of global intraurban intake, or more than double the 15% of the global city population that they contain.

Time-of-day and seasonal patterns in iF

Diurnal trends in atmospheric mixing and population breathing rate lead to variability in *iF* as a function of emissions timing. In general, *iF* is elevated for emissions that occur during periods of weak atmospheric dispersion (e.g., nighttime, Figure 3-7). Considering all cities, the median *iF* for emissions at night (2100 h – 0300 h) is 8.5× greater (IQR: 5.1 - 11×) than for emissions during the day (0900 h – 1500 h). The strong role of atmospheric mixing in driving nighttime maxima in *iF* is highlighted when considering that the model accounts for higher-than-average population breathing rates during daytime hours. Interestingly, diurnal cycles in mixing height are principally responsible for the temporal pattern in a city's short-term *DR*, in contrast to the observation that regional variation in long-term *DR* is primarily attributable to between-city differences in mean wind speed.

Compared to diurnal variability, monthly differences in *iF* are less pronounced. The median ratio of maximum to minimum month-averaged *iF* among all cities is 2.3 (IQR: 1.8 – 2.9). On average, *iF* values in non-tropical cities are 13× greater (IQR: 9.1 - 15×) during winter nights

than summer days (Figure 3-8). Interannual variability in meteorology for the three years considered in this study (2007 – 2009) has negligible (< 1%) effect on global mean *iF* and also little effect on *iF* values for individual cities (10% trimmed range: ~±5%).

City ventilation and per-capita dilution rate

A fundamental determinant of the intake fraction for urban emissions is the degree to which pollutants can be diluted or removed before they are inhaled. A simple illustration of this competition between dilution and inhalation is embodied in the intake fraction for indoor emissions of an inert pollutant, which can be expressed as the ratio of occupants' inhalation rate to the building ventilation rate (Nazaroff, 2006). In an analogous sense, urban environments can be understood as a conceptual extension of other naturally ventilated built environments (e.g., Yang and Li, 2009). City ventilation processes are complex and occur at multiple scales (Britter and Hanna, 2003). The parameter (*DR* / *LPD*) usefully characterizes one aspect of urban-scale city ventilation, the effective per-capita atmospheric dilution rate available for an urban area. Intake fraction is inversely proportional to this per-capita dilution metric.

Table 3-7 provides estimates of (*DR* / *LPD*) disaggregated by region and city size. Globally, the annual mean value of this dilution metric is 7.2 $m^3\ s^{-1}\ person^{-1}$. For scale, consider that typical urban ventilation is rapid compared to building ventilation (~10^{-2} $m^3\ s^{-1}\ person^{-1}$), which explains the lower overall intake fraction of emissions for outdoor releases. Owing to geometric considerations (urbanized land area to perimeter length), small cities experience substantially higher per-capita ventilation than medium or large cities. Global population-weighted mean values of the (*DR* / *LPD*) metric are respectively 14, 5.7, and 2.4 $m^3\ s^{-1}\ person^{-1}$ for small, medium, and large cities. This ventilation metric also varies regionally as a function of urban form and meteorology. For example, the population-weighted mean per-capita ventilation rate is high for cities in land-rich developed countries (~11 $m^3\ s^{-1}\ person^{-1}$) and low for cities in East Asia (~5 $m^3\ s^{-1}\ person^{-1}$). It is interesting to note that the trends in per-capita dilution by region and city size very closely track the patterns in *iF* (i.e., Table 3-2), but not perfectly so. The reason for this imperfect correlation is that (*DR* / *LPD*) values are estimated using the long-term harmonic mean of meteorological data for each city. In contrast, *iF* calculations incorporate time-dependent emissions and breathing patterns and account for non-steady state dilution conditions.

3.3.2 Validation and comparison with prior research

Several previous studies have estimated *iF* of urban vehicle emissions for individual cities, countries or regions, principally in North America and Europe. For large groups of cities with diverse population sizes, prior estimates of population-weighted average *iF* for vehicle emissions are in the range of ~5 – 20 ppm (Greco et al., 2007b; Marshall et al., 2005; Taimisto et al., 2011; Tainio et al., 2009), with higher *iF* values reported for individual large cities (e.g., Mexico City, Hong Kong, Los Angeles) (Loh et al., 2009; Luo et al., 2010; Marshall et al., 2003; Stevens et al., 2007). The higher population-weighed mean *iF* result obtained here (39 ppm) is substantially attributable to the inclusion for the first time of many cities in Africa, Asia, and South America, which tend to have higher *LPD* than urban areas elsewhere (Table 3-3). This study's core result — a global population-weighted mean intraurban *iF* of 39 ppm — is approximately consistent

with the estimated "archetypal" *iF* by Humbert et al. (49 ppm, breathing-rate adjusted) for ground-level emissions (Humbert et al., 2011).

Model results for individual cities and countries compare favorably with those of previous studies after adjusting for differences in breathing rate. Overall, agreement is stronger for groups of cities (e.g., national averages of cities) than for individual urban areas. For example, my estimate for population-weighted mean intraurban *iF* for the 243 US cities with population ≥ 100,000 (21 ppm) is similar to the estimate of Marshall et al. (2005) for US Census "Urban Areas" (17 ppm, breathing-rate adjusted). Two other US studies report lower mean *iF* values. For ground-level emissions and considering inhalation intakes within 50 km of the source, Lobscheid et al. report a nationwide population-weighted mean *iF* = 8.6 ppm (Lobscheid et al., 2012). For counties in metropolitan areas with at least 1 million inhabitants, that study reports population weighted mean *iF* = 14.0 ppm. In a study of intake fractions for 3080 US counties, Greco et al. found emissions-weighted mean *iF* = 2.5 ppm for primary $PM_{2.5}$ emissions (Greco et al., 2007b). However, the spatially coarse county-level exposure model employed in that study is likely to underestimate *iF* for urban emissions.

The present estimate for metropolitan Los Angeles (43 ppm) is consistent with an empirically derived *iF* estimate for the South Coast Air Basin (38 ppm, breathing-rate adjusted) (Marshall et al., 2003). Results for Mexico City and Hong Kong – two cities with notoriously complex terrain – each differ from prior empirical estimates by ~50%, but in opposite directions. For Mexico City, my estimate (140 ppm) is ~60% larger than that of Stevens et al. (87 ppm, breathing-rate adjusted) (Stevens et al., 2007). In contrast, the estimate for Hong Kong (110 ppm) is ~40% lower than the value estimated by Luo et al. (190 ppm, breathing-rate adjusted) (Luo et al., 2010). I obtain more closely comparable *iF* estimates for these two cities (to within ~± 30%) after harmonizing demographic input parameters, which can vary substantially among studies of megacities (Forstall et al., 2009). Overall, results are consistent with an expectation of better than 2× uncertainty in *iF* values for individual cities estimated using the single-compartment Eulerian model.

While beyond the scope of the present study, further empirical validation of urban *iF* results is warranted. For example, emissions and concentration data for opportunistic tracer pollutants have already been used to develop semi-empirical *iF* estimates in several worldwide urban areas; for motor vehicles, example tracer species include CO, benzene, and diesel $PM_{2.5}$ (Loh et al., 2009; Luo et al., 2010; Marshall et al., 2003; Ries et al., 2009; Stevens et al., 2007). Recent improvements in global emissions datasets and satellite remote sensing techniques may permit more extensive use of empirical methods for assessing intake fractions in the future as a complement to the modeling approach employed here.

3.3.3 Sensitivity analysis and limitations

I tested the sensitivity of results to many assumptions and modeling decisions that were necessary to assess *iF* at a global scale. Based on comparison with previous work (§3.3.2), I estimate that overall uncertainty for the aggregated (many-city) *iF* estimates is ~30%.

Base-case analyses evaluate *iF* for nonreactive primary pollutants ($k = 0$). For non-conserved pollutants that follow first-order decay (half-life: 100 h, 10 h), mean *iF* is, respectively, only

0.8% and 7.2% lower than for conserved, non-reactive pollutants. The effect of decay was somewhat larger for large cities (11% for 10-h half-life), owing to the longer residence time of air in cities with greater length scale. Nevertheless, the global patterns of *iF* with respect to region and city size are similar for all 3 pollutant classes considered. Since the half-life for many health-relevant primary pollutants in urban air is larger than 10 h (Atkinson, 2000), these findings imply that *iF* values for nonreactive pollutants may be reasonably applied to many toxic emissions to urban outdoor air. However, the *iF* values reported here may not be applicable to pollutants formed via secondary processes. For example, prior research indicates that intraurban *iF* may be 1-2 orders of magnitude lower for secondary inorganic $PM_{2.5}$ (i.e., nitrate and sulfate aerosols) attributable to urban precursor emissions than for primary $PM_{2.5}$ (Evans et al., 2002; Greco et al., 2007b; Humbert et al., 2011).

In general, results are relatively insensitive to most of the assumptions that I made in pre-processing meteorological parameters (§3.2.3, Table 3-8). However, results for time-averaged *iF* are moderately sensitive to assumptions that relate to transient conditions of poor atmospheric mixing (e.g., during nights with low wind speeds). For example, global mean *iF* is 35% lower in a sensitivity scenario under which urban mixing height is constrained to be at least 100 m at all times. Since dispersion is generally weak at nights, alternative scenarios with higher emissions (E) or breathing rate (Q) at night result in higher *iF* values. Mean *iF* varies by 5 – 15% under a range of plausible assumptions about the diurnal pattern of E and Q (Table 3-9). Refined model inputs for nighttime conditions may improve the accuracy of *iF* estimates in future studies.

An important modeling simplification relates to the aspect ratio, α, the ratio of an urban area's windward to crosswind dimensions (§3.2.3). In the default modeling case, I assume square-plan layout ($\alpha = 1$), as α is not readily estimated for cities in this dataset. In general, *iF* is expected to increase for situations where $\alpha > 1$ (less ventilation per unit land area), with the opposite true for $\alpha < 1$. The intake fraction for individual cities increased (decreased) by ~30% for sensitivity cases in which $\alpha = 2$ ($\alpha = 0.5$). More detailed information on α may therefore improve the precision of *iF* estimates for individual cities. However, additional information on aspect ratio may not improve the accuracy of the mean *iF* estimates for large groupings of cities if the main axis direction of a cities are in general uncorrelated with the mean wind direction.

The modeling approach employed here has limitations. The one-compartment model does not account for within-urban variation in exposure concentrations or for the effects of microenvironments. To the extent that exposures disproportionately occur in near-source regions (e.g., in vehicles on roads), *iF* may be systematically underestimated by the model. Conversely, the model may overestimate *iF* when outdoor-attributable indoor exposure concentrations are attenuated from ambient levels, as is the case for $PM_{2.5}$ encountered in buildings (Riley et al., 2002). Here, I make the simplifying assumption that for emissions of primary, conserved pollutants, the population-average microenvironmental exposure concentration is adequately approximated by the urban ambient concentration attributable to those emissions. Two prior studies of vehicle-associated population intake of conserved pollutants in Southern California found this simplification to be valid to within ± ~15-30%, depending on the pollutant under consideration (Marshall et al., 2006; Marshall et al., 2003). To test this simplification. I carried out the following bounding-case analysis. Consider the sensitivity parameter ε, which represents the percentage difference between an *iF* estimated based on microenvironmental concentrations

and one estimated using a single ambient concentration. Neglecting differences in breathing rate among microenvironments, ε can be estimated as:

$$\varepsilon \sim 100 \times \left(\sum_{\mu=1}^{N} T_\mu \gamma_\mu - 1 \right) \quad [3.6]$$

Here, for one of $\mu = 1 \ldots N$ microenvironments, T_μ represents the fraction of population-time spent in that microenvironment, and γ_μ represents the ratio between the vehicle attributable concentration in that microenvironment and in the overall urban (outdoor) environment. Following Marshall et al. (2003, 2006), I consider three microenvironments: indoors, in-vehicle/near-roadway, and outdoors (not-near roadways). The microenvironmental time distribution (*T,* see Appendix B) is based on analysis of the US NHAPS database (Klepeis et al., 2001). Indoor microenvironments account for an average of 20.9 h d^{-1} of population-time (Table 3-10), with respectively 1.3 h and 1.8 h spent in transit and outdoors. Time-activity data for urban populations are approximately similar elsewhere. For example, a global meta-analysis of human activity patterns reports that populations spend ~20 – 22h indoors, 0.5-2h outdoors, and ~1.5h-2.5h in transit. (Moschandreas, 1981). More recent data from a detailed time-activity budget of 525 urban residents of Chongqing, China, indicate a mean of approximately 20.2 h spent indoors, 1.2 h in transit, and 2.7 h outdoors (Wang et al., 2008). Likewise, a similar microenvironmental time distribution was reported for the population of Hong Kong (Luo et al., 2010). Since the NHAPS time-activity data fall within the range of other reported values, I use these values for the quantitative sensitivity analyses reported below.

Distributions of γ_μ may vary as a function of pollutant dynamics and characteristics of the built environment. Indicative values of γ_μ are reported in Table 3-1 and described here. For non-reactive gaseous primary pollutants (e.g., CO, benzene), $\gamma_\mu = 1$ for indoor conditions (Marshall et al., 2003). In contrast, $PM_{2.5}$ of outdoor origin is partially removed in buildings via deposition and filtration. Particle infiltration is a strong function of building ventilation, and varies as a function of climate and regional building practices. Summarizing results over many studies, I consider an indicative range of $\gamma_\mu = 0.3 - 0.7$ for primary $PM_{2.5}$ (Hodas et al., 2012; MacNeill et al., 2012; Wallace and Williams, 2005; Marshall et al., 2006; Riley et al., 2002). Considering roadway and in-vehicle microenvironments, γ_μ is typically ~3-4 for primary pollutants of vehicular origin (Chapter 2, Marshall et al., 2003; Marshall et al., 2006). Finally, by definition, $\gamma_\mu = 1$ for the outdoor microenvironment. Two pollutant classes for γ_μ, listed as "conserved primary" and "primary $PM_{2.5}$" in Table 3-10, summarize the above data. Considering these two cases, vehicle-attributable intake may be ~16 % higher than predicted by the base-case single compartment model for nonreactive primary pollutants, and ~15-50% lower than base-case estimates for $PM_{2.5}$. I conclude that microenvironments are likely to contribute less than ~30% absolute uncertainty in results for nonreactive pollutants with high indoor penetration efficiency. However, more refined consideration of microenvironmental exposures could more strongly affect conclusions for particles and other pollutants that interact strongly with indoor environments.

A further limitation is that the model only assesses intraurban *iF*, the fraction of a city's emissions that are inhaled by that city's own inhabitants. The results exclude additional intake that may occur in other urban or rural areas downwind of the source city, and therefore may be considered a lower-bound estimate of total *iF*. Limited prior research suggests that intraurban *iF*

for ground-level emissions may reasonably approximate total *iF* in many circumstances (Greco et al., 2007b; Heath and Nazaroff, 2007). Nevertheless, the difference between intraurban and total *iF* may be important in certain cases, such as for emissions in a small urban area that is located upwind and nearby large urban areas. Chapter 4 explores this assumption in further detail, emphasizing reactive and secondary pollutants.

Since inhalation intake is an incomplete indicator of health risk, additional analyses are required to interpret *iF* results more explicitly in terms of health effects. In general, a metric of "intake-based toxicity" (*IBT*, sample units: mortality per mass intake) can be combined with *iF* to yield estimates of health effect per unit emission (Ji et al., 2012; Marshall and Nazaroff, 2002). *IBT* may vary among populations, owing to, for example, different background disease rates or non-linearity in dose-response (Smith and Peel, 2010). Likewise, similar reductions in intake may yield differential health benefits among populations with differing baseline exposure levels, susceptibility, and underlying disease burdens (Levy et al., 2009).

3.3.4 Implications for policy

Given constrained resources for environmental protection, air quality policies may seek to maximize the environmental health benefit achieved per unit cost expended. Intake fraction lends insight into one dimension of this calculus: the population intake benefit associated with a given quantity of emissions reduction. In concert with other information routinely used in air quality management and health risk assessment (e.g., source strengths, cost-of-control curves, pollutant toxicity data), it may be advantageous to prioritize emissions reductions for sources with high *iF* (Nazaroff, 2008; Roumasset and Smith, 1990; Smith, 1993; Tsai, 1999; Smith, 2002). The global average *iF* for urban vehicle emissions (39 ppm) is substantially greater than previous estimates of *iF* for central electric power stations located in California, USA (~1 ppm) or China (~10 ppm) (Heath and Nazaroff, 2007; Zhou et al., 2006), reinforcing the relative importance of vehicle emissions control. Comparing among regions, results suggest that mitigating or avoiding increases in urban vehicle emissions in countries with high *iF* (e.g., India, China, Indonesia) may yield relatively high exposure-reduction benefits per unit of emissions reduction. Moreover, as vehicle fleets in these countries tend to be high emitting and rapidly growing, the marginal costs of emissions abatement may be favorable. The exposure benefits of emissions control in megacities also appear particularly strong. Intake fraction results by season and time-of-day suggest that emissions control measures for ground-level sources with high emissions at night (e.g., trucking (Sathaye et al., 2010)) or during the winter (e.g., solid-fuel combustion for heat) (Ries et al., 2009; Taimisto et al., 2011) may yield relatively high exposure benefits per unit mitigation.

3.4 Conclusions

This chapter considers the intraurban intake fraction of for emissions of conserved, nonreactive pollutants from vehicles and other ground-level sources. I develop intake fraction estimates for a total 3646 worldwide cities accounting for more than 70% of the global urban population in year 2000. The intake fraction of urban vehicle emissions is substantially variable among cities, spanning a range of more than 100× among all world cites, with a 10% trimmed range of 7.7 – 80 ppm. Variability in intake fraction among cities is systematic. A metric of urban form, linear population density (*LPD*), is the most important predictive parameter for the

variability in *iF* observed here. Differences in meteorology account for a smaller but still substantial fraction of global variability in *iF*. Since more populous cities tend to have higher *LPD*, *iF* varies strongly as a function of population. The dense urban form of Asian cities leads to high *LPD* and thus high *iF*, while more sprawling cities in land-rich developed countries have lower *LPD* and low *iF*. These findings indicate that policies to control vehicle emissions in populous, dense cities may result in especially large exposure benefits per unit effort. Conversely, since urban vehicle usage is growing fastest in regions of the world with relatively high *iF* (e.g., China, India), the exposure implications of a failure to manage emissions are likely to be especially high.

The data presented in this chapter may be useful for life cycle assessments, health risk assessments, and other analyses concerned with the health consequences of distributed, ground-level urban emissions. This analysis also substantially contributes to the literature on intake fraction by providing the first consistent, globally comparative assessment of *iF* for urban vehicle emissions. Future developments in the *iF* literature could build on this effort in several ways. Examples include (a) more thorough treatment of regionally varying factors that may affect indoor and microenvironmental exposures, (b) explicit consideration of dynamic pollutants (e.g., ultrafine particles), and (c) comparison of intraurban and beyond-urban inhalation intakes for cities of different sizes. Finally, the policy landscape could benefit from more detailed consideration of *iF* for variety of other major, non-vehicular sources that are relevant to population intake.

3.5 References

Angel, S., Parent, J., Civco, D., Blei, A., Potere, D., 2010. *A Planet of Cities: Urban Land Cover Estimates and Projections for All Countries, 2000-2050*, Cambridge, MA. Available from: http://www.lincolninst.edu/pubs/1861_A-Planet-of-Cities.

Angel, S., Parent, J., Civco, D.L., Blei, A., Potere, D., 2011. The dimensions of global urban expansion: Estimates and projections for all countries, 2000-2050. *Progress in Planning* 75, 53-107.

Atkinson, R., 2000. Atmospheric chemistry of VOCs and NO_x. *Atmospheric Environment* 34, 2063-2101.

Baidya, S., Borken-Kleefeld, J., 2009. Atmospheric emissions from road transportation in India. *Energy Policy* 37, 3812-3822.

Bennett, D.H., Margni, M.D., McKone, T.E., Jolliet, O., 2002a. Intake fraction for multimedia pollutants: A tool for life cycle analysis and comparative risk assessment. *Risk Analysis* 22, 905-918.

Bennett, D.H., McKone, T.E., Evans, J.S., Nazaroff, W.W., Margni, M.D., Jolliet, O., Smith, K.R., 2002b. Defining intake fraction. *Environmental Science & Technology* 36, 206A-211A.

Britter, R.E., Hanna, S.R., 2003. Flow and dispersion in urban areas. *Annual Review of Fluid Mechanics* 35, 469-496.

Butler, T.M., Lawrence, M.G., Gurjar, B.R., van Aardenne, J., Schultz, M., Lelieveld, J., 2008. The representation of emissions from megacities in global emission inventories. *Atmospheric Environment* 42, 703-719.

Cahill, T.M., Mackay, D., 2003. Complexity in multimedia mass balance models: When are simple models adequate and when are more complex models necessary? *Environmental Toxicology and Chemistry* 22, 1404-1412.

Chan, C.K., Yao, X., 2008. Air pollution in mega cities in China. *Atmospheric Environment* 42, 1-42.

Chang, D., Song, Y., Liu, B., 2009. Visibility trends in six megacities in China 1973-2007. *Atmospheric Research* 94, 161-167.

Evans, J.S., Wolff, S.K., Phonboon, K., Levy, J.I., Smith, K.R., 2002. Exposure efficiency: An idea whose time has come? *Chemosphere* 49, 1075-1091.

Forstall, R.L., Greene, R.P., Pick, J.B., 2009. Which are the largest? Why lists of major urban areas vary so greatly. *Tijdschrift voor Economische en Sociale Geografie* 100, 277-297.

Greco, S.L., Wilson, A.M., Hanna, S.R., Levy, J.I., 2007a. Factors influencing mobile source particulate matter emissions-to-exposure relationships in the Boston urban area. *Environmental Science & Technology* 41, 7675-7682.

Greco, S.L., Wilson, A.M., Spengler, J.D., Levy, J.I., 2007b. Spatial patterns of mobile source particulate matter emissions-to-exposure relationships across the United States. *Atmospheric Environment* 41, 1011-1025.

Gurjar, B.R., Lelieveld, J., 2005. New directions: Megacities and global change. *Atmospheric Environment* 39, 391-393.

Gurjar, B.R., Butler, T.M., Lawrence, M.G., Lelieveld, J., 2008. Evaluation of emissions and air quality in megacities. *Atmospheric Environment* 42, 1593-1606.

Guttikunda, S.K., Tang, Y., Carmichael, G.R., Kurata, G., Pan, L., Streets, D.G., Woo, J.-H., Thongboonchoo, N., Fried, A., 2005. Impacts of Asian megacity emissions on regional air quality during spring 2001. *Journal of Geophysical Research* 110, D20301.

Guttikunda, S.K., 2011. Diurnal profiles for Delhi emissions inventory, personal communication. Indian Institute of Technology, Delhi, June 8, 2011.

Hanna, S.R., Briggs, G.A., Hosker, R.P., Jr, 1982. *Handbook on Atmospheric Diffusion*, Washington, DC. Available from: http://www.orau.org/ptp/PTP Library/library/Subject/Meteorology/handbook on atmospheric diffusion.pdf.

He, K., Huo, H., Zhang, Q., He, D., An, F., Wang, M., Walsh, M.P., 2005. Oil consumption and CO_2 emissions in China's road transport: Current status, future trends, and policy implications. *Energy Policy* 33, 1499-1507.

Heath, G.A., 2006. *Redistributing Pollution: Exposure Implications of a Shift Toward Distributed Electricity Generation in California*. PhD Dissertation, University of California, Berkeley.

Heath, G.A., Granvold, P.W., Hoats, A.S., Nazaroff, W.W., 2006. Intake fraction assessment of the air pollutant exposure implications of a shift toward distributed electricity generation. *Atmospheric Environment* 40, 7164-7177.

Heath, G.A., Nazaroff, W.W., 2007. Intake-to-delivered-energy ratios for central station and distributed electricity generation in California. *Atmospheric Environment* 41, 9159-9172.

Hodas, N., Meng, Q., Lunden, M.M., Rich, D.Q., Özkaynak, H., Baxter, L.K., Zhang, Q., Turpin, B.J., 2012. Variability in the fraction of ambient fine particulate matter found indoors and observed heterogeneity in health effect estimates. *Journal of Exposure Science and Environmental Epidemiology* 22, 448-454.

Humbert, S., Marshall, J.D., Shaked, S., Spadaro, J.V., Nishioka, Y., Preiss, P., McKone, T.E., Horvath, A., Jolliet, O., 2011. Intake fraction for particulate matter: Recommendations for life cycle impact assessment. *Environmental Science & Technology* 45, 4808-4816.

Huo, H., Zhang, Q., He, K., Wang, Q., Yao, Z., Streets, D.G., 2009. High-resolution vehicular emission inventory using a link-based method: A case study of light-duty vehicles in Beijing. *Environmental Science & Technology* 43, 2394-2399.

Irwin, J.S., 1979. A theoretical variation of the wind profile power-law exponent as a function of surface roughness and stability. *Atmospheric Environment* 13, 191-194.

Ji, S., Cherry, C.R., Bechle, M.J., Wu, Y., Marshall, J.D., 2012. Electric vehicles in China: Emissions and health impacts. *Environmental Science & Technology* 46, 2018-2024.

Klepeis, N.E., Nelson, W.C., Ott, W.R., Robinson, J.P., Tsang, A.M., Switzer, P., Behar, J.V., Hern, S.C., Engelmann, W.H., 2001. The National Human Activity Pattern Survey

(NHAPS): A resource for assessing exposure to environmental pollutants. *Journal of Exposure Analysis and Environmental Epidemiology* 11, 231-252.

Lai, A.C.K., Thatcher, T.L., Nazaroff, W.W., 2000. Inhalation transfer factors for air pollution health risk assessment. *Journal of the Air & Waste Management Association* 50, 1688-1699.

Levy, J.I., Greco, S.L., Melly, S.J., Mukhi, N., 2009. Evaluating efficiency-equality tradeoffs for mobile source control strategies in an urban area. *Risk Analysis* 29, 34-47.

Lobscheid, A.B., Nazaroff, W.W., Spears, M., Horvath, A., McKone, T.E., 2012. Intake fractions of primary conserved air pollutants emitted from on-road vehicles in the United States. *Atmospheric Environment* 63, 298-305.

Loh, M.M., Soares, J., Karppinen, A., Kukkonen, J., Kangas, L., Riikonen, K., Kousa, A., Asikainen, A., Jantunen, M.J., 2009. Intake fraction distributions for benzene from vehicles in the Helsinki metropolitan area. *Atmospheric Environment* 43, 301-310.

Luo, Z., Li, Y., Nazaroff, W.W., 2010. Intake fraction of nonreactive motor vehicle exhaust in Hong Kong. *Atmospheric Environment* 44, 1913-1918.

MacNeill, M., Wallace, L., Kearney, J., Allen, R.W., Van Ryswyk, K., Judek, S., Xu, X., Wheeler, A., 2012. Factors influencing variability in the infiltration of $PM_{2.5}$ mass and its components. *Atmospheric Environment* 61, 518-532.

Mage, D., Ozolins, G., Peterson, P., Webster, A., Orthofer, R., Vandeweerd, V., Gwynne, M., 1996. Urban air pollution in megacities of the world. *Atmospheric Environment* 30, 681-686.

Marshall, J., Nazaroff, W., 2006. Intake fraction, in: Ott, W., Steinemann, A., Wallace, L. (Eds.), *Exposure Analysis*, CRC Press, Boca Raton, FL, pp. 237-251.

Marshall, J.D., Nazaroff, W.W., 2002. *Risk Assessment of Diesel-Fired Back-up Electric Generators Operating in California,* prepared for Environmental Defense, Oakland, CA.

Marshall, J.D., Riley, W.J., McKone, T.E., Nazaroff, W.W., 2003. Intake fraction of primary pollutants: Motor vehicle emissions in the South Coast Air Basin. *Atmospheric Environment* 37, 3455-3468.

Marshall, J.D., Behrentz, E., 2005. Vehicle self-pollution intake fraction: Children's exposure to school bus emissions. *Environmental Science & Technology* 39, 2559-2563.

Marshall, J.D., Teoh, S.K., Nazaroff, W.W., 2005. Intake fraction of nonreactive vehicle emissions in US urban areas. *Atmospheric Environment* 39, 1363-1371.

Marshall, J.D., Granvold, P.W., Hoats, A.S., McKone, T.E., Deakin, E., Nazaroff, W.W., 2006. Inhalation intake of ambient air pollution in California's South Coast Air Basin. *Atmospheric Environment* 40, 4381-4392.

Marshall, J.D., 2007. Urban land area and population growth: A new scaling relationship for metropolitan expansion. *Urban Studies* 44, 1889-1904.

Molina, M.J., Molina, L.T., 2004. Megacities and atmospheric pollution. *Journal of the Air & Waste Management Association* 54, 644-680.

Moschandreas, D.J., 1981. Exposure to pollutants and daily time budgets of people. *Bulletin of the New York Academy of Medicine* 57, 845-859.

Nazaroff, W.W., 2006. Inhalation intake fraction of pollutants from episodic indoor emissions. *Building and Environment* 43, 269-277.

Nazaroff, W.W., 2008. New Directions: It's time to put the human receptor into air pollution control policy. *Atmospheric Environment* 42, 6565-6566.

Parrish, D.D., Zhu, T., 2009. Clean air for megacities. *Science* 326, 674-675.

Potere, D., Schneider, A., Angel, S., Civco, D.L., 2009. Mapping urban areas on a global scale: Which of the eight maps now available is more accurate? *International Journal of Remote Sensing* 30, 6531-6558.

Pucher, J., Korattyswaropam, N., Mittal, N., Ittyerah, N., 2005. Urban transport crisis in India. *Transport Policy* 12, 185-198.

Rienecker, M.M., Suarez, M.J., Gelaro, R., Todling, R., Bacmeister, J., Liu, E., Bosilovich, M.G., Schubert, S.D., Takacs, L., Kim, G.-K., Bloom, S., Chen, J., Collins, D., Conaty, A., da Silva, A., Gu, W., Joiner, J., Koster, R.D., Lucchesi, R., Molod, A., Owens, T., Pawson, S., Pegion, P., Redder, C.R., Reichle, R., Robertson, F.R., Ruddick, A.G., Sienkiewicz, M., Woollen, J., 2011. MERRA: NASA's modern-era retrospective analysis for research and applications. *Journal of Climate* 24, 3624-3648.

Ries, F.J., Marshall, J.D., Brauer, M., 2009. Intake fraction of urban wood smoke. *Environmental Science & Technology* 43, 4701-4706.

Riley, W.J., McKone, T.E., Lai, A.C.K., Nazaroff, W.W., 2002. Indoor particulate matter of outdoor origin: Importance of size-dependent removal mechanisms. *Environmental Science & Technology* 36, 200-207.

Roumasset, J.A., Smith, K.R., 1990. Exposure trading: An approach to more efficient air pollution control. *Journal of Environmental Economics and Management* 18, 276-291.

Sathaye, N., Harley, R., Madanat, S., 2010. Unintended environmental impacts of nighttime freight logistics activities. *Transportation Research Part A: Policy and Practice* 44, 642-659.

Schneider, A., Friedl, M.A., Potere, D., 2009. A new map of global urban extent from MODIS satellite data. *Environmental Research Letters* 4, 044003.

Seinfeld, J.H., Pandis, S.N., 2006. *Atmospheric Chemistry and Physics: From Air Pollution to Climate Change*, 2nd edition, Wiley-Interscience, Hoboken, NJ.

Smith, K.R., 1993. Fuel combustion, air pollution exposure, and health: The situation in developing countries. *Annual Review of Energy and the Environment* 18, 529-566.

Smith, K.R., 2002. Place makes the poison: Wesolowski Award Lecture — 1999. *Journal of Exposure Analysis and Environmental Epidemiology* 12, 167 - 171.

Smith, K.R., Peel, J.L., 2010. Mind the gap. *Environmental Health Perspectives* 118, 1643-1645.

Stephenson, R., Mohan, R.M., Duffin, J., Jarsky, T.M., 2000. Circadian rhythms in the chemoreflex control of breathing. *American Journal of Physiology - Regulatory, Integrative and Comparative Physiology* 278, R282-R286.

Stevens, G., Wilson, A., Hammitt, J.K., 2005. A benefit-cost analysis of retrofitting diesel vehicles with particulate filters in the Mexico City metropolitan area. *Risk Analysis* 25, 883-899.

Stevens, G., de Foy, B., West, J.J., Levy, J.I., 2007. Developing intake fraction estimates with limited data: Comparison of methods in Mexico City. *Atmospheric Environment* 41, 3672-3683.

Taimisto, P., Tainio, M., Karvosenoja, N., Kupiainen, K., Porvari, P., Karppinen, A., Kangas, L., Kukkonen, J., Tuomisto, J., 2011. Evaluation of intake fractions for different subpopulations due to primary fine particulate matter ($PM_{2.5}$) emitted from domestic wood combustion and traffic in Finland. *Air Quality, Atmosphere & Health* 4, 199-209.

Tainio, M., Sofiev, M., Hujo, M., Tuomisto, J.T., Loh, M., Jantunen, M.J., Karppinen, A., Kangas, L., Karvosenoja, N., Kupiainen, K., Porvari, P., Kukkonen, J., 2009. Evaluation of the European population intake fractions for European and Finnish anthropogenic primary fine particulate matter emissions. *Atmospheric Environment* 43, 3052-3059.

Tsai, F.C., 1999. *Total Exposure and Significant Source Apportionment: The Relationships among Emissions Sources, Concentration, Exposure, and Health Effects of Particulate Matter*. PhD Dissertation, University of California, Berkeley.

US EPA, 2009a. *Metabolically Derived Human Ventilation Rates: A Revised Approach Based Upon Oxygen Consumption Rates*, United States Environmental Protection Agency, National Center for Environmental Assessment, Washington, DC. EPA/600/R-06/129F. Available from: http://cfpub.epa.gov/ncea/cfm/recordisplay.cfm?deid=202543.

US EPA, 2009b. *Exposure Factors Handbook: 2009 Update (External Review Draft)*, United States Environmental Protection Agency, Washington, DC. EPA/600/R-09/052A. Available from: http://cfpub.epa.gov/ncea/cfm/recordisplay.cfm?deid=209866.

US EPA, 2011. *The National Emissions Inventory*, United States Environmental Protection Agency, Washington, DC. Available from: http://www.epa.gov/ttn/chief/net/2008inventory.html.

Wallace, L., Williams, R., 2005. Use of personal-indoor-outdoor sulfur concentrations to estimate the infiltration factor and outdoor exposure factor for individual homes and persons. *Environmental Science & Technology* 39, 1707-1714.

Wang, H., Fu, L., Zhou, Y., Du, X., Ge, W., 2010. Trends in vehicular emissions in China's mega cities from 1995 to 2005. *Environmental Pollution* 158, 394-400.

Wang, S., Zhao, Y., Chen, G., Wang, F., Aunan, K., Hao, J., 2008. Assessment of population exposure to particulate matter pollution in Chongqing, China. *Atmospheric Environment* 153, 247-256.

Westerdahl, D., Wang, X., Pan, X., Zhang, K.M., 2009. Characterization of on-road vehicle emission factors and microenvironmental air quality in Beijing, China. *Atmospheric Environment* 43, 697-705.

Yang, L., Li, Y., 2009. City ventilation of Hong Kong at no-wind conditions. *Atmospheric Environment* 43, 3111-3121.

Zhou, Y., Levy, J.I., Evans, J.S., Hammitt, J.K., 2006. The influence of geographic location on population exposure to emissions from power plants throughout China. *Environment International* 32, 365-373.

Table 3-1. Global summary of intraurban intake fraction, demographic parameters, and meteorology [a,b]

	Intake Fraction ppm		**Population** millions		***LPD*** persons m^{-1}		***DR*** $m^2 s^{-1}$	
Range of values	0.6 - 260		0.1 - 34		5.8 – 780		32 – 10,000	
AM (ASD)	39 (36)	*17 (18)*	4.2 (6.4)	*0.55 (1.4)*	170 (150)	*59 (58)*	540 (460)	*520 (460)*
GM (GSD)	26 (2.5)	*12 (2.2)*	1.5 (4.7)	*0.28 (2 .6)*	110 (2.5)	*45* (*2.0*)	470 (1.6)	*450* (*1.6*)
Median	26	*12*	1.4	*0.21*	110	*41*	450	*430*
IQR	14 - 52	*7.3 - 20*	0.42 - 5	*0.13 - 0.43*	57 - 220	*28 - 67*	370 - 550	*360 - 530*
P_{10} – P_{90}	7.7 - 80	*4.7 - 34*	0.18 - 13	*0.11 - 1.1*	33 - 370	*20 - 110*	300 - 770	*300 - 750*

[a] Non-italicized entries (left side) reflect population-weighted statistics; italicized entries (right side) are unweighted results.
[b] Abbreviations: *LPD* – linear population density, *DR* – normalized dilution rate, AM – arithmetic mean, ASD – arithmetic standard deviation, GM – geometric mean, GSD – geometric standard deviation, IQR – interquartile range, P_{10} and P_{90} – 10^{th} and 90^{th} percentiles of distribution.

Table 3-2. Population-weighted mean intake fraction (*iF*) by region and city size [a]

	Region	***iF*** (ppm)			**Population** (million)			**Number of Cities**		
		S	M	L	S	M	L	S	M	L
SCA	South and Central Asia	14.9	35.5	106	93.5	88.7	105	450	76	13
SEA	Southeast Asia	19.8	45.8	67.1	33.2	22.3	51.8	165	22	9
EAP	East Asia and Pacific	21.8	49.3	70.4	165	194	99.3	716	161	14
SSA	Sub-Saharan Africa	17.9	38.2	98.3	43.4	63.5	25.1	202	52	4
LAM	Latin America	12.7	32.2	68.8	68.8	93.3	96.8	318	73	12
NAF	North Africa	10.0	26.5	56.8	20.4	11.5	21.2	103	8	4
EUJ	Europe and Japan	10.1	21.8	55.4	146	111	143	681	97	18
WAS	Western Asia	12.3	26.6	41.0	29.2	35.5	24.8	125	27	5
LRD	Land-Rich Developed	6.6	14.9	30.1	49.9	67.1	109	222	53	16

[a] Cities sorted by population size range: (S) – small, 100,000 ≤ population < 600,000;
(M) – medium, 600,000 ≤ population < 3,000,000; (L) – large, population ≥ 3,000,000.

Table 3-3. Regional summary of intraurban intake fraction, population density, & meteorology [a]

Region		***iF*** ppm	***LPD*** persons m^{-1}	**Density** persons ha^{-1}	***DR*** $m^2 s^{-1}$	**City pop** millions	***N*** cities
SCA	South and Central Asia	55	230	160	490	290	539
SEA	Southeast Asia	48	170	120	520	110	196
EAP	East Asia and Pacific	44	180	220	480	460	891
SSA	Sub-Saharan Africa	43	160	170	610	130	258
LAM	Latin America	41	170	87	610	260	403
NAF	North Africa	32	180	130	630	53	115
EUJ	Europe and Japan	30	140	59	530	400	796
WAS	Western Asia	26	120	91	550	90	157
LRD	Land-Rich Developed	20	110	29	600	230	291

[a] Population-weighted arithmetic means for cities with population ≥ 100,000. Total population: 2.0 billion people (72% of year 2000 urban population, 32% of global population) in 3646 cities.

Table 3-4. Population-weighted mean intraurban intake fraction for the 10 countries with largest population in cities [a]

Country	***iF*** ppm	**City pop** millions
China	44	412
USA	21	192
India	51	188
Brazil	33	88
Japan	50	85
Russia	32	68
Mexico	65	58
Germany	30	49
Indonesia	53	40
S. Korea	46	36
All 10 countries	41	1216
Other 148 countries	35	796

[a] Cities considered are all urban areas with population ≥ 100,000

Table 3-5. Population-weighted mean intraurban intake fraction for all cities modeled, grouped by country.

Country	Region[a]	*iF* (ppm)	Cities	Pop (millions)
Afghanistan	SCA	49	12	4.4
Albania	EUJ	25	1	0.34
Algeria	NAF	20	33	8.3
Angola	SSA	53	5	3.1
Argentina	LAM	29	28	23
Armenia	WAS	17	3	1.4
Australia	LRD	14	13	13
Austria	EUJ	20	5	2.8
Azerbaijan	WAS	16	3	2.4
Bahamas, The	LAM	1.3	1	0.21
Bahrain	WAS	7	1	0.4
Bangladesh	SCA	190	20	18
Belarus	EUJ	19	15	4.7
Belgium	EUJ	13	11	5.3
Benin	SSA	11	3	1
Bolivia	LAM	12	7	3.6
Bosnia & Herzegovina	EUJ	24	2	0.56
Botswana	SSA	9.2	2	0.38
Brazil	LAM	33	130	88
Bulgaria	EUJ	14	9	2.6
Burkina Faso	SSA	27	2	1.4
Burundi	SSA	16	1	0.32
Cambodia	SEA	52	2	1.2
Cameroon	SSA	52	14	5.4
Canada	LRD	20	29	19
Central African Republic	SSA	30	1	0.58
Chad	SSA	23	2	0.75
Chile	LAM	27	18	9.4
China	EAP	44	830	410
Colombia	LAM	75	26	21
Congo, Democratic Republic	SSA	63	23	12
Congo, Republic	SSA	26	2	1.5
Costa Rica	LAM	27	2	1.1
Cote d'Ivoire	SSA	43	9	5.2
Croatia	EUJ	19	3	1
Cuba	LAM	16	12	4.4
Cyprus	WAS	4.8	2	0.37
Czech Republic	EUJ	11	6	2.2
Denmark	EUJ	7.7	4	1.6
Djibouti	SSA	12	1	0.46
Dominican Republic	LAM	25	8	3.1
Ecuador	LAM	15	14	5.4
Egypt	NAF	49	27	20
El Salvador	LAM	14	4	1.8
Eritrea	SSA	16	1	0.48
Estonia	EUJ	7.3	2	0.5
Ethiopia	SSA	36	6	3.3
Finland	EUJ	15	5	1.8
France	EUJ	25	50	27
Gabon	SSA	3.5	2	0.63
Gambia, The	SSA	9.1	1	0.32

Country	Region[a]	*iF* (ppm)	Cities	Pop (millions)
Georgia	WAS	21	5	1.7
Germany	EUJ	30	73	49
Ghana	SSA	15	5	2.9
Greece	EUJ	17	6	4.6
Guatemala	LAM	19	2	1
Guinea	SSA	30	3	1.6
Guinea-Bissau	SSA	17	1	0.27
Haiti	LAM	30	2	1.9
Honduras	LAM	43	3	1.5
Hungary	EUJ	16	9	3
Iceland	EUJ	5.3	1	0.17
India	SCA	51	340	190
Indonesia	SEA	53	77	40
Iran	SCA	30	61	27
Iraq	WAS	29	22	14
Ireland	EUJ	8.7	2	1.2
Israel	WAS	23	8	4.6
Italy	EUJ	24	43	20
Jamaica	LAM	15	2	0.87
Japan	EUJ	50	100	85
Jordan	WAS	20	2	1.9
Kazakhstan	SCA	12	19	5.3
Kenya	SSA	23	5	3.6
Korea, Dem. Rep.	EAP	31	24	8.5
Korea, Rep.	EAP	46	33	36
Kosovo	EUJ	11	2	0.3
Kuwait	WAS	16	2	2.1
Kyrgyzstan	SCA	15	2	0.98
Laos	SEA	33	3	0.9
Latvia	EUJ	12	2	0.88
Lebanon	WAS	12	4	2.1
Liberia	SSA	100	1	0.69
Libya	NAF	10	14	4.7
Lithuania	EUJ	15	5	1.4
Macedonia	EUJ	17	2	0.6
Madagascar	SSA	29	6	2.1
Malawi	SSA	23	2	0.99
Malaysia	SEA	24	24	13
Mali	SSA	24	4	1.5
Mauritania	SSA	9.7	1	0.6
Mexico	LAM	65	82	58
Moldova	EUJ	13	4	1
Mongolia	EAP	21	1	0.76
Montenegro	EUJ	9.8	1	0.13
Morocco	NAF	35	20	11
Mozambique	SSA	15	9	2.7
Myanmar	SEA	45	15	6.5
Namibia	SSA	9.5	1	0.23
Nepal	SCA	30	4	1.1
Netherlands	EUJ	17	19	9.5
New Caledonia	EAP	0.8	1	0.13
New Zealand	LRD	4.6	6	2.3
Nicaragua	LAM	11	2	1.2
Niger	SSA	17	3	1.1
Nigeria	SSA	72	60	33
Norway	EUJ	39	5	1.4
Oman	WAS	10	3	0.98

Country	Region[a]	*iF* (ppm)	Cities	Pop (millions)
Pakistan	SCA	47	56	34
Panama	LAM	13	3	1.2
Papua New Guinea	EAP	11	2	0.36
Paraguay	LAM	17	2	1.7
Peru	LAM	39	18	12
Philippines	SEA	44	31	18
Poland	EUJ	16	33	14
Portugal	EUJ	15	6	3.7
Puerto Rico	LAM	4.3	7	3.3
Qatar	WAS	6.2	1	0.5
Romania	EUJ	20	25	6.7
Russia	EUJ	32	160	68
Rwanda	SSA	30	1	0.52
Saudi Arabia	WAS	20	21	15
Senegal	SSA	21	7	2.9
Serbia	EUJ	19	5	1.7
Sierra Leone	SSA	20	3	1
Singapore	SEA	58	1	4.1
Slovakia	EUJ	11	2	0.69
Slovenia	EUJ	16	2	0.39
Somalia	SSA	6.9	7	2.3
South Africa	SSA	27	37	23
Spain	EUJ	31	43	20
Sri Lanka	SCA	12	4	1.5
Sudan	NAF	16	14	6.8
Suriname	LAM	4.3	1	0.23
Sweden	EUJ	22	10	3.2
Switzerland	EUJ	15	10	3.4
Syria	WAS	32	10	6.7
Tajikistan	SCA	12	2	0.71
Tanzania	SSA	46	13	6.9
Thailand	SEA	33	17	9.8
Togo	SSA	7.7	1	0.73
Tunisia	NAF	17	6	2.6
Turkey	WAS	31	55	29
Turkmenistan	SCA	11	5	1.3
Uganda	SSA	31	1	1.1
Ukraine	EUJ	15	45	18
United Arab Emirates	WAS	9.5	4	2.4
United Kingdom	EUJ	19	66	32
United States	LRD	21	240	190
Uruguay	LAM	8.6	1	1.3
Uzbekistan	SCA	14	17	5.5
Venezuela	LAM	30	31	14
Vietnam	SEA	71	26	14
West Bank & Gaza	WAS	69	4	1.9
Western Sahara	NAF	5	1	0.17
Yemen	WAS	19	7	3
Zambia	SSA	18	7	2.6
Zimbabwe	SSA	21	5	2.7

[a] See Table 3-2 and Figure 3-5 for definition of regions

Table 3-6. Intake fraction results and summary data for 20 worldwide megacities

Megacity	Country	*iF* (ppm)	Population (millions)	*LPD* [a] (population m^{-1})	*DR* [a] (m^2 s^{-1})
Tokyo	Japan	94	34.5	524	489
New York [b]	USA	48	22.4	270	317
Mexico City	Mexico	145	18.4	520	224
Seoul	S. Korea	75	17.4	484	581
São Paulo	Brazil	68	17.1	369	467
Essen/Ruhr	Germany	52	16.9	291	527
Los Angeles [c]	USA	43	16.4	222	272
Mumbai	India	79	16.1	779	1200
Delhi	India	105	14.4	413	333
Shanghai	China	74	13.1	370	534
Kolkata	India	151	13.1	538	376
Osaka	Japan	25	13.0	300	1150
Buenos Aires	Argentina	45	12.6	295	601
Jakarta	Indonesia	90	11.0	315	307
Rio de Janeiro	Brazil	45	10.8	306	668
Beijing	China	73	10.8	317	383
Cairo	Egypt	71	10.4	400	556
Moscow	Russia	76	10.2	303	470
Dhaka	Bangladesh	262	10.1	715	297
Karachi	Pakistan	67	10.0	419	651

[a] LPD – Linear population density, DR – dilution rate; see text for details.
[b] New York includes New York City, Long Island, Northern New Jersey regions
[c] Los Angeles includes contiguous urban portions of Orange and Riverside counties

Table 3-7 Population-weighted mean per-capita dilution parameter (DR / LPD) (m^3 s^{-1} $person^{-1}$), grouped by region and city size.

	Region	City size[a]			
		S	M	L	All
SCA	South and Central Asia	11.1	3.97	1.22	5.24
SEA	Southeast Asia	15.2	5.01	1.84	6.58
EAP	East Asia and Pacific	8.13	3.53	1.81	4.8
SSA	Sub-Saharan Africa	13.1	5.33	1.38	7.09
LAM	Latin America	17.9	7.73	2.21	8.3
NAF	North Africa	15.5	5.17	2.21	7.89
EUJ	Europe and Japan	16.8	6.68	2.32	8.74
WAS	Western Asia	13.3	5.34	2.64	7.17
LRD	Land-Rich Developed	24.8	10.5	4.95	10.9
	All Regions	14.0	5.69	2.42	7.22

[a] Cities sorted by population size range: (S) – small, 100,000 ≤ population < 600,000; (M) – medium, 600,000 ≤ population < 3,000,000; (L) – large, population ≥ 3,000,000.

Table 3-8. Sensitivity of model results to meteorological inputs.[a]

Model Parameter	Mean [b]	P_{25} [c]	P_{75} [c]
Wind profile cap (default: H_{max} = 200 m)			
H_{max} = 100 m	+ 1.8%	+ 1.0%	+ 3.0%
H_{max}= 150 m	+ 0.6%	+ 0.4%	+ 1.0%
H_{max} = 300 m	- 0.6%	- 1.1%	- 0.4%
H_{max} = ∞	- 1.6%	- 2.4%	- 0.9%
Wind profile exponent (default: p = 0.32)			
p = 0.25	+ 7.9%	- 6.5%	+ 9.2%
p = 0.37	- 5.4%	- 6.2%	- 4.5%
Year of meteorological data	(default: 2007 - 2009)		
2007	- 0.4%	- 5.9%	+ 5.6%
2008	+ 0.1%	- 5.1%	+ 4.7%
2009	+ 0.3%	- 5.3%	+ 6.4%

[a] Sensitivity is defined as 100 × ($iF_{sens_case} - iF_{base_case}$) / iF_{base_case}, where iF_{sens_case} and iF_{base_case} represent iF calculated under sensitivity case and base-case assumptions, respectively.
[b] Population-weighted mean of sensitivity values over all cities.
[c] Population weighted 25th and 75th percentiles of sensitivity estimate over all cities. For example, an interquartile range from -5% to +5% for a given sensitivity scenario implies that the scenario changes iF by less than ±5% for the half of all observations.

Table 3-9. Sensitivity of model results to other inputs. [a]

Model Parameter	Mean [b]	P_{25} [c]	P_{75} [c]
Aspect ratio (L/W, default = 1)			
α = 0.5	- 26%	- 28%	- 22%
α = 2	+ 33%	+ 26%	+ 38%
Breathing profile			
"Flat"	+ 13%	+ 5.2%	+ 22%
"Sine"	+ 16%	+ 11%	+ 21%
SoCAB-1	- 10%	- 13%	- 6.7%
SoCAB-2	+ 9.5%	+ 6.3%	+ 13%
Emissions Profile			
Flat	+ 1.0%	- 3.8%	+ 6.2%
Mexico	+ 1.8%	+ 0.9%	+ 2.7%
Delhi	+ 4.8%	+ 1.9%	+ 7.6%
Beijing	- 6.6%	- 9.1%	- 4.0%
USA NEI	-12%	-18%	-6.8%
Pollutant half-life (default: conserved)			
100 h	- 0.8%	- 1.6%	- 0.3%
10 h	- 7.2%	- 14%	- 2.6%

[a] Sensitivity is defined as 100 × ($iF_{sens_case} - iF_{base_case}$) / iF_{base_case}, where iF_{sens_case} and iF_{base_case} represent iF calculated under sensitivity case and base-case assumptions, respectively.
[b] Population-weighted mean of sensitivity values over all cities.
[c] Population weighted 25th and 75th percentiles of sensitivity values over all cities.

Table 3-10. Parameter values for microenvironment sensitivity analysis

	Microenvironment		
	Indoors	*Vehicle/road*	*Other outdoor*
Time distribution	T_μ (h d^{-1})[a]		
(from NHAPS)	20.9	1.3	1.8
Pollutant class	γ_μ (-)[b]		
conserved primary	1	4	1
primary $PM_{2.5}$	0.3 - 0.7	3	1

[a] T_μ - hours spent by the mean individual in a given microenvironment
[b] γ_μ - microenvironmental adjustment factor; ratio of attributable concentration in microenvironment to urban ambient attributable concentration.

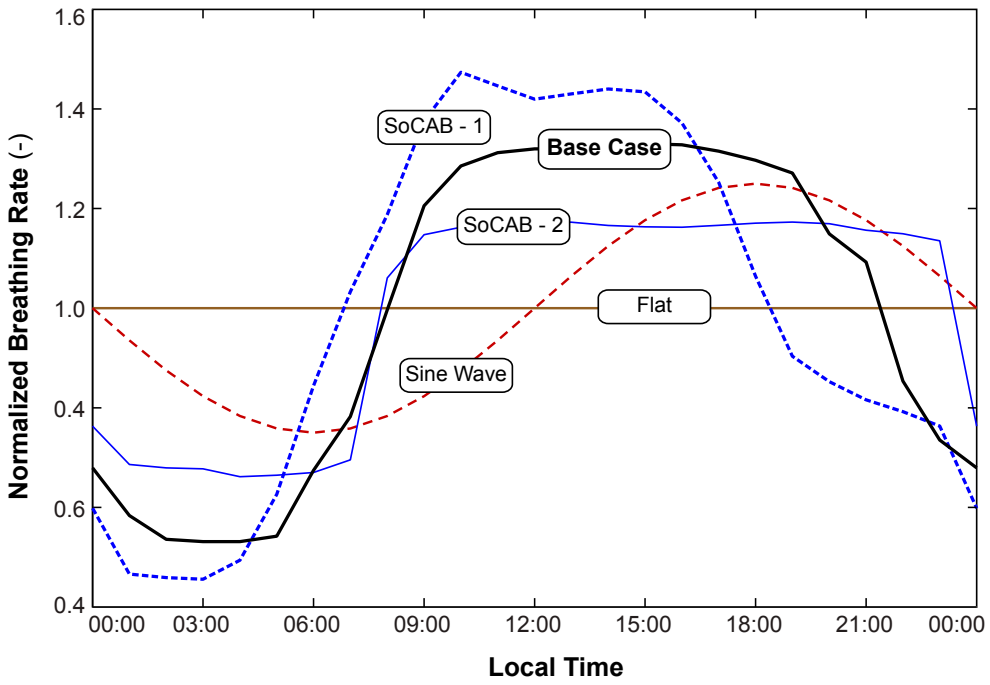

Figure 3-1. Comparison of base case diurnal breathing rate profile with three alternate profiles used for sensitivity analysis. All profiles are normalized to time-averaged breathing rate (14.5 m^3 $person^{-1}$ d^{-1}).

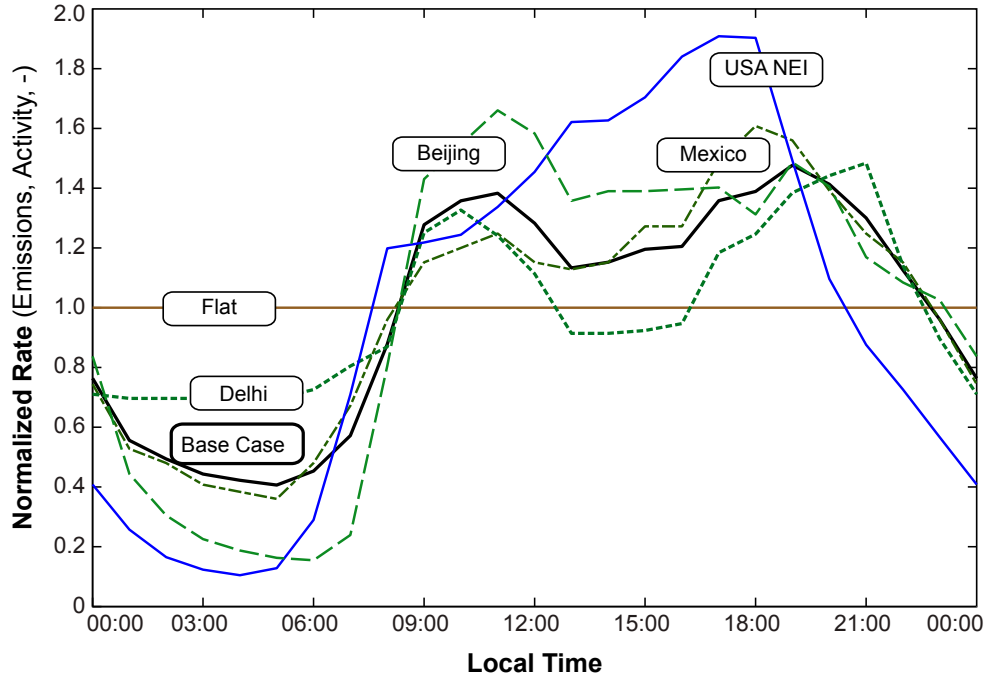

Figure 3-2. Comparison of base case diurnal emissions profile with alternate profiles used for sensitivity analysis. Profiles represent the normalized hourly emissions rate.

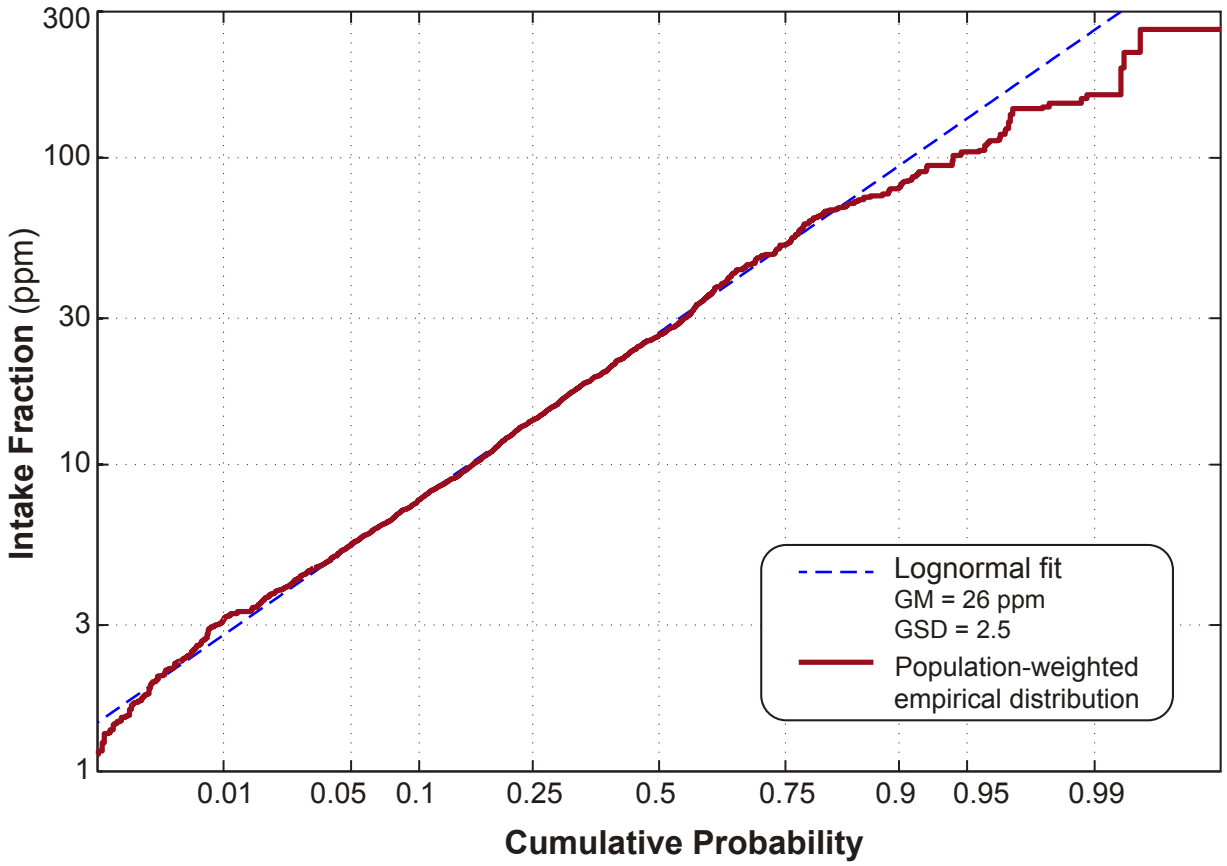

Figure 3-3. Log-probability plot for population-weighted global distribution of intraurban *iF* for emissions of primary, nonreactive pollutants from distributed groundlevel sources. The empirical cumulative distribution of *iF* is reasonably approximated by a lognormal fit (r^2 = 0.92), with excellent fit for the lower 75% of the population-weighted distribution of *iF.*

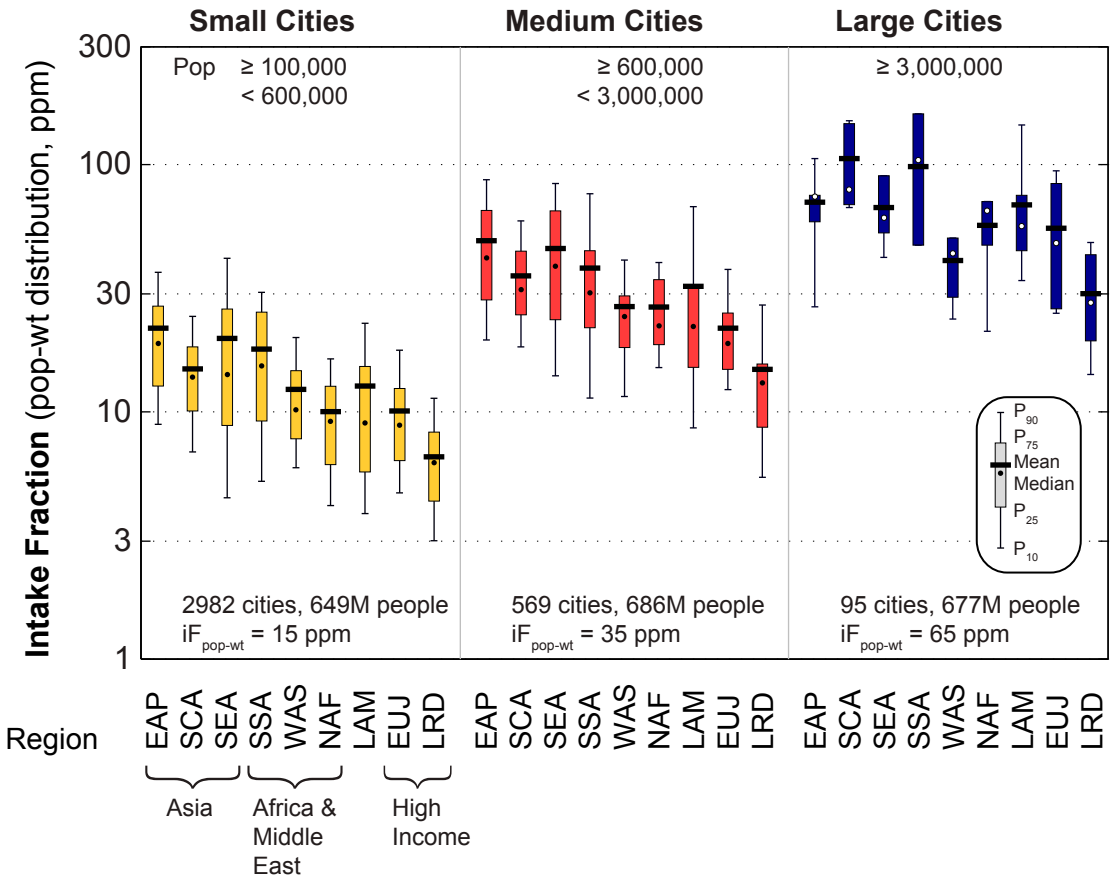

Figure 3-4. Population-weighted distribution of intraurban intake fraction by city size (small, medium, large) and region (labels on horizontal axis, see Table 3-1 and Figure 3-5 for definition of abbreviations). For cities of similar size, *iF* is generally higher in Asia (e.g., EAP, SCA, SEA) and lower in high-income regions (e.g., EUJ, LRD). See Table 3-2 for tabulation of results.

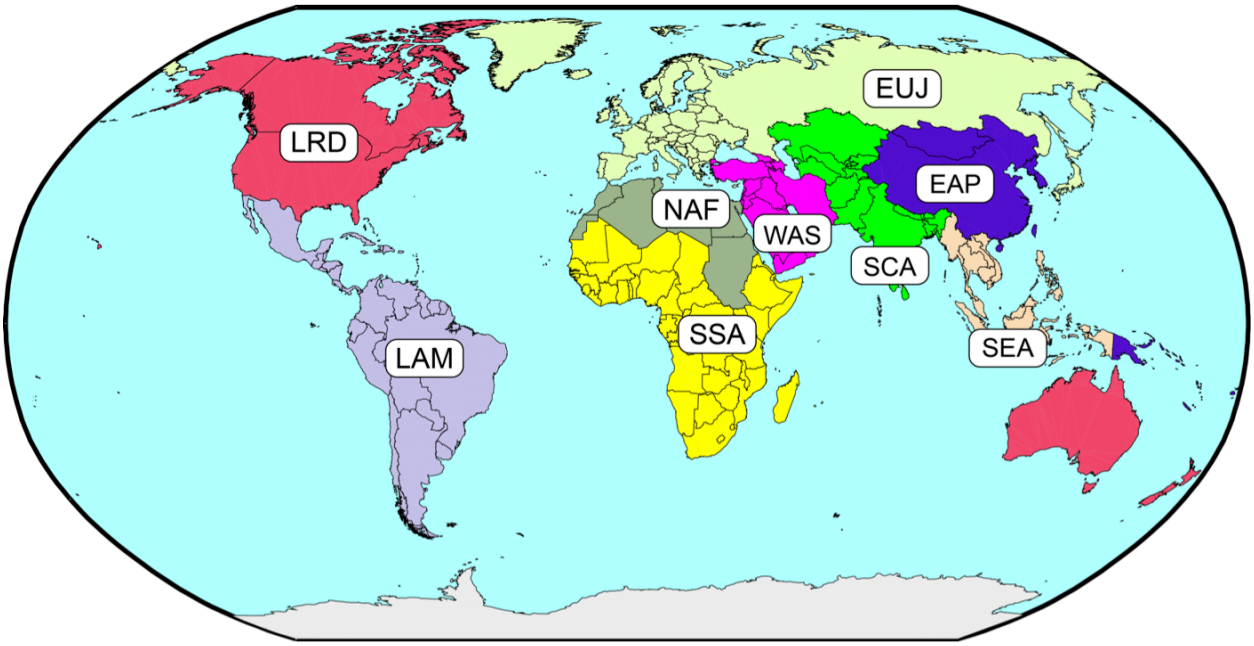

Figure 3-5. Map of nine world regions used for analysis, after Angel et al. (2011). See Table 3-2 for definition of region codes.

Figure 3-6, following 3 pages**.** Regional maps of intraurban intake fraction for groundlevel emissions of primary, noreactive pollutants. Maps consider cities in North and Central America (A), Asia (B), Europe (C), Africa (D), South America (E) and Oceania (F). Values of *iF* are denoted by symbol area. City colors correspond with Figure 1 and indicate population size bins. Intake fractions for selected cities are labeled. Stars (★) designate megacities (population > 10 million). The same scale applies to all maps.

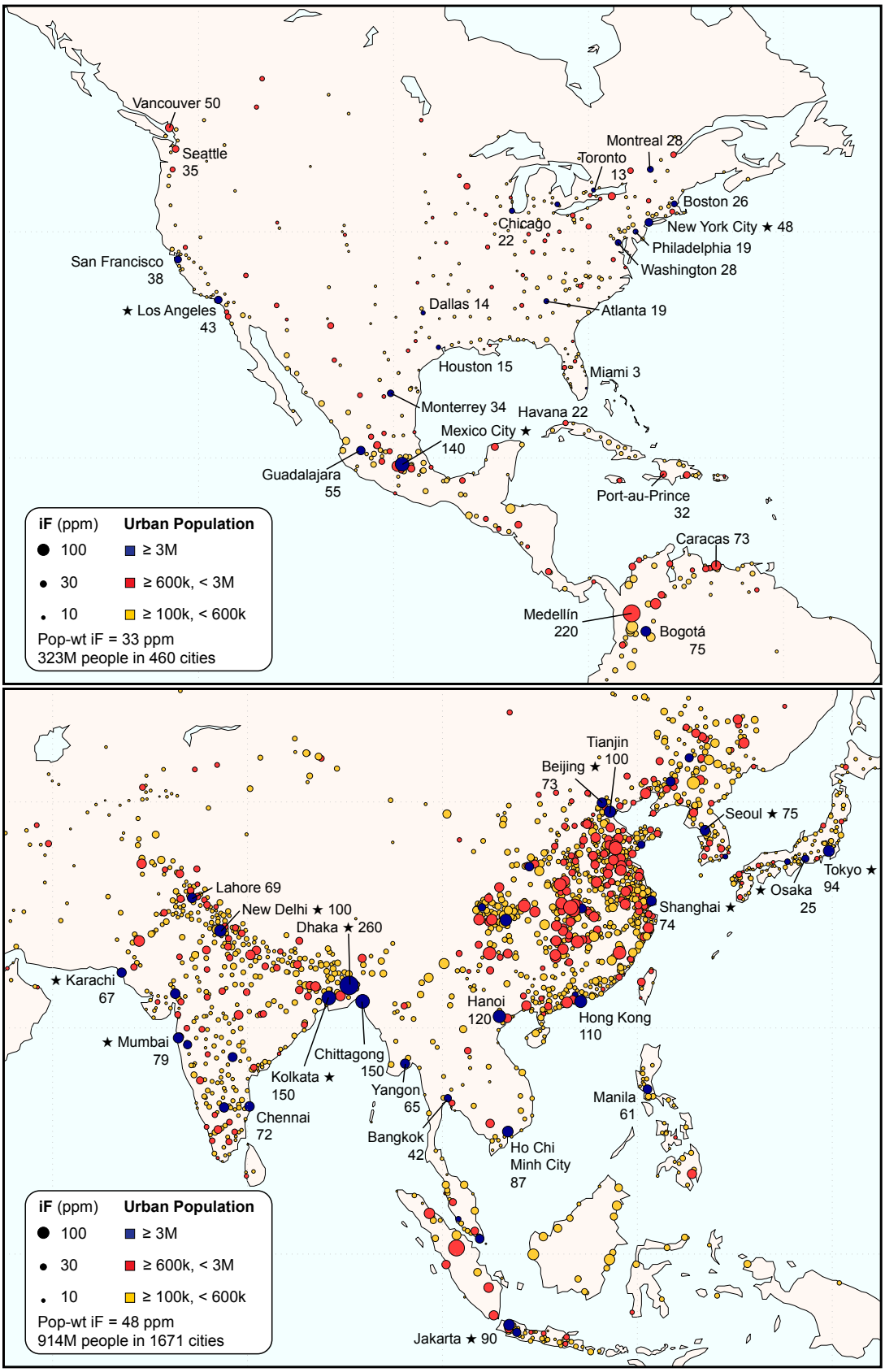

Figure 3-6 (A – upper, B – lower). Map of intraurban *iF* for North America and Asia.

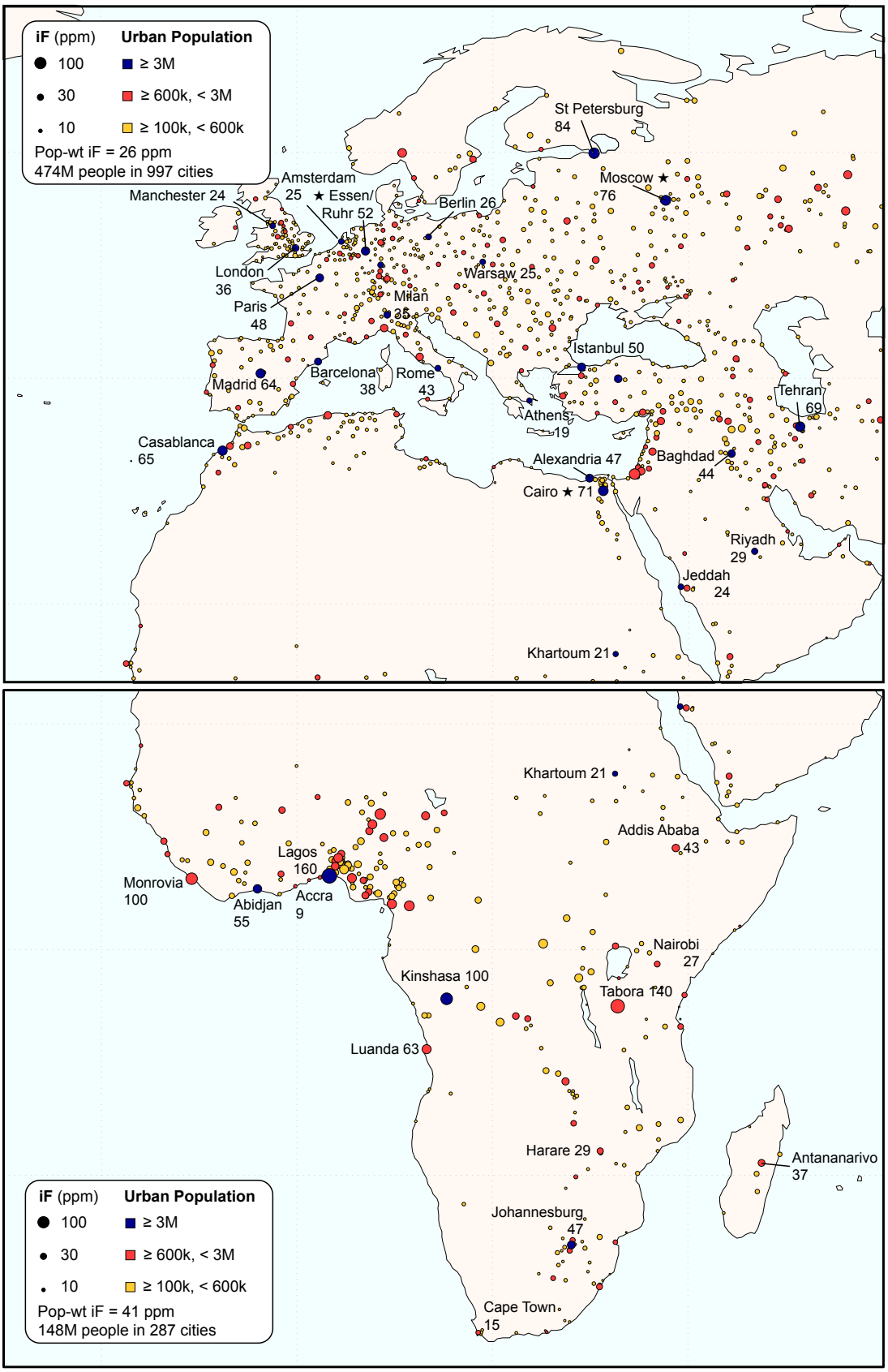

Figure 3-6 (C – upper, D – lower). Map of intraurban *iF* for Europe and Africa.

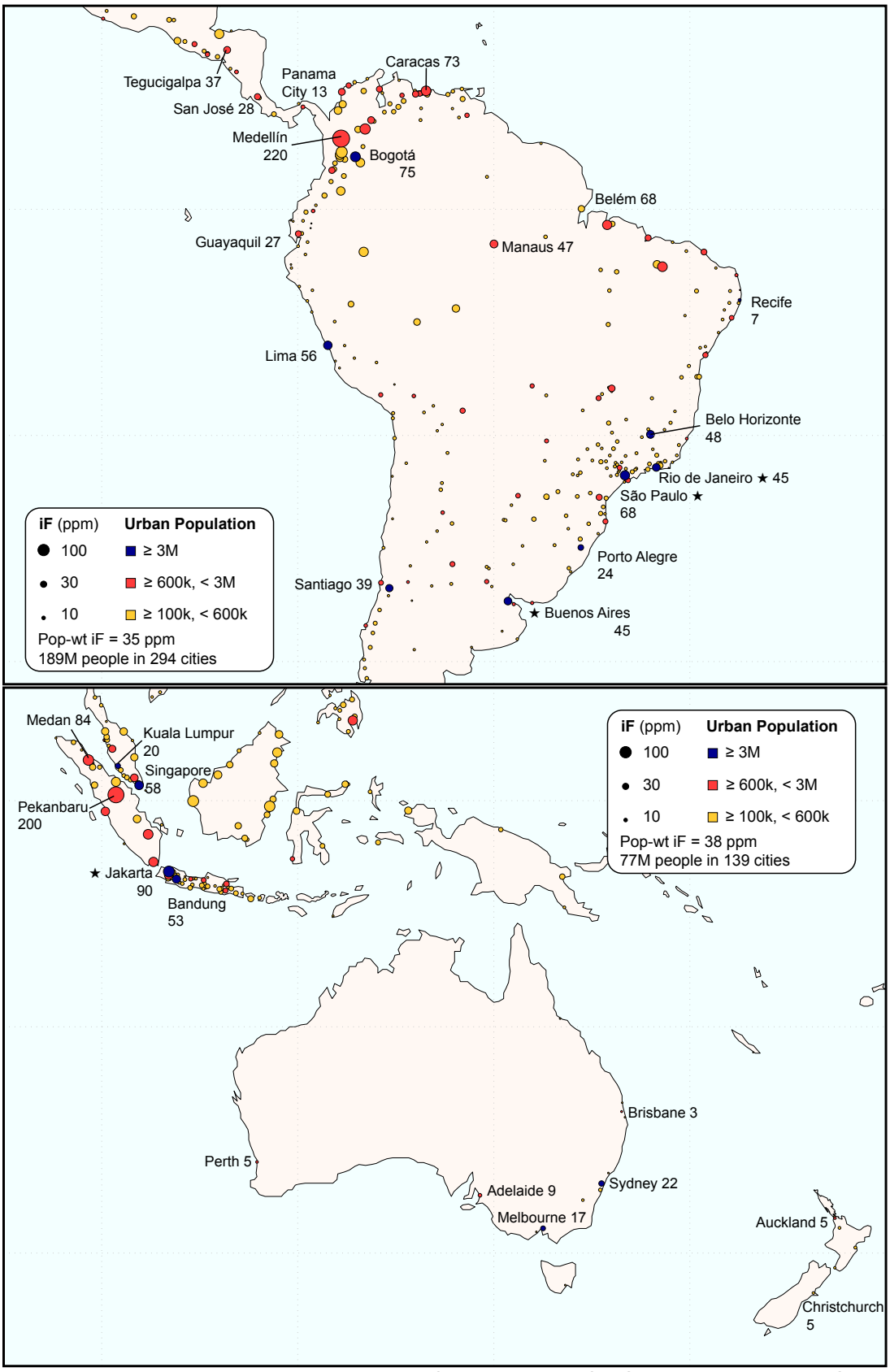

Figure 3-6 (E – upper, F – lower). Map of intraurban *iF* for South America and Oceania.

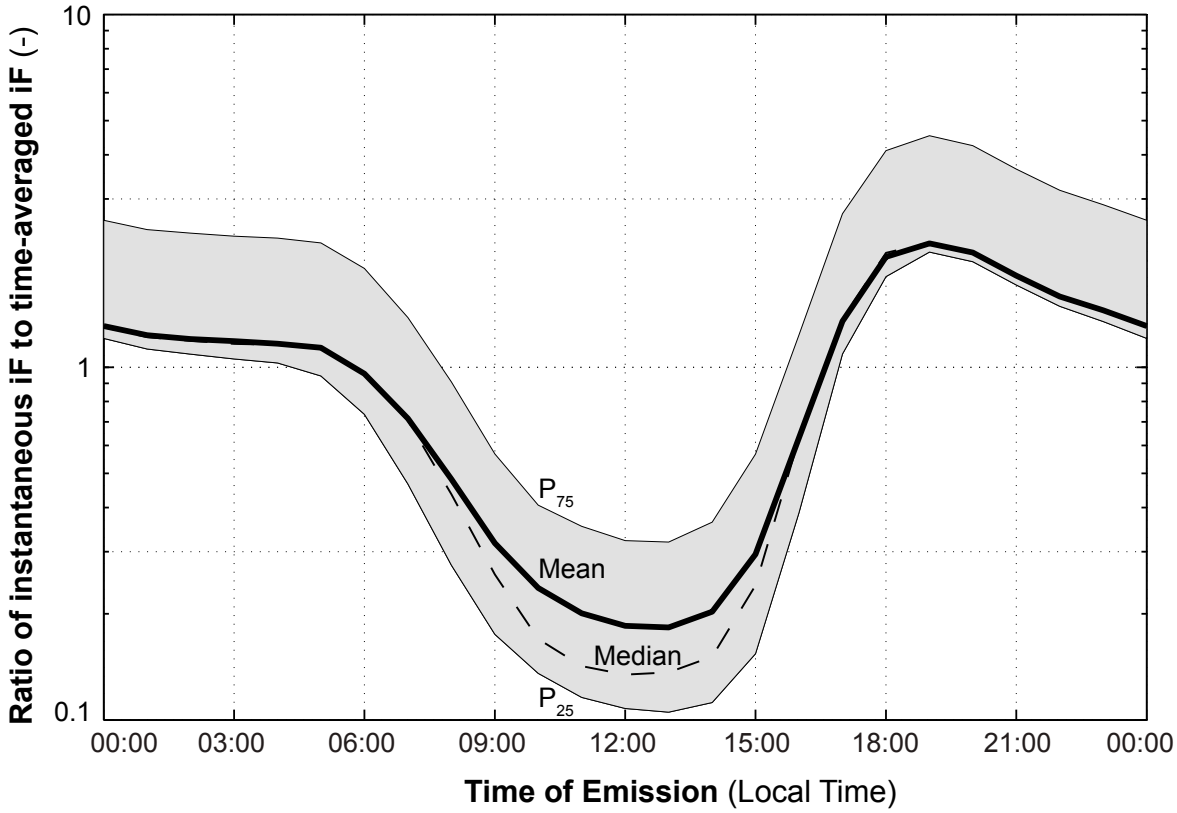

Figure 3-7. Variation in *iF* for emissions occurring at a specified time of day, expressed as a ratio of the time-dependent *iF* to time-averaged *iF* for a given city. Line marked "mean" represents the population-weighted mean value of this ratio for emissions at each hour of the day computed for 3646 cities. Similarly, lines marked median, P_{25} and P_{75} represent the median, 25^{th} and 75^{th} percentiles of the distribution of this ratio for each hour of emissions.

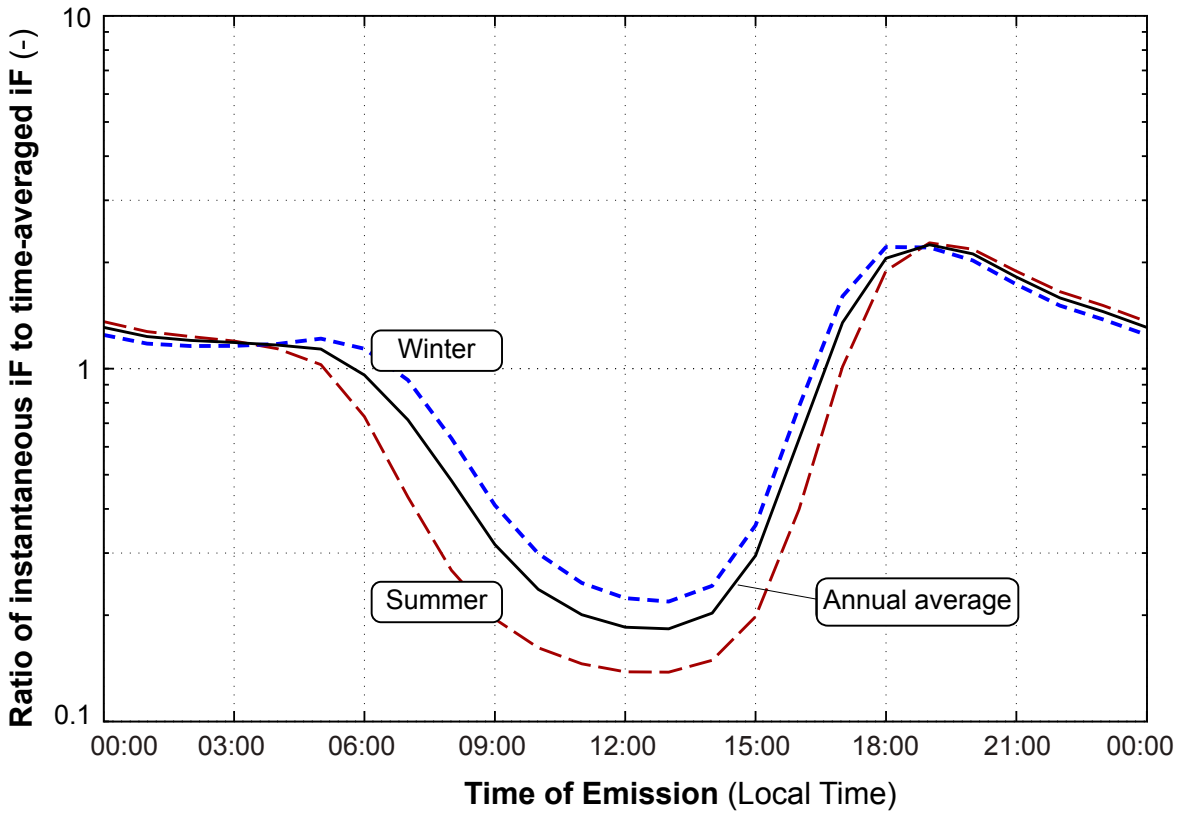

Figure 3-8. Seasonal variation in *iF* for emissions occurring at a specified time of day, expressed as a ratio of the time-dependent *iF* to time-averaged *iF* for a given city. Traces display the population-weighted mean value of this ratio for all non-tropical cities (absolute latitude > 23.5º; 2365 cities, 1.4 billion inhabitants). Line marked “annual average” displays the annual average of this ratio for emissions at a specific time of day. Winter trace represents emissions during Jan – Mar (cities in northern hemisphere) and Jul – Sep (southern hemisphere); summer trace represents emissions during Jul – Sep (northern hemisphere) and Jan – Mar (southern hemisphere).

Chapter 4: Inhalation intake fraction for urban emissions of semivolatile organic compounds from vehicles and other distributed sources

4.1. Introduction

Vehicle emissions are a major source of urban and regional $PM_{2.5}$. In Chapter 3, I presented an analysis of the intraurban intake fraction of urban vehicle emissions of primary, nonreactive pollutant emissions. To properly understand the population intake of vehicle-attributable $PM_{2.5}$, it is necessary to extend the intake fraction framework to incorporate exposures to the reactive and secondary components of fine particle mass. Previous analyses have considered the intake fraction for inorganic secondary $PM_{2.5}$ formed as the result of oxidation of gas-phase precursor emissions, such as NO_x, SO_2, and NH_3 (Evans et al., 2002; Levy et al., 2002; Greco et al., 2007b). However, no previous intake fraction studies have addressed the complex dynamic system that governs population exposures to semivolatile organic vehicular emissions. I aim to address this important gap in the current state of knowledge in this chapter.

It is important that exposure models accurately characterize the behavior of organic emissions from vehicles. Primary $PM_{2.5}$ emissions from vehicles are predominantly comprised of carbonaceous material – i.e., organic carbon (OC) and elemental carbon (EC) (May et al., 2013a; Robinson et al., 2010). Organic emissions dominate total PM mass emissions for many light-duty vehicle technologies and account for a substantial fraction (~25-50%) of PM emissions for heavy-duty vehicles (Schauer et al., 1999; Schauer et al., 2002; Reynolds et al., 2011; Robinson et al., 2010; May et al., 2013a). Given that transportation is a major urban energy end use – and that organic material is also prevalent in other major combustion emission sources (Robinson et al., 2010) – it is perhaps no surprise that organic carbon also accounts for a large or even dominant fraction of ambient $PM_{2.5}$ mass in most urban areas around the world (Zhang et al., 2007).

Whereas EC emissions can be reasonably modeled as a conserved and nonreactive primary pollutant for the purposes of exposure assessment, this assumption cannot be made for OC emissions. Primary particle-phase OC emissions (so-called "primary organic aerosol" or POA) are largely semivolatile. Accordingly, gas-particle partitioning of OC emissions varies strongly as a function of dilution over the range of relevant conditions (Donahue et al., 2006; Robinson et al., 2007; Donahue et al., 2009). When POA in a concentrated exhaust plume is diluted by ambient air, some portion of the semivolatile condensed phase material will evaporate to the vapor phase. Since POA mass is not strictly conserved, an intake fraction assessment for semivolatile organic emissions must consider the dynamic interplay between gas and particle phases of organic material. This chapter emphasizes particle-phase exposures from semivolatile emissions, which is appropriate given the large body of epidemiological evidence for the health effects of PM. However, inhalation of gaseous semivolatile organic vapors may also have important health effects. This investigation explicitly considers both gas- and particle-phase intakes attributable to urban vehicle emissions.

A second consideration of critical importance to human exposure relates to the evolution of primary organic material as it ages in the atmosphere. Ambient monitoring data suggest that highly oxygenated photochemical reaction products constitute a large portion of organic aerosol mass at the urban and regional scale (Jimenez et al., 2009; Zhang et al., 2007). This oxygenated material is a major component of secondary organic aerosol (SOA). Of course, primary organic emissions in the gas and particle phases are key precursors for SOA formation, of which vehicle emissions are one of many important sources (Gentner et al., 2012). SOA formation in the atmosphere is a complex process. For the purposes of SOA formation from vehicle emissions, at least two major routes are important. In the traditional understanding, anthropogenic SOA is principally formed from the atmospheric oxidation of primary emissions of gas-phase volatile organic compounds (VOCs) such as single-ring aromatics. The present analysis emphasizes a second route to SOA formation. Recent research has investigated in detail the role that semivolatile organic carbon emissions play for SOA formation (Donahue et al., 2006; Donahue et al., 2009; Robinson et al., 2007; Robinson et al., 2010; Jimenez et al., 2009). Unlike conventional VOCs, semivolatile SOA precursors may be emitted in either the particle or vapor phase.

In this updated conceptual model, the distinction between POA and SOA is blurred. Consider the dynamic evolution in the atmosphere of vehicle emissions of semivolatile organic material (Robinson et al., 2010; Zhang and Wexler, 2004). Fresh vehicle exhaust is rich in semivolatile organic vapors. As tailpipe exhaust cools rapidly to ambient temperatures, the mass fraction of material in the particle phase increases greatly owing to condensation of semivolatile vapors. In turn, on-road and urban-scale dilution causes some of this POA mass to evaporate back into the vapor phase. Then, over hours and days, the photochemical aging of gases, evaporated vapors, and particles leads to lower-volatility secondary products of primary emissions, augmenting the regional scale background of SOA. At each stage of this process, the potential exists for population exposures to vapor and particle-phase material of vehicular origin. While not directly relevant to population intake, key processes that govern the ultimate atmospheric fate of OC include dry and wet deposition, and fragmentation reactions that oxidize OC to gaseous CO and then to CO_2.

In this chapter, I use a mathematical model to simultaneously address two distinct research questions related to population exposure to vapors and particles attributable to semivolatile organic emissions from vehicles and other distributed, ground-level urban combustion sources. First, I seek to refine the state of knowledge about the *iF* of urban combustion emissions by explicitly characterizing the major dynamic processes that govern dilution, partitioning, and aging of semivolatile organic emissions. Here, an important research question is: “how does the intake fraction of semivolatile organic emissions differ from the intake fraction of primary, conserved pollutants and primary nonreactive particles?” A second objective of this investigation is to re-interpret the existing findings of the atmospheric organic aerosol literature from the perspective of human exposure. In a review of the dynamic processes that shape the evolution of semivolatile combustion emissions, Robinson et al. (2010) write: “Secondary PM production often greatly exceeds the direct or primary PM emissions; therefore, secondary PM must be included in any assessment of the contribution of combustion systems to ambient PM concentrations.” Here, I aim to critically assess this proposition from the perspective of human exposure, rather than through a lens focused on ambient concentrations or atmospheric burdens. I therefore seek to address the following question: “what is the relative importance of primary

versus secondary material for the population inhalation intake of particulate matter attributable to semivolatile organic vehicle emissions?"

4.2. Methods and conceptual framework

4.2.1 Fundamental considerations: Dynamics of semivolatile compounds

Given the tremendous number of individual organic compounds present in combustion exhaust and in human-occupied microenvironments, it remains an insurmountable task to explicitly account for the emissions, dynamic behavior, and inhalation intake of organics on a species-by-species basis. To address this challenge, I use the volatility basis set (VBS) framework, which enables a parsimonious and physically realistic description of dynamic gas-particle partitioning behavior of organic compounds in the atmosphere (Donahue et al., 2006). Within this framework, organic compounds are classified on the basis of their volatility, as measured by their saturation concentration C^*. A simplified description of the system is achieved by using a volatility set with a small number of representative volatilities C_i^*, termed here "bins." Following previous modeling efforts, I employ here the following 9-member VBS with order-of-magnitude bin spacing (Robinson et al., 2007; Shrivastava et al., 2008):

$$\{C_i^*\} = \{10^{-2}, 10^{-1}, 1, 10, 100, 10^3, 10^4\ 10^5, 10^6\}\ \mu g\ m^{-3} \text{ at } T = 298\ K \qquad [4.1]$$

Briefly, the VBS is used to represent the dynamics of the atmospheric organic aerosol as follows. Material of a given volatility is assigned to the individual VBS bin with the closest mean C_i^* value. For example, all material with $10^{-0.5} \leq C^* < 10^{0.5}$ μg m^{-3} is represented by the VBS member with $C^* = 1$ μg m^{-3}. Emissions and removal processes (advection, deposition) affect abundances (concentrations) within each VBS bin. Transformation processes that modify the volatility distribution of the aerosol are represented by shifting mass from one bin to another. Finally, shifts in gas-particle partitioning (e.g., owing to changing temperature) do not directly alter the volatility distribution, but instead change the fraction of material within each bin that is in the gas or particle phase.

Absorptive partitioning theory

For a given organic compound, gas-particle partitioning depends on intrinsic properties and environmental conditions. In a model system with a single compound, when the abundance of that compound exceeds its saturation concentration, then it will partition predominantly into the particle phase. Of course, the environment is a considerably more complex system, with a tremendous number of individual organic compounds present in the gas and particle phases. Gas-particle partitioning of organic compounds is primarily an absorptive process (May et al., 2013a; Roth et al., 2005b). Here, I assume that the absorptive partitioning model of Pankow holds, in which semivolatile organic vapors are absorbed into an condensed-phase organic solution (Pankow, 1994). The assumption of strictly absorptive partitioning is appropriate for many exposure-relevant conditions, but may be incomplete for near-road and in-plume conditions in which adsorption to soot also contributes to gas-particle partitioning (Roth et al., 2005b; Roth et al., 2005a). In the Pankow model, the partitioning behavior of any single compound with C_i^* depends on the condensed-phase abundance of all species present in the system. In other words,

the partitioning of any *single* species depends on the total organic aerosol concentration C_{OA} summed over *all* species (Donahue et al., 2006; Pankow, 1994). For a compound with saturation concentration C_i^*, the particle-phase partitioning coefficient ξ_i (mass-per-mass basis) is:

$$\xi_i = \left(1 + \frac{C_i^*}{C_{OA}} \right)^{-1} \quad [4.2]$$

Here, the partitioning coefficient represents the mass fraction of organic material that is present in the particle phase. This simple model encapsulates the powerful effect of dilution on partitioning for semivolatile compounds. Consider a single-compound system with C_i^* = 100 μg m^{-3}. Under conditions typical of a weakly diluted exhaust plume (C_{OA} = 1000 μg m^{-3}), this compound would partition predominantly into the particle phase ($\xi_i \approx 0.91$). However, after dilution to levels more typical of ambient conditions (C_{OA} = 10 μg m^{-3}), this compound would substantially evaporate into the gas phase ($\xi_i \approx 0.09$). Note that in this system, the total organic aerosol concentration C_{OA} itself depends on the concentration and partitioning of its N constituent species, as follows:

$$C_{OA} = \sum_{i=1}^{N} C_i \xi_i \quad [4.3]$$

To account for the interdependence of equations [4.2] and [4.3], I use the following iterative routine to determine gas-particle partitioning: (1) start with an initial guess of C_{OA}; (2) determine the partitioning coefficient ξ_i for each of $i = 1 \ldots N$ species; (3) estimate C_{OA} based on the known abundance C_i of each species; (4) and then repeat steps (2) and (3) until the value of C_{OA} converges to a stable estimate. Since this iterative routine is solved for only a small system of compounds (the 9-member VBS of C^* values), it remains computationally tractable. I determined that the solution generated by this iterative routine was robust to the choice of initial value of C_{OA} by conducting a large number of trial simulations with initial guesses in the concentration range 10^{-6} to 10^{9} μg m^{-3}. Note that the theory invoked here assumes that equilibrium partitioning is reached rapidly relative to the other timescales in the system (i.e., advection). Although this assumption is consistent with prior modeling investigations of semivolatile organics in outdoor air (Donahue et al., 2006; Shrivastava et al., 2008), the assumption may be inaccurate in certain scenarios, such as partitioning of lower-volatility compounds into coarse-mode particles (Weschler and Nazaroff, 2008; Weschler and Nazaroff, 2010). While I do not address this concern in the present analysis, I acknowledge that adsorptive and non-equilibrium partitioning behaviors may be important phenomena for thorough assessments of certain exposure microenvironments, such in on-road/near-field conditions and indoors.

Evolving partitioning

Gas-particle partitioning evolves substantially over the minutes, hours, and days that elapse between the emission and subsequent inhalation intake of semivolatile organics. I consider three major processes that shape the gas-particle partitioning of semivolatile organics: dilution, shifts in temperature, and photochemical aging.

Dilution

Dilution processes most strongly affect partitioning in settings where concentration gradients approach order-of-magnitude or greater scale. For urban vehicle emissions, the sharpest OA concentration gradients exist in evolving exhaust plumes in the near-field region ("tailpipe-to-road"), where ~1000× dilution is accomplished over length and time scales of just a few meters and seconds, respectively (Zhang and Wexler, 2004). Since such fine spatial and temporal scales pose difficulty for accurate representation of tailpipe-to-road processing, I omit the near-road microenvironment from consideration in the present analysis. Gradients between urban-ambient and continental background OA mass concentrations span ~3-10 × (Zhang et al., 2007). Owing to the long length scales for this dilution process (~100-1000 km and hours to days), the potential exists for tens of millions of people to be exposed at relatively dilute levels. In the present analysis, I restrict consideration to the dilution and partitioning processes that affect urban and regional-scale exposures, and neglect within-urban variations in dilution. In-vehicle and near-road exposures are an important topic for future study.

Temperature

Shifts in temperature affect the gas-particle partitioning of individual compounds by changing the saturation concentration C_i^*, with higher temperatures favoring evaporation into the gas phase. The steepest temperature gradients are found in cooling exhaust plumes; however, tailpipe-to-road processes are not explored here owing to modeling constraints. Diurnal and seasonal shifts in temperature of scale 20 ºC or more can have a substantial (~2-3×) effect on gas-particle partitioning and subsequent photochemical aging (Donahue et al., 2006; Robinson et al., 2007; Shrivastava et al., 2008), as discussed in the following section. The effect of such temporal patterns on the population intake of semivolatile compounds is explored in sensitivity cases. The effect of temperature T on C_i^* is modeled using the Clausius-Clapeyron relation (Donahue et al., 2006; Jathar et al., 2011):

$$C_i^*(T) = C_i^*(T_{\text{ref}}) \exp\left[\frac{\Delta H_{\text{V}}}{R}\left(\frac{1}{T_{\text{ref}}} - \frac{1}{T}\right)\right]\frac{T_{\text{ref}}}{T}, \text{ where } T_{\text{ref}} = 298 \text{ K}. \qquad [4.4]$$

Here, T_{ref} represents the reference temperature for which the base-case VBS is defined (298 K), R is the ideal gas constant, and ΔH_{v} is the enthalpy of vaporization for a model compound at each given volatility bin. Prior studies have indicated a weak dependence of ΔH_{v} on C^*, with lower enthalapies of vaporization for more volatile compounds (Donahue et al., 2006; Robinson et al., 2007; Shrivastava et al., 2008). In keeping with other modeling studies that employ the VBS modeling framework, I adopt the same estimates of ΔH_{v} values as used by Shrivastava et al. (2008), reproduced here in Table 4-1. These are indicative estimates for the large saturated organic compounds that are abundant in primary emissions; thermodynamic considerations underlie the constant spacing of ΔH_{v} between successive volatility bins (Donahue 2006). Following Donahue et al. (2006), shifts in temperature are incorporated into the VBS framework by dynamically redefining the basis set when temperatures deviate from T_{ref} = 298 K.

Photochemical aging

When coupled with the dilution processes outlined above, photochemical aging exerts a profound influence on several exposure-relevant properties of semivolatile organic emissions, gas-particle partitioning, and chemical composition. For typical combustion emissions sources and considering semivolatile emitted compounds with $C^* \leq 10^6$ μg m^{-3}, mass emissions rates increase with increasing C^*, such that the most volatile compounds account for the majority of all mass emissions (Donahue et al., 2006; Lipsky and Robinson, 2006; Donahue et al., 2009; Grieshop et al., 2009; Robinson et al., 2010). Several lines of evidence indicate that primary emissions of lower volatility compounds are unlikely to account for the observed levels of organic aerosol at urban and rural sites. Rather, photochemical oxidation of semivolatile material is thought to account for a substantial fraction of the lower-volatility and oxygenated compounds observed in field measurements of organic aerosols (Robinson et al., 2007; Zhang et al., 2007).

Since prior organic aerosol research has developed a large lexicon of overlapping terms and concepts, is worthwhile to briefly introduce and define some nomenclature. Here, I primarily employ the classification scheme of Robinson et al. (2007). In that framework, the adjective "semivolatile" is applied to a broad class of compounds that are neither VOCs in the traditional sense ($C_i^* > 10^6$ μg m^{-3}) or non-volatile ($C_i^* < 0.01$ μg m^{-3}, i.e., predominantly in the condensed phase under nearly any atmospheric condition). Somewhat confusingly, the broad class of compounds adjectivally described as "semivolatile" is further subdivided into two groups: "SVOCs" ($10^{-2} – 10^4$ μg m^{-3}) and intermediate volatility "IVOCs" ($10^4 – 10^6$ μg m^{-3}). This distinction reflects the observation that unlike SVOCs, IVOCs will not partition substantially into the particle phase even at C_{OA} levels typical of tailpipe conditions, yet can rapidly be oxidized to C^* levels in the SVOC range. To further distinguish SVOCs and IVOCs from traditional VOCs (i.e., $C_i^* > 10^6$ μg m^{-3}), gas-phase SVOC and IVOC material will be referred to here as "vapors", while gas-phase VOC material will be termed "gases".

Robinson et al. (2007) proposed a crucial refinement to the conceptual model of atmospheric "secondary" organic aerosol (SOA). In earlier conceptual frameworks, SOA was thought to be produced chiefly via oxidation of gas-phase VOCs, while "primary" organic aerosol (POA) was thought to be largely inert. This conceptualization did not account for the effects of dilution and evaporation. At the same time, traditional SOA models were often unable to reproduce the high levels of low-volatility, highly oxygenated OA observed in field measurements. Robinson et al. hypothesized that the large mass of semivolatile vapors produced by diluting POA emissions could serve as an important precursor for the formation of "SOA." In this updated conceptual model, the low-volatility oxygenated aerosol blurs the distinction between "secondary" and "primary", since a substantial fraction of precursor material is already semivolatile in its as-emitted state and therefore partitions into the particle phase under tailpipe conditions, although not necessarily under ambient conditions. Acknowledging the relatively cursory oxidation required to produce low-volatility products from semivolatile emissions, this oxidized material is therefore referred to as OPOA (oxidized POA). This conceptual model accommodates the possibility that OPOA can be produced by either gas phase chemistry (i.e., vapors evaporated from POA are oxidized by gas-phase radicals) or by other means (including heterogeneous chemistry on the surface of POA particles, or aqueous chemistry via dissolved oxidizing agents in liquid droplets). Oxidation reactions can also *increase* the volatility of material by

fragmentation of carbon-carbon bonds. However, I do not explicitly consider fragmentation in the present analysis, as elaborated below.

In this analysis, I adopt the simplified treatment of organic aerosol aging that was introduced by Shrivastava et al. (2008) and Robinson et al. (2007). Reactions that "age" primary material can have the effect of either decreasing the volatility of compounds (via functionalization or oligomerization) or alternatively increasing volatility via fragmentation (Jimenez et al., 2009). However, the *net* effect of the first few days of oxidation is unambiguous: on average, aging reduces the volatility of primary emissions (Donahue et al., 2009; Donahue et al., 2006; Zhang et al., 2007). The description of aging here is phenomenological, and thus does not retain complete fidelity to the underlying physical and chemical mechanisms. In particular, net aging is represented with a simplified mechanism in which each oxidation step results in a reduction in volatility. A single pathway, functionalization, is used to represent this net reduction in volatility. Because chemistry proceeds most rapidly in the gas-phase, only gas-phase oxidation reactions are considered here (Donahue et al., 2006). As an additional simplification, the effects of multiple oxidation pathways (e.g., those initiated by OH, O_3, NO_3) are represented using only OH. The model mechanism introduced by Robinson et al. (2007) therefore does not constitute a complete description of organic carbon oxidation chemistry in the atmosphere. However, the model provides a clear window for observing one of the most salient features of this physical system. In doing so, the model is able to usefully illustrate the effects on human exposure of the production of low-volatility products (largely in the particle phase) from the emission of higher volatility precursors.

To operationalize this conceptual framework in terms of the volatility basis set, I define population intake of POA as the inhalation intake of any particle-phase material for which the C_i^* is the same as its emitted state, whereas OPOA intake is defined as inhalation intake of particle-phase material for which the C_i^* is lower than its as-emitted state. Here, OPOA production is assumed to occur solely via gas-phase oxidation initiated by the OH radical of evaporated POA vapors. Following Robinson et al. (2007), this process is simulated with a simplified reaction mechanism (Figure 4-1) in which each reaction step reduces the saturation concentration C_i^* of input material by a single volatility bin (i.e., by one order of magnitude). In base case simulations, I employ a second-order reaction rate coefficient $k_{OH} = 4 \times 10^{-11}$ cm^3 molecule^{-1} s^{-1} and incorporate a time-dependent diurnal profile for OH radical concentrations. As an example, for typical regional summer daytime OH concentrations of ~4×10^6 molecules s^{-1}, this value of k_{OH} corresponds to a characteristic time for a one-bin reduction in C^* of ~1.7 h. Since semivolatile vapors represent only a small fraction of all gas-phase organic material that would react with OH in an urban airshed, I adopt the assumption of Shrivastava et al. (2008) that OH concentrations can be treated independently of the organic aerosol aging process.

To link the emission of semivolatile material to ultimate population intake, I separately track the evolving volatility distributions of material originally emitted into each of $i = 1 \ldots N$ volatility bins C_i^* as it ages into $j = 1 \ldots N$ volatility bins. Within this $N \times N$ matrix of volatilities, aged condensed-phase material with saturation concentration $C_{i,j}^*$ is classified as POA when it remains at its originally emitted volatility level i (i.e., the aging index $j = i$) and is classified as OPOA when it is found in a lower-than-emitted volatility bin (i.e., the aging index $j <$ emitted-

state index *i*). As described above, note that this model does not consider fragmentation or other reaction pathways that may increase the volatility of material relative to its originally emitted state.

The volatility reduction associated with oxidation chemistry is accompanied by an increase in OA mass, since functionalization reactions introduce oxygen and other atomic constituents to OA molecules that are absent in primary emissions (Jimenez et al., 2009). I represent this increase in OA mass with photochemical transformation using a scheme developed by Robinson et al. (2007), in which the OA mass is assumed to increase by 7.5% for each order-of-magnitude reduction in C^*. This increase in mass is equivalent to, for example, adding a single oxygen atom to a C_{15} precursor alkane, or two carbon atoms to a C_{30} precursor. Additional model scenarios consider larger or smaller increases in OA mass with each order-of-magnitude reduction in VBS bin. To facilitate intake fraction calculations (§4.2.3), the model employs an accounting scheme that separately tracks organic carbon mass (OC) and the mass of non-carbon organic aerosol constituents. The total OA mass is the sum of these two terms. Note that OC mass is assumed to be conserved in functionalization reactions, whereas the mass of the non-carbon constituents increases with each reaction step.

4.2.2 Nested multi-compartment model

I use a multi-compartment exposure model in order to represent population exposure to emissions at multiple spatial and temporal scales. The exposed population is distributed into a small, densely populated urban compartment, a "periurban" compartment with intermediate population density, and a large, more sparsely populated regional compartment (Figure 4-2). Vehicle-associated emissions into each compartment are assumed to occur on an equal per-capita basis. I assume concentrations in each compartment are horizontally and vertically well mixed, which is a reasonable approximation for spatially distributed ground-level emissions (Chapter 3). Emissions in each compartment are diluted as the result of air flows, modeled here as the product $W \times [u(t) \times H(t)]$, where W is the crosswind width of the compartment, $H(t)$ is the time-dependent mixing height for the compartment, and $u(t)$ is the time-dependent wind speed averaged through the mixing depth. Material (pollution) in the inner ("urban") compartment is supplied by emissions in the urban compartment and by inflow from the periurban compartment. Material in the periurban compartment is supplied by emissions in that compartment and by inflow of material from both the regional and urban compartments. Similarly, material the outermost regional compartment derives from emissions in the regional compartment and from the inflow of air from the periurban compartment and a fixed continental background boundary condition. In base-case model runs, the contribution from the continental background is assumed to be negligible ($C = 0$). In each compartment, the outflow of material to other compartments and eventually to the system boundary is a major or dominant loss process. The differential material balance for this model system is discussed in more detail below.

The sizing of model compartments is intended to represent key exposure-relevant gradients in an idealized fashion. Compared to their surrounding hinterlands, cities are islands of high primary pollutant concentrations and high population density. In the default model parameterization, the urban box is sized to represent an "archetypal" US urban area with population of 1.5 million in a square-plan urbanized land area of 25 × 25 km, which corresponds to a population density of 2400 km^{-2} and linear population density (*LPD*) of 60 m^{-1}. These

parameter values agree closely with the remotely-sensed urban form data for US cities that formed part of the intake fraction analysis presented in Chapter 3 (Angel et al., 2011). Specifically, for the 238 U.S. cities in that dataset with population in the range 100,000 – 7 million, I compute the following population-weighted mean metrics: population (1.9 million), urbanized length-scale (26 km), population density (2500 km^{-2}) and linear population density *LPD* (59 m^{-1}; see Chapter 3 for definition of *LPD*). These 238 cities incorporate a year-2000 population of 129 million, and exclude the 62 million people that inhabit the 5 most populous US urban areas (New York, Los Angeles, Chicago, Washington, San Francisco). I developed a separate archetype to consider global megacities (population ≥ 10 million), which account for a substantial fraction of the worldwide urban population (~15%) despite being relatively few in number (Forstall et al., 2009). Year-2000 population weighted-mean metrics for the 20 worldwide megacities in the Angel et al. (2011) dataset are: population (17 million), length scale (45 km), population density (12,500 km^{-2}) and *LPD* (414 m^{-1}). I used these central-tendency values as the inspiration for the megacity archetype described in Table 4-2 (population = 18 million, length scale = 40 km, population density = 11,250 km^{-2}, *LPD* = 450 km^{-2}). Additional sensitivity scenarios consider other configurations of urban form.

Near-urban ("periurban") populations are distributed at a population density that is substantially lower than the urban core, but much greater than the regional average. Because of their proximity to the urban core, periurban populations are exposed to urban emissions at a lower level of dilution than the overall regional population. Here, I define the periurban compartment as a 100-km box. Analysis of gridded US population data (Seirup and Yetman, 2006) indicates that for a grid cell resolution of 100 km, the population-weighted mean population density of the USA is ~390 km^{-2}, which I round here to 400 km^{-2}. At this population density, the cumulative population enclosed by the 100 km periurban box is 4 million, of which 1.5 million people reside within the urban core and 2.5 million reside within the periurban compartment. For the megacity scenario, the periurban box has the same overall spatial extent, but a larger population (6 million). Thus, the urban compartment for the megacity scenario represents the most heavily urbanized "core", while the periurban compartment is indicative of a populous urban fringe.

The sizing of the regional-scale box determines the overall residence time of air within the model system, and thus has a strong effect on the amount of photochemical aging that can take place in the model system. In base-case simulations, I consider a 400-km regional domain, which results in a residence time of ~1 day under the wind speeds considered here. In the same gridded US population data as above, the population-weighted mean population density of the USA is ~100 km^{-2} for grid cells of 400 km size. Thus, the combined population within a 400 km domain is approximately 16 million. For the base-case and megacity models, the incremental population in the outer regional box is assumed to be 12 million.

The terminology and conceptual model used to describe and develop the model compartments merits brief elaboration here. The principal focus of this analysis is on the inhalation intake consequences of urban emissions, which are represented with releases into the core urban compartment. Note, however, that the periurban and regional population also partially resides within cities, because the average spacing between US cities is smaller than the 400 km length scale of the model domain. In the terminology employed here, the descriptor "urban" is reserved exclusively for the core urban model compartment, and the term "intraurban" refers to

exposures to material of urban origin that take place within the core urban compartment. All population in the outermost compartment is described as "regional", regardless of whether that regional population resides in a city or a rural area. Thus, the term "regional" should not be conflated with "rural." Note also that this simplified three-compartment geometry imposes a small downward bias on the level of OA exposure that might take place within cities located in the regional compartment. Since cities typically have higher OA concentrations than the areas that surround them, the partitioning of semivolatile regionally transported material tends to shift further into the particle phase as it advects into a city. This feature is accounted for in the core urban compartment, but is not incorporated into the regional compartment. This simplification imposes a small (~5% - 10%) downward bias on the exposures that would take place in cities located in the regional compartment.

4.2.3 Intake fraction for semivolatile compounds in a multi-compartment system

Owing to the atmospheric transformations of emitted semivolatile compounds, the intake fraction for organic carbon emissions requires a more precise definition than has been presented in previous chapters or other studies (e.g., (Bennett et al., 2002; Marshall et al., 2003)). As a source-oriented metric, the intake fraction must be able to trace the material inhaled in any arbitrary compartment back to the compartment in which the emissions originally occurred. In a conceptually similar fashion, the intake fraction as defined here attributes semivolatile material inhaled in any arbitrary volatility bin to the emitted volatility bin of its original precursor material. Thus, it is possible to define an intake fraction for emissions into each of $y = 1 \ldots M$ model compartments for emissions of each of $i = 1 \ldots N$ volatility bins C_i^*. In the present scheme, $M = 3$ (i.e., urban, periurban and regional compartments), and $N = 10$ (ten individual VBS volatility bins). The following system of subscripts is employed here to attribute the concentration C of semivolatile material in any compartment to its source model compartment and originally emitted volatility bin. For the N volatility bins that comprise the VBS here, the subscript i represents the volatility bin of material at the time of emission. To track the evolving volatility distribution of this material, the subscript j represents the current volatility level at a given model time step. Likewise, emissions into each of M compartments are tagged with subscript $y = 1 \ldots M$, and are tracked as they move into compartments $z = 1 \ldots M$. Thus, a total of $M^2 \times N^2$ tagged species are tracked in this model.

A related issue is the set of units used to track material between emissions and inhalation intake. Most studies express iF as a dimensionless ratio of mass inhaled to mass emitted. Here, I adopt a slight modification, focusing exclusively on the flow of organic carbon atoms through the model system. Intake fraction values are computed as the mass ratio of inhaled organic carbon atoms to emitted organic carbon atoms. This modified accounting approach is necessary to avoid over-counting the inhalation intakes of relatively more oxidized material, since the total weight of organic molecules increases as the result of reactions that add oxygenated functional groups to organic precursors (Jimenez et al., 2009). Thus, the accounting basis for iF calculations (dimensionless mass ratio of organic carbon atoms) contrasts with the basis used to present OA mass concentrations, which fully accounts for the non-carbon atoms that also contribute mass to the molecular constituents of the organic aerosol.

For emissions of semivolatile material into a compartment y, the intake fraction iF_y can be represented as a summation over a set of partial intake fraction values ($iF_{y,z}$) which represent the

intake fraction for populations exposed in each of M compartments z in which inhalation intakes occur. Formally, this summation is represented as follows:

$$iF_y = \sum_{z=1}^{M} iF_{y,z} \text{ where } iF_{y,z} = \frac{P_z \sum_{i=1}^{N}\sum_{j=1}^{N}\left(\int_{T_1}^{T_2} q_B(t) C_{i,j,z,y}(t)\,\mathrm{d}t\right)}{\sum_{i=1}^{N}\left(\int_{T_1}^{T_2} E_{i,y}(t)\,\mathrm{d}t\right)} \quad [4.5]$$

Here, the summation term in the denominator of $iF_{y,z}$ considers organic carbon emissions distributed over volatility bins $i = 1 \ldots N$. In the numerator, the double set of summations accounts the effects of atmospheric aging, which redistributes fresh organic carbon emissions into $j = 1 \ldots N$ volatility bins. Accordingly, this iF metric represents the emissions-weighted average intake fraction evaluated over the entire volatility distribution, including material emitted in the particle and vapor phases. The concentration C in each compartment z is assumed to represent the population-average exposure concentration of organic carbon for the P_z individuals in that compartment. Individuals in all compartments inhale air at a time-dependent rate q_B, expressed in units of $m^3\ s^{-1}$. Assumptions for the population-weighted mean breathing rate (equivalent to 14.5 $m^3\ d^{-1}$) and diurnal profile of breathing are consistent with those in Chapter 3 (Figure 3-1; also see Appendix B).

Note here that the integrals in both numerator and denominator are evaluated over the time domain (T_1, T_2), in contrast to a more common formulation of the iF metric where the upper time limit of the numerator integral is evaluated as $T_2 \rightarrow \infty$ (e.g., (Marshall et al., 2003). An analytical approximation is employed here to obtain an unbiased estimate of the time-averaged iF, based on the observation that the simulated temporal pattern of emissions, meteorology, and inhalation intake follows a diurnal cycle that repeats on a time scale (24 h) that is much shorter than the integration length ($T_2 - T_1$). Here, I employ a 5-day spinup period to reach a consistent diurnal pattern for concentrations, and then evaluate the intake fraction using trapezoidal integration over the 5-day time period from $T_1 = 120$ h to $T_2 = 240$ h. The emissions-to-concentration model (described below) is solved using a variable time-step differential equation solver (MATLAB routine: *ode15s*), with minimum precision of 0.1% for hourly reported solutions.

The average intake fraction iF_y (equation [4.5]) can be disaggregated in a manner that provides useful insight into the location and phase partitioning of population intake of semivolatile material originally emitted into compartment y. For example, for emissions of semivolatile material into urban area y, it is valuable to understand the relative distribution of population intake of that material between urban area y's own residents (intraurban intake) and populations who live outside of city y (downwind intake). Similarly, emitted semivolatile material will be inhaled as some mixture of POA, OPOA or vapors. Each of these contributions to intake differs in its different spatial distribution among model compartments. Formally, I disaggregate iF_y into the following series of additive terms:

$$iF_y = \sum_{z=1}^{M}\left(iF_{y,z}^{\mathrm{POA}} + iF_{y,z}^{\mathrm{OPOA}} + iF_{y,z}^{\mathrm{vap}}\right) \quad [4.6]$$

This expression separately considers the contributions to intake of material inhaled as POA, OPOA and vapors in each of $z = 1 \ldots M$ compartments. The partial inhalation intake fractions for POA, OPOA and vapor-phase material emitted into compartment y by residents in compartment z are defined as follows:

$$iF_{y,z}^{\mathrm{POA}} = \frac{P_z \sum_{i=1}^{N} \int_{T_1}^{T_2} q_B(t) C_{i,j=i,z,y}(t) \xi_{j=i,z}(t) \mathrm{d}t}{\sum_{i=1}^{N} \left(\int_{T_1}^{T_2} E_{i,y}(t) \mathrm{d}t \right)} \quad [4.7]$$

$$iF_{y,z}^{\mathrm{OPOA}} = \frac{P_z \sum_{i=1}^{N} \sum_{j=1}^{i-1} \int_{T_1}^{T_2} q_B(t) C_{i,j,z,y}(t) \xi_{j,z}(t) \mathrm{d}t}{\sum_{i=1}^{N} \left(\int_{T_1}^{T_2} E_{i,y}(t) \mathrm{d}t \right)} \quad [4.8]$$

$$iF_{y,z}^{\mathrm{vap}} = \frac{P_z \sum_{i=1}^{N} \sum_{j=1}^{N} \int_{T_1}^{T_2} q_B(t) C_{i,j,z,Y}(t) \left(1 - \xi_{j,z}(t)\right) \mathrm{d}t}{\sum_{i=1}^{N} \left(\int_{T_1}^{T_2} E_{i,y}(t) \mathrm{d}t \right)} \quad [4.9]$$

Note that in each of these three expressions, the denominator (emitted mass) remains identical to that in equation [4.5], in which the entire emitted volatility distribution is considered as the basis for computing *iF*. Here, for any compartment *z,* the parameter $\xi_{j,z}(t)$ represents the particle-phase partitioning coefficient for the material in volatility bin *j* at time *t.*

In implementation, POA and OPOA intakes are distinguished by the selection of volatility subscripts *j* included in the numerator's summation term in the above equations [4.7] and [4.8]. Material that remains in its emitted volatility bin ($j = i$) is considered to be POA, whereas material that has been aged into a lower volatility bin ($j < i$) is treated as OPOA. The intake fraction for vapors $iF_{y,z}^{\mathrm{vap}}$ considers all vapor-phase material without regard to degree of aging.

Finally, it is worthwhile to briefly introduce a companion metric to intake fraction, the population intake rate ("intake") *I.* For a given emissions source compartment *y* and receptor compartment *z,* the time-averaged population intake rate $I_{y,z}$ (units: mass of semivolatile material inhaled per time) is the time average of the product of the attributable concentration $C_{y,z}$ and the population breathing rate ($P_z \times q_B$). If organic material is accounted for strictly in terms of its organic carbon mass (i.e., neglecting other atomic constituents), *I* is also equivalent to the product of the mass emissions rate E_y and the intake fraction $iF_{y,z}$. If organic material is

accounted on a full mass basis including its non-carbon constituents, the proportionality $I \sim E \times iF$ is approximate rather than precise.

As with the intake fraction, further aggregation, disaggregation, or specification of population intake is possible. For example the metrics I^{OA} (particle phase) and I^{vap} (vapor phase) are used here to represent the population intake rate of organic material attributable to a particular source. The intake rate metric most usefully adds new information when comparing the inhalation exposure consequences of two or more emissions sources with differing characteristics (e.g., emissions rates). For a fixed basis of emissions, intake fraction and intake rate behave similarly. For example, for a single emissions source that causes exposures in multiple model compartments, the proportional contribution of populations in each compartment to the total intake fraction and to the total population intake will be similar (if expressed in terms of total organic mass) or precisely the same (if expressed in terms of organic C atoms). Here, I adopt the following accounting conventions in reporting the inhalation intake rate. In contexts where the term "intake" is used to explain how intake fraction results may be disaggregated, I report results computed on the standard carbon-only basis used for *iF* calculations. In contrast, when directly reporting the inhalation intake rate as an independent physical quantity, I do so on the basis of the full organic mass (i.e., for particle phase intakes, I [=] gOA d^{-1}).

4.2.4 Differential material balance

The following differential material balance describes the physico-chemical evolution of semivolatile material as it moves through various model compartments.

$$V_z \frac{\mathrm{d}\left(C_{i,j,y,z}\right)}{\mathrm{d}t} + C_{i,j,y,z} \frac{\mathrm{d}\left(V_z\right)}{\mathrm{d}t} = F^{\mathrm{in}}_{i,j,y,z} + E_{i,j,y,z} + P_{i,j,y,z} - D_{i,j,y,z} - F^{\mathrm{out}}_{i,j,y,z} \qquad [4.10]$$

Here, within any compartment *z, V* represents the volume of that compartment*; C* represents the concentration of material in that compartment using the subscripting scheme described below; F^{in} represents the inflow of material from other compartments in the model system, *E* represents the emission of new material*, P* represents the net photochemical production of material, *D* represents deposition and/or destructive removal of material from the model system, and F^{out} represents removal of material from the model compartment via outflow (advection). Each of these processes is described in further detail below. Equation [4.10] partially accounts for the effects on dilution of temporally variant mixing heights (and thus temporally varying model volume *V*), as elaborated below.

The time-dependent inflow F^{in} and outflow F^{out} of material from a given model compartment *z* depends on meteorology and the concentration of material in each compartment in the model system. For advection between any two compartments, Q = *WHu* where *W* is the crosswind length scale of the interface (m), *H* is the mixing height (m), and *u* is the wind speed averaged over the mixing depth. Consider the flow of material in and out of a single model compartment *Z.* Advective flows from all other $z = 1 \ldots M$ model compartments into compartment *Z* are represented with a vector of values $Q_{z \to Z}$. For a compartments that do not interface with *Z*, $Q = 0$; likewise, $Q_{Z \to Z}$ is by definition zero since each compartment is already assumed to be well

mixed. Then, the net flow of material into a specific compartment Z is simply the sum of influent material flow rates into that compartment from all other $z = 1\ldots M$ compartments for which interfaces exist. Formally, this inflow F^{in} is given as:

$$F^{\text{in}}_{i,j,y,Z} = \sum_{z=1}^{M} C_{i,j,y,z} Q_{z \to Z} \qquad [4.11]$$

Correspondingly, the outflow depends on the concentration of material within compartment Z and the advection of air into other compartments. Here, the outflow of air to all other $z = 1\ldots M$ compartments $Q_{Z \to z}$ is simply summed, and thus the outflow of material from compartment Z to all other compartments is formally given as:

$$F^{\text{out}}_{i,j,y,Z} = \left(C_{i,j,y,Z}\right) \sum_{z=1}^{M} Q_{Z \to z} \qquad [4.12]$$

Photochemistry transforms the volatility distribution j of material in each compartment. In the simplified reaction mechanism employed here (Figure 4-1), aging is represented by gas-phase oxidization of organic vapors initiated by the OH radical. Each oxidation reaction reduces the volatility of gas-phase material by one VBS bin. The transformation of material is described by $P_{i,j,y,z,}$ which represents the net photochemical production minus loss of material in each volatility bin j. For compactness of notation, the following discussion will neglect the subscripts for model compartments (y, z) and for the originally emitted volatility bin (i). For a VBS with $j = 1\ldots N$ volatility bins, the net production minus loss P_j is defined as follows:

$$P_j = \left(k_{\text{OH}} C_{\text{OH}}\right) \times T_j \text{ where } \mathrm{T}_j = \left\{ \begin{array}{cc} C^{\text{vap}}_{j+1} & \text{for } j = 1 \\ \left(C^{\text{vap}}_{j+1} - C^{\text{vap}}_{j}\right) & \text{for } j = 2\ldots(N-1) \\ -C^{\text{vap}}_{j} & \text{for } j = N \end{array} \right\} \qquad [4.13]$$

Here, k_{OH} is the second-order photochemical rate coefficient for oxidation initiated by OH radicals (cm^3 molecules^{-1} s^{-1}), C_{OH} is the OH radical concentration (molecules cm^{-3}), and C^{vap} is the vapor-phase concentration of organic material to be oxidized. Considering the intermediate members of the VBS, gas-phase material with a given value of C^* is produced by the oxidation of more volatile material, and then subsequently transformed via oxidation to a lower volatility level. Note that there is no photochemical production of material in the most volatile VBS bin ($j = N$), and no further reduction in volatility beyond the lowest bin ($j = 1$). Following Robinson et al. (2007) and Shrivastava et al. (2008), I assume a k_{OH} value of 4×10^{-11} cm^3 molecule^{-1} s^{-1}. Shrivastava et al. (2008) note that this rate constant estimate is "slightly higher than average." Thus, model results may provide an overestimate of the amount of photochemical conversion of material from vapor to particle phase. I test the effects of slower photochemistry by perturbing C_{OH} values, as described below. (Note that the net rate of photochemical production P_j is proportional to the product $k_{\text{OH}}C_{\text{OH}}$.) Finally, note that the modeling framework makes the simplifying assumption that k_{OH} is constant across all volatility bins and independent of

temperature and other environmental variables. This assumption is commonly made elsewhere in the VBS literature and represents an idealization of a more complex reality (Donahue et al., 2006; Robinson et al., 2007; Shrivastava et al., 2008).

Since photochemistry is assumed to proceed only in the gas phase, total photochemical production is proportional to the vapor-phase concentration vector C^{vap}, which in turn depends on the gas-particle partitioning in the compartment. For each volatility bin j, the vapor-phase partitioning coefficient is simply the complement of the particle phase partitioning coefficient (i.e., $[1-\xi_j]$.) Since this partitioning coefficient depends on the total OA loading in the compartment (see equation [4.2] and equation [4.3]), the evaluation of the differential mass balance for any single compound must simultaneously consider all contributions to OA from each source volatility bin i and each source compartment y.

This model accounts for the effects of temporal variation in mixing height on inhalation exposure, as follows. In general, nighttime mixing heights in all model compartments are substantially lower than for daytime conditions (see §4.2.5 for details). In the model formulation embodied in equation [4.10], the time-variant mixing height imposes two distinct effects on the mixing of material in the model compartment. First, under conditions where H is high, emissions will be diluted into a greater volume than when H is low. Thus, the attributable concentration that results from a fixed unit of emissions is inversely proportional to the mixing height. A secondary consideration that requires careful elaboration here relates to the effect of *changing* mixing heights on the entrainment and removal of material contained in aloft air layers. In Chapter 3, the dynamic box model explicitly considers the effect of rising and falling mixing heights. In that model (equation [3.2]), I assume that clean aloft air ($C = 0$) is entrained into the single model compartment under periods of rising mixing height. This assumption has the effect of providing a modest increase in the dilution of urban emissions under periods of rising mixing height. In contrast, under conditions of falling mixing height, there is no exchange of material through the top of the model "box," since contaminated material is assumed to remain aloft while concentrations at ground level are unaffected. A crucial assumption in the single-compartment model is that the contaminated material in the aloft layer is entirely removed from that layer before the mixing height increases again (thus, in equation [3.2], $\phi = 1$ for periods of rising mixing height, and $\phi = 0$ at all other times). This assumption poses a key challenge in the present multi-compartment model considered here.

In the present analysis, I consider the additional vertical dilution that occurs under conditions of rising mixing height for the urban compartment, and neglect this process for the regional and periurban model compartments. The reason for the simplified treatment in the outer two model compartments is that the vertical exchange of aloft material is difficult to represent in a physically realistic manner for a multi-compartment system. A key challenge relates to the scale dependence of the entrainment phenomenon using the model formulation presented in Chapter 3. The amount of dilution provided by mixing with aloft layers scales with the land area of each model compartment. In contrast, the amount of dilution that results from advection scales with the characteristic length of each compartment. For the 25 km urban model compartment, the entrainment of clean aloft air increases dilution by ~15%. In contrast, addition of this entrainment term would increase dilution by more than 3× for the 400-km regional domain, such that the advective (wind-driven) component of dilution accounts for <25% of the overall removal of contaminated material. Clearly, this treatment of entrainment is not physically realistic at large

length scales. The reason for this puzzling result lies with the assumption that material "left behind" in an aloft layer during periods of falling mixing height is not re-entrained during periods of rising mixing height. While this assumption may be nearly true for a small urban compartment, substantial re-entrainment seems quite plausible for a model compartment that is several hundred kilometers in length. In order to adequately account for this re-entrainment, an additional model dimension that accounts for transport in aloft layers would be required. Instead of adding this layer of complexity, I make the simplifying assumption here that all material excluded from the model system in the periurban and regional compartments during periods of falling mixing height is re-entrained into the same model compartment during periods of rising mixing height. In doing so, the additional contribution to dilution from the $C \times \mathrm{d}V/\mathrm{d}t$ term on the left hand side of equation [4.10] is neglected for these two outer compartments. Future analyses could usefully refine this treatment of aloft material.

In the default model case, dry deposition for particles is the only removal process considered. Dry deposition is modeled using a time invariant deposition velocity v_{dep}. A time-dependent effective first-order deposition loss coefficient $k_{\mathrm{dep},z}$ for compartment z is then defined as $k_{\mathrm{dep},z} = v_{dep} / H_{z,}$ where H_z is the time-dependent mixing height in compartment z. The loss process is then given as:

$$D_{i,j,y,z} = k_{\mathrm{dep},z}\left(C_{i,j,y,z} \times \xi_{j,z}\right) . \qquad [4.14]$$

Here, $\xi_{j,z}$ is the particle phase partitioning coefficient for material in compartment z with saturation concentration C_j^*. In base-case modeling, I employ a default deposition velocity of 2.5 mm s^{-1}, which implies a time-averaged quasi-first-order loss timescale ($\tau_{\mathrm{dep}} = k_{\mathrm{dep}}^{-1}$) of ~30 h. This value is consistent with a widely-cited midpoint estimate of the deposition velocity for ~300 nm particles (Zhang et al., 2001). Sensitivity scenarios consider non-depositing particles, as well as alternate values of v_{dep} (1 mm s^{-1}, 5 mm s^{-1}, 7.5 mm s^{-1}) that roughly bound plausible conditions for accumulation mode particles. Once dry deposition occurs, I assume that all deposited material is completely removed from the model system, and no further gas-particle exchange occurs between the deposition surfaces and the airborne semivolatile material in the compartment. This assumption is adequate for compartments with large volumes (i.e., urban or regional airsheds); however, it may be inappropriate to maintain this assumption if this model were later extended to include smaller compartments or indoor environments (Weschler and Nazaroff, 2008; Weschler and Nazaroff, 2010). Finally, note that dry deposition of gas-phase material is not considered here. Wet deposition of particles and gases is likewise neglected.

4.2.5 Other model input variables

Wind speed and mixing height

To develop an archetypal diurnal cycle of the meteorological parameters relevant to dilution, I obtained hourly wind speed and mixing height data for 243 US cities for the years 2007-2009 from the NASA MERRA reanalysis dataset used in Chapter 3 (Rienecker et al., 2011). I used the power-law wind speed model described in Chapter 3 to estimate hourly mixing-depth averaged wind speeds for each city in the dataset. For each city, I constructed a "typical meteorological

day" by computing the harmonic mean values of wind speed U, mixing height h and the normalized dilution rate $h \times U$ for each hour of the day over all observations in the 3-year data set. Finally, I developed a single archetypal meteorological profile for the entire US dataset (Figure 4-3) by computing the mean of the hourly values over all 243 cities' typical meteorological days for wind speed and mixing height. For this combination of diurnal profiles, the harmonic mean dilution rate (harmonic mean of the product $h \times U$) is ~600 $m^2 s^{-1}$, which is consistent with the population-weighted mean dilution rate ~610 $m^2 s^{-1}$ estimated for land-rich developed countries in Chapter 3 (Table 3-4) and slightly more than the global population-weighted mean estimate of 540 $m^2 s^{-1}$. The mixing-depth averaged harmonic mean wind speed over the diurnal cycle is ~4.6 m s^{-1}, which leads to an advection time scale of ~24 h for a 400 km model domain.

I assume that this archetypal mixing height and wind speed profile holds for the urban model compartment. For the periurban and regional compartments, I follow the approach of Humbert et al., wherein the "rural" mixing height exceeds the urban mixing height to account for the greater vertical dilution that can take place over longer spatial scales (Humbert et al., 2011). Here, I adopt the simplifying assumption that the mixing height of the periurban and regional compartments is twice that of the urban compartment at any given hour. The wind speed does not vary among the three model compartments. In alternative sensitivity scenarios, I consider the effects of slower wind speeds, regionally invariant mixing heights, and minimum mixing heights.

OH radical profiles and ambient temperatures

Aging of gas-phase material depends on the concentration of OH radicals, C_{OH}, which varies in time (diurnally, seasonally) and in space (e.g., varying between model compartments). I use a mean-normalized diurnal profile of OH concentrations (Figure 4-4) measured under urban summertime conditions in New York City to represent the time evolution of OH radicals in all model compartments over the course of a day (Ren et al., 2003). In this profile, peak afternoon (1300 h – 1500 h) OH concentrations are ~2.5× higher than the 24 h average and overnight minimum radical concentrations (0300 h – 0600 h) are ~80% lower than the 24 h average. For base-case model runs, I assume that the 24 h mean (daily peak) C_{OH} is 1.5 (3.9) × 10^6 molecules cm^{-3} in the regional compartment. Radical levels are typically higher in the immediate downwind region of the urban core, and attenuated in the urban core (e.g., Mollner et al., 2010) owing to reaction with elevated levels of nitrogen oxides ($NO_2 + OH \rightarrow HNO_3$) in areas with high levels of primary combustion emissions. In base case modeling, I account for this phenomenon by assuming that OH concentrations are equal in the urban and regional compartments, and 50% higher in the periurban compartment. Overall, these spatial and temporal patterns are broadly consistent with summertime field observations in the Eastern USA (Ren et al., 2003; Ren et al., 2005). Alternative sensitivity scenarios consider the effect of perturbing the mean value and spatial distribution OH radical concentrations, and incorporate winter as well as summer conditions (Ren et al., 2006). To simulate diurnal shifts in gas-particle partitioning associated with temperature, I use a default temperature profile with daily mean temperature of 25 ºC. The peak temperature of 32 ºC is achieved at 3 pm, relaxing to a nighttime minimum of 17 ºC at 6 am. I consider alternative temperature profiles as sensitivity scenarios, including profiles more representative of wintertime conditions.

4.2.6 Emissions

The volatility distribution of organic emissions matches the distribution used in the simulations of Robinson et al. (2007) and Shrivastava et al. (2008), reproduced here in Table 4-1 and Figure 4-5. This distribution was derived by applying partitioning theory (i.e., equations [4-2] and [4-3]) to isothermal dilution sampler measurements of diesel exhaust emissions (Lipsky and Robinson, 2006; Robinson et al., 2007). Since the quartz filter sampling approach employed by Lipsky et al. is unable to efficiently collect IVOC material, Robinson et al. estimated the emissions contributions from IVOCs using top-down constraints and simulated aging experiments (Robinson et al., 2007). The gas-particle partitioning of emissions depends on the dilution level at which they are measured. To avoid the "moving target" that is inherent to dynamic shifts in partitioning, emissions for *iF* calculations do not distinguish between particle and vapor phase material. Aggregate intake fraction calculations consider the total emitted mass of all semivolatile material (i.e., both SVOCs and IVOCs) in the denominator. Additional disaggregated *iF* calculations separately consider SVOC emissions, IVOC emissions, and emissions into individual volatility bins, as described below.

The volatility distribution of Robinson (Figure 4-5) should be considered a highly stylized representation of semivolatile organic emissions from one type combustion source (diesel engines) that is relevant to on-road emissions. Fuel-related emissions from different vehicle fleets, fuel types (e.g., gasoline, diesel, CNG) and engine technologies are likely to have different volatility distributions, whereas lubricating oil contributions to semivolatile emissions may be similar for different vehicle technologies. Data on the emissions volatility distribution for vehicle fleets are only just becoming available (May et al., 2013a). The modeling approach used here could be adapted to incorporate such data in the future.

The total mass emissions rate of semivolatile material into each model compartment is assumed to be proportional to the population in the compartment. A single global parameter, the per-capita emissions rate, is provided as a model input parameter. I tuned this per-capita emissions rate in order to obtain realistic values of C_{OA}. In base-case model simulations, the emissions rate of semivolatile organic material is ~25 g person^{-1} day^{-1}. This base-case value is reconcilable with top-down estimates. For example, Shrivastava et al. (2008) synthesized emissions inventory data to estimate total US anthropogenic semivolatile POA emissions at ~1.1 Tg y^{-1} (~ 10 g person^{-1} d^{-1}), and estimated an additional contribution from unaccounted IVOC emissions at ~15 g person^{-1} d^{-1}. The temporal distribution of emissions matches the default model input employed in the global *iF* analysis described Chapter 3 (Figure 3-2) where emissions peak during morning and evening rush hours (~1.5× the 24 h average), and are at a minimum at night and early morning hours (~0.5× the 24 h average). Because this modeling analysis emphasizes the emission-to-intake relationship for urban combustion emissions, I neglect here the additional emissions contributions from biogenic sources.

In addition to the semivolatile organic species that are the emphasis of this chapter, I also consider the intake fraction for primary, nonreactive species. The utility of inert tracer species for this analysis is twofold. First, the *iF* estimates for primary nonreactive pollutants determined here can be compared directly with the results from Chapter 3. Second, the nonreactive pollutant provides a useful benchmark for comparison with the semivolatile organic species. This comparison can yield useful insights about the relative contribution of dilution vs. pollutant

dynamics in governing the intake fraction of semivolatile species. Model runs therefore also include intake fraction estimates for the emission of two types of inert tracer species: a conserved pollutant ($iF^{conserved}$), and an inert (nonreactive) particle that experiences quasi-first-order losses by dry deposition ($iF^{inertPM}$). The dry deposition velocity for inert particles matches the default v_{dep} for organic particles (base case: 2.5 mm s^{-1}). The temporal pattern of emissions for both nonreactive species is identical to that of the semivolatile organic emissions.

4.3. Results and discussion

4.3.1 Concentration results

Since gas-particle partitioning is a strong function of C_{OA}, an accurate determination of intake fraction requires that the model produce realistic estimates of organic aerosol concentrations. This section summarizes key aspects of model performance related to the simulation of organic aerosol concentrations. Concentrations are expressed in this section in terms of total OA mass, that is, including the mass of the non-carbon constituents of the organic aerosol.

Particle and vapor-phase concentrations of semivolatile material are reported in Table 4-2, Figure 4-6 and Figure 4-7 for the base-case and megacity scenarios. The per-capita emissions rate (see §4.2.6) was tuned to produce a time-averaged urban C_{OA} concentration consistent with the mean urban concentrations reported by a large global meta-analysis of organic aerosol concentrations (Zhang et al., 2007). For the base-case model simulation, the resulting time-averaged C_{OA} levels for the urban, periurban and regional compartments were respectively 7.4 μg m^{-3}, 5.4 μg m^{-3} and 2.8 μg m^{-3}. This concentration gradient reasonably approximates the mean C_{OA} levels reported by Zhang et al. (2007) for urban, urban downwind (<100 km from major urban areas), and remote sites (>100 km from major urban areas), reported as 7.6 μg m^{-3}, 4.7 μg m^{-3} and 2.8 μg m^{-3}. This comparison suggests that the simulated levels of C_{OA} are consistent with observations, and thus gas-particle partitioning in each model compartment is likely to be realistic. However, note that the present modeling does not consider the additional contributions to ambient OA from biogenic sources. Biogenic OA accounts for a non-negligible (~25%) fraction the global atmospheric OA burden (Jathar et al., 2011), and thus presumably accounts for some portion of the continental OA background summarized in the analysis of Zhang et al. (2007). Accordingly, anthropogenic emissions might be overestimated in the current analysis.

In the base-case scenario considered here, the relative contributions of primary (POA) and oxidized OA (OPOA) to total organic aerosol mass differ among the three compartments. The OPOA contribution to total OA mass in lowest in the urban compartment (67%) and higher in the periurban and regional compartments (respectively 89% and 93% of total OA mass, Table 4-3). This finding is in line with expectations. Theory suggests that the contribution of primary material will be greatest in near-source regions, since the elevated local emissions will contribute a higher fractional amount of total OA mass. Likewise, the short residence time of air within the urban compartment precludes substantial conversion of fresh local emissions into OPOA. In the base-case scenario, locally emitted material contributes ~43% of total OA mass in the urban compartment; only ~35% of that mass was aged into OPOA (Table 4-3).

Because functionalization reactions simultaneously reduce volatility and increase organic aerosol mass through the introduction of non-carbonaceous elements (e.g., oxygen), the ratio of OA mass to OC mass varies as a function of photochemical aging. The OA:OC mass ratio is greatest for material with a high fraction of substantially aged OPOA, and lowest for fresh POA. Overall, the addition of non-carbon atoms from photochemical aging increases the total mass of the organic aerosol by respectively 21%, 32%, and 36% in the urban, periurban, and regional compartments.

The modeled spatial distribution of OPOA and POA is also consistent with field observations. As a point of comparison, Zhang et al. (2007) employed factor analysis of 37 worldwide aerosol mass spectrometer (AMS) datasets to gain insight into the chemical composition and degree of atmospheric aging of OA source and downwind regions. In that work, Zhang et al. apportion total OA mass into two broad factor groupings, abbreviated OOA and HOA. The "oxygenated OA" (OOA) factor is thought to be dominated by oxidized material produced by photochemical aging, while the "hydrocarbon-like OA" (HOA) factor is considered more representative of primary emissions (Zhang et al., 2007). Averaged over all sites, the OOA factor contributed 63% of OA mass in urban sites, with higher fractional OOA contributions in urban downwind (83%) and remote sites (95%). Although the OOA-HOA factors of Zhang et al. do not map perfectly to the OPOA-POA construct employed here, findings from Zhang et al. are at least consistent with the spatial distribution of primary vs. aged material modeled here.

For the base-case scenario, the concentration of vapor-phase semivolatile material exceeds particle-phase concentrations (C_{OA}) in all compartments (Table 4-3). Here, it is useful to define the particle-phase partitioning coefficient $\xi_{p,}$ which represents the mass fraction of all semivolatile organic material in a given model compartment that is present in the particle phase. The partitioning coefficient ξ_p increases from 23% in the urban compartment to respectively 39% and 43% in the periurban and regional compartment. The higher ξ_p values in the periurban and regional compartments are attributable to photochemical aging of the vapor-phase material, which shifts the volatility distribution towards to lower C^* levels. Even so, on average most semivolatile mass resides in the vapor phase.

Particle-phase concentrations exhibit diurnal variability owing to temporal patterns in emissions, atmospheric dispersion, photochemical aging, and gas-particle partitioning (Fig 4-7). Emissions are assumed to peak during the morning and evening rush hours. However, the most substantial peak in OA levels occurs near midnight, when atmospheric dispersion is especially weak. A secondary peak occurs during the early morning hours as emissions begin to rise before daytime mixing conditions take hold. In the urban compartment, the overall contribution of POA to OA loadings varies substantially between nighttime (~40-50%) and mid-afternoon (~10-15%) conditions, primarily as a result of the daytime peak in OH radicals (Figures 4-6 and 4-7). High rates of photochemical conversion during the afternoon lead to an afternoon peak in the particle-phase partitioning coefficient ξ_p (Figure 4-6). Since higher afternoon temperatures promote evaporation of material into the vapor phase, these latter two findings suggest that the diurnal variability of OH radical availability has a more pronounced effect than temperature-induced shifts in partitioning for base-case conditions.

The megacity-scenario differs from the base-case scenario in several key regards. Organic aerosol loadings are higher in all compartments and the urban-to-background concentration

gradients are sharper compared to the base-case scenario (Table 4-3). The high urban OA loading (41 $\mu g\ m^{-3}$) in the megacity scenario is attributable primarily to the very large urban and periurban populations (respectively 18 and 6 million); per-capita emissions-rates are unchanged from the base case. The fractional contribution of local emissions (84%) and of POA (53%) is substantially higher for the urban compartment in the megacity case than under the base-case scenario (Table 4-3 and Figure 4-7). Similarly, a very large fraction of the ambient OA concentration in the regional compartment is attributable to the emissions of the urban compartment (48% for the megacity scenario, compared to 10% in the base-case scenario). Owing to the higher overall OA loading in all compartments, the particle-phase partitioning coefficients ξ_p are somewhat higher in the megacity scenario (Table 4-3). Finally, diurnal variability in total OA concentrations within the urban compartment is more pronounced for the megacity scenario, owing to the larger fractional contribution of local emissions to the total OA loading.

4.3.2 Intake fraction for primary, nonreactive pollutants

The intake fraction for distributed, ground level urban emissions of primary, nonreactive pollutants is summarized in Tables 4-4 and 4-5. For the base-case scenario (Table 4-4), the intraurban intake fraction for conserved, nonreactive pollutants ($iF^{conserved}$) is 11.5 ppm. The intraurban intake fraction for inert particles ($iF^{inertPM}$), which accounts for dry deposition losses, is 10.0 ppm. For comparison, the population weighted-mean intraurban *iF* for conserved pollutants in the 237 US cities with population < 7 million modeled in Chapter 3 is 12.3 ppm. This value is comparable to other published *iF* estimates for the US (Lobscheid et al., 2012; Marshall et al., 2005). Marshall et al. (2005) report a best estimate intraurban *iF* of 14 ppm for nonreactive ground-level emissions into US urban areas. For conserved, ground-level emissions and considering inhalation intakes within 50 km of the source, Lobscheid et al. report a nationwide population-weighted mean *iF* of 8.6 ppm. For counties in metropolitan areas with at least 1 million inhabitants, that study reports population-weighted mean *iF* of 14.0 ppm.

An important aspect of this study is the consideration of beyond-urban inhalation intakes. For urban emissions, exposed populations in the periurban and regional compartments each contribute additional incremental *iF* of 2.7 ppm for conserved, nonreactive pollutants. Thus, the considering intakes over the entire model domain, $iF^{conserved}$ is 16.9 ppm. Notably, the population of the urban compartment (1.5 million) constitutes < 10% of the total population in the model domain, whereas intraurban exposures accounts for ~68% of the total $iF^{conserved}$ for emissions into the urban compartment. For nonreactive particles ($iF^{inertPM}$) emitted in the urban compartment, the fractional contribution of intraurban intakes is further amplified, owing to more substantial dry deposition losses in outer model compartments. Overall, 78% of the domain-wide inhalation intake of urban emissions of inert particles takes place within the urban compartment. Out of the total domain-wide $iF^{inertPM}$ of 12.9 ppm for urban emissions, inhalation intakes in the periurban and regional compartments contribute *iF* of respectively 1.8 ppm and 1.1 ppm.

In the megacity scenario, the intraurban $iF^{conserved}$ (85 ppm) is comparable to my previous estimate for the global population-weighted mean intraurban *iF* for megacity emissions of conserved pollutants (~86 ppm, Chapter 3), but lower than point estimates for several prominent megacities (e.g., Dhaka, Mexico City, Kolkata, Hong Kong). Owing to the exceptionally high

LPD for the urban compartment (400 people m^{-1}), for the megacity scenario the intraurban *iF* accounts for a large majority (91%) of the total within-domain *iF* (94 ppm) for urban emissions (Table 4-5). For urban emissions of nonreactive particles in the megacity scenario, the domain-wide $iF^{inertPM}$ is 74 ppm, of which intraurban intakes (67 ppm) contribute the vast majority (94%) of total intake.

To summarize, for urban emissions of primary nonreactive pollutants, the intraurban *iF* accounts for a very large fraction (~68–94%) of the cumulative population intake that occurs within the 400 km model domain. Other studies have reached similar conclusions about the high relative importance of intraurban intakes for urban, ground-level emissions of nonreactive pollutants (Heath et al., 2006; Greco et al., 2007a).

4.3.3 Intake fraction for semivolatile organic compounds

Base-case model

The intake fraction of semivolatile organic emissions has a fundamental difference from the *iF* for primary, nonreactive emissions. Emitted semivolatile material can be inhaled in either the vapor or particle phase. Owing to the dynamic partitioning of semivolatile organics, the relative balance between inhalation intakes in the particle or gas phase varies strongly in space (e.g., between different model compartments), in composition (i.e., primary vs. aged material), and as a function of the volatility of emitted material. In the default model scenarios, dry deposition of particles (but not gases) means that the total *iF* for all emitted semivolatile material is lower than the *iF* for nonreactive, non-depositing species ($iF^{conserved}$), but higher than the *iF* for inert particles ($iF^{inertPM}$). For example, the sum of intraurban partial *iF* values for particle-phase (1.5 ppm) and vapor-phase (9.8 ppm) exposures to semivolatile urban emissions gives rise to a total *iF* for semivolatile emissions of 11.2 ppm (Table 4-4). This value is lower than the intraurban *iF* for nonreactive, conserved pollutants ($iF^{conserved}$ is 11.5 ppm), but higher than the *iF* for inert particles ($iF^{inertPM}$ is 10.0 ppm), since organic vapors are assumed not to experience depositional loss in the present model. This example also illustrates a key point about the phase partitioning of inhaled material. In the default emissions scenario, the volatility distribution of precursor material is skewed strongly towards more volatile compounds (Figure 4-5); ~80% of emissions have $C^* \geq 1000$ μg m^{-3}. A consequence of the highly volatile emissions distribution is that a large fraction of inhalation intake is in the vapor phase. Here, only ~14% of intra-urban inhalation intake of emitted semivolatile material is in the particle phase. It is useful to introduce a new metric here, X_p, defined as the fraction of *iF* (or equivalently, the fraction of inhalation intake of organic carbon) that occurs in the particle phase. In most circumstances considered here, a substantial or even dominant portion of the inhalation intake of emitted semivolatile compounds is in the vapor phase, rather than as particles (i.e., $X_p << 1$). Of course, this result is dependent on the volatility of emitted material. Subsequent sections and sensitivity analyses explore how this result varies for emissions with different degrees of volatility.

In the base-case scenario, and considering exposed populations throughout the model domain, only ~26% of the inhalation intake of semivolatile urban emissions is in the particle phase. However, the X_p for urban emissions varies substantially among the compartments in which exposures take place (Table 4-4). Consider here emissions to the urban compartment. As mentioned above, for intraurban exposures, the partial intake fractions for vapor (iF^{vap}) and

particle (iF^{OA}) exposures are respectively 9.8 ppm and 1.5 ppm (X_p ~17%). For residents of the periurban compartment, the relative importance of OA exposures increases (X_p ~29% for urban emissions); partial *iF* values for urban emissions are 1.7 ppm (vapor) and 0.7 ppm (OA). In the regional compartment, the partitioning of urban-attributable OA intake is nearly equal between particle and vapor phases (X_p ~47% for urban emissions). This pattern reflects the increasing photochemical transformation of urban emissions into low-volatility products (OPOA) as they advect from the urban compartment into the periurban and regional compartments. Since the X_p of urban emissions grows with increasing "downwind" distance, the overall contribution of beyond-urban exposures to the organic aerosol intake fraction iF^{OA} is much greater than for primary conserved pollutants. Considering the cumulative base-case iF^{OA} of 3.1 ppm for urban emissions, 29% of the domain-wide inhalation intake of urban emissions (0.9 ppm) is in the regional compartment, 23% (0.7 ppm) is in the periurban compartment, and only 48% of the total iF^{OA} is intraurban (1.5 ppm). Therefore, in contrast to conserved nonreactive pollutants, beyond-urban intakes constitute an important part (52% for the base case scenario) of the population exposure to particulate matter attributable to urban semivolatile vehicle emissions.

The spatial pattern of particle-phase intake fraction iF^{OA} has another important dimension: whether the inhaled material is primary (POA) or photochemically transformed (OPOA). Consider the base-case scenario for urban semivolatile vehicle emissions. Overall, iF^{OA} (3.1 ppm) is dominated by OPOA (iF^{OPOA} = 1.9 ppm), while primary material contributes ~38% of intake (iF^{POA} = 1.2 ppm). However, the POA:OPOA balance differs substantially among the compartments in which the products of urban emissions are inhaled. For intraurban intakes, iF^{POA} (1.0 ppm) substantially exceeds iF^{OPOA} (0.5 ppm). In contrast, primary material accounts for an order of magnitude less exposure than aged material in the regional compartment (iF^{OPOA} = 0.05 ppm; iF^{OPOA} = 0.85 ppm). It is this photochemical conversion of evaporated vapors into OPOA that is responsible for the large proportion (52%) of total domain-wide *iF* for urban emissions that occurs within the regional and periurban compartments.

Further insight into the dynamics of this system can be gleaned by directly linking inhalation intakes to the specific VBS volatility bin of originally emitted precursor material. While the emissions distribution for semivolatile organics is skewed towards compounds with the highest C^* values (IVOCs, $10^4 \leq C^* \leq 10^6$ μg m^{-3}; see Figure 4-5), partitioning dictates that lower-volatility primary emissions can produce substantial OA exposures with little or no aging. This tension poses an important question: which volatility bins are most capable of producing population intake of OA? It will become evident that the answer to this question depends on the choice of metric. In general, low-volatility emissions are particularly efficient at producing particle-phase exposures (iF^{OA} is high). However, the lowest volatility bins have rather low emissions rates, so the aggregate population intake rate I^{OA} (gOA inhaled per day) is not especially high. The pattern is opposite for the most volatile emissions, which do not lead to high OA exposures per unit emission (low iF^{OA}), yet result in a large population intake rate (I^{OA}) by virtue of their high emissions.

Volatility-bin specific estimates of *iF* and population intake rate (*I*) for semivolatile urban emissions are presented in Figure 4-8 (particle-phase: POA and OPOA) and Figure 4-9 (vapor phase). In the base-case model, the particle-phase intake fraction (Figure 4-8A) is dominated by primary, urban exposures for the emissions of less volatile species ($C^* <$ ~10 μg m^{-3}). For the lowest volatility bin (C^* = 0.01 μg m^{-3}), iF^{POA} is equivalent to the intake fraction for a

nonreactive primary particle, while $iF^{OPOA} \approx 0$. This result is a consequence of partitioning: for this volatility bin, nearly all emitted material partitions into the particle phase under atmospherically relevant conditions. As the volatility of emissions increases, three key trends emerge. First, X_p decreases with increasing volatility. For IVOC emissions, the emissions-weighted mean iF^{OA} is 1.6 ppm ($X_p = 10\%$), as compared to an iF^{OA} of 6.3 ppm ($X_p = 42\%$) for SVOC emissions (Table 4-4). The reason for this trend is that higher-volatility emissions require extensive aging in order to result in particle-phase intakes. A second trend is that the ratio iF^{OPOA}:iF^{POA} increases with increasing volatility of urban emissions. For example, for emissions with $C^* = 10$ μg m^{-3}, 42% of the resulting particle exposure is attributable to OPOA intakes, whereas for $C^* = 1000$ μg m^{-3}, 96% of the domain-wide particle exposure is attributable to OPOA. That finding makes sense; for a highly volatile compound to be inhaled in the particle-phase, the compound first needs to age and thereby become less volatile. Third, intraurban intakes are the largest contributor to iF^{OA} for low-volatility emissions, whereas beyond-urban intakes dominate iF^{OA} for high-volatility emissions. For urban SVOC emissions, intraurban intake accounts for ~50% of iF^{OA}. For IVOC emissions, the beyond-urban exposures account for ~80% of iF^{OA} (Table 4-4). For vapor-phase exposures (iF^{vap}, Figure 4-9A), these patterns are reversed. Higher-volatility emissions are predominantly inhaled in the vapor phase. For urban emissions with $C^* \geq$ ~100 μg m^{-3}, iF^{vap} substantially exceeds iF^{OA}. Considering all urban IVOC emissions, ~90% of inhalation intake occurs as vapors (Table 4-4). Interestingly, intraurban exposures contribute a disproportionately large fraction of the domain-wide exposure to vapors of urban origin (~77% of iF^{vap} is intraurban, see Table 4-4), since photochemical aging tends to shift downwind semivolatile material into the particle phase. As higher-volatility compounds (e.g., IVOCs) are emitted in especially high abundance (Figure 4-5), they contribute disproportionately to overall population intakes of vapor-phase emissions. IVOC emissions account for nearly ~80% of total urban-attributable I^{vap} (Figure 4-9B) owing to the high iF^{vap} for IVOC emissions (Table 4-4) and the large fractional contribution of IVOCs to total emissions (68%, Figure 4-5).

Megacity scenario

In the megacity scenario, the physico-chemical composition and spatial patterns of exposure to semivolatile urban emissions differ substantially from the base-case scenario. Table 4-5 presents *iF* estimates for this scenario. Given the population within the urban compartment, intraurban exposures are especially important. Here, I introduce the metric f^{urban} to quantify the fraction of material of urban origin that is inhaled within the urban compartment, evaluated on the basis of organic carbon atoms (i.e., neglecting non-carbon mass). For particle and vapor phase intakes, f^{urban} is respectively 86% and 94%. Compared to the base-case scenario, a somewhat larger fraction of all exposure is in the particle phase (iF^{OA} is 18 ppm, X_p is 21%). POA accounts for almost half of total OA exposure (43%). The distribution of population exposure by emitted volatility bin (Figures 4-8C and 4-8D) reinforces the notion that intraurban and POA exposures are especially important for megacity emissions. Overall, the megacity-attributable intake rate I^{OA} is more skewed towards lower-volatility emissions than for the base-case model. Although SVOCs account for only 32% of all organic emissions, these lower-volatility emissions account for nearly ~80% of the inhalation intake of OA. Interestingly, the distribution of OPOA exposures is much more strongly tilted towards intraurban exposures in the megacity scenario. In the base case model, the urban population only accounted for ~25% of I^{OPOA} of urban origin, whereas in the megacity scenario, intraurban intakes accounted for nearly

75% of I^{OPOA}. Thus, whereas atmospheric aging of a city's own emissions tends to chiefly result in beyond-urban exposures for a more typically sized city, photochemistry can have substantial effect on intraurban intakes for megacity emissions.

It is also worthwhile to compare the relative inhalation intakes that take place in the base-case and megacity scenario on a per-capita basis. Interestingly, the per-capita intraurban *iF* is somewhat lower for the megacity scenario than for the base-case scenario. In the analytical solution for the *iF* of primary, conserved pollutants in the single compartment model reported in equation [3.8], intraurban *iF* scales with the linear population density (*LPD*). In contrast, the per-capita intake fraction scales with the square root of urbanized land area ($A^{-0.5}$), but has no population dependence. Because the spatial extent of the megacity's intraurban compartment is larger than that for the base-case model, this simple analytical solution suggests that per-capita intraurban *iF* would be ~20% lower for the megacity model than for the base-case model for emissions of a primary, conserved species. For the full dynamic model simulation of a nonreactive particle subject to depositional loss, the per-capita intraurban *iF* is ~15% lower in the megacity model than in the base-case model. In contrast, for intraurban OA intakes attributable to urban emissions, the per-capita iF^{OA} is 34% larger in the megacity case than in the base case, owing to the higher fraction of semivolatile material that partitions into the particle phase in the megacity scenario. Accordingly, per-capita iF^{vap} is ~17% lower in the megacity model than under base-case conditions. In contrast to the per-capita *iF*, the per-capita population intake rate *I* is ~8.5× higher for the megacity scenario than for the base-case scenario. This increase in per-capita intake occurs because emissions are assumed here to scale linearly with population. Thus, even though the per-capita intake fraction is lower for the megacity model, overall emissions are substantially higher, and therefore the per-capita intake rate is much higher in the megacity model.

4.3.5 Contribution of beyond-urban emissions to urban exposures

In keeping with the focus of this dissertation on the exposure implications of urban emissions, the emphasis of this chapter is on the domain-wide exposures to semivolatile material that are attributable to urban emissions. However, it is also worthwhile to consider the effects of beyond-urban emissions on the anthropogenic OA intakes that take place in the urban compartment. In contrast to the (urban-) source-oriented perspective adopted elsewhere this chapter, in this section I adopt a receptor-oriented lens and consider urban exposures to domain-wide emissions. This perspective could be more relevant to local policy makers who might wish to reduce exposures within a given urban area. The suite of policy options available to mitigate regional and long-range contributions to urban exposures may be quite different than those for local emissions. Note that all figures in this sub-section are presented on the basis of total organic mass, including non-carbon constituents.

Considering the base-case scenario, for domain-wide emissions of a primary, conserved pollutant, 77% of the urban inhalation intake is attributable to the urban source. Emissions in the periurban and regional compartments respectively contribute another 14% and 9% of the total urban intake of this primary, conserved pollutant. Beyond-urban sources make a more pronounced contribution to urban intake of semivolatile organic particles. Regional, periurban, and urban sources contribute respectively 36%, 24% and 40% of total OA intake in the urban compartment. Given the more regional nature of photochemically aged material, beyond-urban

sources account for a very large fraction of urban intakes of OPOA. Thus, regional and periurban emissions account for respectively 49% and 29% of urban OPOA intake. Conversely, a large fraction of urban intake of POA is of urban origin (84%), owing to the high urban background of primary material and the highly aged nature of regional material. Overall, 92% of the beyond-urban contribution to urban OA intake is attributable to OPOA.

For the megacity case, urban sources account for a much larger fraction of urban OA exposures. Two factors explain this result. First, since the urban population produces a larger overall fraction of domain-wide emissions in the megacity scenario, the contribution of beyond-urban sources to urban exposures is relatively diminished. Second, the high population density of the megacity compartment imposes a high intraurban intake fraction, thereby magnifying the intraurban intake of urban emissions.

4.3.4 Comparing metrics: source-oriented exposure vs. atmospheric burden

Thus far, I have principally related results from the perspective of source-oriented exposure. The conclusions that I reach here at times align well with the conclusions of the existing literature on atmospheric organic aerosols. At other times, the "exposure" lens offers diverging insights from an atmosphere-oriented perspective. It is worthwhile to reflect on these similarities and differences.

The results of my simplified model broadly reproduce commonly observed gradients in organic aerosol concentration and composition, resulting in similar conceptual conclusions as those commonly made in the literature. In summary, for urban semivolatile emissions, dilution and evaporation result in a substantially lower particle-phase intake fraction for organic emissions than would be expected for nonreactive pollutants. However, the large reduction in volatility achieved after many hours of photochemical aging of evaporated vapors allows for downwind particle exposures to account for a much larger fraction of the total iF^{OA} than would be the case for a conserved pollutant. Whereas attributable concentrations of primary, nonreactive pollutants from a given source drop sharply with downwind distance, continuous conversion of material from the vapor to particle phase creates a much shallower downwind concentration gradient for OA attributable to an urban source (Robinson et al., 2007; Shrivastava et al., 2008; Wagstrom and Pandis, 2011a). Accordingly, when tens of millions of people live downwind, this widespread OPOA "plume" can create rather large downwind exposures. There is also an important receptor-oriented dimension to this phenomenon that complements the source-oriented *iF* perspective that I employ in this analysis. Since exposed populations are also sources of emissions themselves, it should be unsurprising that regional transport from elsewhere typically accounts for a large fraction of the ambient OA burden in any given urban area. In the present model, 57% (78%) of the ambient OA (OPOA) loading in the urban compartment is attributable to sources beyond the urban compartment (see Figure 4-7). Another modeling investigation reported similar findings for secondary organic aerosol in Pittsburgh, PA, where 63% of the local urban-ambient OA mass was attributed to transport from upwind regions ~100 – 600 km away (Wagstrom and Pandis, 2011b).

The exposure focus that I employ in this analysis contrasts sharply with "mass-in-atmosphere" perspective that is frequently employed by atmospheric scientists (eg., Jathar et al., 2011; Robinson et al., 2007). Metrics that consider the atmosphere as the unit of analysis, such as

the atmospheric OA burden, inherently tend to discount the experience of exposed individuals, because the earth's population has highly uneven spatial distribution and yet many important pollution sources, such as motor vehicles, are spatially correlated with population. For example, >50% of the world's population lives in cities that account for <0.5% of total land area (Schneider et al., 2009). Exposure metrics such as population intake and *iF* emphasize the conditions that prevail in cities and other human settlements. Whereas mass-in-atmosphere metrics are useful for understanding regional-scale and global phenomena (e.g., aerosol effects on climate; visibility impairment), exposure-oriented metrics are more relevant for understanding the human health impacts of air pollution.

It is worthwhile to contrast these two perspectives using the model simulation results of the present analysis. For base-case conditions, considering the atmospheric OA burden attributable to semivolatile urban emissions, only ~1.3% of the total OA mass is contained within the urban compartment, while 80% of the total mass is contained within the regional compartment. In contrast, ~43% of the domain-wide inhalation intake of organic aerosol mass of urban origin takes place solely within the urban compartment. Likewise, only 6% of the total urban-attributable OA burden in the entire model domain is POA, but 31% of the mass-based I^{OA} is primary. For lower-volatility emissions, the difference between these two perspectives is even starker. Roughly 60% of the domain-wide population OA intake of urban SVOC emissions takes place in the urban compartment, but only ~2.5% of the domain-wide atmospheric OA burden of SVOC emissions is contained within the urban compartment. In sum, domain-wide POA and intraurban OA concentrations account for only a small fraction of the total atmospheric OA burden, but play an important role in determining the population intake of organic aerosol attributable to urban emissions.

4.3.5 Sensitivity analyses

Table 4-6 summarizes *iF* results for sensitivity analyses. In this section, I evaluate sensitivity scenarios with respect to several key metrics that describe the distribution of intake fraction between vapor and particle phase, between urban and beyond-urban exposures, and between primary (POA) and aged (OPOA) material.

Emissions: magnitude and volatility

In Chapter 3, I argue that for primary, conserved pollutants, the intake fraction is independent of the bulk (time-averaged) emissions rate, since the numerator of the *iF* expression (the attributable population intake rate) changes in linear proportion to the denominator of the *iF* expression (the emissions rate). Strictly speaking, this property does not hold for semivolatile emissions, since phase partitioning and subsequent atmospheric aging is a function of ambient concentrations, which in turn depend on the emissions rate. As a consequence of partitioning, a higher per-capita emissions rate results in a higher iF^{OA} and lower iF^{vap}. However, the overall sensitivity is not large, even for substantial changes in emissions. For example, increasing (decreasing) the per-capita emissions rate by 3× increases (decreases) iF^{OA} by 15% (14%) and decreases (increases) iF^{vap} by 5% (4%). For a tripling in emissions, the overall fraction of population OA intake that is attributable to POA rises modestly to 44%, from 38% in the base-case scenario. This result represents an interesting consequence of partitioning: higher emissions

lead to higher C_{OA} levels, which in turn prevent the vaporization of material which could be subsequently oxidized into OPOA.

An additional sensitivity scenario was considered in which the bulk emissions rate was held constant, but assumed to be temporally invariant. For a flat diurnal emissions profile, the overall *iF* increases by ~25% compared to the base-case, owing to increased emissions during overnight periods with low mixing height. However, a shift to a time-invariant emissions rate does not substantially alter the phase partitioning or POA-OPOA balance of population intake.

Shifts in the volatility distribution that reweight emissions towards more volatile or less volatile species can have a more substantial effect on the volatility-weighted iF^{OA} and iF^{vap} values. As an example, I re-ran the base-case scenario using an alternative volatility distribution (Table 4-7) reported for diesel generator emissions (Grieshop et al., 2009). In that volatility distribution, SVOC emissions are skewed towards higher volatility levels, such that ~3× less material is emitted into the lowest three volatility bins ($0.01\ \mu g\ m^{-3} \leq C^* \leq 1\ \mu g\ m^{-3}$), with that reduction in emitted mass reassigned to higher-volatility SVOC bins ($10\ \mu g\ m^{-3} \leq C^* \leq 1000\ \mu g\ m^{-3}$). In this sensitivity case, the POA fraction of OA intake ($f^{POA} = iF^{POA} / iF^{OA}$) is substantially reduced (from 38% to 26%) and iF^{OA} is slightly reduced (from 3.1 ppm to 2.8 ppm). Opposite conclusions are reached for alternative emissions volatility distributions that reduce the contribution of IVOC emissions. For example, I considered modified version of the default emissions volatility distribution which halves the emissions rate for three most volatile emissions bins (IVOCs; $10^4\ \mu g\ m^{-3} \leq C^* \leq 10^6\ \mu g\ m^{-3}$). The net effect of de-emphasizing IVOC emissions is to increase iF^{OA} (by 20% for this scenario), since IVOC emissions tend to have substantially lower iF^{OA} than lower-volatility emissions (e.g., Figure 4-8). Moreover, particle-phase exposures attributable to urban IVOC emissions are almost exclusively in the form of OPOA. Consequently, reducing IVOC emissions somewhat increases the contribution of urban and POA exposures to domain-wide intake. Overall, these results suggest that a refined treatment of the emitted volatility distribution may alter the overall conclusions of this analysis, and more importantly that conclusions given here may or may not apply to specific emissions sources (whose volatility distribution may vary).

Meteorology and dispersion

As described in §4.3.1, the multi-compartment model realistically reproduces urban and regional patterns in OA concentrations and composition. However, the simplified treatment of dispersion is a key limitation of the present modeling approach. Accordingly, model results are sensitive to alternative assumptions about wind speed, mixing height, and the geometry of the multi-compartment system. In base-case simulations, mixing heights in the regional and periurban compartments are assumed to be twice as high as in the urban compartment. I considered an alternative sensitivity case in which the lower urban mixing height was applied to all three model compartments. This scenario resulted in a substantial increase in the domain-wide *iF* for urban emissions of nonreactive, conserved species (24 ppm, +39%), as well as for iF^{OA} (4.3 ppm, +40%) and iF^{vap} (16 ppm, +25%). For this scenario, much of the increase in *iF* occurs in the periurban and regional compartments. As a consequence, OPOA exposures make a larger overall contribution to population intake of urban emissions. Sensitivity scenarios that apply a global "floor" (120 m or 200 m) to the regionally varying mixing heights tend to reduce the

overall *iF* without substantially altering the ratio of intraurban to beyond-urban intakes or the ratio of vapor to particle-phase intakes.

Dry deposition

To test the sensitivity of results to the base-case dry deposition rate (v_{dep} = 2.5 mm s^{-1}), I evaluated two alternative scenarios that amplify or eliminate dry deposition (respectively 7.5 mm s^{-1}, 0 mm s^{-1}). For the case with no dry deposition, $iF^{inertPM}$ is 31% higher than base case, and is equivalent to the result for $iF^{conserved}$ (domain-wide $iF^{conserved}$ for urban emissions is 17.0 ppm). Because deposition has the largest effect on concentrations in the regional compartment (longer residence time), eliminating dry deposition substantially increases exposures to OPOA in the regional compartment, thereby increasing the domain-wide iF^{OA} for urban emissions (48% higher than base-case). In contrast, increasing v_{dep} by a factor of three (to 7.5 mm s^{-1}) reduces the domain-wide $iF^{inertPM}$ and iF^{OA} for urban emissions by respectively 25% and 31%. Higher rates of dry deposition have a larger effect on regional and OPOA intakes than on urban and POA intakes.

Compartment parameterization: population and land area

I consider sensitivity scenarios that increase the residence time of air in the model domain by either reducing the wind speed or increasing the overall size of the regional compartment. Halving the global wind speed slightly raises X_p (higher attributable concentrations shift partitioning toward the particle phase), but this change does not substantially alter the spatial distribution of exposure. In contrast, expanding the overall domain size by increasing the length scale of the regional compartment strongly influences *iF*, X_p, and the urban-regional balance of exposures. I considered two bounding-case sensitivity scenarios in which the outermost regional compartment is expanded in length-scale from 400 km to 800 km, corresponding to a mean air residence time of ~48 h. In the first scenario, the regional box is expanded while holding its total population (12 million) constant. Since the effective population density is dramatically reduced, I term this scenario "sprawl," following the typology of Marshall et al. (2005a). In the second scenario, termed "constant density", the regional box is expanded at constant average population density, thereby increasing that compartment's population to 60 million. In the sprawl case, the *iF* for urban-attributable exposures in the regional compartment decreases substantially (Table 4-6), since the regional population is spread more thinly and concentrations of urban origin are more thoroughly diluted. The domain-wide *iF* is reduced modestly for $iF^{conserved}$ and iF^{vap} (respectively -11% and -5%), and substantially reduced for iF^{OA} (-27%). The large reduction in iF^{OA} reflects the high *iF* contribution of regional-scale OPOA exposures to urban emissions in the base-case scenario. In sum, a larger regional compartment substantially increases the conversion of primary vapors into OPOA, but this increase in aging is more than offset by increased dilution and a lower population density.

The constant-density growth scenario results in very different outcome. Here, the population in the regional compartment increases substantially (by 5×). As a result, regional-scale OPOA exposures contribute a very large portion of the domain-wide iF^{OA} for urban emissions. Compared to the base-case, domain-wide $iF^{conserved}$ increases by 20%, iF^{OA} increases by 33%, while iF^{vap} increases by only ~2%. Here, the relatively large increase in OA intake is nearly entirely attributable to additional regional-scale exposures to OPOA of urban origin.

Accordingly, the intraurban fraction of total OA intake is lower than in the base-case (36% vs. 48%), and the fractional contribution of POA to overall OA intake is lower than in the base case (32%, down from 38%). However, the increase in OPOA intakes means that particle phase intakes constitute a larger fraction of total exposure to urban semivolatile emissions (X_p ~24%, compared to 20% in the base case).

Model results are also sensitive to the parameterization of the urban compartment. I considered two sensitivity scenarios that reduce the overall spatial extent of the urban compartment from its default size (25 km length scale). The first scenario is broadly representative of conditions for a typical Asian non-megacity (length 10 km, population 1.8 million), resulting in an urban linear population density 3× higher than under the base case. In this scenario, domain-wide $iF^{conserved}$ for urban emissions increases by 2.4× (41 ppm), and domain-wide iF^{OA} increases by 2.1× (6.4 ppm). Intraurban and POA exposures to urban emissions are strongly emphasized in this scenario: 73% of the domain-wide iF^{OA} of urban origin occurs in the urban compartment, and 61% of that material is as POA. In contrast, conditions more typical of a small, low-density US city reduce the importance of intraurban and POA exposures. A second sensitivity scenario idealizes conditions indicative of US cities with less than 600,000 inhabitants (LPD 25 m^{-1}, population ~310,000, length ~12.5 km). For this scenario, intraurban intakes account for only 24% of the iF^{OA} for urban emissions, and POA accounts for only 28% of iF^{OA}.

To summarize, this model's results are quite sensitive to changes in the way the individual model compartments are parameterized. Moreover, this sensitivity is directly relevant to this study's core questions about the relative importance of primary, intraurban exposures vs. secondary, regional exposures to urban emissions. In future work, side-by-side comparison of this model's results with more detailed chemical transport modeling is warranted.

Photochemistry

A final group of sensitivity runs considers parameters that govern the model's treatment of photochemistry. A simplified treatment of OH radical concentrations, in which C_{OH} does not vary among the three model compartments, resulted in only a small reduction in model-wide iF. Likewise, substantially reducing urban core OH levels (e.g., to account for titration of OH by primary NO_x emissions) reduces domain-wide iF^{OA} by less than 10%. These results are line with expectations. Since the residence time of air is relatively short in the urban and periurban compartments, lowering C_{OH} in these boxes does not lead to a large overall change in domain-wide OPOA production, which is dominated by the regional compartment. On the other hand, turning off all photochemistry (by setting $C_{OH} = 0$ or $k_{OH} = 0$) leads to a very large (69%) reduction in iF^{OA} and a moderate (26%) increase in iF^{vap}. Smaller perturbations in the regional level of OH radical on the scale of ± 30% alter domain-wide iF^{OA} on the scale of ± 15%, primarily by changing the production of OPOA. Regional scale photochemical aging of vapor-phase material into OPOA is clearly a very important contributor to the overall population intake of OA of urban origin.

Base-case model runs assume that oxidation chemistry contributes additional non-carbon mass to OA with each reaction step: OA mass is assumed to increase by 7.5% for each order-of-magnitude reduction in C^*. Sensitivity runs demonstrate that iF^{OA} is only weakly dependent on

the assumed amount of added mass. Doubling the amount of added non-carbon mass to a 15% OA mass increase per VBS bin reduction increases the domain-wide iF^{OA} by ~6%, and does not alter the spatial distribution of exposure. For a scenario in which no additional OA mass is contributed oxidation, iF^{OA} is reduced by 6% compared to base-case conditions. This weak dependence on the additional mass contribution of aging is to be expected, since iF^{OA} is computed solely on the basis of organic carbon atoms, which are conserved in the functionalization reactions that are represented here. The slight shifts observed in iF^{OA} are attributable to partitioning behavior.

The principal emphasis of this analysis is on summertime conditions, which favor photochemical conversion of vapors into OPOA. Sensitivity runs consider conditions that may be more representative of winter. First, I examine the effect of lowering C_{OH} by a factor of 3 in all compartments, such that the time-averaged C_{OH} is reduced in the regional compartment from 1.5×10^6 molecules cm^{-3} to 0.5×10^6 molecules cm^{-3}. As I found above, reducing C_{OH} results in less regional production of OPOA, thereby lowering the domain-wide iF^{OA} for urban emissions (here, 1.8 ppm, vs 3.1 ppm in base case). Likewise, X_p is reduced, but intraurban and POA intakes account for a larger fraction of the reduced iF. Of course, ambient temperatures are also lower in winter, which shifts partitioning into the particle phase. In two additional scenarios, I consider a 20 ºC and 40 ºC reduction in the default temperature profile, wherein temperatures range from respectively -3 ºC and -23 ºC (overnight minimum) to respectively 12 ºC and -8 ºC (afternoon peak). These reduced temperature scenarios shift partitioning of primary emissions towards the particle phase, thereby also altering the spatial distribution of exposure. For the milder winter scenario (20 ºC cooler), domain-wide iF^{OA} increases by 18%, while POA and urban exposures each account for ~60% of the domain-wide iF^{OA}, substantially higher than under base-case assumptions. For the more extreme winter scenario, spatial patterns of exposure are similar, but partitioning shifts much more substantially to the particle phase (iF^{OA} is ~2× the base case at 6.1 ppm, and X_p ~37%). These results are qualitatively consistent with the findings of Shrivastava et al. (2008), which suggest that lower temperatures and slower photochemistry increase the relative contributions of POA to regional OA concentrations during the winter. In summary, under cold and low OH-radical conditions, intraurban exposures to POA account for an especially large fraction of total OA intake of urban origin.

4.3.6 Limitations and future research

The simplified modeling framework that I employ in this analysis has a variety of additional limitations and uncertainties that are more difficult to explore quantitatively. Most prominently, the stylized treatment of photochemical aging of organic aerosol precursors is a major simplification. This investigation emphasizes a single aging pathway (functionalization) that produces OA from vapor-phase precursor material. The results of this analysis demonstrate that such reactions alone may produce population exposures to semivolatile organic material that are substantially different in character from those of primary, nonreactive emissions. However, the effects on population exposure of other OA aging pathways (e.g., fragmentation; heterogeneous- and condensed-phase oxidation processes) are not well characterized here. Future analyses might build on this work by incorporating a more detailed treatment of these processes, for example, by using a 2-D volatility basis set framework that explicitly accounts for transformations in both volatility and chemical composition (Jimenez et al., 2009; Donahue et al., 2011).

Model results generated in this analysis appear to reasonably agree with prior estimates and observations of inert pollutant intake fraction and organic aerosol concentration gradients. However, the simplified and archetypal treatment of atmospheric processes represents a substantial simplification relative to the state of the art in organic aerosol chemical transport modeling. Key areas for future refinement include the treatment of vertical pollutant mixing (e.g., the coupling between concentrations at ground level and in aloft layers), and in the modeling of radical concentrations (e.g., OH) that are responsible for initiating the oxidation of primary semivolatile emissions. Model results and sensitivity analyses also demonstrate that iF^{OA} is substantially dependent on the assumed volatility distribution of primary semivolatile emissions. Future analyses could usefully incorporate recent additions to the state of knowledge about SVOC and IVOC emissions from motor vehicle fleets (May et al., 2013a; May et al., 2013b). A further refinement would be to explicitly account for the contribution of biogenic emissions to regional OA concentrations.

An additional set of limitations relates to the exclusion of microenvironmental variation in exposure concentrations, especially within the urban compartment. Ambient conditions are an imperfect proxy for attributable exposure concentrations. Indoor exposures represent an especially large limitation in the current model treatment. The US population averages > 85% of the day indoors (Klepeis et al., 2001). Indoor airborne concentrations will almost certainly differ from outdoor ambient concentrations. Particles and semivolatile vapors penetrate buildings with < 100% efficiency, and sorptive interactions with surfaces, films, and settled dust make semivolatile dynamics indoors substantially more complex (Riley et al., 2002; Weschler and Nazaroff, 2008; Weschler and Nazaroff, 2010). Especially within the urban compartment, neglecting on-road and near-road exposures is another simplification in the current treatment. A substantial fraction of the urban population lives in near-road environments where OA concentrations are likely elevated above the urban background (e.g., see Chapter 2). Partitioning between the vapor and particle phase may be substantially different in near-source microenvironments compared to urban-ambient conditions.

4.4 Conclusions

The investigation contained in this chapter substantively updates the conceptual understanding of the intake fraction of urban vehicle emissions by considering semivolatile organic species. Similarly, this analysis extends previous research on organic aerosol dynamics by explicitly considering human exposure. The archetypal model used here indicates that the intake fraction of organic emissions differs from that of primary, conserved pollutants in several key regards. Inhalation intakes of semivolatile material have a strong dependence on the volatility distribution of emissions. As a consequence of equilibrium partitioning, and considering the base-case emissions evaluated here (majority high-volatility species), the partial intake fraction for particle-phase inhalation exposures (iF^{OA}) is substantially lower than the partial intake fraction for gas-phase material (iF^{vap}). This finding is important: depending on how volatility is treated when determining emission factors, models that treat vehicular $PM_{2.5}$ emissions as nonreactive may overstate the intake fraction for organic species. In contrast, model results indicate that population inhalation intakes of semivolatile organic vapors may substantially exceed the inhalation rates of condensed-phase material. The health effects of these vapor-phase exposures are not well studied, but merit further attention.

The spatial distribution of inhalation intake for semivolatile organic aerosol differs considerably from that of a primary, conserved species. Considering the base-case volatility distribution and a 400-km model domain, beyond-urban exposures account for more than half of the total OA inhalation intake that is attributable to urban emissions of semivolatile material. Photochemical oxidation makes an important contribution to the total population intake of urban-attributable OA, accounting for nearly 70% of total inhalation intake within the model domain. Intraurban OA intake is predominantly attributable to primary organic aerosol emissions, whereas beyond-urban OA inhalation intakes are dominated by photochemically aged material. In contrast to the more regionally dispersed OA exposures, intraurban intakes account for the dominant fraction of population exposure to organic vapors.

By focusing on an exposure-oriented set of metrics (intake fraction and inhalation intake rate), this analysis reaches conclusions that diverge somewhat from key findings in the atmospheric science literature, in which researchers tend to emphasize atmospheric burdens as opposed to population exposure. The results of this analysis reinforce previous findings that the atmospheric loading of organic aerosol is overwhelmingly made up of oxidized or "secondary" material. However, from the perspective of exposure, intraurban exposures to primary compounds comprise a substantial fraction of the inhalation intake attributable to urban emissions of semivolatile material. A proper accounting of the inhalation intake consequences of urban vehicle emissions therefore requires exposure assessment technique with sufficiently fine-scale spatial resolution to accurately represent intraurban exposures.

4.5 References

Angel, S., Parent, J., Civco, D.L., Blei, A., Potere, D., 2011. The dimensions of global urban expansion: Estimates and projections for all countries, 2000–2050. *Progress in Planning* 75, 53-107.

Bennett, D.H., McKone, T.E., Evans, J.S., Nazaroff, W.W., Margni, M.D., Jolliet, O., Smith, K.R., 2002. Defining intake fraction. *Environmental Science & Technology* 36, 206A-211A.

Donahue, N.M., Robinson, A.L., Stanier, C.O., Pandis, S.N., 2006. Coupled partitioning, dilution, and chemical aging of semivolatile organics. *Environmental Science & Technology* 40, 2635-2643.

Donahue, N.M., Robinson, A.L., Pandis, S.N., 2009. Atmospheric organic particulate matter: From smoke to secondary organic aerosol. *Atmospheric Environment* 43, 94-106.

Donahue, N.M., Epstein, S.A., Pandis, S.N., Robinson, A.L., 2011. A two-dimensional volatility basis set: 1. organic-aerosol mixing thermodynamics. *Atmospheric Chemistry and Physics* 11, 3303-3318.

Evans, J.S., Wolff, S.K., Phonboon, K., Levy, J.I., Smith, K.R., 2002. Exposure efficiency: An idea whose time has come? *Chemosphere* 49, 1075-1091.

Forstall, R.L., Greene, R.P., Pick, J.B., 2009. Which are the largest? Why lists of major urban areas vary so greatly. *Tijdschrift voor Economische en Sociale Geografie* 100, 277-297.

Gentner, D.R., Isaacman, G., Worton, D.R., Chan, A.W.H., Dallmann, T.R., Davis, L., Liu, S., Day, D.A., Russell, L.M., Wilson, K.R., Weber, R., Guha, A., Harley, R.A., Goldstein, A.H., 2012. Elucidating secondary organic aerosol from diesel and gasoline vehicles through detailed characterization of organic carbon emissions. *Proceedings of the National Academy of Sciences* 109, 18318-18323.

Greco, S.L., Wilson, A.M., Hanna, S.R., Levy, J.I., 2007a. Factors influencing mobile source particulate matter emissions-to-exposure relationships in the Boston urban area. *Environmental Science & Technology* 41, 7675-7682.

Greco, S.L., Wilson, A.M., Spengler, J.D., Levy, J.I., 2007b. Spatial patterns of mobile source particulate matter emissions-to-exposure relationships across the United States. *Atmospheric Environment* 41, 1011-1025.

Grieshop, A.P., Miracolo, M.A., Donahue, N.M., Robinson, A.L., 2009. Constraining the volatility distribution and gas-particle partitioning of combustion aerosols using isothermal dilution and thermodenuder measurements. *Environmental Science & Technology* 43, 4750-4756.

Heath, G.A., Granvold, P.W., Hoats, A.S., Nazaroff, W.W., 2006. Intake fraction assessment of the air pollutant exposure implications of a shift toward distributed electricity generation. *Atmospheric Environment* 40, 7164-7177.

Humbert, S., Marshall, J.D., Shaked, S., Spadaro, J.V., Nishioka, Y., Preiss, P., McKone, T.E., Horvath, A., Jolliet, O., 2011. Intake fraction for particulate matter: Recommendations for life cycle impact assessment. *Environmental Science & Technology* 45, 4808-4816.

Jathar, S.H., Farina, S.C., Robinson, A.L., Adams, P.J., 2011. The influence of semi-volatile and reactive primary emissions on the abundance and properties of global organic aerosol. *Atmospheric Chemistry and Physics* 11, 7727-7746.

Jimenez, J.L., Canagaratna, M.R., Donahue, N.M., Prévôt, A.S.H., Zhang, Q., Kroll, J.H., DeCarlo, P.F., Allan, J.D., Coe, H., Ng, N.L., Aiken, A.C., Docherty, K.S., Ulbrich, I.M., Grieshop, A.P., Robinson, A.L., Duplissy, J., Smith, J.D., Wilson, K.R., Lanz, V.A., Hueglin, C., Sun, Y.L., Tian, J., Laaksonen, A., Raatikainen, T., Rautiainen, J., Vaattovaara, P., Ehn, M., Kulmala, M., Tomlinson, J.M., Collins, D.R., Cubison, M.J., E, Dunlea, J., Huffman, J.A., Onasch, T.B., Alfarra, M.R., Williams, P.I., Bower, K., Kondo, Y., Schneider, J., Drewnick, F., Borrmann, S., Weimer, S., Demerjian, K., Salcedo, D., Cottrell, L., Griffin, R., Takami, A., Miyoshi, T., Hatakeyama, S., Shimono, A., Sun, J.Y., Zhang, Y.M., Dzepina, K., Kimmel, J.R., Sueper, D., Jayne, J.T., Herndon, S.C., Trimborn, A.M., Williams, L.R., Wood, E.C., Middlebrook, A.M., Kolb, C.E., Baltensperger, U., Worsnop, D.R., 2009. Evolution of organic aerosols in the atmosphere. *Science* 326, 1525-1529.

Klepeis, N.E., Nelson, W.C., Ott, W.R., Robinson, J.P., Tsang, A.M., Switzer, P., Behar, J.V., Hern, S.C., Engelmann, W.H., 2001. The National Human Activity Pattern Survey (NHAPS): A resource for assessing exposure to environmental pollutants. *Journal of Exposure Analysis and Environmental Epidemiology* 11, 231-252.

Levy, J.I., Wolff, S.K., Evans, J.S., 2002. A regression-based approach for estimating primary and secondary particulate matter intake fractions. *Risk Analysis* 22, 895-904.

Lipsky, E.M., Robinson, A.L., 2006. Effects of dilution on fine particle mass and partitioning of semivolatile organics in diesel exhaust and wood smoke. *Environmental Science & Technology* 40, 155-162.

Lobscheid, A.B., Nazaroff, W.W., Spears, M., Horvath, A., McKone, T.E., 2012. Intake fractions of primary conserved air pollutants emitted from on-road vehicles in the United States. *Atmospheric Environment* 63, 298-305.

Marshall, J.D., Riley, W.J., McKone, T.E., Nazaroff, W.W., 2003. Intake fraction of primary pollutants: Motor vehicle emissions in the South Coast Air Basin. *Atmospheric Environment* 37, 3455-3468.

Marshall, J.D., Teoh, S.K., Nazaroff, W.W., 2005. Intake fraction of nonreactive vehicle emissions in US urban areas. *Atmospheric Environment* 39, 1363-1371.

May, A.A., Presto, A.A., Hennigan, C.J., Nguyen, N.T., Gordon, T.D., Robinson, A.L., 2013a. Gas-particle partitioning of primary organic aerosol emissions: (1) gasoline vehicle exhaust. *Atmospheric Environment* 77, 128-139.

May, A.A., Presto, A.A., Hennigan, C.J., Nguyen, N.T., Gordon, T.D., Robinson, A.L., 2013b. Gas-particle partitioning of primary organic aerosol emissions: (2) diesel vehicles. *Environmental Science & Technology*, 130710122712000.

Mollner, A.K., Valluvadasan, S., Feng, L., Sprague, M.K., Okumura, M., Milligan, D.B., Bloss, W.J., Sander, S.P., Martien, P.T., Harley, R.A., McCoy, A.B., Carter, W.P.L., 2010. Rate of gas phase association of hydroxyl radical and nitrogen dioxide. *Science* 330, 646-649.

Pankow, J.F., 1994. An absorption model of the gas/aerosol partitioning involved in the formation of secondary organic aerosol. *Atmospheric Environment* 28, 189-193.

Ren, X., Harder, H., Martinez, M., Lesher, R.L., Oliger, A., Simpas, J.B., Brune, W.H., Schwab, J.J., Demerjian, K.L., He, Y., Zhou, X., Gao, H., 2003. OH and HO_2 chemistry in the urban atmosphere of New York City. *Atmospheric Environment* 37, 3639-3651.

Ren, X., Brune, W.H., Cantrell, C.A., Edwards, G.D., Shirley, T., Metcalf, A.R., Lesher, R.L., 2005. Hydroxyl and peroxy radical chemistry in a rural area of central Pennsylvania: observations and model comparisons. *Environmental Monitoring and Assessment* 52, 231-257.

Ren, X., Brune, W.H., Mao, J., Mitchell, M.J., Lesher, R.L., Simpas, J.B., Metcalf, A.R., Schwab, J.J., Cai, C., Li, Y., Demerjian, K.L., Felton, H.D., Boynton, G., Adams, A., Perry, J., He, Y., Zhou, X., Hou, J., 2006. Behavior of OH and HO_2 in the winter atmosphere in New York City. *Atmospheric Environment* 40, Supplement 2, 252-263.

Reynolds, C.C.O., Grieshop, A.P., Kandlikar, M., 2011. Climate and health relevant emissions from in-use Indian three-wheelers fueled by natural gas and gasoline. *Environmental Science & Technology* 45, 2406-2412.

Rienecker, M.M., Suarez, M.J., Gelaro, R., Todling, R., Bacmeister, J., Liu, E., Bosilovich, M.G., Schubert, S.D., Takacs, L., Kim, G.-K., Bloom, S., Chen, J., Collins, D., Conaty, A., da Silva, A., Gu, W., Joiner, J., Koster, R.D., Lucchesi, R., Molod, A., Owens, T., Pawson, S., Pegion, P., Redder, C.R., Reichle, R., Robertson, F.R., Ruddick, A.G., Sienkiewicz, M., Woollen, J., 2011. MERRA: NASA's modern-era retrospective analysis for research and applications. *Journal of Climate* 24, 3624-3648.

Riley, W.J., McKone, T.E., Lai, A.C.K., Nazaroff, W.W., 2002. Indoor particulate matter of outdoor origin: Importance of size-dependent removal mechanisms. *Environmental Science & Technology* 36, 200-207.

Robinson, A.L., Donahue, N.M., Shrivastava, M.K., Weitkamp, E.A., Sage, A.M., Grieshop, A.P., Lane, T.E., Pierce, J.R., Pandis, S.N., 2007. Rethinking organic aerosols: semivolatile emissions and photochemical aging. *Science* 315, 1259-1262.

Robinson, A.L., Grieshop, A.P., Donahue, N.M., Hunt, S.W., 2010. Updating the conceptual model for fine particle mass emissions from combustion systems. *Journal of the Air & Waste Management Association* 60, 1204-1222.

Roth, C.M., Goss, K.-U., Schwarzenbach, R.P., 2005a. Sorption of a diverse set of organic vapors to diesel soot and road tunnel aerosols. *Environmental Science & Technology* 39, 6632-6637.

Roth, C.M., Goss, K.-U., Schwarzenbach, R.P., 2005b. Sorption of a diverse set of organic vapors to urban aerosols. *Environmental Science & Technology* 39, 6638-6643.

Schauer, J.J., Kleeman, M.J., Cass, G.R., Simoneit, B.R.T., 1999. Measurement of emissions from air pollution sources. 2. C 1through C 30 organic compounds from medium duty diesel trucks. *Environmental Science & Technology* 33, 1578-1587.

Schauer, J.J., Kleeman, M.J., Cass, G.R., Simoneit, B.R.T., 2002. Measurement of emissions from air pollution sources. 5. C1−C32 organic compounds from gasoline-powered motor vehicles. *Environmental Science & Technology* 36, 1169-1180.

Schneider, A., Friedl, M.A., Potere, D., 2009. A new map of global urban extent from MODIS satellite data. *Environmental Research Letters* 4, 044003.

Seirup, L., Yetman, G., 2006. *U.S. Census Grids (Summary File 1), 2000*, NASA Socioeconomic Data and Applications Center (SEDAC), Palisades, NY. Available from: http://sedac.ciesin.columbia.edu/data/set/usgrid-summary-file1-2000.

Shrivastava, M.K., Lane, T.E., Donahue, N.M., Pandis, S.N., Robinson, A.L., 2008. Effects of gas particle partitioning and aging of primary emissions on urban and regional organic aerosol concentrations. *Journal of Geophysical Research* 113, D18301.

Wagstrom, K.M., Pandis, S.N., 2011a. Source–receptor relationships for fine particulate matter concentrations in the Eastern United States. *Atmospheric Environment* 45, 347-356.

Wagstrom, K.M., Pandis, S.N., 2011b. Contribution of long range transport to local fine particulate matter concerns. *Atmospheric Environment* 45, 2730-2735.

Weschler, C.J., Nazaroff, W.W., 2008. Semivolatile organic compounds in indoor environments. *Atmospheric Environment* 42, 9018-9040.

Weschler, C.J., Nazaroff, W.W., 2010. SVOC partitioning between the gas phase and settled dust indoors. *Atmospheric Environment* 44, 3609-3620.

Zhang, K.M., Wexler, A.S., 2004. Evolution of particle number distribution near roadways--Part I: analysis of aerosol dynamics and its implications for engine emission measurement. *Atmospheric Environment* 38, 6643-6653.

Zhang, L., Gong, S., Padro, J., Barrie, L., 2001. A size-segregated particle dry deposition scheme for an atmospheric aerosol module. *Atmospheric Environment* 35, 549-560.

Zhang, Q., Jimenez, J.L., Canagaratna, M.R., Allan, J.D., Coe, H., Ulbrich, I., Alfarra, M.R., Takami, A., Middlebrook, A.M., Sun, Y.L., Dzepina, K., Dunlea, E., Docherty, K., DeCarlo, P.F., Salcedo, D., Onasch, T., Jayne, J.T., Miyoshi, T., Shimono, A., Hatakeyama, S., Takegawa, N., Kondo, Y., Schneider, J., Drewnick, F., Borrmann, S., Weimer, S., Demerjian, K., Williams, P., Bower, K., Bahreini, R., Cottrell, L., Griffin, R.J., Rautiainen, J., Sun, J.Y., Zhang, Y.M., Worsnop, D.R., 2007. Ubiquity and dominance of oxygenated species in organic aerosols in anthropogenically-influenced Northern Hemisphere midlatitudes. *Geophysical Research Letters* 34, L13801.

Table 4-1. Volatility basis set and assumed parameters for emitted material[a]

Lumped Species C* ($\mu g\ m^{-3}$)	**Percent of emissions** (%)	**Enthalpy of vaporization** ΔH_v ($kJ\ mol^{-1}$)
10^{-2}	1.2	112
10^{-1}	2.4	106
10^{0}	3.6	100
10^{1}	5.6	94
10^{2}	7.2	88
10^{3}	12	82
10^{4}	16	76
10^{5}	20	70
10^{6}	32	64

[a] Data from Shrivastava et al. (2008).

Table 4-2. Demographic parameters and sizing for base-case and megacity scenarios.

			Within-compartment [a]		**Cumulative values** [b]	
Scenario	**Compartment**	**Length** (km)	**Population** (million)	**Density** (pop km^{-2})	**Population** (million)	**Density** (pop km^{-2})
Base case	Urban	25	1.5	2,400	1.5	2,400
	Periurban	100	2.5	250	4	400
	Regional	400	12	75	16	100
Megacity	Urban	40	18	11,250	18	11,250
	Periurban	100	6	600	24	2,400
	Regional	400	12	75	36	225

[a] Within-compartment values represent exclusively the population residing within a given compartment
[b] Cumulative values represent the cumulative population residing in a given compartment and all other compartments nested within that compartment. For example, the cumulative values for the regional compartment represent the total population and average population density for the entire model domain.

Table 4-3. Concentrations of semivolatile material by compartment

		Concentrations ($\mu g\ m^{-3}$)[a]		
Scenario	**Pollutant**	*Urban*	*Periurban*	*Regional*
Base case	OA	7.4	5.4	2.8
	% POA [b]	33%	11%	7%
	% from urban [c]	43%	17%	10%
	% from regional [d]	35%	51%	72%
	ξ_p [e]	23%	39%	43%
	Vapors	25.1	8.3	3.8
Megacity	OA	41.0	18.2	6.3
	% POA	53%	18%	7%
	% from urban	84%	61%	48%
	% from regional	6%	15%	33%
	ξ_p	22%	36%	49%
	Vapors	144	32.1	6.5

[a] Total concentration of semivolatile material contained within a given compartment, expressed on the basis of total organic mass (i.e., including non-carbon constituents).
[b] Ratio of total POA concentration to total OA concentration for a given compartment.
[c] Fractional contribution of OA emitted in urban compartment to total OA mass within compartment.
[d] Fractional contribution of OA emitted in regional compartment to total OA mass within compartment.
[e] ξ_p – Particle phase partitioning coefficient, i.e., fraction of total semivolatile mass in particle phase.

Table 4-4. Intake fractions for urban emissions in base-case scenario

		Partial intake fractions for urban emissions (ppm)			
Pollutant	**Phase**	*Urban* [a]	*Periurban* [b]	*Regional* [c]	*Total* [d]
Nonreactive [e]	Conserved	11.5	2.7	2.7	16.9
	Particle	10.0	1.8	1.1	12.9
All semivolatile [f]	OA + vapor	11.2	2.4	1.9	15.6
	OA only	1.5	0.70	0.90	3.1
	POA	0.99	0.13	0.053	1.2
	OPOA	0.49	0.57	0.85	1.9
	Vapor only	9.8	1.7	1.0	12.5
SVOC only [g]	OA + vapor	10.9	2.2	1.6	14.8
	OA only	4.0	1.2	1.1	6.3
	POA	3.1	0.40	0.16	3.7
	OPOA	0.88	0.79	0.94	2.6
	Vapor only	6.9	1.0	0.52	8.5
IVOC only [h]	OA + vapor	11.4	2.5	2.0	16.0
	OA only	0.3	0.46	0.81	1.6
	POA	0.0024	0.0002	-	0.0026
	OPOA	0.3	0.46	0.81	1.6
	Vapor only	11.1	2.1	1.2	14.4

[a-c] Inhalation intake fraction for urban emissions inhaled in urban, periurban or regional compartment.
[d] Total iF for inhalation intakes in any compartment of material emitted into urban compartment.
[e] Two distinct nonreactive species are considered. “Conserved” nonreactive pollutants are removed exclusively by advection. The “Particle” case considers a nonreactive primary particle that experiences removal by dry deposition.
[f] Emissions- and volatility-weighted average *iF* for material emitted into all VBS volatility bins
[g] Emissions- and volatility-weighted average *iF* for material emitted into the SVOC volatility bins (C^* = [-2…3]).
[h] Emissions- and volatility-weighted average *iF* for material emitted into the IVOC volatility bins (C^* = [4…6]).

Table 4-5. Intake fractions for urban emissions in megacity scenario

		Partial intake fractions for urban emissions (ppm)			
Pollutant	**Phase**	*Urban* [a]	*Periurban* [b]	*Regional* [c]	*Total* [d]
Nonreactive [e]	Conserved	85.0	6.0	2.5	93.5
	Particle	68.6	3.7	0.98	73.3
All semivolatile [f]	OA + vapor	80.9	5.2	1.7	87.8
	OA only	15.9	1.7	0.84	18.4
	POA	9.8	0.37	0.0059	10.2
	OPOA	6.0	1.3	0.78	8.2
	Vapor only	65.0	3.5	0.86	69.4
SVOC only [g]	OA + vapor	75.9	4.6	1.4	81.9
	OA only	39.9	2.8	0.98	43.7
	POA	30.5	1.1	0.19	31.8
	OPOA	9.4	1.7	0.79	11.9
	Vapor only	36.0	1.8	0.41	38.2
IVOC only [h]	OA + vapor	83.2	5.5	1.8	90.6
	OA only	4.6	1.2	0.77	6.5
	POA	0.099	0.001	-	0.10
	OPOA	4.5	1.2	0.77	6.4
	Vapor only	78.7	4.3	1.1	84.1

[a-c] Inhalation intake fraction for urban emissions inhaled in urban, periurban or regional compartment.
[d] Total iF for inhalation intakes in any compartment of material emitted into urban compartment.
[e] Two distinct nonreactive species are considered. “Conserved” nonreactive pollutants are removed exclusively by advection. The “Particle” case considers a nonreactive primary particle that experiences removal by dry deposition.
[f] Emissions- and volatility-weighted average *iF* for material emitted into all VBS volatility bins
[g] Emissions- and volatility-weighted average *iF* for material emitted into the SVOC volatility bins (C^* = [-2…3]).
[h] Emissions- and volatility-weighted average *iF* for material emitted into the IVOC volatility bins (C^* = [4…6]).

Table 4-6. Key results from sensitivity scenarios.

Sensitivity case	Notes	Intake fraction (ppm) [a] $iF^{conserved}$	$iF^{inertPM}$	iF^{OA}	iF^{vap}	X_p [b] (%)	f^{POA} [c] (%)	f^{urban} (%) [d] NR [e]	OA	Vapor
Base case	Unperturbed base-case scenario	**17.0**	**12.9**	**3.1**	**12.5**	**20%**	**38%**	**78%**	**48%**	**78%**
Emissions	Emissions decrease by 67%	17.0	12.9	2.9	12.7	19%	36%	78%	47%	78%
	Emissions decrease by 33%	17.0	12.9	3.1	12.5	20%	38%	78%	48%	78%
	Emissions increase by 1.5 ×	17.0	12.9	3.2	12.3	21%	40%	78%	49%	78%
	Emissions increase by 3.0 ×	17.0	12.9	3.6	11.9	23%	44%	78%	52%	79%
	Grieshop et al. (2009) volatility distribution[g]	17.0	12.9	2.7	12.9	18%	26%	78%	43%	78%
	IVOC emissions reduced by 50% from base	17.0	12.9	3.7	11.7	24%	45%	78%	54%	78%
	Temporally invariant emissions	20.3	15.2	3.9	14.7	21%	39%	76%	48%	77%
Meteorology	Mixing height same for all compartments	23.5	14.7	4.3	15.6	22%	33%	72%	43%	67%
	H_{min} = 120m	16.1	12.3	3.1	11.7	21%	35%	75%	45%	76%
	H_{min} = 200 m	13.7	10.6	2.8	9.7	23%	31%	70%	41%	72%
	Wind speed halved	29.8	19.7	6.0	19.2	24%	35%	82%	51%	84%
Dry Deposition	No PM dry deposition	17.0	17.0	4.6	12.4	27%	33%	68%	41%	78%
	PM deposition velocity v_{dep} = 7.5 mm s^{-1}	17.0	9.7	2.1	12.6	14%	41%	85%	54%	78%
Domain sizing	Regional 800 km 12 M population ("sprawl")	15.1	12.0	2.3	11.9	16%	46%	83%	59%	83%
	Reg'. 800 km, 60 M pop ("constant density")	20.3	13.6	4.1	12.8	24%	32%	73%	36%	75%
	"US small city": urban 12.5 km, 300,000 pop	10.7	7.8	2.2	7.3	23%	28%	58%	24%	59%
	"Asia non-megacity": urban 10 km, 1.8M pop	41.2	36.7	6.4	33.3	16%	65%	91%	73%	91%

Table continues on following page

[a] Domain-wide intake fraction of urban emissions. $iF^{conserved}$ – for emissions of primary, nonreactive, conserved pollutants; $iF^{inertPM}$ – for emissions of nonreactive PM with dry deposition losses; iF^{PM} – particle-phase *iF* for semivolatile organic emissions; iF^{vap} –vapor-phase *iF* for semivolatile organic emissions.

[b] X_p – Proportion of domain-wide intake of urban semivolatile organic emissions that is in the particle phase. $X_p = iF^{OA} / (iF^{OA} + iF^{vap})$.

[c] f^{POA} – Proportion of domain-wide OA intake attributable to urban semivolatile organic emissions that is POA. $f^{POA} = iF^{POA} / (iF^{POA} + iF^{OPOA})$.

[d] f^{urban} – Intraurban proportion of domain-wide intake fraction of urban emissions. This metric is evaluated for a conserved species, for OA, and for vapors.

[e] "NR" – primary, nonreactive, conserved pollutant (e.g., comparable to $iF^{conserved}$).

[f] OH concentrations refer to regional compartment. In base-case model, C_{OH} is 50% higher in periurban compartment.

[g] See Table 4-7.

Table 4-6. Key results from sensitivity scenarios, continued

Sensitivity case	Notes	Intake fraction (ppm) [a] $iF^{conserved}$	$iF^{inertPM}$	iF^{OA}	iF^{vap}	X_p [b] (%)	f^{POA} [c] (%)	f^{urban} (%) [d] Inert [e]	OA	Vapor
Base case	Unperturbed base-case scenario	**17.0**	**12.9**	**3.1**	**12.5**	**20%**	**38%**	**78%**	**48%**	**78%**
Photo-chemistry	C_{OH} at regional levels in all compartments	17.0	12.9	2.8	12.9	18%	41%	78%	49%	77%
	k_{OH} = 0 (no photochemical aging)	17.0	12.9	0.96	15.8	6%	100%	78%	85%	67%
	Daily average[f] OH = 1.0×10^6 molec cm^{-3}	17.0	12.9	2.6	13.3	16%	45%	78%	51%	75%
	Daily average[f] OH = 2.0×10^6 molec cm^{-3}	17.0	12.9	3.5	12.0	22%	34%	78%	47%	80%
	4× lower OH concentration in urban box	17.0	12.9	2.9	12.7	19%	41%	78%	46%	78%
	No added OA mass with photochemical aging	17.0	12.9	2.9	12.7	19%	38%	78%	48%	78%
	2× default added OA mass per aging step	17.0	12.9	3.3	12.3	21%	38%	78%	48%	79%
	Time-invariant OH concentrations	17.0	12.9	3.3	12.2	21%	35%	78%	48%	79%
Winter conditions	Daily average[f] OH = 250,000 molec cm^{-3}	17.0	12.9	1.3	15.2	8%	79%	78%	72%	69%
	Daily average[f] OH = 500,000 molec cm^{-3}	17.0	12.9	1.8	14.5	11%	62%	78%	61%	71%
	… and *T* profile 20ºC cooler	17.0	12.9	3.6	12.7	22%	60%	78%	60%	72%
	… and *T* profile 40ºC cooler	17.0	12.9	6.1	10.2	37%	62%	78%	62%	74%

[a] Domain-wide intake fraction of urban emissions. $iF^{conserved}$ – for emissions of primary, nonreactive, conserved pollutants; $iF^{inertPM}$ – for emissions of nonreactive PM with dry deposition losses; iF^{PM} – particle-phase *iF* for semivolatile organic emissions; iF^{vap} –vapor-phase *iF* for semivolatile organic emissions.

[b] X_p – Proportion of domain-wide intake of urban semivolatile organic emissions that is in the particle phase. $X_p = iF^{OA} / (iF^{OA} + iF^{vap})$.

[c] f^{POA} – Proportion of domain-wide OA intake attributable to urban semivolatile organic emissions that is POA. $f^{POA} = iF^{POA} / (iF^{POA} + iF^{OPOA})$.

[d] f^{urban} – Intraurban proportion of domain-wide intake fraction of urban emissions. This metric is evaluated for a conserved species, for OA, and for vapors.

[e] "NR" – primary, nonreactive, conserved pollutant (e.g., comparable to $iF^{conserved}$).

[f] OH concentrations refer to regional compartment. In base-case model, C_{OH} is 50% higher in periurban compartment.

[g] See Table 4-7.

Table 4-7. Emissions volatility distribution for diesel generators [a]

Lumped Species C* ($\mu g\ m^{-3}$)	**Percent of emissions** (%)
10^{-2}	0.4
10^{-1}	0.4
10^{0}	1.6
10^{1}	8.4
10^{2}	7.2
10^{3}	18
10^{4}	12
10^{5}	20
10^{6}	32

[a] Data from Grieshop et al. (2009).

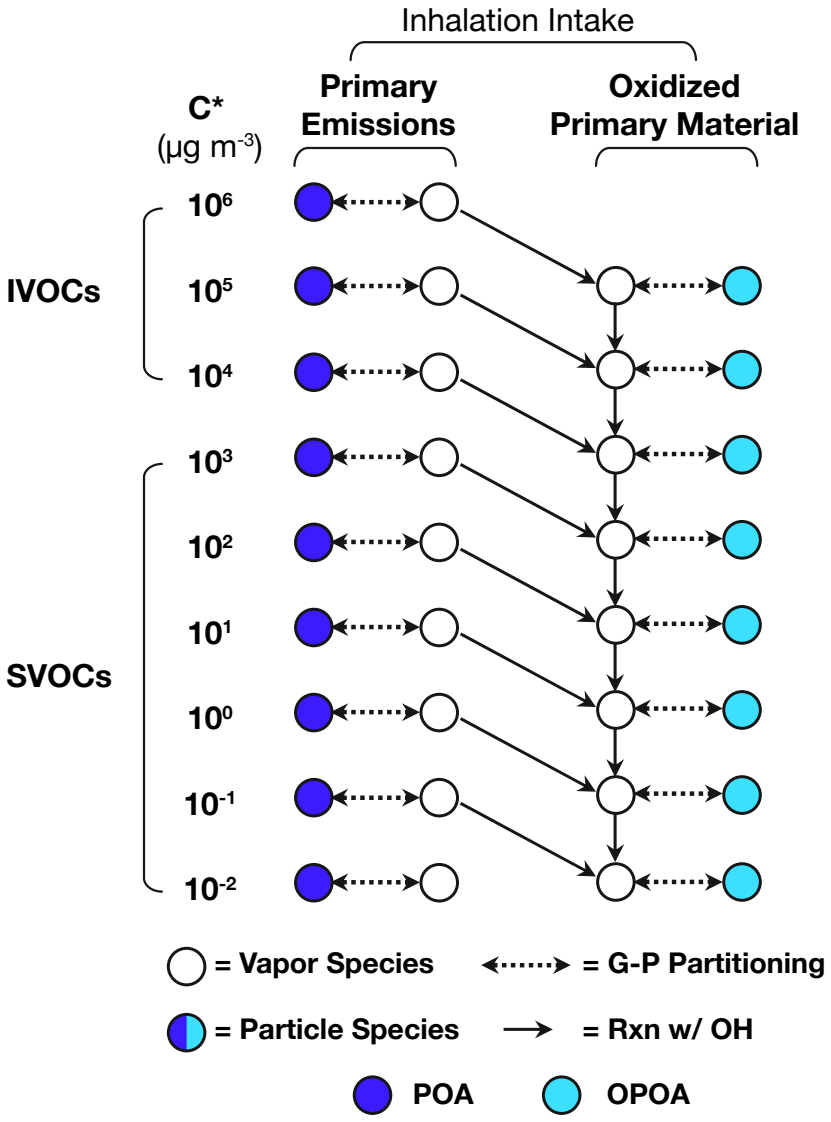

Figure 4-1. Model schematic and aging mechanism. Emitted semivolatile material includes vapors and primary organic aerosol (POA). Vapor and particle phases exist in dynamic equilibrium owing to gas-particle portioning processes ("G-P partitioning"). The photochemical aging mechanism (reaction with OH radicals) reduces volatility of vapor-phase material by one volatility bin (C*) per oxidation reaction step. Photochemically aged material that partitions into particle phase is termed oxidized POA (OPOA). Figure adapted from Shrivastava et al., 2008.

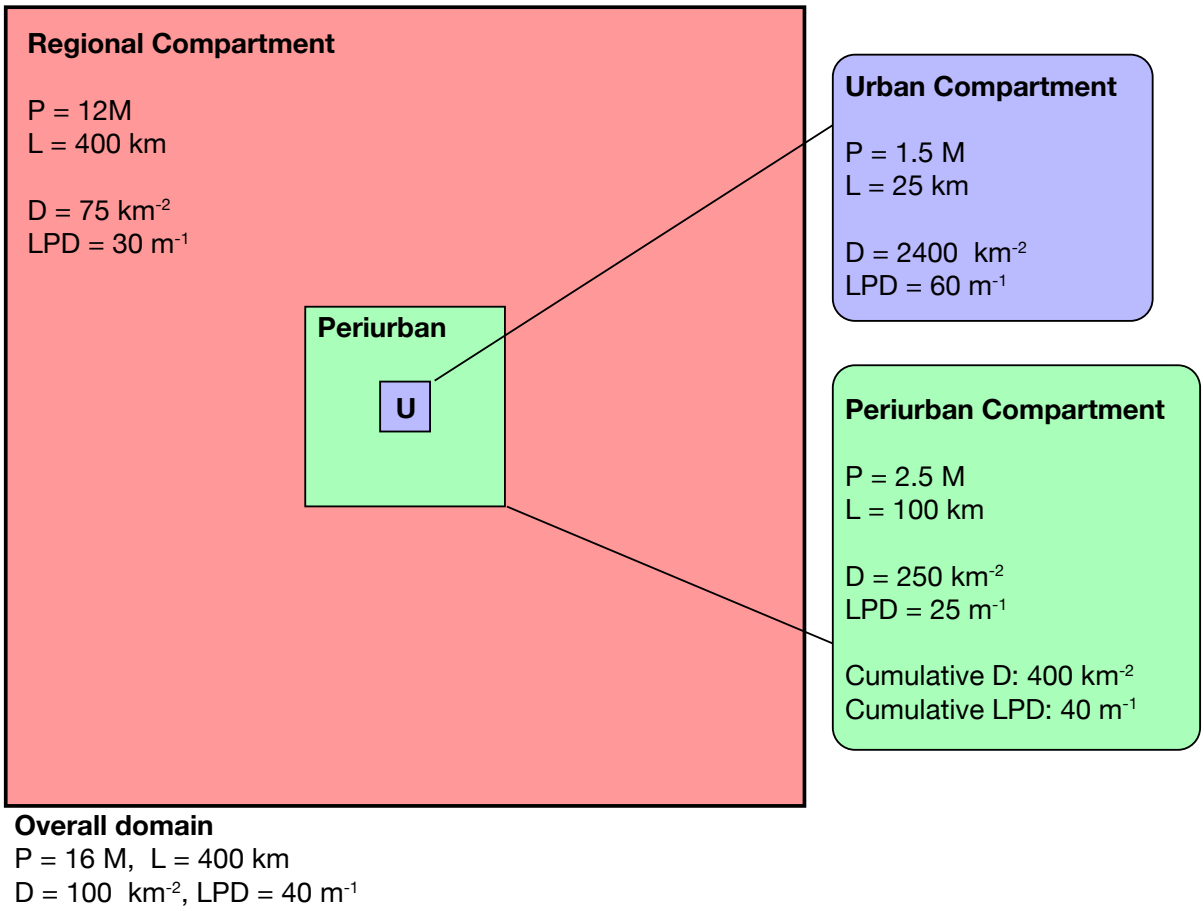

Figure 4-2. Geometry of 3 compartment nested model. Properties for base-case model are illustrated here and reproduced in Table 4-2. Geometries and population differ for the "megacity" scenario; see Table 4-2.

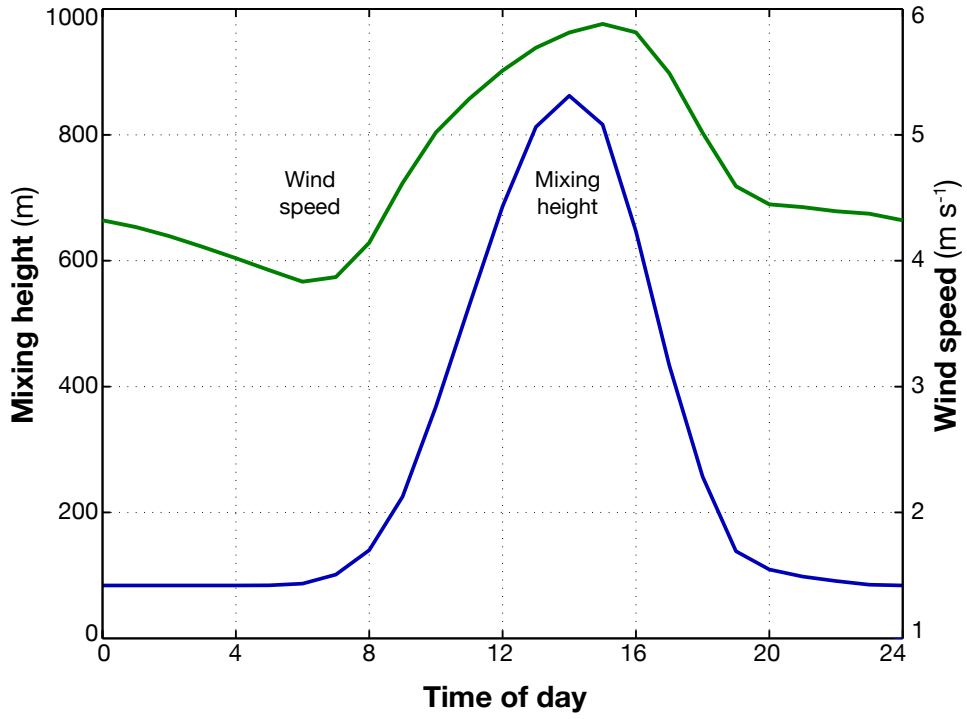

Figure 4-3. Diurnal cycle of urban mixing height (left axis) and wind speed (right axis). Base-case scenarios assume that mixing heights in the periurban and regional compartments are twice as high as in the urban compartment.

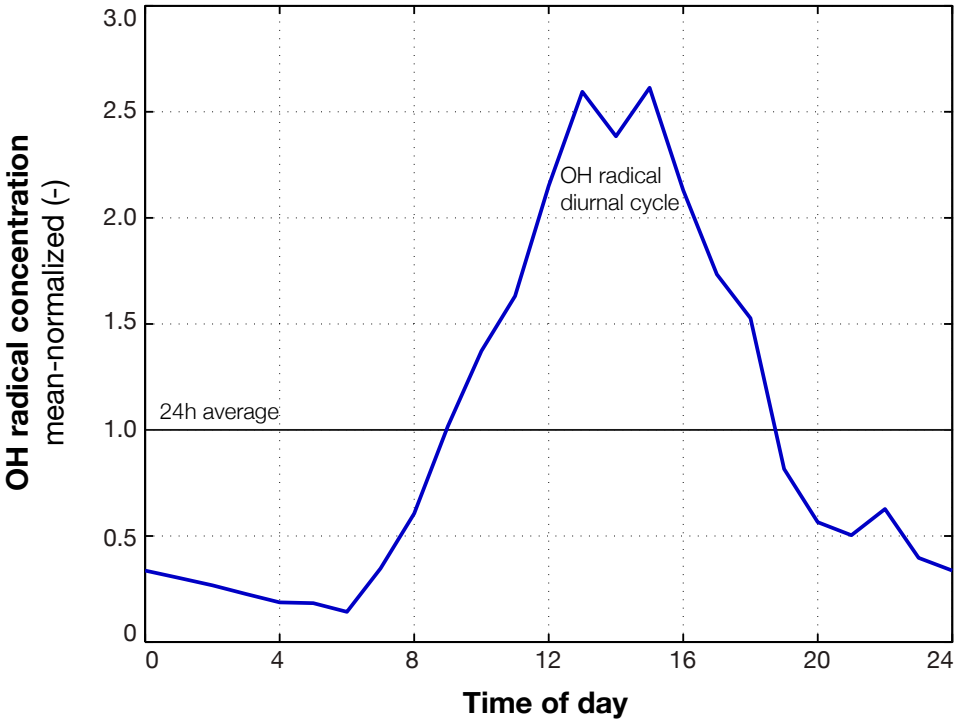

Figure 4-4. Mean-normalized diurnal cycle of OH radical concentrations.

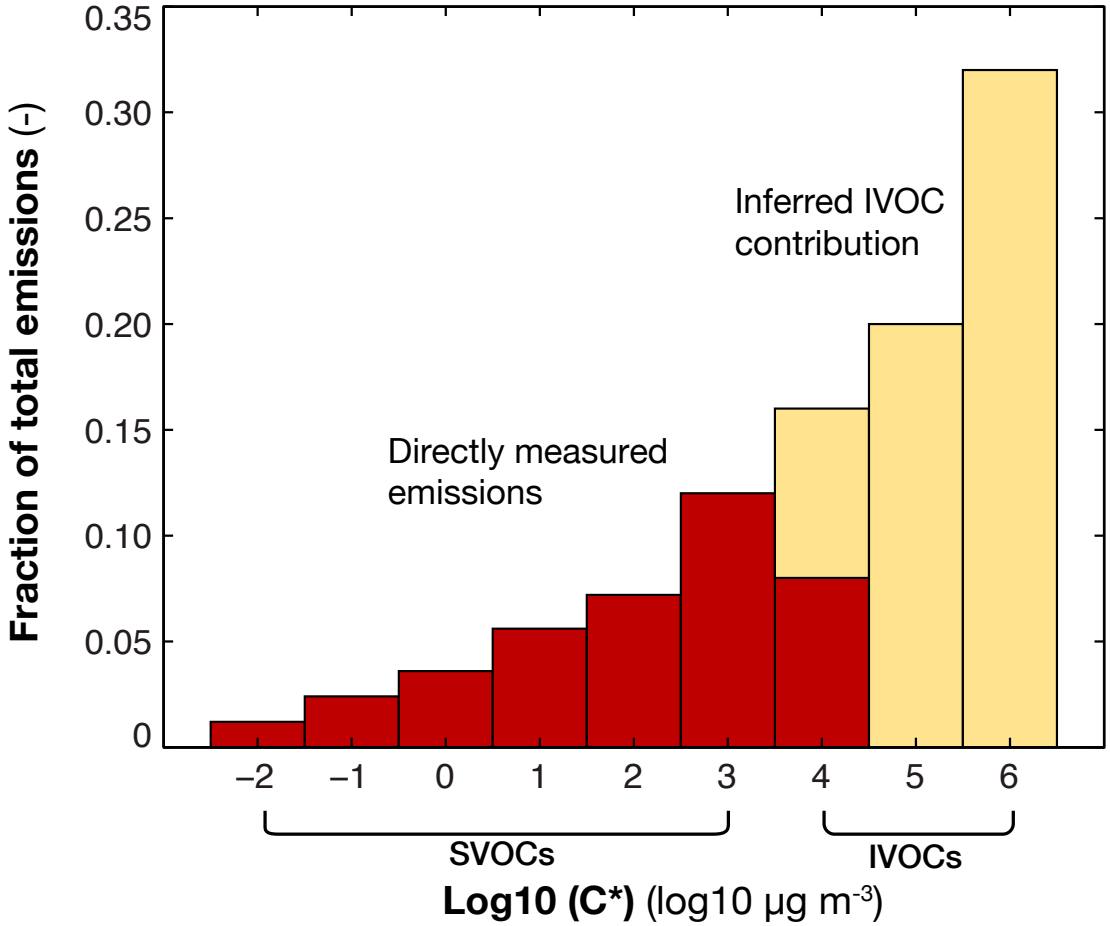

Figure 4-5. Assumed volatility distribution of emissions for default model runs (Shrivstava et al., 2008). Emissions contribution from SVOCs is estimated on the basis of filter measurements, while IVOC contribution is inferred from top-down constraints. Values here are reproduced in Table 4-1. Note that the modeling approached used here assigns to all SVOCs and IVOCs within a plotted bar the saturation concentration at the center of the log scale (i.e., discrete values with integer powers of 10).

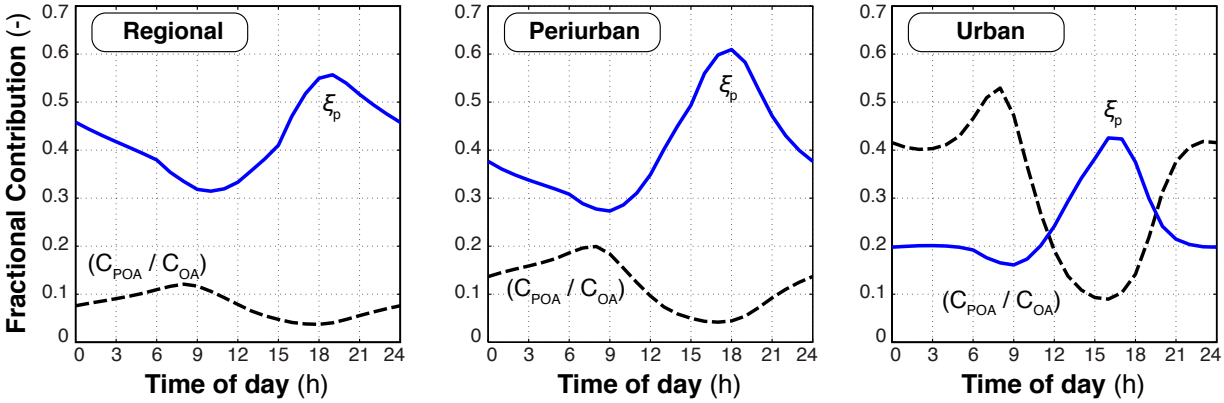

Figure 4-6. Diurnal variation in particle-phase partitioning coefficient (ξ_p, solid blue line) and primary fraction of total OA mass (C_{POA} / C_{OA}, dashed black line) in base-case scenario.

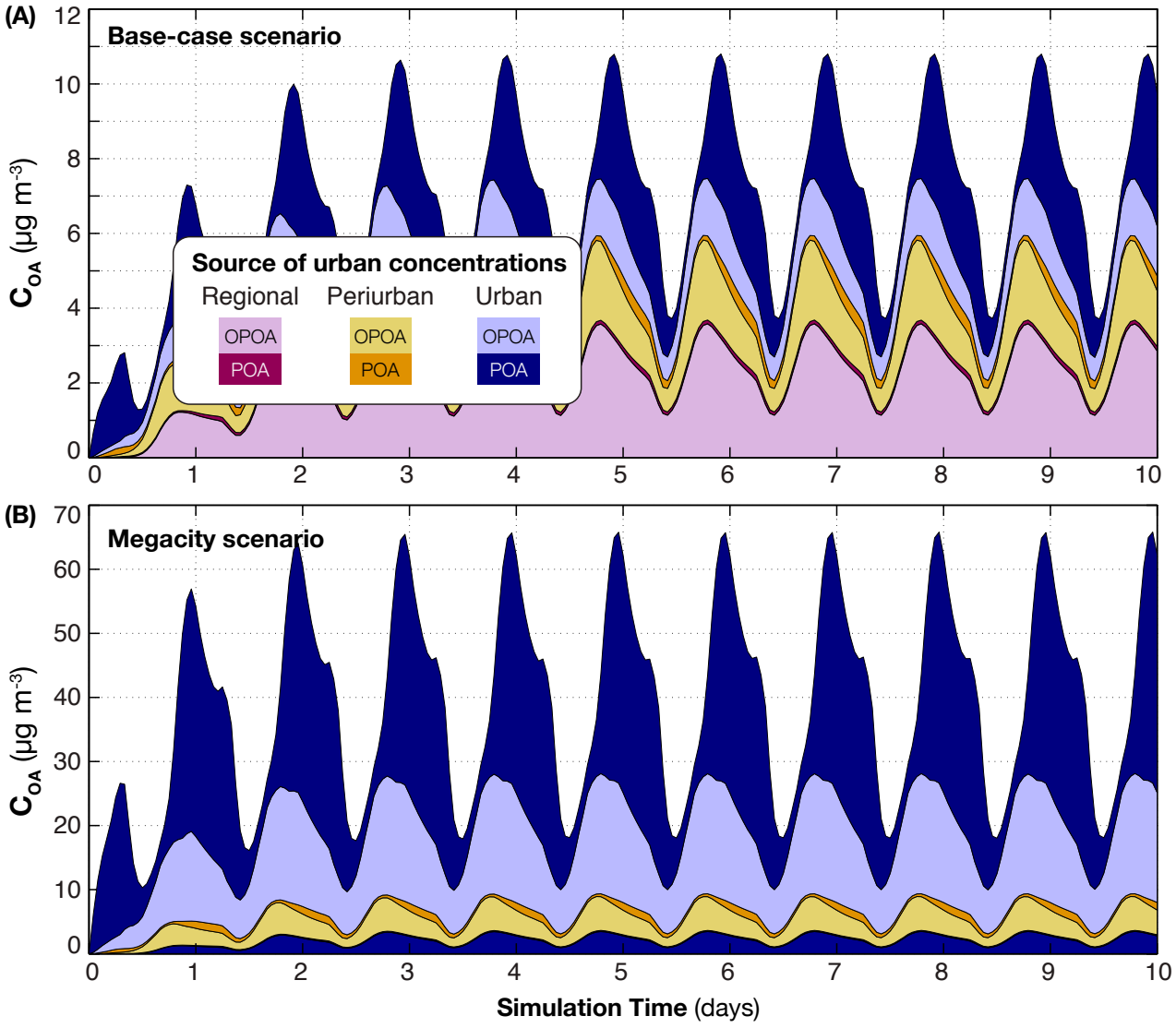

Figure 4-7. Source contributions to organic aerosol concentrations within the innermost urban compartment. Plots disaggregate POA and OPOA contributions to total urban OA concentrations from sources in the urban, periurban and regional compartments. Here and elsewhere, OA mass concentrations are presented on the basis of total organic mass, including non-carbon constituents of the OA. Upper panel A shows base-case scenario; lower panel B shows megacity scenario.

Figure 4-8. (Following pages). Plots of OA intake fraction (ppm, upper panels A,C) and population intake rate (gOA d^{-1}, lower panels B,D) for urban emissions of organic semivolatile precursor material (vapors and particles). Base case scenario is shown in panels A-B; megacity scenario is shown in panels C-D. Inhalation intake of urban emissions is disaggregated by the compartment in which inhalation occurs (i.e., by residents of the urban, periurban, regional compartments) and by whether the inhaled OA is primary (POA) or has experienced gas-phase photochemical aging from higher volatility precursors (OPOA). Separate values are displayed for each individual VBS volatility bin of emitted material (horizontal axis). For material in a given emitted volatility bin, the inhalation intake rate (lower panel) is approximately proportional to the product of intake fraction (upper panel) and the mass emissions rate (not shown). In the scenarios shown here, higher-volatility compounds are emitted in greater abundance than lower volatility compounds (see Figure 4-5). Note that the modeling approached used here assigns to all SVOCs and IVOCs within a plotted bar the saturation concentration at the center of the log scale (i.e., discrete values with integer powers of 10). Finally, note that population intake is plotted here the basis of total organic aerosol mass, while iF is computed on the basis of the organic carbon mass ratio, which neglects added non-carbon mass from photochemical aging.

Figure 4-9. (Following pages). Plots of *vapor-phase* intake fraction (ppm, upper panels A,C) and population intake rate (g organic vapors d^{-1}, lower panels B,D) for urban emissions of semivolatile organic precursor material (vapors and particles). Base case scenario is shown in panels A-B; megacity scenario is shown in panels C-D. Inhalation intake of urban emissions is disaggregated by the compartment in which inhalation occurs (i.e., by residents of the urban, periurban, regional compartments). Separate values are displayed for each individual VBS volatility bin of emitted material (horizontal axis). For material in a given emitted volatility bin, the inhalation intake rate (lower panel) is approximately proportional to the product of the intake fraction (upper panel) and the mass emissions rate (not shown). In the scenarios shown here, higher-volatility compounds are emitted in greater abundance than lower volatility compounds (see Figure 4-5). Note that the modeling approached used here assigns to all SVOCs and IVOCs within a plotted bar the saturation concentration at the center of the log scale (i.e., discrete values with integer powers of 10). Finally, note that population intake is presented on the basis of total organic mass, while iF is computed on the basis of the organic carbon mass ratio, which neglects added non-carbon mass from photochemical aging

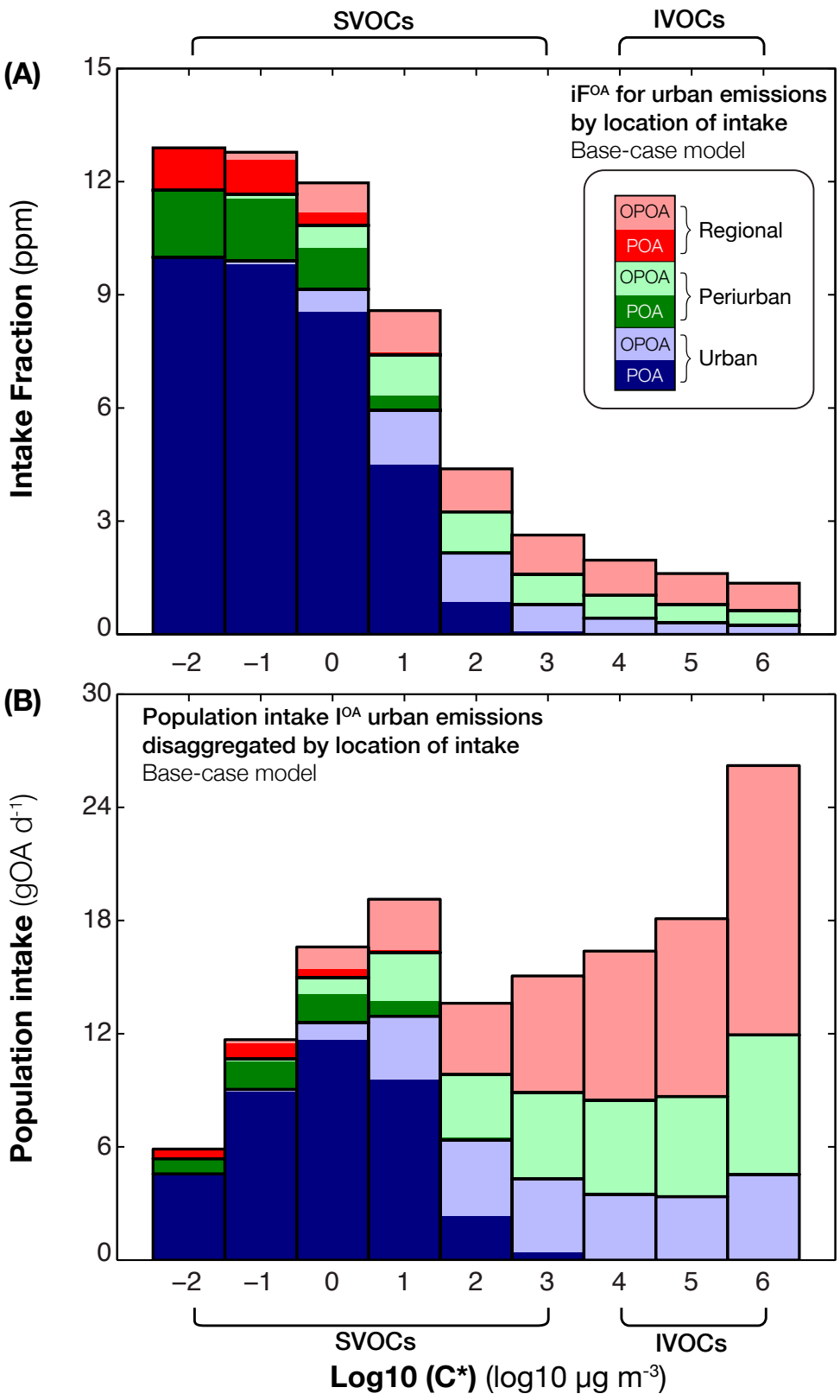

Figure 4-8. Continues on following page. Organic aerosol iF^{OA} and population intake rate I^{OA}.

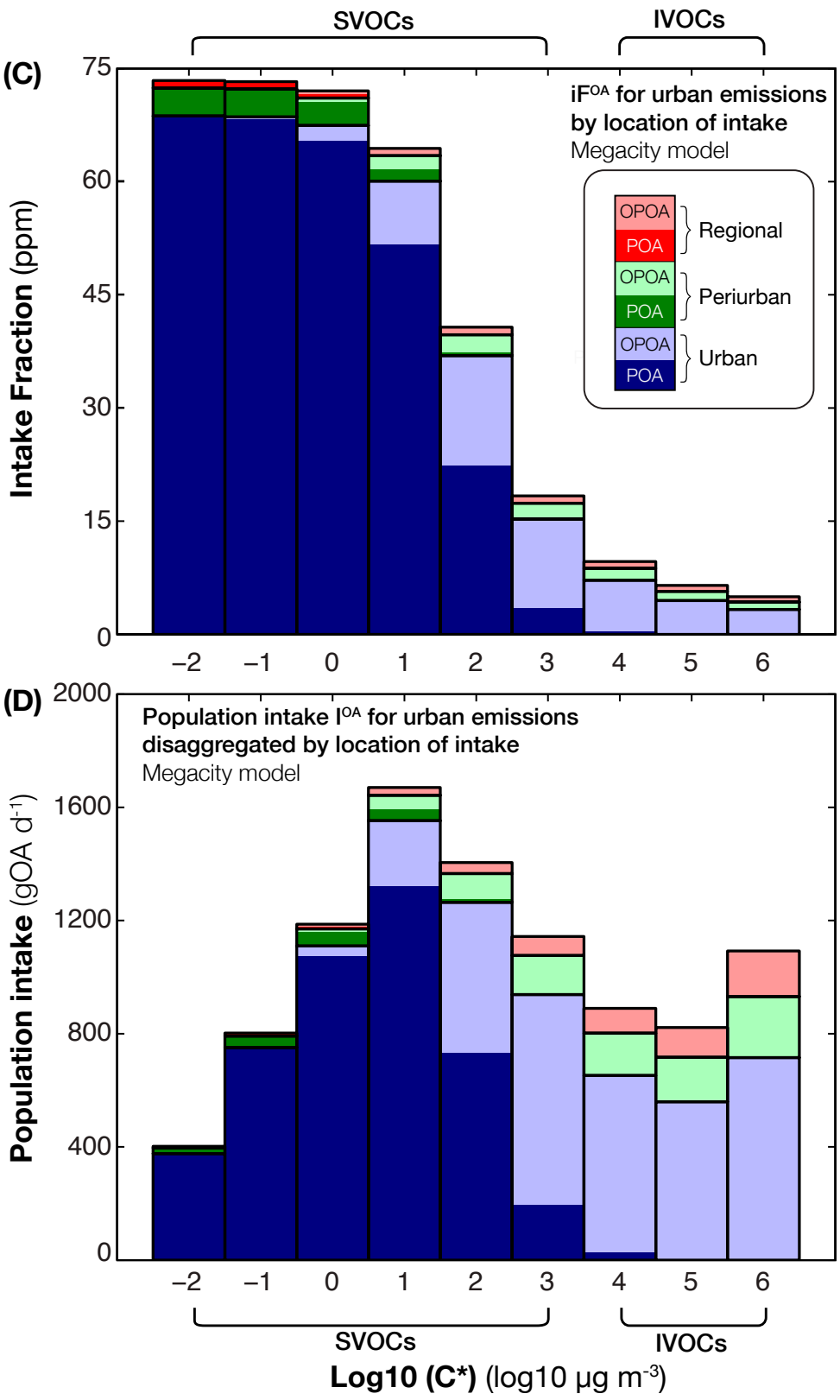

Figure 4-8. Organic aerosol iF^{OA} and population intake rate I^{OA}. Caption above.

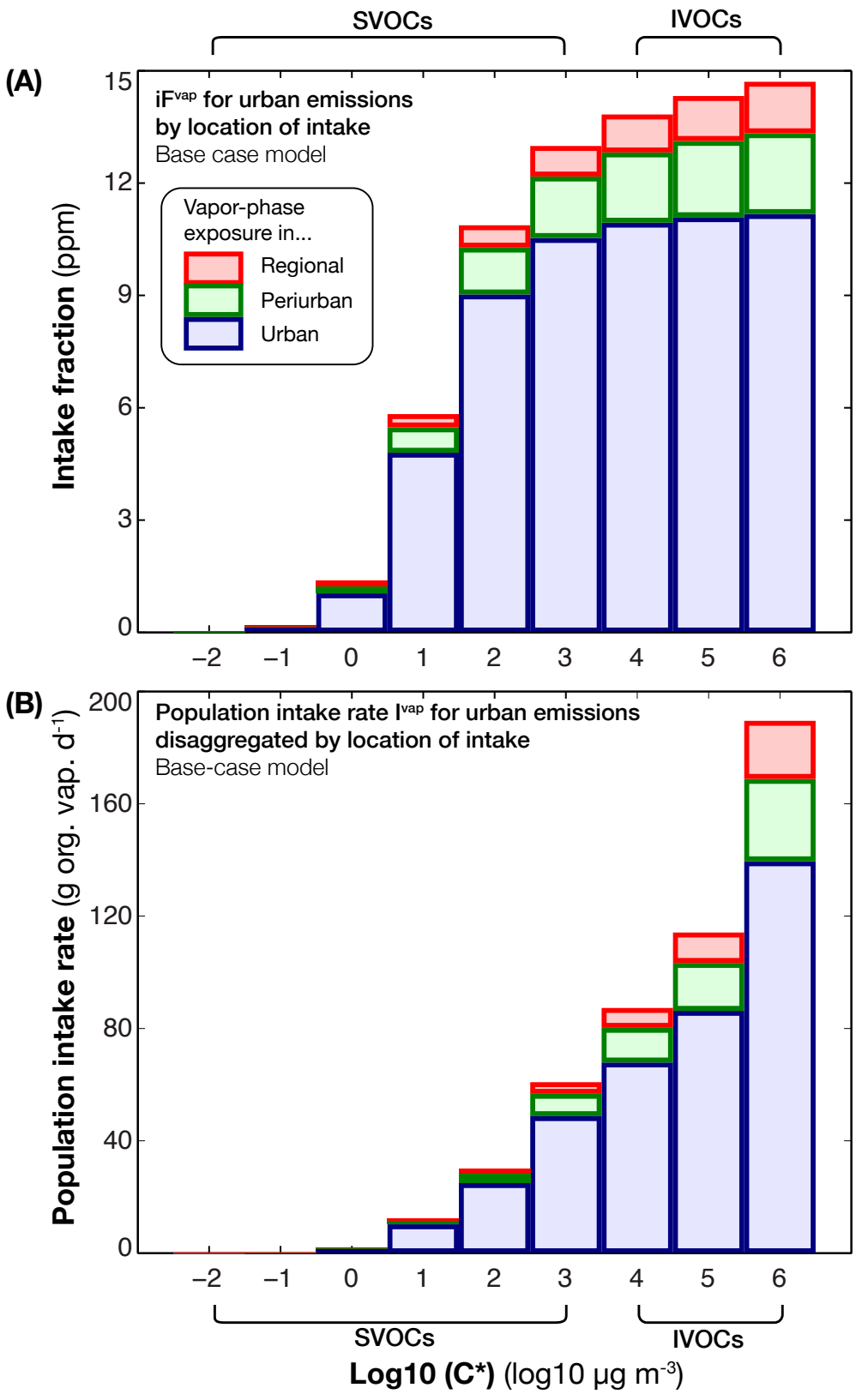

Figure 4-9. Continues on following page. Organic vapor iF^{vap} and population intake rate I^{vap}.

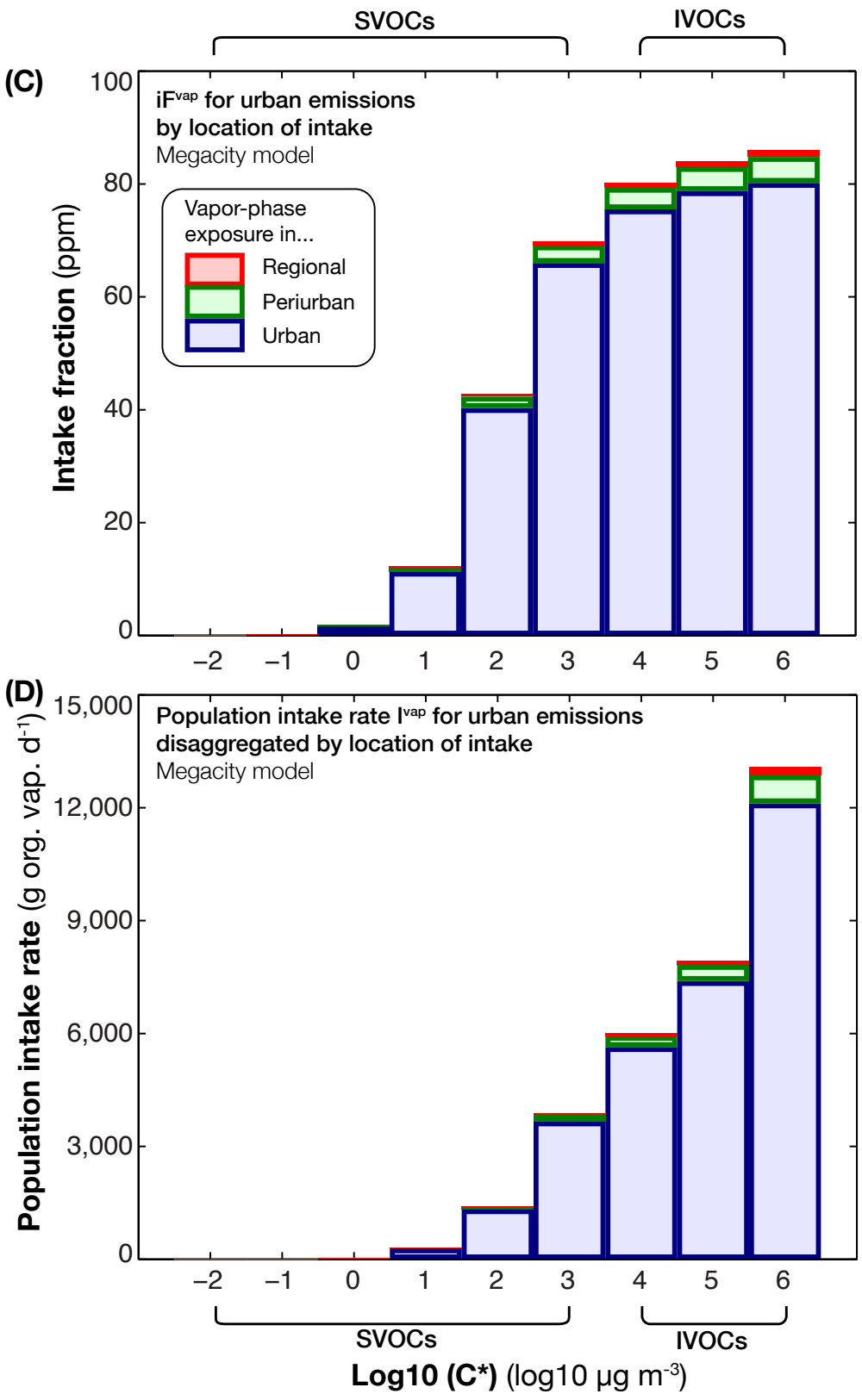

Figure 4-9. Organic vapor iF^{vap} and population intake rate I^{vap}. Caption above.

Chapter 5: Conclusions

In this concluding chapter, I summarize the results of investigations reported in the previous chapters, and discuss the implications of this work for policy and for future research.

5.1 Summary of results

In the individual studies that comprise this dissertation, I have explored several themes: (i) the role of proximity to sources influencing human exposure to primary air pollution; (ii) the effect of dynamic pollutant behavior on human exposure; and (iii) exposure conditions in developing world cities.

In Chapter 1, I provide background, motivation, and context for the dissertation. In Chapter 2, I report on a field investigation of traffic-related particle air pollution in New Delhi, India. Using real-time instruments, I measured fine ($PM_{2.5}$) and black carbon (BC) particle mass concentrations and ultrafine particle number (PN) concentrations inside vehicles traveling along congested roadways. The field study focused on exposure conditions inside unenclosed auto-rickshaws, a common type of commuter vehicle in many Asian cities. A total of ~160 h of measurement data were acquired in 62 individual 39-km trips sampled over a 3-month period. Contemporaneously with the in-vehicle measurements, I monitored ambient particle concentrations at a rooftop fixed site. In-vehicle particle concentrations substantially exceeded ambient concentrations. PM levels in both settings were very high. Geometric means of trip-averaged concentrations were 190 $\mu g\ m^{-3}$ $PM_{2.5}$, 42 $\mu g\ m^{-3}$ BC and 280×10^6 particles cm^{-3}. At the ambient fixed site, the geometric means of contemporaneously measured concentrations were, respectively, 130 $\mu g\ m^{-3}$ $PM_{2.5}$, 12 $\mu g\ m^{-3}$ BC and 35×10^6 particles cm^{-3}. The in-vehicle measurements rank among the highest levels reported in the literature for routine exposures in a transportation microenvironment. In addition to high time-averaged concentrations, the data from all three sampling devices exhibited prominent short-duration peaks. Typical peak concentrations for a trip exceeded trip-averaged concentrations by a factor of ~1.5– 2.5, with more prominent extremes for PN and BC than for $PM_{2.5}$.

The high in-vehicle particle exposures reported here point to a potentially important amplification in health risk that is not well quantified by traditional ambient air quality monitoring systems. In-vehicle levels are elevated above background levels owing to proximity to on-road emissions. The degree of elevation in vehicles varied strongly among the three monitored PM constituents. Whereas in-vehicle $PM_{2.5}$ concentrations were only moderately higher than background levels (1.5×), in-vehicle BC and PN concentrations were much more elevated relative to ambient levels (respectively 3.6× and 8.4×). This pattern of in-vehicle exposure amplification may be explained by differences in both emissions sources and pollutant dynamics. Primary $PM_{2.5}$ is emitted from vehicles but also from many non-traffic sources. In addition, long-range transport and secondary formation further elevate urban background $PM_{2.5}$ concentrations in a manner that tends to be spatially homogeneous on the urban scale. In contrast, BC is an exclusively primary pollutant for which vehicles likely constitute the most important urban emissions source. Thus, BC levels are more substantially elevated in proximity to traffic than are $PM_{2.5}$ levels. Similarly, PN concentrations are dominated by ultrafine particles, for which vehicles are a major emissions source. In comparison to the other two metrics ($PM_{2.5}$ and BC), PN concentrations evolve much more rapidly in space and time owing to dynamic loss

mechanisms that strongly affect ultrafine particles, such as deposition, coagulation and possibly evaporation. Ambient PN concentrations in Delhi are markedly lower than for in-vehicle or on-road conditions. This finding reinforces a growing body of evidence that ambient fixed-site measurements are especially ill suited for characterizing population exposures to pollutants such as UFP (e.g., Sioutas et al., 2005) that are strongly influenced by rapid dynamic processes.

In Chapters 3 and 4, I use the intake fraction (*iF*) metric to explore population exposure to urban vehicle emissions. Intake fraction summarizes the emissions-to-exposure relationship for a given source or source category as the fraction of emissions that are ultimately inhaled by an exposed population. In Chapter 3, I model intraurban *iF* for spatially distributed ground-level emissions of primary pollutants for 3,646 worldwide urban areas. The primary intent is to build an improved understanding of the source-receptor relationships for motor vehicle emissions on a global scale. The dataset includes all cities with a population above 100,000; cumulatively, the study encompasses a combined year-2000 population of 2.0 billion people, roughly 70% of the world's urban population at that date. The study develops *iF* estimates for vehicle emissions for many regions of the world, such as Asia and Africa, for which detailed *iF* data were not previously available. For emissions of conserved pollutants, I estimate a global population-weighted mean intraurban *iF* of 39 ppm, expressed equivalently as 39 g of pollutants inhaled per tonne emitted. For non-conserved pollutants that follow first-order decay with half-life of 10 h, the mean *iF* is 7.2% lower.

Global variation in intraurban intake fraction among the cities considered here is substantially larger than the range of *iF* results reported in earlier studies, with a range (population-weighted IQR) of 0.6 – 260 ppm (14 – 52 ppm). Systematic variation in *iF* among urban areas is explained by differences in population size, population density, and meteorology. Sorting by size, population-weighted mean *iF* values are 65 ppm, 35 ppm, and 15 ppm, respectively, for cities with populations larger than 3 million, 0.6 – 3 million, and 0.1 – 0.6 million. Country-average *iF* values vary by a factor of 3 among the 10 nations with the largest urban populations. Mean intraurban *iF* values are greatest in Asia and lowest in land-rich high-income regions such as the United States and Australia. For example, population weighted mean intraurban *iF* values for Chinese and Indian cities (respectively 44 ppm and 51 ppm) are more than twice as large as for United States cities (21 ppm). The 20 megacities considered here have especially high intake fraction values owing to very large linear population density, with an overall population-weighted mean *iF* of 83 ppm.

Chapter 4 considers the inhalation intake of semivolatile organic emissions from urban vehicles and other distributed ground-level sources. Population exposure to organic vehicle emissions is strongly affected by photochemical oxidation ("aging"), dilution, and other processes that alter gas-particle partitioning. In Chapter 4, I develop and apply a mechanistic exposure model to explicitly account for the dynamic evolution of semivolatile material between its emission from urban vehicles and resulting population inhalation intakes that occur at multiple spatial scales. Using an idealization of typical US urban population distribution patterns, I consider intraurban and beyond-urban exposures to urban emissions in a 400-km model domain.

The emissions-exposure relationship for semivolatile organic emissions differs from that of primary, conserved pollutants in several key aspects. The relative balance between particle- and

vapor-phase exposures to semivolatile emissions is a strong function of the volatility of emissions as well as the degree of dilution and photochemical aging that occurs. Since a large portion of the emitted material partitions into the vapor phase under ambient conditions, the overall particle-phase intake fraction for semivolatile organic emissions is substantially lower than for primary, conserved pollutants. In general, the phase partitioning of population intake is a strong function of the volatility of emissions. Less volatile emissions (i.e., compounds with saturation concentration $C^* < 1\ \mu g\ m^{-3}$) result in population intakes that are predominantly in the form of primary particles. In contrast, more volatile emissions (e.g., $C^* \geq 1000\ \mu g\ m^{-3}$) produce inhalation intakes that are predominantly in the vapor-phase. Semivolatile compounds with volatilities between these two extremes result in population intakes that are a combination of primary particles, aged (quasi-secondary) particles produced by gas-phase oxidation, and vapor-phase material. In the default volatility distributions considered in this analysis, emissions are weighted towards the most volatile material. Accordingly, the dominant fraction of the overall population intake of semivolatile emissions takes place in the vapor phase. Considering the lower-volatility portion of the default emissions distribution ($C^* < 1000\ \mu g\ m^{-3}$; 40% of total emitted mass), roughly 60% of total emitted organic carbon is inhaled in the vapor phase, ~25% is inhaled as primary particles, and ~15% is inhaled as quasi-secondary (oxidized) particles. Scenarios with alternative emissions volatility distributions result in a different apportionment of population intake among these three groupings. However, the overall *iF* (particle + vapor phase) for semivolatile organic emissions is not highly dependent on the volatility distribution of emissions.

The scenarios modeled in Chapter 4 consider population exposures attributable to a given city's emissions that occur within the same city (intraurban) and also in the population living outside the source city (beyond-urban). Intraurban and beyond-urban exposures differ substantially in character. In comparison to intraurban exposures, beyond-urban exposures typically affect a much larger population at more dilute concentrations. Intraurban organic aerosol exposures are predominantly primary, since the relatively short residence time of air precludes substantial photochemical aging. In contrast, beyond-urban exposures to organic aerosol of urban origin consist almost exclusively of photochemically aged material. In the base-case scenario, ~70% of the domain-wide exposure to organic aerosol of urban origin is photochemically aged. The remaining ~30% of total organic aerosol exposure is primary, and takes place nearly exclusively in the intraurban compartment. For urban emissions of organic vapors and for primary, conserved pollutants, more than two thirds of domain-wide exposure is intraurban. These results point to the important contribution to total population intake of intraurban exposures. Such exposures are likely to be substantially underrepresented in medium-scale (~30 km grid) and coarse-scale (>100 km grid) chemical transport models that are commonly used for modeling atmospheric pollution and that are sometimes employed for exposure analysis.

5.2 Implications for policy and future research

In this section, I briefly explore the implications of this dissertation for future research and policy. The discussion of future research is approached from two distinct perspectives. On one hand, I aim to illuminate opportunities to extend the analyses contained herein to explore related topics and/or address uncertainties. On the other, I seek to illustrate fundamental questions on the research frontier whose resolution may allow additional insights to be derived from the present

investigations. This discussion focuses on three particular policy-relevant issues on the research frontier: (i) assessment of near-source exposures; (ii) health effects of vehicle emissions; and (iii) implications for the development and deployment of more environmentally sustainable transportation systems.

5.2.1 Near-source exposures

Human exposure to vehicle emissions occurs at multiple spatiotemporal scales. For example, in this dissertation, I consider exposures in the near-source region (Chapter 2), for urban ambient conditions (Chapters 2 – 4), and at the regional or "beyond-urban" scale (Chapter 4). Human populations and vehicle emissions correlate in space and time. Accordingly, high-resolution investigations often reveal important contributions to exposure attributable to close proximity that are not evident at a coarser scale of analysis (e.g., Gouge et al., 2010; Greco et al., 2007; Marshall and Behrentz, 2005; Zhou and Levy, 2008). This conclusion may itself apply at multiple spatial scales. For example, Chapter 2 demonstrates that in-vehicle exposures in New Delhi are substantially amplified above urban background levels. In turn, Chapter 4 demonstrates that elevated urban background levels of organic aerosol make a substantial contribution to population exposure to urban emissions of semivolatile organic compounds that would be sharply discounted if evaluated at the scale of a regional model. In each of these examples, the importance of proximity is especially large for dynamic primary pollutants with short atmospheric lifetimes.

Considering the broader context of the state of knowledge, near-source exposures to health-relevant pollutants are not yet well characterized, especially relative to the current understanding of ambient pollution. Future research that aims to evaluate the relationship between emissions and human exposure at high spatiotemporal resolution could provide important new insights. One fundamental issue relates to better understanding the spatial and temporal association of human occupancy, emissions, and concentrations in source-impacted environments (e.g., near roadways). The advent of ubiquitous GPS-enabled devices (e.g., smartphones) means that very large datasets (e.g., so-called "big data") are now available for analysis of time-activity patterns. It may be possible to use these data to inform multi-scale mechanistic assessments of the emissions-to-exposure relationship for major sources such as vehicles. In turn, the refinement of this understanding can aid prioritization efforts and policy design and can indicate new avenues for exposure control. Moreover, a more complete understanding of the relationship between personal exposures and ambient concentrations may help resolve issues at the research frontier of air quality epidemiology, such as those that relate to the public health consequences of ultrafine particle exposures. Of course, one should also anticipate diminishing returns associated with any effort to completely characterize population exposure to air pollution. Future research could usefully explore the question of "how fine-scale is fine enough?" In other words, to what degree will refinements in spatiotemporal resolution uncover further exposures that are not evident at coarser analysis scales? It is likely that the answer to this question is highly contextual, depending on the spatial and temporal distributions of emissions and exposed populations, the pollutant under consideration, and the required level of precision and accuracy.

At a more focused scale, a key opportunity to extend the present research relates to better understanding the roles played by buildings and other enclosed environments (e.g., automobile passenger cabins) in modifying population exposure to vehicle emissions. For example,

particulate matter of outdoor origin penetrates the envelope of buildings and automobiles and persists with substantially lower than 100% efficiency (e.g., Riley et al., 2002; Hudda et al., 2012; Hodas et al., 2012; Chen and Zhao, 2011). Because parameters that govern particle penetration and persistence vary regionally, the results for Chapter 3 could be refined specifically for the case of particulate matter with a more regionally explicit treatment of these parameters. In the case of semivolatile emissions (Chapter 4), another potential refinement relates to indoor environmental effects on gas-particle partitioning. Several variables may alter indoor SVOC exposures to material of outdoor origin, including shifts in temperature and humidity and sorptive interactions with building materials and indoor SVOC "reservoirs" such as surface films and settled dust (Weschler and Nazaroff, 2008; Weschler and Nazaroff, 2010). Future work might build on the findings in Chapter 4 by explicitly considering indoor exposures in the mechanistic treatment of the emissions-to-exposure relationship for semivolatile emissions.

5.2.2 Health effects of vehicle emissions

This dissertation adds new texture to existing understanding of the relationship between vehicle emissions and human exposure. A key motivation for undertaking this research relates to the need to better characterize the linkage between emissions sources (e.g., vehicles) and adverse human health impacts. Epidemiological studies provide much of the basis for our understanding of the relationship between air pollution exposures and adverse health outcomes (e.g., excess morbidity and premature mortality). Most epidemiological studies utilize ambient concentration measurements as an explanatory variable, rather than intake or personal exposures, which are the key metrics of interest in this dissertation. In this section, I comment on refinements in the state of knowledge that might be necessary to more fully grasp the relationship between vehicle emissions and health effects.

Decision makers and analysts concerned with environmental health seek information about the connection between emissions (or changes in emissions) and health effects (or changes in health effects). By connecting emissions to population intake, *iF* data provide a useful link in this conceptual chain (intake per unit emission). However, additional data are required to explicitly interpret population intakes in terms of health effects. In the following discussion, I focus on particulate matter, owing to the outsized health effects associated with this pollutant class. Additional data required to link PM exposures to health effects include information on baseline disease incidence rates and on exposure-response relationships. The exposure-response relationship deserves special attention. Two major refinements may be necessary to develop a reliable estimate of an "intake-based toxicity" parameter (units: health effect per unit population intake). First, the choice of exposure metric used in exposure-response functions requires careful attention. Most studies of fine particle health effects employ ambient concentrations as a proxy exposure metric, thereby producing a concentration-response function (CRF) that is linked to ambient levels. To the extent that ambient concentrations provide a biased estimate of exposure concentrations, these data must be interpreted with caution to extract useful information about the health risk associated with a unit of inhalation intake. Studies that specifically identify the exposure-response relationship for non-ambient exposures to material of ambient origin may help fill this important data gap. A related issue is the usage of intake, rather than personal exposure concentrations, as the independent exposure variable of interest in epidemiological studies. In general, concentration-based exposure metrics enjoy wide currency in the air quality epidemiology community, whereas intake-based metrics do not. In principle, however, if

sufficient data were available to measure or model the relationship between personal exposure concentrations and personal intake rates for study subjects, future epidemiological studies may be able to develop intake-response functions to complement concentration-response functions. Such data would allow for health impact assessors to treat the linkage between emissions, intake-based metrics (e.g., *iF*) and resulting health effects with greater conceptual rigor.

A second major issue relates to the shape of ambient CRFs. For $PM_{2.5}$, emerging evidence suggests that the shape of the CRF may be nonlinear, starting with a steep slope at low concentrations and flattening to a shallower slope at higher levels (Crouse et al., 2012; Pope et al., 2011; Smith and Peel, 2010). Much remains to be learned about the shape of the CRF for $PM_{2.5}$, especially at higher ambient and indoor concentrations for which few epidemiological data currently exist. Thus, it is not yet possible to provide a rigorous evaluation of, for example, the prospective health benefits of a given level of emissions reduction in a polluted city compared to the same level of reduction in a clean city. Further research could usefully investigate the shape of the concentration-response curve for $PM_{2.5}$ at concentrations above 30 $\mu g\ m^{-3}$, for example, by including conditions more representative of polluted cities and polluted indoor conditions.

Chapter 2 demonstrates that time-averaged in-vehicle particle exposures may substantially exceed ambient concentrations in some circumstances. Short-duration peaks in exposure owing to transient encounters with exhaust plumes can account for a substantial fraction of on-road exposure. Prior studies have demonstrated associations of subclinical effects (e.g., markers of oxidative stress) and acute outcomes (e.g., myocardial infarction, asthma attacks) with exposure to traffic (Peters et al., 2004; Riediker et al., 2004; McConnell et al., 2010), although the relative contributions of air pollution and other traffic-related stressors (e.g., noise) is not completely understood. Overall, relatively little is known about the potential long-term health effects of short-duration exposures to high levels of pollution. Future studies may help elucidate the health consequences of in-traffic exposures at different time scales. One issue relates to the relative toxicity of ambient vs. near-roadway air pollution: fresh combustion aerosols might have higher or lower health effects per unit inhaled mass than more aged ambient air pollution. A second unresolved issue relates to the health effects of transient (i.e., shorter than 1 minute) exposures to high particle concentrations, which may pose different risks than lower, less-variable exposures at the same time-averaged concentration.

5.2.3 Sustainable transportation for an urbanizing world

Transportation has important environmental consequences that extend beyond the human health impacts of urban and regional-scale air pollution exposures. Chief among these concerns ranks the emission of climate-active pollutants such as CO_2, CH_4 and BC. An environmentally sustainable trajectory of development over the coming century will require a dramatic departure from current trends of increasing emissions of climate- and health-relevant pollutants (Sager et al., 2011; Scown et al., 2013). A portfolio approach can help achieve the order-of-magnitude scale reduction in transportation's climate footprint that is especially necessary in highly motorized countries, and the similar scale of reduction in transportation-related air pollution exposures that is especially needed in many low-income cities. In this section, I briefly explore how intake fraction and other concepts from this dissertation can play a role in envisioning,

planning, and analyzing options for achieving a more environmentally sustainable future for urban transportation.

Strategies for reducing transportation's environmental impact may be classified into three broad groupings: avoiding demand (vehicle kilometers traveled, VKT), reducing emissions per unit activity, and mitigating the environmental impact per unit emissions (Table 5-1). Progress in reducing environmental impact has and will likely continue to entail a suite of measures drawn from engineering, urban planning, and policy. Many potential mitigation measures may produce simultaneous benefits ("co-benefits") for climate and health (Haines et al., 2007; Smith and Haigler, 2008). For example, engineering strategies to reduce vehicle fuel consumption can reduce CO_2 and health-relevant pollutant emissions simultaneously. Likewise, compact, mixed-use urban planning can substantially reduce the need for private motor vehicle use. Vehicle electrification has the potential to reduce both CO_2 emissions (electric motors are more efficient than internal combustion engines) and urban exposures (rural tall-stack emissions have lower intake fractions than urban tailpipe emissions).

Important tradeoffs between climate and health also exist in the effort to design a sustainable transportation sector. For example, vehicle electrification may not decrease climate and health impacts if the electricity generation system remains highly dependent on coal with incomplete emission controls (Williams et al., 2012; Ji et al., 2012). Likewise, increasing urban density without reducing emissions could increase population intakes (Marshall et al., 2005). Some emissions control treatments may trade one benefit for another (e.g., fuel economy vs. emissions; particle mass vs. particle number). The intake fraction of urban emissions can be reduced via active air filtration in indoor environments, but doing so may increase building energy consumption.

It is probable that specific strategies for reducing the environmental impact of transportation will be appropriate to different degrees in different world regions. For example, efforts to mitigate vehicle emissions may provide greater health benefits in regions with high intake fraction than in more sparsely populated regions. Bold shifts in urban form are likely to be more feasible in locales with strong, centralized control of urban planning than in areas with more diffuse decision-making. Although an appropriate set of strategies might differ among regions, a common set of metrics (e.g., Table 5-1) coupled with tools for addressing transportation sustainability could have broad applicability for analysts and policy makers.

Energy analysts have long employed scenario analysis as a means to explore the technical, economic, and policy considerations associated with the evolution of the energy system towards some envisioned future state (e.g., Lovins, 1976; Williams et al., 2012). An emerging body of literature uses similar techniques to explore the potential climate and health co-benefits of various proposed policy inventions (e.g., Woodcock et al., 2009; Shindell et al., 2011; Shindell et al., 2012). Interdisciplinary exposure analysts have important contributions to make to this new conversation. For example, co-benefit analyses frequently employ simplified emissions-to-impact models for health effects that overlook large differences in intake fraction among major source categories. Reduced-form health impact models that more accurately account for key differences in the emissions-to-impact relationship among various mitigation options could enable refined and more accurate analyses in the future. Such models and datasets can play an important role in screening analyses to identify actions that would lead to especially high climate

and health benefits per unit effort. The models and data that I report on in this dissertation make a contribution towards developing this set of analytical tools.

5.3 References

Chen, C., Zhao, B., 2011. Review of relationship between indoor and outdoor particles: I/O ratio, infiltration factor and penetration factor. *Atmospheric Environment* 45, 275-288.

Crouse, D.L., Peters, P.A., van Donkelaar, A., Goldberg, M.S., Villeneuve, P.J., Brion, O., Khan, S., Atari, D.O., Jerrett, M., Pope, C.A., Brauer, M., Brook, J.R., Martin, R.V., Stieb, D., Burnett, R.T., 2012. Risk of nonaccidental and cardiovascular mortality in relation to long-term exposure to low concentrations of fine particulate matter: a Canadian national-level cohort study. *Environmental Health Perspectives* 120, 708-714.

Gouge, B., Ries, F.J., Dowlatabadi, H., 2010. Spatial distribution of diesel transit bus emissions and urban populations: Implications of coincidence and scale on exposure. *Environmental Science & Technology* 44, 7163-7168.

Greco, S.L., Wilson, A.M., Hanna, S.R., Levy, J.I., 2007. Factors influencing mobile source particulate matter emissions-to-exposure relationships in the Boston urban area. *Environmental Science & Technology* 41, 7675-7682.

Haines, A., Smith, K.R., Anderson, D., Epstein, P.R., McMichael, A.J., Roberts, I., Wilkinson, P., Woodcock, J., Woods, J., 2007. Policies for accelerating access to clean energy, improving health, advancing development, and mitigating climate change. *The Lancet* 370, 1264-1281.

Hodas, N., Meng, Q., Lunden, M.M., Rich, D.Q., Özkaynak, H., Baxter, L.K., Zhang, Q., Turpin, B.J., 2012. Variability in the fraction of ambient fine particulate matter found indoors and observed heterogeneity in health effect estimates. *Journal of Exposure Science and Environmental Epidemiology* 22, 448-454.

Hudda, N., Kostenidou, E., Sioutas, C., Delfino, R.J., Fruin, S.A., 2012. Vehicle and driving characteristics that influence in-cabin particle number concentrations. *Environmental Science & Technology* 45, 8691-8697.

Ji, S., Cherry, C.R., Bechle, M.J., Wu, Y., Marshall, J.D., 2012. Electric vehicles in China: Emissions and health impacts. *Environmental Science & Technology* 46, 2018-2024.

Lovins, A., 1976. Energy strategy: The road not taken? *Foreign Affairs* 55, 65-96.

Marshall, J.D., Behrentz, E., 2005. Vehicle self-pollution intake fraction: Children's exposure to school bus emissions. *Environmental Science & Technology* 39, 2559-2563.

Marshall, J.D., McKone, T.E., Deakin, E., Nazaroff, W.W., 2005. Inhalation of motor vehicle emissions: effects of urban population and land area. *Atmospheric Environment* 39, 283-295.

McConnell, R., Liu, F., Wu, J., Lurmann, F., Peters, J., Berhane, K., 2010. Asthma and school commuting time. *Journal of Occupational and Environmental Medicine* 52, 827-828.

Peters, A., von Klot, S., Heier, M., Trentinaglia, I., Hörmann, A., Wichmann, H.E., Löwel, H., 2004. Exposure to traffic and the onset of myocardial infarction. *New England Journal of Medicine* 351, 1721-1730.

Pope, C.A., III, Burnett, R.T., Turner, M.C., Cohen, A., Krewski, D., Jerrett, M., Gapstur, S.M., Thun, M.J., 2011. Lung cancer and cardiovascular disease mortality associated with ambient air pollution and cigarette smoke: Shape of the exposure-response relationships. *Environmental Health Perspectives* 119, 1616-1621.

Riediker, M., Cascio, W.E., Griggs, T.R., Herbst, M.C., Bromberg, P.A., Neas, L., Williams, R.W., Devlin, R.B., 2004. Particulate matter exposure in cars is associated with cardiovascular effects in healthy young men. *American Journal of Respiratory and Critical Care Medicine* 169, 934-940.

Riley, W.J., McKone, T.E., Lai, A.C.K., Nazaroff, W.W., 2002. Indoor particulate matter of outdoor origin: Importance of size-dependent removal mechanisms. *Environmental Science & Technology* 36, 200-207.

Sager, J., Apte, J.S., Lemoine, D.M., Kammen, D.M., 2011. Reduce growth rate of light-duty vehicle travel to meet 2050 global climate goals. *Environmental Research Letters* 6, Art. 024018.

Scown, C.D., Taptich, M., Horvath, A., McKone, T.E., Nazaroff, W.W., 2013. Achieving deep cuts in the carbon intensity of US automobile transportation by 2050: Complementary roles for electricity and biofuels. *Environmental Science & Technology*, in press, DOI: 10.1021/es4015635.

Shindell, D., Faluvegi, G., Walsh, M., Anenberg, S.C., Van Dingenen, R., Muller, N.Z., Austin, J., Koch, D., Milly, G., 2011. Climate, health, agricultural and economic impacts of tighter vehicle-emission standards. *Nature Climate Change* 1, 59-66.

Shindell, D., Kuylenstierna, J.C.I., Vignati, E., van Dingenen, R., Amann, M., Klimont, Z., Anenberg, S.C., Muller, N., Janssens-Maenhout, G., Raes, F., Schwartz, J., Faluvegi, G., Pozzoli, L., Kupiainen, K., Hoglund-Isaksson, L., Emberson, L., Streets, D., Ramanathan, V., Hicks, K., Oanh, N.T.K., Milly, G., Williams, M., Demkine, V., Fowler, D., 2012. Simultaneously mitigating near-term climate change and improving human health and food security. *Science* 335, 183-189.

Sioutas, C., Delfino, R.J., Singh, M., 2005. Exposure assessment for atmospheric ultrafine particles (UFPs) and implications in epidemiologic research. *Environmental Health Perspectives* 113, 947-955.

Smith, K.R., Haigler, E., 2008. Co-benefits of climate mitigation and health protection in energy systems: Scoping methods. *Annual Review of Public Health* 29, 11-25.

Smith, K.R., Peel, J.L., 2010. Mind the gap. *Environmental Health Perspectives* 118, 1643-1645.

Weschler, C.J., Nazaroff, W.W., 2008. Semivolatile organic compounds in indoor environments. *Atmospheric Environment* 42, 9018-9040.

Weschler, C.J., Nazaroff, W.W., 2010. SVOC partitioning between the gas phase and settled dust indoors. *Atmospheric Environment* 44, 3609-3620.

Williams, J.H., DeBenedictis, A., Ghanadan, R., Mahone, A., Moore, J., Morrow, W.R., Price, S., Torn, M.S., 2012. The technology path to deep greenhouse gas emissions cuts by 2050: The pivotal role of electricity. *Science* 335, 53-59.

Woodcock, J., Edwards, P., Tonne, C., Armstrong, B.G., Ashiru, O., Banister, D., Beevers, S., Chalabi, Z., Chowdhury, Z., Cohen, A., Franco, O.H., Haines, A., Hickman, R., Lindsay, G., Mittal, I., Mohan, D., Tiwari, G., Woodward, A., Roberts, I., 2009. Public health benefits of strategies to reduce greenhouse-gas emissions: Urban land transport. *The Lancet* 374, 1930-1943.

Zhou, Y., Levy, J.I., 2008. The impact of urban street canyons on population exposure to traffic-related primary pollutants. *Atmospheric Environment* 42, 3087-3098.

Table 5-1. Potential routes for reducing health and climate impacts from transportation

	Sample metrics [a]	Example measures
Reduce vehicle usage	**VKT y^{-1}**	
Shorten trips	PKT y^{-1}	Mixed use planning, telecommuting
Higher vehicle occupancy	VKT PKT^{-1}	Carpooling, mass transit
Reduce emissions intensity	**gCO_2 VKT^{-1}; $gPM_{2.5}$ VKT^{-1}**	
Reduce energy consumption	MJ_{fuel} VKT^{-1}	Vehicle mass, drivetrains, electrification
Decrease emission factor	g CO_2 MJ^{-1}_{fuel}, g $PM_{2.5}$ MJ^{-1}_{fuel}	Emissions aftertreatment, fuel switching
Reduce impact of emissions	**various**	
Lower population intake per unit emissions	*iF*	Electrification, reduce population proximity, active remediation of indoor air
Reduce health risk per unit population intake	DALY per g-inhaled	Address other risk factors for cardiovascular disease
Reduce climate impact of GHG emissions	various	Air capture of CO_2, geoengineering to increase albedo

[a] Abbreviations:
PKT, passenger kilometers traveled
VKT, vehicle kilometers traveled
DALY, disability-adjusted life year

Appendix A: Post-processing of aethalometer black carbon measurements

During initial field sampling for Chapter 2, it became apparent that the early production Magee Scientific AE-51 "microAethalometer" instruments had strong sensitivity to mechanical shock and vibration that yielded spurious "spikes" in measured BC concentrations (Figure A-1). Controlled testing of the instrument under clean-air conditions revealed that sudden, forceful movement of the instrument caused a characteristic "spike" of ± 200 – 2000 μg m^{-3} that was typically short-lived (1-3 s). The pattern of spikes typically involved a very large positive and negative excursion in reported BC in close succession, within 1-3 s of each other. However, I found that the net contribution of a set of positive and negative BC concentration spikes typically *did not* average to zero over the duration of each mechanical shock event. As this spurious signal likely introduced bias into the sample, I developed a post-processing algorithm to identify the characteristic signature of affected data points and exclude them from analysis. The algorithm identifies affected points by searching for instances of high relative deviation between an individual observation and surrounding data points, as follows:

1. Establish a moving baseline range of instrumental noise in the 1 Hz BC signal.

    a. For each 1-s observation compute the difference between each individual 1-s measurement of BC and the 30-s moving average of BC around that point. This time series is termed the "local deviation," or *LD*. For each time point *i,* the local deviation LD_i is computed as:

$$LD_i = BC_i^{raw} - \frac{1}{30}\sum_{i-15}^{i+14} BC_i^{raw} \qquad [A.1]$$

    Here, BC_i^{raw} is the raw reported BC signal from the microAeth at time point *i*.

    b. For every 1-s observation, compute the 5-min moving-window 25th and 75th percentile of the local deviation time series generated by equation [A.1]:

$$LD_i^{5\,\mathrm{min},p75} = \mathrm{P}^{75}\left(LD_{i-150},\ldots,LD_{i+149}\right) \qquad [A.2a]$$

$$LD_i^{5\,\mathrm{min},p25} = \mathrm{P}^{25}\left(LD_{i-150},\ldots,LD_{i+149}\right) \qquad [A.2b]$$

    Notation: the operator P^n computes the n^{th} percentile of a series. For example, $LD_i^{5\,\mathrm{min},p75}$ is the 75th percentile of the local deviation time series *LD*, evaluated over a 5-minute period of the *LD* time series centered on time point *i*, and extending over the 5 minutes (300 seconds) from point (*i* – 150) to point (*i* + 149).

2. Identify individual 1-s observations as "candidate extreme values" for exclusion if the local deviation (step 1a) of that observation is more than 5 times larger (smaller) than the 75th (25th) percentile of the 5-min moving-window instrumental noise, as calculated in step 1b:

$$CEV_i = \left\{ \begin{array}{l} IF\left(\begin{array}{l} \left[LD_i > \left(5 \times LD_i^{5\,\mathrm{min},p75} \right) \right] \\ OR\ \left[LD_i < \left(5 \times LD_i^{5\,\mathrm{min},p25} \right) \right] \end{array} \right), \text{ then } \quad TRUE \\ \qquad\qquad\qquad\qquad\qquad\qquad \ldots \text{else } FALSE \end{array} \right\} \qquad [A.3]$$

Here, CEV_i represents whether an individual time point is determined to be a candidate extreme value ($CEV_i = TRUE$) or not ($CEV_i = FALSE$).

3. Search for negative BC concentrations within 2 s of each candidate extreme value identified in the previous step. Candidate extreme values that are negative or that have a negative BC measurement within ± 2 s are classified as spurious observations (*SO*). Each individual data point is evaluated for being a spurious observation with the following expression:

$$SO_i = \left\{ \begin{array}{l} IF\left(\begin{array}{l} \left(CEV_i = TRUE \right) \\ AND\left(\left[\sum_{i-2}^{i+2} \left(BC_i^{raw} < 0 \right) \right] > 0 \right) \end{array} \right), \text{ then } \quad TRUE \\ \qquad\qquad\qquad\qquad\qquad\qquad \ldots \text{else } FALSE \end{array} \right\} \qquad [A.4]$$

Here, SO_i represents whether an individual time point is determined to be a spurious observation ($SO_i = TRUE$) or not ($SO_i = FALSE$). In the summation notation employed here, the number instances for which $BC_i^{raw} < 0$ are summed. Thus, the "*AND"* condition tests to see whether any negative values are contained in the immediate proximity of a candidate extreme value.

4. Remove each spurious BC observation and the other four BC observations within ± 2 s of the spurious value from analysis.

After applying this algorithm, I computed cleaned BC time series using the "sensor" and "reference" raw optical signals from the instrument, which measure the intensity of light (λ= 880 nm) transmitted through, respectively, the BC-laden filter spot and an area of filter unexposed to sample air. To remove inherent 1-s instrumental noise, I applied a 10-s moving average smoothing function to the sensor and reference optical signals, resulting in the variables I_S and I_R, respectively. Next, I computed BC concentrations for each observation at time $t = i$ using the following relations (Hansen et al., 1984):

$$I_{S_i}^* = I_{S_i} \left(I_{R_{i=1}} / I_{R_i} \right) \qquad [A.5]$$

$$\mathrm{d}ATN_i^* = -100 \ln\left(I_{S_i}^* / I_{S_{(i-1)}}^* \right) \qquad [A.6]$$

$$BC_i = \frac{A}{V_i}\left(\frac{\mathrm{d}ATN_i^* / 100}{\sigma}\right) \qquad [A.7]$$

In equation [A.5], I^*_{Si} represents the smoothed sensor beam signal at $t = i$, normalized for any change in the smoothed reference beam signal I_R between $t = 1$ and $t = i$. In equation [A.6], the instantaneous change in filter light attenuation dATN is computed using a Beer-Lambert type relation based on the change in instantaneous filter transmission. Equation [A.7] computes the instantaneous BC (units: g m^{-3}) concentration at $t = i$. Here, A represents the area of the filter spot (7.1×10^{-6} m^2), V_i represents the air volume swept through the filter between t = i-1 and $t = i$ (for 150 mL min^{-1} flow rate and 1 Hz data logging, $V = 2.5 \times 10^{-6}$ m^3), and σ is the attenuation coefficient, which for the manufacturer's default calibration is 12.5 m^2 g^{-1}. The effect of the cleaning algorithm is visible when comparing Figures A-1a-c.

I further corrected BC measurements to account for the decreased instrumental sensitivity to BC with increased filter loading based on the empirical calibration of Kirchstetter and Novakov (2007):

$$BC = BC_o \left(0.88\,Tr + 0.12\right)^{-1} \qquad [2.4]$$

Kirchstetter and Novakov attribute this effect to the true attenuation coefficient (σ, equation [A.7]) diminishing as filter transmission decreases (Tr), which corresponds with increased filter loading (Kirchstetter and Novakov, 2007). In contrast, the default manufacturer's calibration of the instrument implies that σ is not affected by changes in filter loading. The coefficient values of 0.88 and 0.12 in equation [2.4] were empirically derived from laboratory experiments based on comparison of time-resolved aethalometer measurements with alternative non-filter based time-resolved methods and thermo-optical analysis of time-integrated filter samples (Kirchstetter and Novakov, 2007). As a large set of colocated BC measurements was collected with two separate microAethalometers during the fieldwork for Chapter 2, I was able to validate the choice of these particular coefficient values. The study protocol included regular cross-comparison measurements between the two aethalometers (in-vehicle and at CRP) immediately before in-vehicle sampling, when filters in both instruments were clean. I repeated the same cross-comparison BC measurements immediately following in-vehicle sampling, when the instrument filters had differential BC mass loading.

For each pre- and post-trip comparison session, I computed the difference between the mean ambient BC concentrations measured by each instrument over the duration of the session. The median difference in concentration reported by the two instruments was close to zero for the pre-trip comparison sessions (Figure A-2). The effect of applying the correction equation [2-4] of Kirchstetter and Novakov (2007) was small for the pre-trip BC measurements, as both instruments started the session with fresh filters and therefore both had near-zero filter loading. In contrast, for post-trip measurements, filter loading was typically higher for the in-vehicle instrument than for the ambient fixed-site instrument, owing to higher on-roadway BC levels. As a result, the uncorrected post-trip ambient concentrations measured by the in-vehicle instrument were typically lower than the same concentrations measured simultaneously by the ambient site instrument (median difference: -2.7 μg m^{-3} BC, Figure A-2b). However, after correcting BC

measurements for loading (equation [2-4]), the median bias between the two instruments was reduced to nearly zero (median difference: -0.3 μg m^{-3} BC over ~43 comparison sessions). I therefore conclude that equation [2-4] appropriately corrects for aethalometer loading effects under the conditions encountered in Chapter 2.

Refereneces

Hansen, A.D.A., Rosen, H., Novakov, T., 1984. The aethalometer -- An instrument for the real-time measurement of optical absorption by aerosol particles. *Science of The Total Environment* 36, 191-196.

Kirchstetter, T.W., Novakov, T., 2007. Controlled generation of black carbon particles from a diffusion flame and applications in evaluating black carbon measurement methods. *Atmospheric Environment* 41, 1874-1888.

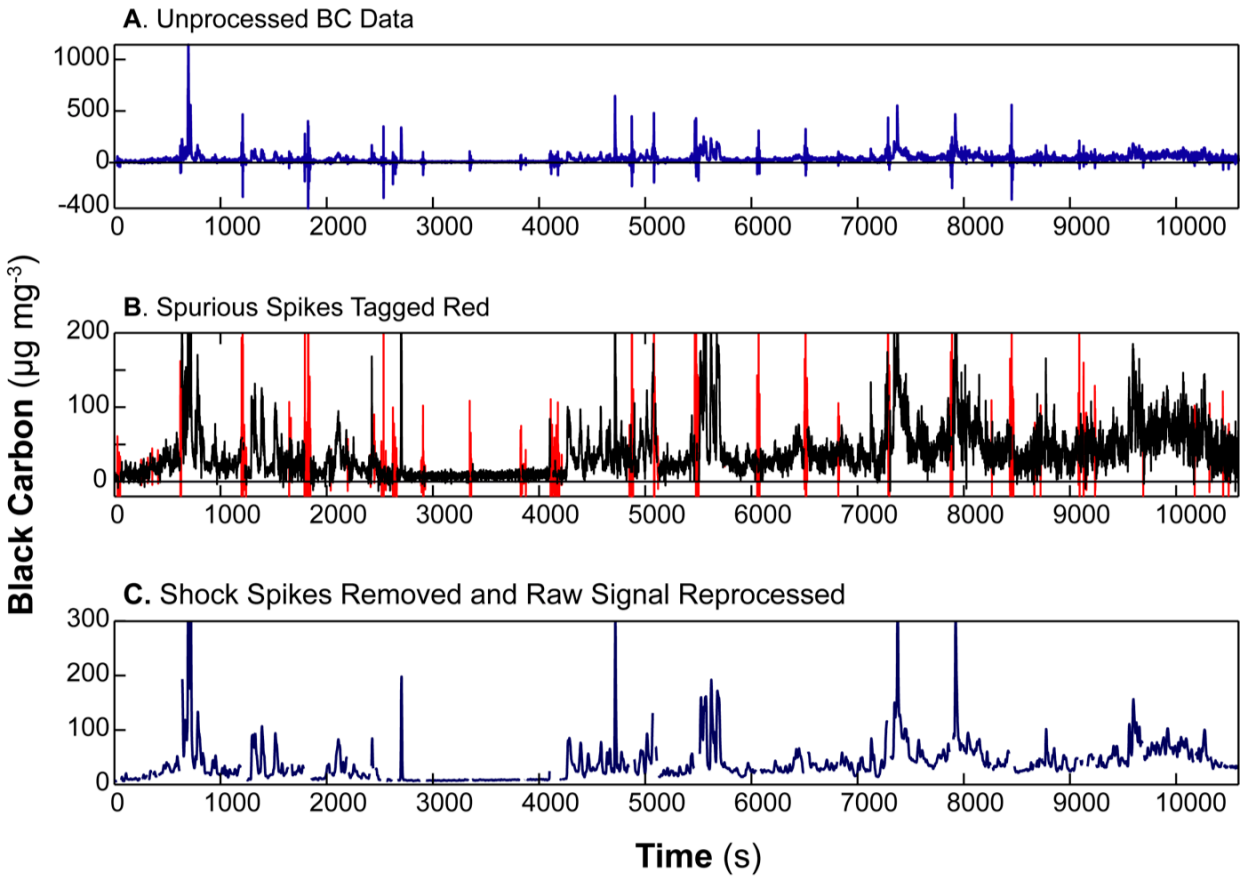

Figure A-1. Effect of post-processing algorithm on aethalometer black carbon (BC) data. Raw data from aethalometer is shown in (A), with extreme short-duration (1-3 s) excursions in measured BC evident. These spurious measurements are detected by the post-processing algorithm and are identified in red color in (B). The post-processed and smoothed time series is shown in (C).

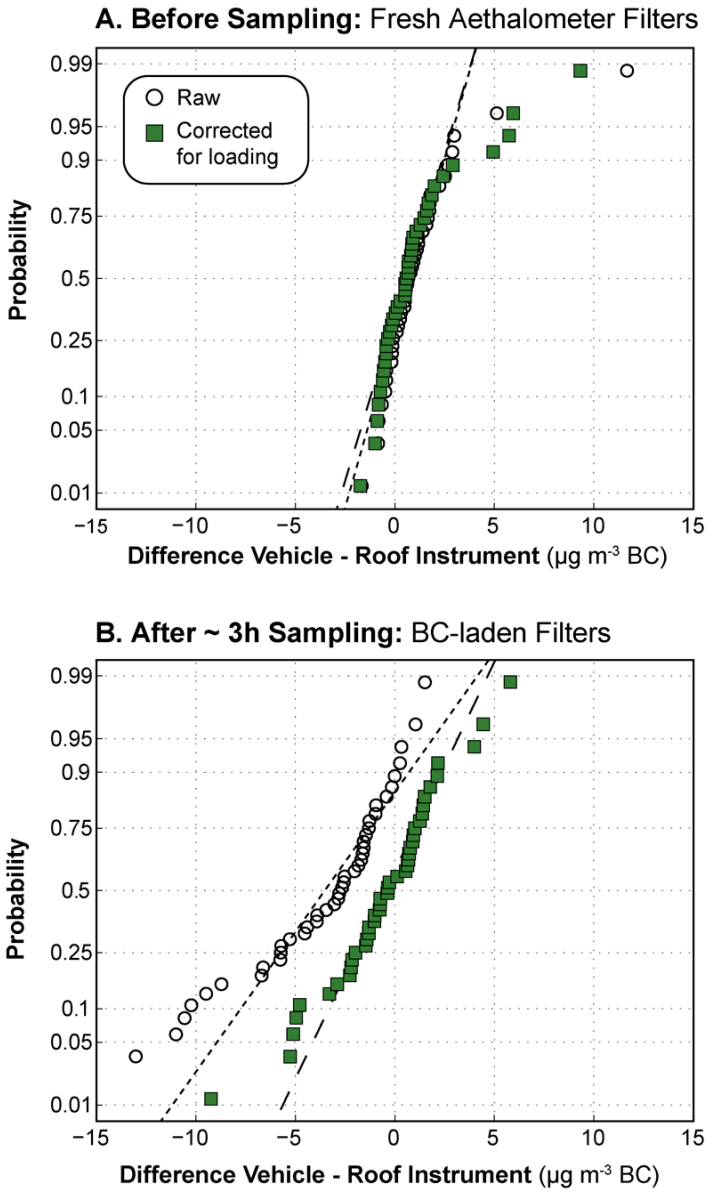

Figure A-2. Effect of filter loading correction (equation [2-4]) on colocated BC measurements collected in the field study described in Chapter 2. Horizontal axis is the difference in measured concentration at the ambient fixed site between two instruments operating simultaneously: the instrument typically used for in-vehicle measurements, and the instrument typically used for rooftop ambient measurements. The vertical axis displays the cumulative probability of the distribution of differences. Note that the effect of correction is small for fresh filters (A), while the effect of the correction is more pronounced for BC-laden filters (B). For loaded filters, the median difference between colocated measurements after correction approaches zero (B).

Appendix B: Development of diurnal profiles for population breathing rates

The diurnal profile of population mean breathing rate (units: $m^3\ d^{-1}\ person^{-1}$) is attributable to temporal profile of activity intensity within a population. For example, population mean breathing rate is lower at night, when much of the population is sleeping. The US Environmental Protection Agency (US EPA) provides activity-specific estimates of mean instantaneous breathing rate for discrete age groups (US EPA, 2009a). Activities are clustered into five intensity levels: "sleep/nap," "sedentary," "light," "moderate," and "heavy." I used US Census Bureau population age structure data for 2009 (http://www.census.gov/popest/national/asrh/NC-EST2009-sa.html) to eliminate the age-dependence of the US EPA breathing rate dataset, resulting in population mean breathing rates for each of the five activity levels. Mean breathing rates were only slightly sensitive to the age distribution employed. For example, compared to the default age distribution (US, mean age: 37 y), mean activity-specific breathing rates for the Japanese and Indian population-age distributions (mean ages: 44, 28 y) differed by ±1-4%. Table B-1 provides estimates of mean breathing rate and hours spent at each activity level for the US population.

I used data from the US National Human Activity Pattern Survey (NHAPS) (Klepeis et al., 2001) to convert activity-specific inhalation rates into an estimate of the diurnal profile of population breathing rate. For each hour of the day, NHAPS reports the distribution of the US population by microenvironment. I categorized microenvironments into four groups: indoor-residence, vehicles, other indoor, and outdoors (Figure B-1). For each microenvironment and hour of the day, I made best-judgment estimates of the fraction of population-time spent at each activity level. I then used the data in Table B-1 as a constraint on the total person-time that could be spent at each activity level over the course of a day. The results of this apportionment are summarized in Table B-2 and Figure B-2. Finally, activity-specific breathing rates in Table B-1 were applied to the diurnal activity profile (Figure B-2), resulting in the diurnal breathing rate profile depicted in Figure B-3. The time-weighted average breathing rate for this constructed diurnal profile is 15.4 $m^3\ person^{-1}\ d^{-1}$. To match the long-term population mean breathing rate recommended by the US EPA Exposure Factors Handbook (14.5 $m^3\ person^{-1}\ d^{-1}$) (US EPA, 2009b), I then applied a constant scaling factor of 0.94 to the population breathing rate at each hour of the day.

To test the sensitivity of results to the breathing rate profile, I considered four alternate temporal patterns of population breathing rate (Figure 3-1): (a) time-invariant ("flat"); (b) a sinusoidal daily cycle ("sine wave") with amplitude set at ± 25% of the mean, minimum (maximum) at 0600 h (1800 h) (Stephenson et al., 2000); and two profiles developed by Marshall et al. for the population of the South Coast Air Basin (in the Los Angeles, USA region) based (c) on author assumptions ("SoCAB-1") (Marshall et al., 2003) and (d) a local time-activity survey ("SoCAB-2") (Marshall et al., 2006). Compared with the base case, all sensitivity cases except SoCAB-1 assume relatively more population inhalation during night hours (2100 h – 0300h) and less inhalation during daytime hours (0900 h – 1500 h).

References

Klepeis, N.E., Nelson, W.C., Ott, W.R., Robinson, J.P., Tsang, A.M., Switzer, P., Behar, J.V., Hern, S.C., Engelmann, W.H., 2001. The National Human Activity Pattern Survey (NHAPS): A resource for assessing exposure to environmental pollutants. *Journal of Exposure Analysis and Environmental Epidemiology* 11, 231-252.

Marshall, J.D., Riley, W.J., McKone, T.E., Nazaroff, W.W., 2003. Intake fraction of primary pollutants: Motor vehicle emissions in the South Coast Air Basin. *Atmospheric Environment* 37, 3455-3468.

Marshall, J.D., Granvold, P.W., Hoats, A.S., McKone, T.E., Deakin, E., Nazaroff, W.W., 2006. Inhalation intake of ambient air pollution in California's South Coast Air Basin. *Atmospheric Environment* 40, 4381-4392.

Stephenson, R., Mohan, R.M., Duffin, J., Jarsky, T.M., 2000. Circadian rhythms in the chemoreflex control of breathing. *American Journal of Physiology - Regulatory, Integrative and Comparative Physiology* 278, R282-R286.

US EPA, 2009a. *Metabolically Derived Human Ventilation Rates: A Revised Approach Based Upon Oxygen Consumption Rates*, United States Environmental Protection Agency, National Center for Environmental Assessment, Washington, DC. EPA/600/R-06/129F. Available from: http://cfpub.epa.gov/ncea/cfm/recordisplay.cfm?deid=202543.

US EPA, 2009b. *Exposure Factors Handbook: 2009 Update (External Review Draft)*, United States Environmental Protection Agency, Washington, DC. EPA/600/R-09/052A. Available from: http://cfpub.epa.gov/ncea/cfm/recordisplay.cfm?deid=209866.

Table B-1. Activity-specific breathing rates for the US population [a]

Activity Mode	Breathing rate (m^3 $person^{-1}$ d^{-1})	Time spent (h d^{-1})
Sleep / Nap	6.9	8.8
Sedentary	6.8	4.5
Light	17	6.3
Moderate	37	4.1
Heavy	69	0.3

[a] Adapted from US EPA data (US EPA, 2009)

Table B-2. Apportionment of average person time (h d^{-1}) by microenvironment and breathing rate for US population in NHAPS

	Sleep	Sedentary	Light	Moderate	High	Total
Residence	8.7	2.5	3.4	1.8	0.15	**16**
Other Indoor	0.13	1.2	2.0	1.0	0.04	**4.4**
In-Vehicle	-	0.53	0.53	0.26	-	**1.3**
Outdoor	-	0.22	0.45	1.0	0.11	**1.8**
Total	**8.8**	**4.5**	**6.3**	**4.1**	**0.30**	**24**

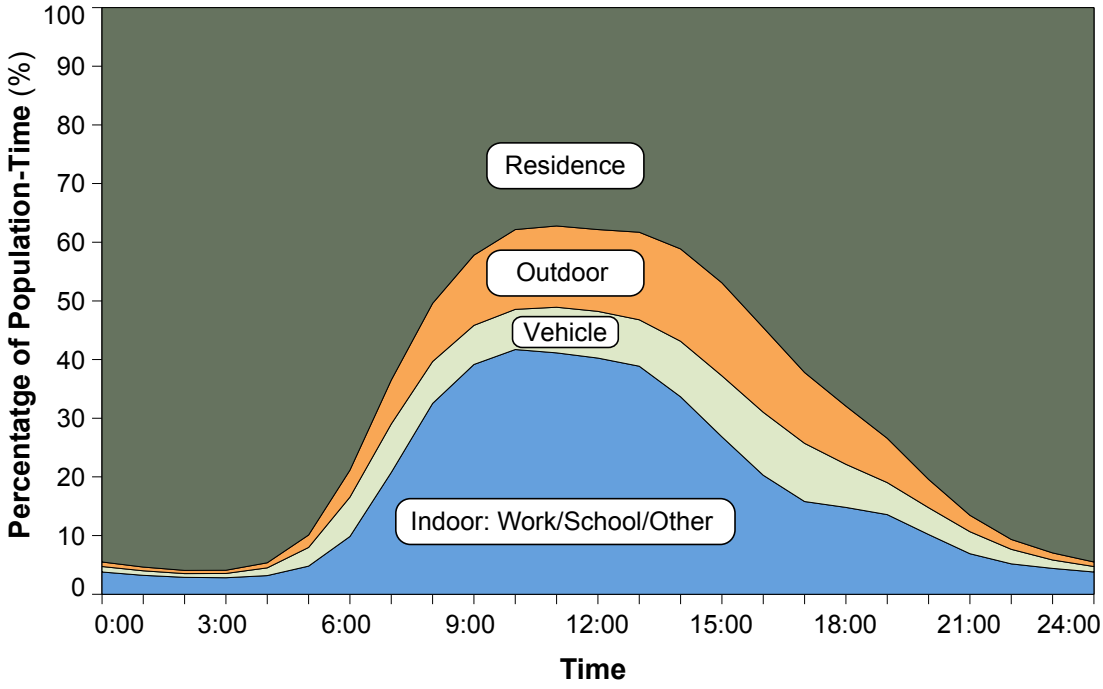

Figure B-1. Fraction of total person time in NHAPS for each of four microenvironment groupings.

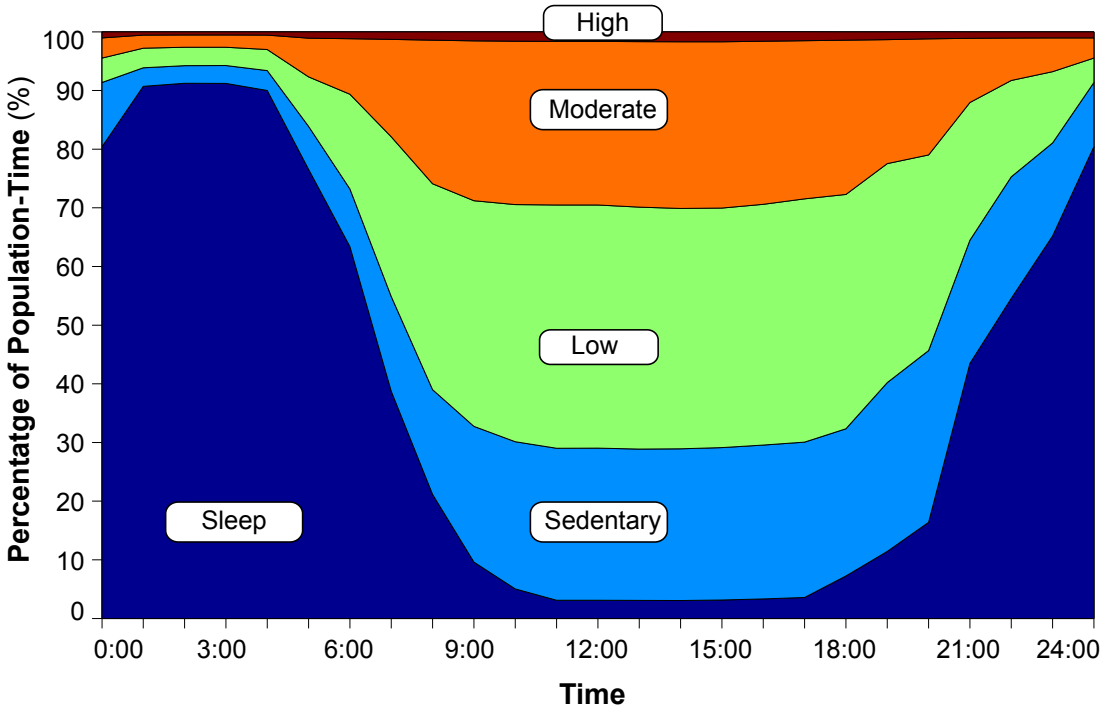

Figure B-2. Estimated fraction of US population-time in each of five breathing rate modes by hour of day.

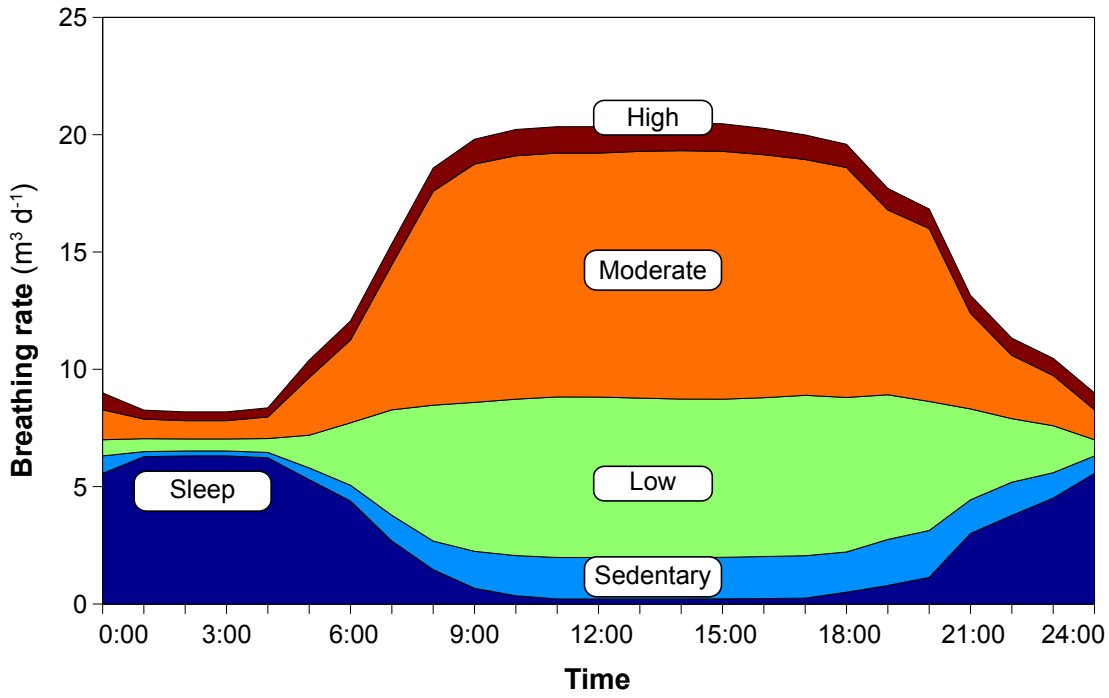

Figure B-3. Diurnal breathing rate profile for the US population estimated using US EPA and NHAPS data.